HIGH OXIDATION STATE NIOBIUM AND TANTALUM COORDINATION CHEMISTRY: A SOLUTION AND SOLID STATE INVESTIGATION

by

RENIER KOEN

Submitted in fulfilment of the requirements in respect of the
Doctoral degree qualification

PHILOSOPHIAE DOCTOR

in the

DEPARTMENT OF CHEMISTRY

in the Faculty of

NATURAL- AND AGRICULTURAL SCIENCES

at the

UNIVERSITY OF THE FREE STATE

Supervisor

Prof. Hendrik G. Visser

Co-Supervisor

Prof. Andreas Roodt

JANUARY 2016

Acknowledgements

First and foremost, I thank the Lord Almighty for equipping me with the wisdom, insight and perseverance to make my success possible. Without Your guidance and love I would be a lost case. To you God, I give you this and I give my all. Thank you for the countless blessings that you have given me.

To Prof. Deon Visser, a simple thank you does not justify my gratitude. You are not only an enthusiastic promoter but a great role model and friend. The value of the advice and support that you've given me over time cannot be quantified. You are truly a legend!!!

To Prof. André Roodt, thank you for all the guidance and laughs shared. It is a well-known fact that you are not only a prodigious scientist but also a great person. The advice that you have given me, both professionally and personally will always be appreciated. I'm truly honoured to be associated with a man such as you.

To my colleagues, thank you for all the fun, the jokes and the occasional drink that makes going to work worthwhile. There are too many to personally thank but to all; thank you for sharing knowledge and always being there to give advice and answer the stupid questions.

To Dr. Johann Nel, thank you for all the effort that you not only put into our work and projects but also the effort you put in behind the scenes. Sometimes you don't get enough credit for all that you do for us, but be assured it does not go unnoticed and is greatly appreciated.

To my friends, thank you for always being there for me during all the difficult times but also not forgetting all the laughs. Without you bunch of freaks my life would be unbelievably boring. Thank you for some of the best years of my life.

To my parents, Johan and Veronica, thank you for shaping me into the man I am today. I can attribute all my successes to your support and sacrifices through the years. I could not ask for better role models and support system. I wish you both could be alive to share in this great moment in my life.

To my fiancé, Heléne, I can truly say, meeting you has been the greatest success story of my life. The love and effort you put into everything you do for me is indescribable and I'm eternally grateful. Thank you for helping me through the tough times while, not only writing this thesis, but all the challenges I've faced in the last few years. I'm really looking forward to tackling a lifetime of trials and sharing an eternity of laughter with you.

And last, but not least; the financial assistance from the Advanced Metals Initiative (AMI) and the Department of Science and Technology (DST) of South Africa, as well as the New Metals Development Network (NMDN) and the South African Nuclear Energy Corporation Limited (Necsa) is gratefully acknowledged. Without your input this project would be non-existent. Thank you for shaping us into the scientists of the future.

Abbreviations and Symbols

Abbreviation	Meaning
acacH	*2,4*-Pentanedione
3Cl-acacH	*3*-Chloro-*2,4*-pentanedione
tffaH	*4,4,4*-Trifluoro-*1*(*2*-furyl)-*1,3*-butanedione
ttfaH	*4,4,4*-Trifluoro-*1*(*2*-thienyl)-*1,3*-butanedione
btfaH	*4,4,4*-Trifluoro-*1*-benzoyl-*1,3*-butanedione
tfaaH	*1,1,1*-Trifluoro-*2,4*-pentanedione
hfaaH	*1,1,1,5,5,5*-Hexafluoro-*2,4*-pentanedione
ntfaH	*4,4,4*-Trifluoro-*1*(*2*-naphtyl)-*1,3*-butanedione
tropH	Tropolone
Z	Number of molecules in a unit cell
Å	Angstrom
NMR	Nuclear Magnetic Resonance spectroscopy
IR	Infrared spectroscopy
XRD	X-ray Diffraction
ν	Stretching frequency on IR
δ	Chemical shift
ppm	Units of chemical shift (parts per million)
π	pi
σ	Sigma
α	Alpha
β	Beta
γ	Gamma
λ	Wavelength
°	Degrees
°C	Degrees Celsius
K	Kelvin
ε	Extinction coefficient
g	Gram
M	$mol.dm^{-3}$
k_{obs}	Observed pseudo-first order rate constant
K_{eq}	Equilibrium constant
k_{fwd}	Observed rate of simplified forward reaction
k_{rev}	Observed rate of simplified reverse reaction

pK_a	Acid dissociation constant
T	Temperature
UV	Ultraviolet region in light spectrum
Vis	Visible region in light spectrum
MeCN	Acetonitrile
Acetonitrile-d_3	Deuterated Acetonitrile
CSD	Cambridge Structural Database
s	Singlet in NMR spectroscopy
d	Doublet in NMR spectroscopy
m	Multiplet in NMR spectroscopy
d(⋯)	Distance
Hz	Hertz

Table of Contents

Chapter 3: Synthesis of Various Nb(V)- and Ta(V) Compounds

Chapter 4: Chrystallographic Evaluation of New Nb(V)- and Ta(V) Synthons

Chapter 5: Chrystallographic Evaluation of [$NbOCl_3$(*β*-diket)] Complexes (1)

Chapter 6: Chrystallographic Evaluation of [$NbOCl_3$(*β*-diket)] Complexes (2)

Chapter 7: Crystallographic Evaluation of Nb(V)- and Ta(V) Tropolonato Complexes

Chapter 8: Kinetic/Mechanistic Study of the Coordination of *β*-diketones to Nb(V)- and Ta(V) Metal Centres

Chapter 10: Evaluation of Study and Future Aims

Appendices

Chapter 1: Introduction

1.1 Tantalum and Niobium: A Brief History and Insight

Tantalum (previously known as tantalium) was originally discovered by the Swedish chemist Anders Gustaf Ekeberg in 1802, when he was examining new mineral samples found in Ytterby, Sweden.[1] The word "tantalum" is derived from the Greek mythological god, Tantalus, whom was most famously known to have revealed the divine secrets of the gods to ordinary mortals.[2] In 1809, a British chemist, William Hyde Wollaston, was conducting studies into two different mineral samples of columbite and tantalite (consisting mainly of columbium and tantalum respectively). On completion of his study Wollaston concluded that columbium and tantalum were, in fact, the same element.[1] There was no argument concerning his conclusion until 1844 when Heinrich Rose could distinguish between these two elements by differences in valence state, with columbium exhibiting +3 and +5 oxidation states and tantalum only +5 as stable entities.[3] Accordingly, he renamed columbium as niobium after Niobe, the daughter of Tantalus, due to their very similar chemical and physical properties.[2]

Tantalum and niobium are two transition metals found in the vanadium triad of the periodic table and always occur together in nature.[4] The average tantalum content of the earth's crust has been estimated at about 1.7 parts per billion *vs.* niobium which

[1] A. Agulyansky, (2004). *The Chemistry of Tantalum and Niobium Fluoride Compounds*, Elsevier, Amsterdam, Netherlands.

[2] G. L. Miller, (1959). *Tantalum and Niobium*, Academic Press, New York, United States of America.

[3] J. B. Lambert, (2011). *Kirk-Orthmer Encyclopaedia of Chemical Technology*, John Wiley and Sons, New Jersey, United States of America.

[4] L. G. Hubert-Pfalzgraf, M. Postel and J. G. Reiss, (1987). *Comprehensive Coordination Chemistry*, Elsevier:Pergamon, Oxford, United Kingdom.

is 10 times as abundant.[5] The minerals of tantalum and niobium are known as tantalates and niobates (columbates) and are mainly salts of metaniobic and metatantalic acids. They are usually found as oxidic materials, complexed with other minerals such as tin, titanium, uranium, thorium and rare earths.[1]

1.2 Nuclear Industrial Application of Niobium and Tantalum

Niobium finds a very important application in the nuclear industry. This has been ascribed to the high melting point, strength, resistance to chemical attack and the low neutron absorption cross-section (NAC) of the metal.[3] A smaller NAC correlates to a lower affinity for absorbing thermal neutrons (nuclear energy); this cross section of an element is measured in barns (1 barn = 10^{-24} cm^2).[6] Niobium has a NAC of 1.10 barn which makes it an ideal applicant for cladding material in control rods of nuclear reactors.[3] These rods usually contain uranium or plutonium oxides, called fuel pellets. Due to the intense reactivity within the reactor, these pellets are cladded with niobium-zirconium alloys that have high anti-corrosive properties and have a low NAC to prevent leakage of nuclear reactive materials.[7]

Tantalum, on the other hand, has a much more limited application in the nuclear industry. It is mainly used in combination with carbon to form tantalum carbide which is used as a lining agent within the nuclear reactor (due to the corrosion resistance of tantalum).[8] Since tantalum and niobium are always found together in mineral ores, tantalum is actually seen as a “pollutant” by nuclear chemists.

---

[5] R. L. Rudnick and S. Gao, (2004). *Composition of the Continental Crust*. Elsevier:Pergamon, Oxford, United Kingdom.

[6] J. B. Lambert and J. Rausch, (1990). *Metals Handbook*, ASM International, Ohio, United States of America.

[7] M. Benedict, T. H. Pigford and H. W. Levi, (1981). *Nuclear Chemical Engineering*, McGraw-Hill Publishing, United States of America.

[8] S. L. Chawla and R. K. Gupta, (2010). *Materials Selection for Corrosion Control*, ASM International, Ohio, United States of America.

1.3 The Separation of Niobium and Tantalum

The separation of tantalum and niobium is extremely difficult due to the very similar chemical and physical characteristics. This similarity in behaviour has mainly been ascribed to lanthanide contraction and because of their similar ionization energies. These elements replace each other isomorphously in their minerals and are also sometimes replaced by elements of similar atomic radius, such as tin, antimony and bismuth.[1]

Separation of tantalum and niobium from their mineral ores has long presented a problem and challenge to both chemist and metallurgist but several tantalum-niobium separation techniques have been identified. The methods which are currently industrially applicable are listed below and will be discussed in greater detail in Chapter 2.

- Marignac Process[9]
- Solvent Extraction[10]
- Chlorination Separation[10]

Of these methods listed, the solvent extraction process has been most successfully implemented on an industrial and economically viable scale.

1.4 The Need for Improvement in Separation

In recent times, attempts have been made not only to quantify the "greenness" of a chemical process like separation, but to always factor in other variables such as yields, price of reagents, safety in handling chemicals, hardware demands, ease of product workup and purification.[11]

---

[9] J. Emsley, (2003). *Nature's Building Blocks: An A-Z Guide to the Elements*, Oxford University Press, Oxford, United Kingdom.

[10] D. K. Bose and C. K. Gupta, (2001). *Miner. Process. Extr. Metall. Rev.*, **22**, 389-399.

[11] R. A. Sheldon, I. W. Arends and U. Hanefeld, (2007). *Green Chemistry and Catalysis*, John Wiley and Sons, New Jersey, United States of America.

Green chemistry, also known as sustainable chemistry, is a philosophy of chemical research and engineering that encourages the design of products and processes that minimalizes the use of and generation of hazardous substances and excess waste products. In recent years companies have been encouraged to apply principles of green chemistry to their industrial processes.

The current industrial tantalum and niobium separation methods are relatively effective but unfortunately these methods have several flaws (discussed in detail in Chapter 2).[9,10] These include:

- Processes are very expensive.
- Reactors and hardware require high temperature to be effective.
- Coordination processes of the chemicals required for separation, generate waste gas containing noxious fumes such as chlorine and phosgene.
- Hazardous waste products are generated from these processes (e.g. metal fluorides).
- Some of these methods require the use of dangerous acids such as hydrofluoric acid (HF).
- And finally, all of these methods are labour intensive.

When considering the negative aspects noted above, it would be very advantageous to study the possibility of another, less expensive and greener separation method.

1.5 The Aim of This Study

The information presented above clearly shows that there is scope for improvements in the metallurgical methods of purification of niobium and separation from tantalum. A detailed literature review revealed a considerable shortage of knowledge with relation to the chelation behaviour of tantalum and niobium with different organic bidentate or multidentate ligands. The key to the effective and simplified separation of these two elements could possibly be found in the chemical differences in the chemical properties of two similar organic chelated moieties of these metals. When conducting a search for a unique chemical state difference, it is crucial to investigate

metal compounds with ligand systems that allow for the effective characterization and evaluation of these metal complexes. By studying the solid and solution state behaviour of tantalum and niobium with selected coordination agents, as well as the rates at which these interactions take place, a clearer image of how improvements on known methods can be obtained.

The main focus of this study will therefore be placed on coordination of organic bidentate ligands, especially focussing on acetylacetone-type (acacH) as well as tropolone (tropH) ligands to Nb(V) and Ta(V) metal centres. These ligand systems are relatively inexpensive, safe, rather simple to characterize and are also known to be easily functionalized, providing scope to study electron donating and -withdrawing effects (based on the Bronsted pK_a). Accordingly, a significant part of this investigation was focussed on the synthesis and characterization of these metal-acetylacetonato and -tropolonato complexes.

The aims of this Ph.D. investigation of tantalum- and niobium coordination compounds can thus be summarized as follows:

- Most of the recorded literature indicates that tantalum(V) and niobium(V) bidentate complexes can only be synthesized under inert and anhydrous conditions.[12] In an attempt to overcome this problem, the synthesis of a more robust, inexpensive metal(V) synthon is required for application in atmospheric conditions. This could improve the stability and ease of formation of the corresponding coordination compounds.

- Application of these stable synthons in the synthesis of novel tantalum(V) and niobium(V) coordination compounds with a range of *O,O'*-donor bidentate ligands and subsequent characterization thereof by means of a range of analytical techniques, such as UV/Vis-, IR and NMR spectroscopies and X-Ray crystallography. The acetylacetone-type and tropolone-type ligands intended for this study are discussed in detail in Chapter 2.

[12] R. Koen, (2012). *High Oxidation State Tantalum Coordination Chemistry: A Solution and Solid State Investigation*, M.Sc. Dissertation, University of the Free State, South Africa.

- Solid state structural characterization of crystalline products of the complexes described above, intended at elucidating the nuances of chelation and variances in geometry that can be detected by means of single crystal X-Ray Diffraction (XRD). With this type of investigation, a comparison of similar niobium(V) and tantalum(V) compounds could yield valuable insight into physical and/or chemical state differences to be exploited for purification/separation endeavours.

- Solution state assessment of the intrinsic formation mechanism of the synthesized and characterised compounds of niobium(V) and tantalum(V). This investigation is accomplished by means of detailed time resolved UV/Vis kinetic studies and reaction rate modelling with the purpose of shedding light into the equilibrium effects in these processes that could possibly be exploited for solution extraction methodology.

- Finally, to conduct an overarching correlation of the ligand effects including the evaluation of intra- and intermolecular interactions in the different coordination compounds. The purpose of this is to obtain potential trends relating to the electronic and steric effects of the introduced ligands on the isolated tantalum(V) and niobium(V) bidentate complexes. It is envisaged that this correlation will potentially clarify properties such as complex stability, acidity and other physical properties, including the propensity of the compounds to sublimate.

In the following chapter, the theory related to this study will be presented in a systematic fashion, which will be followed by the presentation and discussion of experimental results in six chapters. The study will conclude with a comprehensive discussion and comparison of the different parameters by which the niobium(V) and tantalum(V) complexes were analyzed to evaluate any trends and relationships that exist for the different complexes.

Chapter 2: Theoretical Background Related to This Investigation

Often associated geologically, but with different end-uses, tantalum (^{181}Ta) and niobium (^{91}Nb), the chemical twins of the vanadium triad have found considerable interest in scientific research.[1,2,3,4]

In the average continental crust the overall abundances of ^{91}Nb (8.0 ppm) and ^{181}Ta (0.7 ppm) are relatively low.[5] These transition metals do not naturally occur as free metals, but are essential components in a range of mineral species.[2] The majority of these are oxide minerals; silicates do exist but are relatively rare. Tantalite ($(Fe,Mn)Ta_2O_6$), columbite ($(Fe,Mn)Nb_2O_6$), columbite-tantalite (Coltan), pyrochlore ($(Na,Ca)_2Nb_2O_6(OH,F)$) and euxenite ($(Y,Ca,Ce,U,Th)(Nb,Ta,Ti)_2O_6$) constitute the major primary sources for these elements and are most common in Australia, Canada, Brazil, Nigeria, Zaire and Russia.[6]

[1] Tantalum-Niobium International Study Center, (2011). *Tantalum and Niobium – Early history*. http://tanb.org/history. Last accessed 20/06/2015.

[2] British Geological Survey, (2011). *Tantalum and Niobium*, London, United Kingdom.

[3] A. Agulyansky, (2004). *The Chemistry of Tantalum and Niobium Fluoride Compounds*, London, United Kingdom.

[4] G. L. Miller, (1959). *Tantalum and Niobium*, Academic Press, New York, United States of America.

[5] R. L. Rudnick and S. Gao, (2003). *Composition of the Continental Crust*, Oxford: Elsevier-Pergamon, London, United Kingdom.

[6] O. S. Ayanda and F. A. Adekola, (2011). *JMMCE*, **10**, 245-256.

As transitions metals they function over a wide range of applications, from catalysis to alloyed metal components.[7,8,9,10,11,12] However, because of the strong chemical similarity of the two metals, it makes it difficult to refine either free metal from each other in the mineral ores. Separation of these metals can be accomplished *via* several means, but is a difficult and labour intensive process.[3,4]

2.1 Tantalum vs. Niobium

Niobium and tantalum are members of the refractory metals family, which are characterized by very high melting points, with similarity going far beyond occurrence and discovery. It has been well noted that ^{181}Ta and ^{91}Nb also share many physical and chemical characteristics with some examples listed in the following paragraph.

Both of these elements are members of group 5 on the periodic table with a variety of oxidation states. Further research revealed that the +5 state is the most common and stable, which could be attributed to the lack of valence s- and d-electrons of these elements.[9] These metals are known to replace each other isomorphously in their minerals and are also sometimes replaced by elements of similar atomic radius, such as tin, antimony and bismuth.[4] In addition, they also display similar chemical behaviour due to lanthanide contraction and because of their similar ionization energies.[13] Table 2.1 depicts a chemical comparison of the elements.

[7] T. Ushibuko, (2000). *Catal. Today*, **57**, 331-338.

[8] P. L. Tau, (2007). *Study of Titanium, Tantalum and Chromium Catalysts for Use in Industrial Transformations,* Ph.D. Thesis, Rhodes University, South Africa.

[9] A. G. Knapton, (1960). *J. Less Com. Met.*, **2**, 113-124.

[10] E. Albert, E. Fromm and R. Kirchhein, (1983). *Metall. Trans. A.*, **14**, 2117-2118.

[11] S. Y. Yu, J. R. Scully and C. M. Vitus, (2001). *J. Electrochem. Soc.*, **148**, B68-B78.

[12] V. Livramento, M. T. Marques, J. B. Correia, A. Almeida and R. Vilar, (2006). *Mater. Sci. Forum*, **514**, 707-711.

[13] L. G. Hubert-Pfalzgraf, M. Postel and J. G. Riess, (1987). *Comprehensive Coordination Chemistry*, **3**, Pergamon, London, United Kingdom.

Table 2.1 Comparison of some chemical and physical properties of tantalum and niobium.[14,15]

Name	Tantalum (^{73}Ta)	Niobium (^{41}Nb)
Principal Oxidation States	5,4,3,2,-1	5,4,3,2,-1
Lattice-type	Body centered cubic	Body centered cubic
Standard atomic weight (g. mol^{-1})	180.95	92.91
Atomic Radius (pm)	146	146
Covalent Radius (pm)	170	164
Ionization Energy (eV)	6.67	7.30
Melting Point (K)	3290	2750
Boiling Point (K)	5731	5017
Thermal Conductivity (W. m^{-1} K^{-1})	54.4	57.3
Hardness (mohs)	6.5	6.0
Thermal Neutron Cross-Section (barns)	21.3	1.1
Density (g. cm^{-1}) (near r.t.)	16.69	8.57

Both these elements are tough, ductile metals which can be formed into nearly any shape. Because of their corrosion resistant nature and excellent formidability, they are often used in environments which no other metals can withstand.[15]

The most notable differences among the chemical properties of the elements are the atomic masses, densities and thermal neutron absorption cross-sections. These deviations contribute to the differences in industrial application of the metals. An obvious example of this in the nuclear industry can be attributed to the low thermal neutron absorption of niobium.[16] This characteristic makes niobium-zirconium alloys ideal in nuclear fuel rod cladding. In contrast, tantalum has the ability to absorb neutrons, is highly corrosion resistant and has remarkable mechanical strength, making it ideal for use in the production of control rods in a nuclear reactor.[17]

[14] J. B. Lambert, (2011). *Kirk-Othmer Encyclopedia of Chemical Technology*, John Wiley & Sons, Inc., New York, United States of America.

[15] N. E. Holden, (2004). *CRC Handbook of Chemistry and Physics,* **85**, CRC Press, Boca Raton, United States of America.

[16] C. A. Hampel, (1961). *Rare Metals Handbook*, **2**, Reinhold, United Kingdom.

[17] D. R. Sadoway and S. N. Flengas, (1980). *Metall. Trans. B,* **11**, 57-62.

Separation of tantalum and niobium from their mineral ores has long presented a problem to both chemist and metallurgist. Even so, separation of the elements has been relatively successfully implemented on an industrial and economically viable level.[18]

2.2. Industrial Separation Processes of Tantalum and Niobium

2.2.1 Marignac Process[19]

The Marignac process was the preferred industrial separation method up until the mid-1950's. The process starts directly from tantalite ore which has been solubilized with hydrofluoric acid. Potassium salts are added to the tantalum-niobium containing filtrate. This addition leads to the crystallization of insoluble potassium heptafluorotantalate(V) ($K_2[TaF_7]$) (to be further purified by recrystallization) and the more soluble oxofluoroniobate(V) ($K_2[NbOF_5]$) remains in the filtrate. This niobium containing filtrate is then precipitated as the oxide hydrate, which can be processed directly to ferroniobium.

2.2.2 Pegmatite Mining and Solvent Extraction (Methyl Isobutyl Ketone (MIBK) – HF/H_2SO_4)

Most tantalum (Ta) and niobium (Nb) containing pegmatite deposits are mined in either one of two ways, either from open-pit mines (Australia) or in underground mines (Canada). The excavation of these pegmitites is done by conventional techniques such as blasting and crushing of the rocks. The minerals are then concentrated mainly by gravitational methods.[20] This has already separated the tantalum from some other fewer useful deposits. The remaining Ta, Nb and other

[18] D. K. Bose and C. K. Gupta, (2005). *Mineral Processing and Extractive Metallurgy Review*, **22**, 389-412.

[19] J. Emsley, (2003). *Nature's Building Blocks: An A–Z Guide to the Elements*. Oxford University Press, United Kingdom.

[20] M. Forest, (2002). *Mater. World*, **10**, 14-16.

elements (including tin (Sn)) are then collected in the form of tin 'slags' (Ta_2O_5 : Nb_2O_5 = 0.2 – 17 % : 34%).[20]

After tin 'slag' upgrading, a raw synthetic concentrate with relatively high Ta- and Nb-content is obtained. This concentrate is finely ground and digested in hydrofluoric acid (HF) and sulphuric acid (H_2SO_4) to acidity greater than 8 M, at an elevated temperature. This causes the formation of the heptafluorides, $H_2[TaF_7]$ and $H_2[NbF_7]$, which easily dissolve along with manganese (Mg), titanium (Ti) and iron (Fe).[15,18] The other impurities, such as calcium (Ca) and aluminium (Al) remain as insoluble residues and are removed by simple filtration.[14]

The aqueous Ta-Nb solution in HF is then extracted several times with the organic solvent methyl isobutyl ketone (MIBK), using extraction columns. The impurities such as Ti, Mg and Fe remain in the aqueous phase. The organic phase containing the Ta and Nb is extracted again but this time against H_2SO_4 (3 – 6 M). It is important to note that at high concentrations of H_2SO_4 (> 8 M), both Ta and Nb are extracted, at lower H_2SO_4 concentrations (< 8 M) only Nb gets extracted.[13] Accordingly, the fluoroniobate gets extracted into the aqueous phase, while the fluorotantalate remains in the organic phase. The resultant aqueous phase is re-extracted with MIBK to remove any excess traces of co-extracted Ta.[14]

The final step is to extract the Ta salt from the organic phase with an aqueous ammonium fluoride solution or water. This process has been optimized to such an extent that 99 % purity has been obtained.[15,21] Figure 2.1 is a graphic illustration of the processing of Ta-Nb raw materials via the solvent extraction process discussed in this section.

[21] G. P. Sabol, R. J. Comstock and U. P. Nayak, (2000). *Zirconium in the Nuclear Industry,* **14**, 525-530.

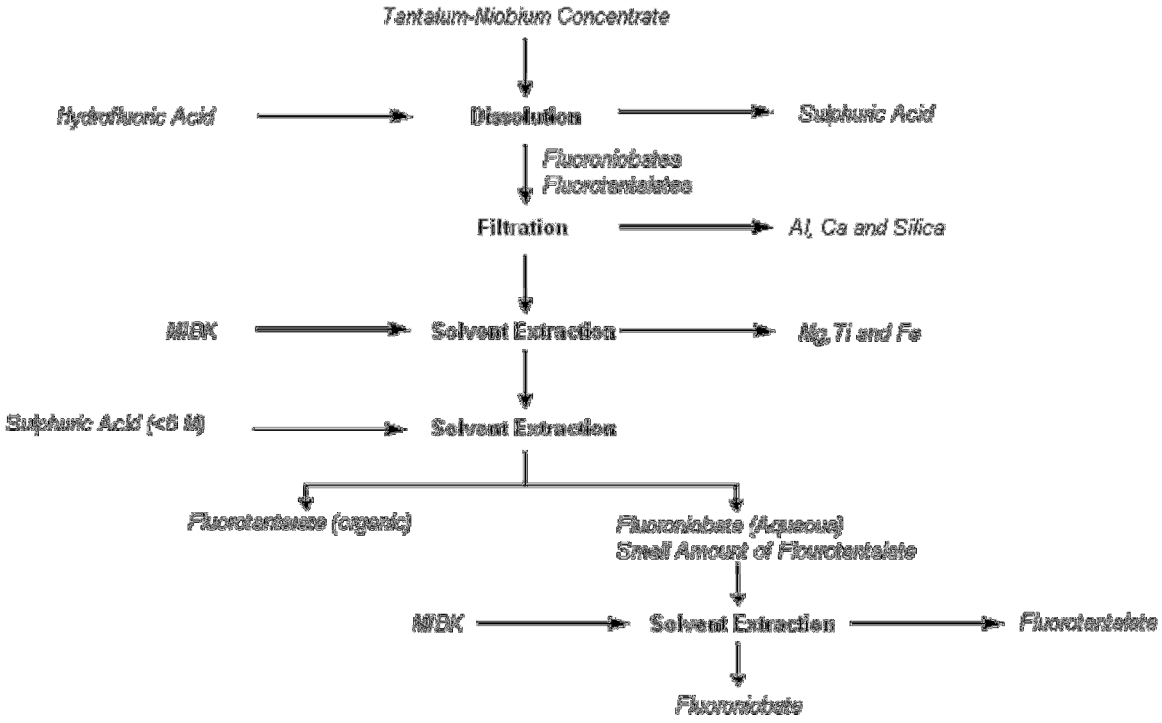

Figure 2.1 Processing of Ta-Nb raw materials *via* solvent extraction process.[22]

2.2.3 Chlorination Separation[14]

An alternative separation procedure currently being used industrially is reductive chlorination. The Ta-Nb concentrate obtained from tin 'slags' such as discussed in Section 2.2.2 is pelletized with coke and pitch. This mixture is dried and left to react in a stream of chlorine at roughly 850 °C.

Using this ingenious approach, the non-volatile earth metal chlorides remain precipitated in the bottom of the reactor, while the volatile chlorides of tungsten (W), niobium (Nb), tantalum (Ta), tin (Sn) and titanium (Ti) are collected and fractionally distilled.

[22] Schematic of: *Processing Ta-Nb Raw Materials via Solvent Extraction Process,* adapted from: D. K. Bose and C. K. Gupta, (2005). *Mineral Processing and Extractive Metallurgy Review*, **22**, 389-412.

.

2.2.4 Evaluation of Separation Methods

When considering the aforementioned industrial separation techniques for tantalum and niobium, it becomes apparent that these methods focus to exploit small differences in chemical behaviour and physical states of these metals. These methods are highly efficient affording extremely pure Ta and Nb but are very wasteful and have negative environmental implications.

- **Marignac Process**[19] – exploits the $K_2[TaF_7]$ preferential crystallization *vs*. the more soluble $K_2[NbOF_5]$ which remains in HF-solution to be furthered purified. This process is very laborious and hazardous hydrofluoric acid waste is created.

- **Solvent Extraction**[20] – takes advantage of the fact that the fluoroniobate gets extracted into the aqueous phase at H_2SO_4 concentrations lower than 8 M, while the fluorotantalate remains in the organic phase. Even though it is so efficient, it remains a very laborious, expensive and potentially hazardous process. Much HF waste is generated and a large amount of solvent waste is produced.

- **Chlorination Separation**[14] – benefits from Ta and Nb affinity for chlorine gas and the different temperatures at which these complexes can be distilled. Unfortunately, this is a very expensive process, extremely high temperatures are needed and the waste gas containing chlorine and phosgene needs to carefully be controlled.

When taking some of these aspects in consideration, it becomes plausible to plan a systematic approach to find an easier and better separation method by developing a method that exploits subtle nuances of the chemical behaviour which in some way alters the physical attributes or characteristics of these metals/metal complexes. Attention must just be given to minimalize the adverse aspects of these processes.

The proposal to study novel tantalum and niobium coordination compounds as well as their solution state behavioural characteristics, for separation purposes, is

fundamental to this study. It is important to take into account the successes with regard to known chelators, solvents and other contributors that have already been successfully applied on an industrial scale.[19,20] The electronic and steric effects of organic chelators have a massive impact on the behaviour of the respective metal complexes. These aspects are of prime importance when considering improvement of known separation methods.

2.3. Tantalum(V) and Niobium(V) Complexes

The key to effective separation of these elements could be found in the differences in the chemical properties of two similar organic chelated moieties of these metals. When attempting to find a unique chemical state difference, it is crucial to investigate metal compounds with ligand types which allow for effective and accurate characterization and evaluation of these metal complexes.[3] Postulation of a reaction mechanism will also assist in the clarification of the chemical behaviour, which the metal undergoes during substitution with organic ligands in the solution state.[23] In this study focus was placed on bidentate ligand systems, eg. functionalized *β*-diketone- and tropolone ligands.

Ligand coordination studies for the two heaviest elements of group 5, is essentially related to the multiple uses of these elements in advanced materials for high technology applications.[24,25] Even though a relatively large amount of work has been done in this field, knowledge of the aqueous chemistry of these two elements is still limited.

[23] M. Steyn, (2014). *A Solid State and Mechanistic Study of Multidentate Ligand Zirconium(IV) Halido Complexes.* Ph.D. thesis, University of the Free State, South Africa.

[24] D. Bayot and M. De Villiers, (2006). *Coord. Chem. Rev.,* **250**, 2610-2626.

[25] L. Herbst, (2012). *A Solution and Solid State Study of Niobium Complexes,* M.Sc. Dissertation, University of the Free State, South Africa.

2.3.1 Bidentate Ligands

2.3.1.1 An Overview of *β*-diketones

The *β*-diketone bidentate ligands are used widely as a type of conjugated ligand system in organometallic chemistry. In solution, these ligands exist in a keto-enol tautomeric equilibrium, depicted in Figure 2.2. Interestingly, this equilibrium is generally strongly shifted towards the enol form due to the formation of the resonance structure as a six-membered ring.[26,27] The extent to which the equilibrium may depend on the solvent polarity, temperature, the concentration, and the structure of the compound.[28] *β*-diketones have the ability to form stable complexes with most metals and is a direct consequence of the occurrence of the enol form of these compounds.[29,30]

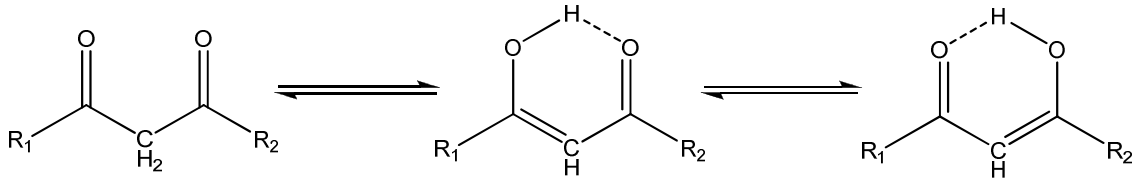

Figure 2.2 Keto-enol tautomerism of a *β*-diketone.[31]

When considering *β*-diketones currently used in synthetic chemistry, it would seem that pentane-2,4-dione (acetylacetone, acacH) is deemed as a favourite.[32] These ligand systems are very useful because of its highly coordinative nature, good solubility but also due to the ability to be functionalized with various substituents on

[26] W. Urbaniak, K. Jurek, K. Witt and A. Goracko, (2011). *CHEMIK*, **65**, 273-282.

[27] W. R. Cullen and E. B. Wickenheiser, (1989*). J. Organomet. Chem*., **370**, 141-148.

[28] G. K. Schweitzer and E. W. Benson, (1968), *J. Chem. Eng. Data*, **13**, 452-453.

[29] F. D. Lewis, A. M. Miller and D. G. Salvi, (1995). *Inorg. Chem*, **34**, 3173-3183.

[30] W. H. Hegazy, (2001). *Monatshefte für Chemie*, **132**, 639-650.

[31] Schematic of: *Keto-enol Tautomerism of a β-diketone*, adapted from: http://en.wikipedia.org/wiki/Beckmann_rearrangement: Last accessed 15/06/2015.

[32] M. Steyn, (2009). *Speciation And Interconversion Mechanism Of Mixed Halo And O,O'- And N,O-Bidentate Ligand Complexes Of Zirconium*, M.Sc. Dissertation, University of the Free State, South Africa.

the carbonyl carbons.[33] Ability to 'tweak' these substituents could be very useful for enhancing small differences in coordination between tantalum and niobium complexes for separation purposes.

Replacements of the methyl groups on the carbonyl carbons for these ligand systems are mainly achieved by organic groups. Basic examples of these functionalities include; phenyl, tertiary-butyl and trifluoromethyl moieties. Unsymmetrical ligands are also produced such as the substitution of a single methyl group with trifluoromethyl.[29] Figure 2.3 illustrates the functionalization of the acacH-backbone with various substituents. *β*-diketones with fluorinated functionalities form a significant part of the interest in this investigation and properties that govern ligand selection will be discussed in Section 2.3.1.3.

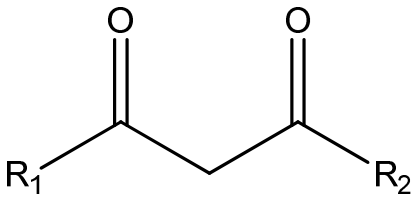

Figure 2.3 Graphical representation of the basic acetylacetone type ligand structure. *(R_1=R_2=**CH_3**, (2,4-pentanedione (acacH); R_1= R_2=**Ph**, (1,3-diphenyl-1,3-propanedione (dpaaH)); R_1= R_2= **tBu**, (2,2,7,7-tetramethyl-3,5-heptanedione (dtbaH)); R_1= R_2=**CF_3**, (1,1,1,5,5,5-hexafluoro-2,4-pentanedione (hfaaH)); R_1=**CF_3** & R_2=**CH_3**, (1,1,1-Trifluoro-2,4-pentanedione (tfaaH)))*.

2.3.1.2 *β*-diketonato Complexes of Tantalum(V) and Niobium(V)

Some examples of Ta(V)- and Nb(V)-*β*-diketonato complexes have been synthesized in the past. In a vast majority of the cases, these compounds were synthesized under an inert atmosphere and favoured a *mono*- chelated moiety.[34,35,36] The cause of the instability of these complexes in ambient conditions can be

[33] J. A. Viljoen, (2009). *Speciation and Interconversion Mechanism of Mixed Halo O,O'- and N,O-Bidentate Ligand Complexes of Hafnium*, M.Sc. Dissertation, University of the Free State, South Africa.

[34] H. O. Davies, T. J. Leedlam and A. C. Jones, (1999). *Polyhedron*, **18**. 3165-3172.

[35] P. Wendrup and V. G. Kessler, (2001). *J. Chem. Soc., Dalton Trans*, 574-579.

[36] E. L. Lippert and M. R. Truter, (1960). *J. Chem. Soc. A.*, **33**, 309-311.

ascribed to the hydrolysis of the halides on the metal synthon, e.g. $[NbCl_5]_2$ or $[TaCl_5]_2$.[37,38,39,40,41,42] Some exceptions are observed where *mono*- coordination of the bidentate ligand had taken place in hydrous conditions but this seems to be an exception, rather than the norm.[43,44]

Increasing the stability of the various metal(V)-*β*-diketonato complexes is crucial to improving the potential separation possibilities to an industrial level. Accordingly, more stable synthons need to be obtained. A paper by Kergoat *et al.* focuses on niobium synthon stabilization with a tetraethylammonium counterion. A graphic postulation of this formation compound of $[(C_2H_5)_4N][NbOCl_4(H_2O)]$ is illustrated in Figure 2.4.[45] This durable starting reagent has been proven to be more favourable for stable complexation with *β*-diketones than the 'regular' niobium pentachlorides and pentoxides. An additional advantage is that these complexes form rapidly, without any special manipulations, minimal solvent waste is evolved and forms in 85+ % yields.[45] This approach is much more cost effective, environmentally friendly and accordingly ideal to further a separation study.

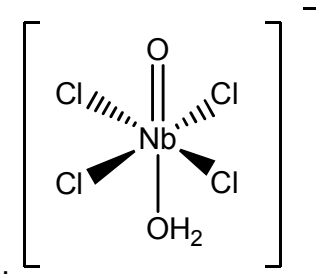

Figure 2.4 Postulation of the structure of the $[NbOCl_4(H_2O)]^-$ synthon by Kergoat *et al*.[45]

[37] G. J. Bullen, R. Mason and P. Pauling, (1965). *Inorg Chem.*, **4**, 456-461.

[38] F. Preuss, G. Lambing and S. Mueller-Becker, (1994). *Z. Anorg. Allg. Chem.,* **620**, 1812-1821.

[39] P. A. Williams, A. C. Jones, P. J. Wright and M. J. Crosbie, (2002). *Chem. Vap. Dep.*, **8**, 110-116.

[40] M. J. Crosbie, P. J. Wright, P. A. Lane, A. C. Jones and T. J. Leedham, (1999). *J. Phys. IV.*, **9**, 919-935.

[41] H. Funk, (1934). *Ber. Dtsch. Chem. Ges.*, **62**, 1801-1805.

[42] C. K. Gupta and A. K. Suri, (1993). *Extractive Metallurgy of Niobium*, CRC Press, Boca Raton, United States of America..

[43] L. Herbst, H. G. Visser, A. Roodt and C. Pretorius, (2012). *Acta Cryst.*, **E68**, m1392-1394

[44] L. Herbst, H. G. Visser and A. Roodt, (2013). *Z. Krist. NCS.*, **228**, 397-398.

[45] R. Kergoat and J. E. Guerchais, (1975). *J. Less Com. Met.*, **39**, 91-98.

2.3.1.3 Chemical and Physical Properties of Fluorinated M-*β*-Diketonato Complexes

Sievers *et al.* published some interesting results relating the volatility of a M-*β*-diketonato complex to the extent of fluorination on the ligand.[46] From this study it was concluded that the complexes containing highly fluorinated ligands are more volatile than their hydrogenated counterparts. Similar studies have also revealed that fluorine ligands not only reduce the intramolecular forces within the molecule but also that fluorine atoms in the periphery of complex decreases the van der Waals interaction and intermolecular hydrogen bonding.[47,48] Moreover it has been proven that the more ionic bonding with the larger resulting dipoles in the *β*-diketonato complex would render them more volatile.[48] The argument being that the bulky ligands form a hydrocarbon shell around the complex, which shields the polar groups from interactions with the neighbouring molecules.[49] Accordingly, investigation of the effect of fluorination and steric bulk on the Ta(V) and Nb(V) complexes could prove insightful with relation to finding differences in volatility to be exploited in vacuum sublimation separation.[50]

The advantages using these properties for a possible separation method are numerous and will be mentioned in Section 2.4. Ideally, the determination of a sublimation prediction model is of cardinal importance. If it is possible to envisage at which temperatures certain complexes sublime or the properties influence rate or temperature of sublimation one can gain great insight into these systems. With this enhanced knowledge base, the finding of idealized conditions for maximum separation of Ta(V)- and Nb(V)-complexes can be obtained. This solid state crystallographic study will greatly attribute to a better understanding of the intra- and inter molecular interactions of these complexes.

---

[46] R. E. Sievers and J. E. Sadlowski, (1978). *Science*, **201**, 217-241.

[47] M. L. Bhaumik, (1965a). *J. Inorg. Nucl. Chem.*, **27**, 243-252.

[48] M. L. Bhaumik, (1965b). *J. Inorg. Nucl. Chem.*, **27**, 261-267.

[49] T. J. Anderson, M. A. Newman and G. A. Melson, (1973). *Inorg. Chem.*, **12**, 927-936.

[50] A. Amano, A. Sato and S. Suzuki, (1979). *Radiochem. Radioanal. Lett.*, **39**, 441-448.

β-diketone ligands have also been introduced in past separation studies as an extracting agent.[51] Fluorination of the extracting agent increases its acidity by the electron-withdrawing effect of the fluorinated group. Accordingly the agent can be used to extract metal ions from more acidic aqueous solutions.[51] This property is of prime importance for the extraction of metal ions that are easily hydrolyzed e.g. Nb(V) and Ta(V).

A study by Umetani *et al.* on rare earth *β*-diketonato compounds used a solution state examination combined with a crystallographic investigation to evaluate this hypothesis on rare earth elements.[52] The authors found that the rare earth elements were indeed extracted at lower pH values. However the separation was also influenced by the bite angle of the ligand. It was concluded that the separation of the rare-earth ions is improved by shorter O···O bite distances in the metal complexes (i.e. a smaller bite angle). This angle can be manipulated and the O···O distance controlled by the introduction of bulky substituents at suitable positions to create a steric effect and improve the extent of separation.

2.3.1.4 A Brief Summary of Some Aspects of Tropolones

The tropolone anion ligand is ideally suited to the formation of structures with high coordination numbers. This is ascribed to the planarity and compactness of the ligand and the rigidity of the functionality.[53,54] Due to the special nature of the seven-membered ring, it demonstrates similar aromaticity to that found in a benzene ring.[55] Tropolone has different resonance structures and similar characteristics to polyenes and polyenones.[56] A representation of the general structure of the molecule is illustrated in Figure 2.5.

[51] J. C. Reid and M. Calvin, (1950). *J. Am. Chem. Soc.*, **72**, 2048-2065.

[52] S. Umetani, Y. Kawase and M. Matsui, (2000). *J. Chem. Soc. Dalton Trans.*, **33**, 2787-2799.

[53] E. L. Muetteries and C. M. Wright, (1965). *J. Am. Chem. Soc.*, **87**, 4706-4717.

[54] E. L. Muetteries and C. M. Wright, (1964). *J. Am. Chem. Soc.*, **86**, 5132-5141.

[55] T. N. Hill, M. S. Manguela and G. Steyl, (2012). *Acta Cryst.,* **E68**, o941-944

[56] G. Steyl and A. Roodt, (2006). *S. Afr. J. Chem.*, **59**, 21–27.

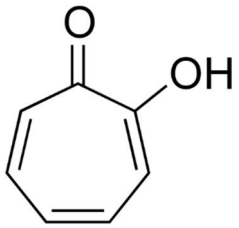

Figure 2.5 General structure of tropolone (tropH).

2.3.1.5 Tropolonato Complexes of Tantalum(V) and Niobium(V)

According to Muetteries *et al*., niobium(V) and tantalum(V) pentachlorides react with acidic aqueous solutions of tropolone to form the tetrakistropolonato cations $[Nb(Trop)_4]^+$ and $[Ta(Trop)_4]^+$, with near quantitative yields.[53] The hydrolytic stabilities of the Ta(V) and Nb(V) analogues differ significantly. In strongly acidic media both $[Nb(Trop)_4]^+$ and $[Ta(Trop)_4]^+$ species were found to be stable. With increasing temperature or pH, the niobium chelate undergoes partial hydrolysis to $[NbO(Trop)_3]$ which separates from solution. As the solution becomes basic, the niobium cation is rapidly and completely hydrolysed. In contrast the tantalum cation is resistant to hydrolysis provided the pH is not appreciably above 7.[53,54]

Due to the dissimilarities in chemical nature between the tantalum and niobium analogues in solution some research into this phenomenon will be attempted. As is the case with *β*-diketones, tropolones can also be functionalized and tailored to requirements.[55,56] These additions could further enhance the differences by influencing hydrolytic stabilities. By capitalizing on the difference in charge around the metal centre, a negatively charged ion resin can be used to extract the cationic Ta complex while the neutral Nb complex precipitates out of solution. If both of the compounds precipitate out of solution simultaneously other techniques, e.g. sublimation purification, could in principle be used to separate the complexes at differing temperatures, under reduced pressure. It would also be advantageous to investigate the solid state structures of these compounds to ascertain which factors govern the extent of ligand coordination as well as the intermolecular interactions that influence complex stability and volatility. The theory of sublimation purification/separation and the advantages thereof will be discussed in Section 2.4.

The solution state investigation of Muetteries *et al.* was very thorough but minimal attention was given to the solid-state coordination geometries of the *tris*-bidentate seven-coordinate ([$M(Bid)_3(X)$]), [$NbO(Trop)_3$] and the *tetrakis*-bidentate eight-coordinate ([$M(Bid)_4$]), $[Nb(Trop)_4]^+$ and $[Ta(Trop)_4]^+$ cationic, solid state compounds. No crystal structures were reported in their investigation as they were not focussing on a separation method but rather enhancement of chemical knowledge. Accordingly, a crystallographic investigation of the coordination modes and intermolecular interactions could shed even more light on this nuance between Ta(V) and Nb(V) behaviour.

2.3.2 Seven-Coordinate [$M(Bid)_3(X)$] Complexes

The total number of points of attachment to the central element is termed the coordination number and can vary from two to as many as sixteen. [$M(Bid)_3(X)$] complexes like [$NbO(Trop)_3$] discussed in the previous section, a seven-coordinate geometry is expected. This coordination mode is a well-defined molecular entity, although not frequently observed in literature.[57] An idealized representation of this seven-coordinate structure can be obtained by adding an additional vertex (ligand) to a regular octahedron. This addition can be achieved in one of three ways as illustrated in Figure 2.6. Addition of an extra ligand along an octahedral edge causes a relatively minor rearrangement of the four vertices co-planar to the new vertex. This arrangement is described as pentagonal bipyramidal geometry (D_5h). Alternatively, a facial addition may generate either a capped octahedron (C_3v) or a capped trigonal prism (C_2). There are various examples of each coordination mode found in published structures for a wide variety of metal centres, but in the case of Nb(V) and Ta(V) the data is very limited. For this reason, a crystallographic investigation of these compounds will provide additional insight of the coordination preferences and modes.

[57] R. Hoffmann, B. F. Beier, E. L. Muetteries and A. R. Rossi, (1977). *Inorg. Chem.*, **3**, 511-522.

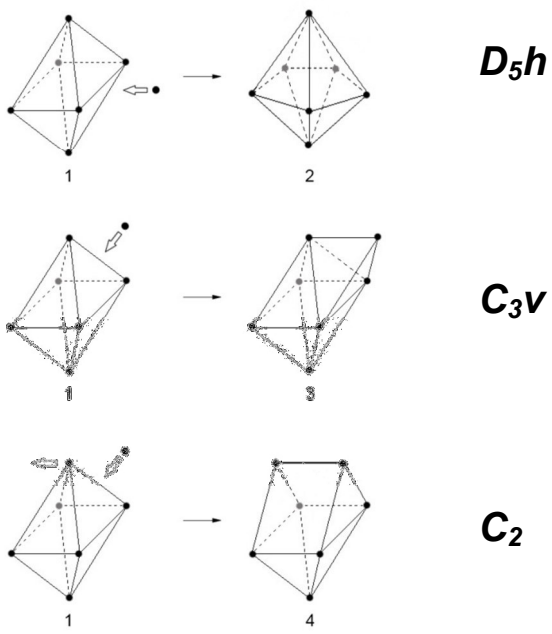

Figure 2.6 Illustration of vertex addition to the regular octahedral geometry to afford the various seven-coordinated isomers.[57]

2.3.2.1 C_2-Capped Trigonal Prism

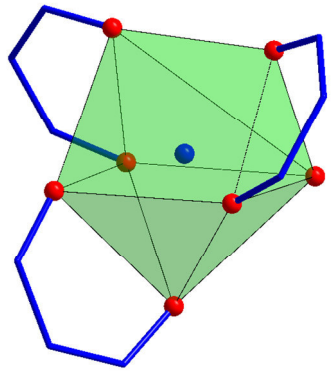

Figure 2.7 Illustration of the C_2-capped trigonal prism geometry.

C_2-capped trigonal prismatic (CTP) structures as illustrated in a general representation in Figure 2.7 are often encountered in seven coordinate systems. This geometry has been described for a wide range of metal centres for both neutral and ionic compounds. An example of this, is the aqua-*tris*(*tert*-

butylacetylacetonato)dysporium(V) cation is noted in Figure 2.8.[58] Interestingly, this geometry has not been encountered for any tantalum and niobium metal centres.

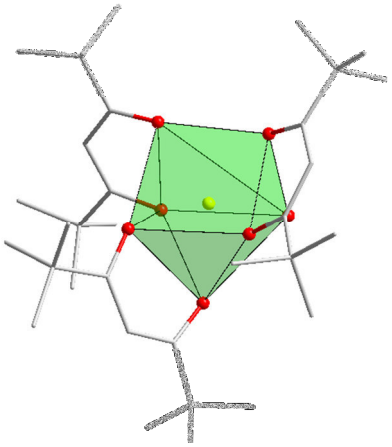

Figure 2.8 Illustration of the C_2-capped trigonal prismatic geometry of aqua-*tris*(*tert*-butylacetylacetonato)dysporium(V) cation.

2.3.2.2 C_3v-Capped Octahedral Geometry

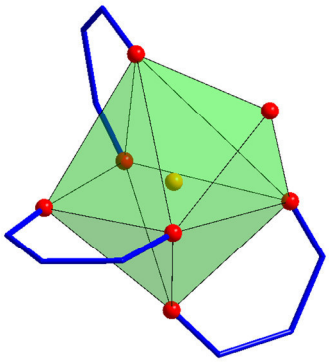

Figure 2.9 Illustration of the C_3v-capped octahedral isomer.

The C_3v-capped octahedral (CO) geometry is the second most common of the seven-coordinate geometries encountered and is illustrated in a general representation in Figure 2.9. Many examples of this geometry are encountered for larger metal centres (lanthanides and actinides). An example is the aqua-

[58] C. S. Erasmus and J. C. A. Boeyens, (1971). *J. Cryst. Mol. Struct.*, **1**, 83-87.

tris(dibenzoylacetylacetonato)holmium(III) cation is noted in Figure 2.10.[59] Once again no Nb(V) or Ta(V) structures with this coordination mode was found in literature; however a single Ta(IV) structure of fluorido-*tris*(oxalato)tantalum(IV), has been characterized. A depiction of this compound is given in Figure 2.11.[60]

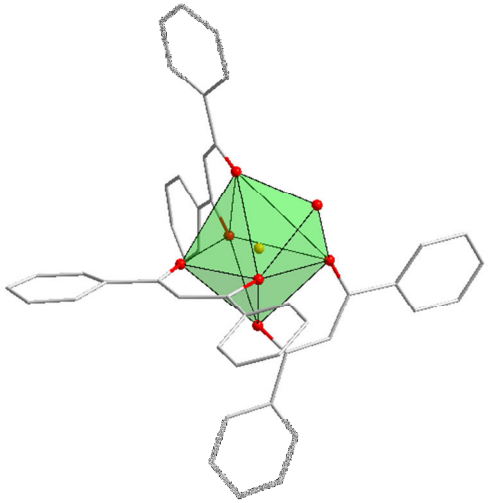

Figure 2.10 Illustration of the C_3v-capped octahedral geometry in the aqua-*tris*(dibenzoylacetylacetonato)holmium(III) cation.

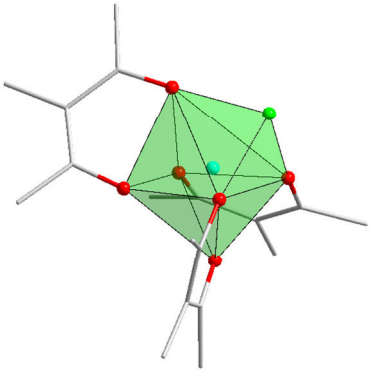

Figure 2.11 Illustration of the C_3v-capped octahedral geometry in fluorido-*tris*(oxalato)tantalum(IV).

[59] A. Zalkin, D. H. Templeton and D. G. Karraker, (1969). *Inorg Chem.*, **8**, 2680-2689.

[60] F. Marchetti, G. Pampaloni and G .Zacchini, (2007). *Dalton Trans.*, **38**, 4343-4351.

2.3.2.3 D_5h-Pentagonal Bipyramidal Geometry

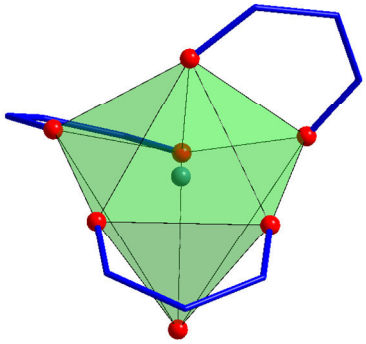

Figure 2.12 Illustration of the D_5h-pentagonal bipyramidal geometry.

D_5h-pentagonal bipyramidal (PB) geometry is not completely uncommon for $[M(Bid)_3(X)]$ isomers but is not found as frequently as the CTP or CO conformations. A general representation of PB geometry is noted in Figure 2.12. A supreme example of this coordination mode is encountered for fluorido-*tris*(tropolonato)tin(IV) (Figure 2.13).[61] The only example of this *tris*-bidentate ligand coordination related to either tantalum(V) or niobium(V) is the structure of oxido-*tris*(oxalato)niobium(V) (Figure 2.14).[62]

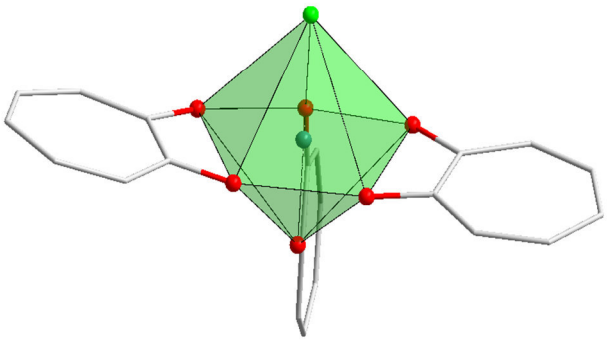

Figure 2.13 Illustration of the D_5h-pentagonal bipyramidal of fluorido-*tris*(tropolonato)tin(IV).

[61] J. J. Park, D. M. Collins and J. L. Hoard, (1970). *J. Am. Chem Soc.*, **92**, 3636-3645.

[62] G. Mathern and R. Weiss, (1971). *Acta Cryst.*, **B27**, 1610-1618.

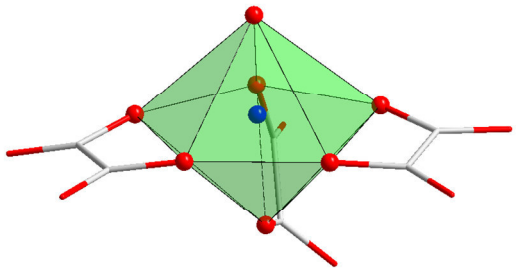

Figure 2.14 Illustration of the D_{5h}-pentagonal bipyramidal geometry in oxido-*tris*(oxalato)niobium(V).

From this preliminary investigation a noticeable shortage of $[M(Bid)_3X]$ isomers of Ta(V) and Nb(V) was found. Additional insight into preferred solid-state binding modes and the factors that govern these aspects in tantalum and niobium compounds will be advantageous to this separation study.

2.3.3 Eight-Coordinate ((M-Bidentate)$_4$) Metal-Bidentate Complexes

There are various examples of eight-coordination of *O,O'*-bidentate ligands found in literature of early transition metals, lanthanides and actinides. In many of these cases the *tetrakis*-bidentate ligand coordination mode is regularly cited.[63,64,65] From these publications it was concluded that certain metal centres prefer a certain maximum coordination (eight) by bidentate ligands. This phenomenon has been ascribed to the fact that this coordination mode most likely has the lowest, most stable crystallization state.[66] *Tetrakis*-coordination is also well known to favour a square anti-prismatic (SAP) polyhedron or geometry as was observed for $[Hf(acac)_4]$ and is illustrated in Figure 2.15. [67,68,69]

---

[63] J. K. Burdett, R. Hoffmann and R. C. Fay, (1978). *Inorg. Chem.*, **17**, 2553-2569.

[64] S. P. Sovilj, G. Vuckovic, V. M. Leovac and D. M. Minic, (2000). *Polish J. Chem.*, **74**, 945-954.

[65] V. S. Tyurin, Y. P. Yashchuk and I. P. Beletskaya, (2008). *Russ. J. Org. Chem.*, **44**, 1378-1383.

[66] J. E. Huheey, E. A. Keiter and R. L. Keiter, (1993). *Inorganic Chemistry – Principles of Structure and Reactivity*, **4**, Harper Collins College Publishers, New York, United States of America.

[67] J. V. Silverton and J. L. Hoard, (1963). *Inorg. Chem.*, **2**, 243-249.

[68] J. L. Hoard and J. V. Silverton, (1963). *Inorg. Chem.*, **2**, 235-242.

[69] N. B. Morazova, K. V. Zherikova, I. A. Badina and N. V. Glenfold, (2005). *Monogr. Ser. Int. Cont. Conf. Coord. Chem.*, **7**, 246-252.

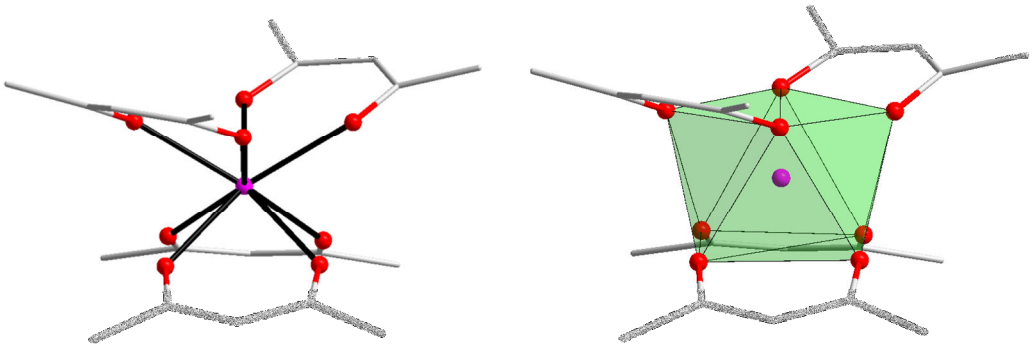

Figure 2.15 Illustration of SAP geometry for *tetrakis*(acetylacetonato)hafnium(IV).

It is quite obvious from Figure 2.15 that there is not only one isomer possible for this SAP coordination geometry. Hoard *et al.* noted that three isomers are possible for the square anti-prismatic geometry, specifically for metal complexes with *tetrakis-O,O'*-bidentate ligands. In the case of ideal SAP geometry the polyhedron is defined as the D_{4d}-*82m* antiprism with all vertices equivalent as illustrated in Figure 2.16. However this obviously does not hold for $[Ta(acac)_4]$ complex, and is clearly dependant on, amongst others, the metal centre size and the ligand bite angles.

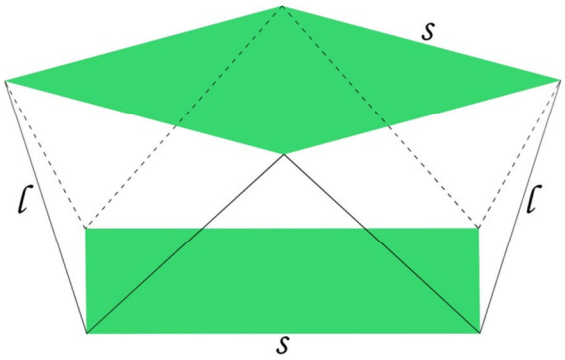

Figure 2.16 Illustration of general SAP geometry as defined by Hoard *et al.*[68]

(s = 1st defined coordination face/edge, l = 2nd defined coordination face/edge).

From Figure 2.16 it is noticed that the 16 (8x2) structural edges of the polyhedron is equally divided between two symmetry types (*s* and *l*, as defined by Hoard *et al.*), with the central metal atom being the intersection point of the 4 two-fold axes.[68] These two-fold axes pass through the mid-point of two opposite *l* polyhedron edges.

Because of this conformation, three possible isomers for *tetrakis-O,O'*-bidentate ligand complexes can be obtained and are discussed in the following sections;

2.3.3.1 D_2-Square Antiprismatic Geometry (D_2-222/ssss)

This specific type of coordination geometry often encountered in the $[M(Bid)_4]$ types of compounds. A general illustration of this isomer is illustrated in Figure 2.17. D_2-222 geometry for a *tetrakis*-coordinated complex is very easily identified and characterized by the fact that all four ligands are coordinated to the vertices of the *s*-symmetry edges of the square antiprism.

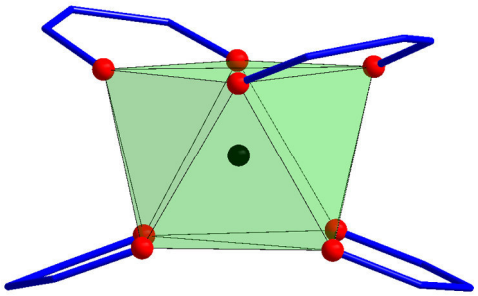

Figure 2.17 Illustration of the *s*-edge coordinated D_2-square antiprismatic geometry.

Various cases of these D_2-*s*-edge bonded structures are found in literature for a wide range of metal centres for both neutral and cationic compounds. Examples include *tetrakis*(tropolonato)hafnium(IV), *tetrakis*(trifluoronaphtylacetylacetonato)europium(V) cation and *tetrakis*(acetylacetonato)zirconium(IV) which are illustrated in Figure 2.18.[70,71,72] A substantial decrease in the number of *tetrakis*-coordinated *O,O'*-structures for tantalum and niobium metal centres with this coordination mode was observed. All of the structures display a slightly distorted D_2-geometry. Examples of

[70] D. Tranqui, A. Tissier, J. Laugier and P. Boyer, (1977). *Acta Cryst.*, **B33**, 392-394.

[71] S. M. Bruno, R. A. S. Ferreira and F. A. A. Paz, (2009). *Inorg. Chem.*, **48**, 4882-4891.

[72] B. Allard, (1976). *J. Inorg. Nucl. Chem.*, **38**, 2109-2116.

tetrakis(oxalato)niobium(IV) and *tetrakis*(oxalato)tantalum(IV) are illustrated in Figure 2.19.[73,74]

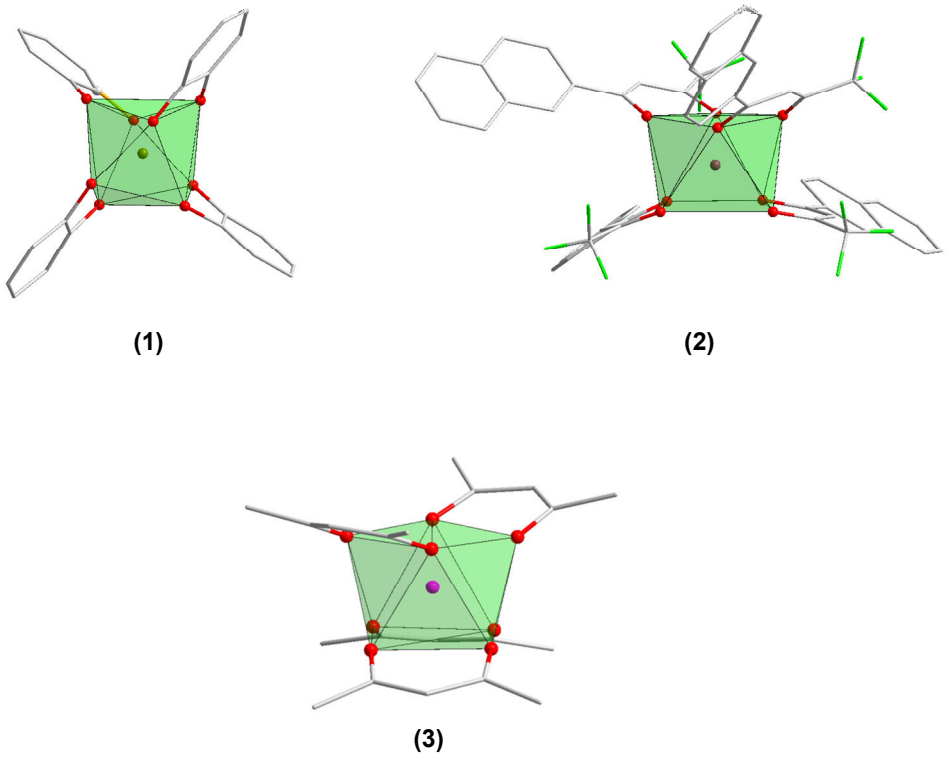

(1) **(2)**

(3)

Figure 2.18 Various examples of D_2-coordinated square antiprismatic compounds of several metal centres.(**(1)** *tetrakis*(tropolonato)hafnium(IV), (**2**) *tetrakis*(trifluoronaphtylacetylacetonato)europium(V) cation, **(3)** *tetrakis*(acetylacetonato)zirconium(IV)).

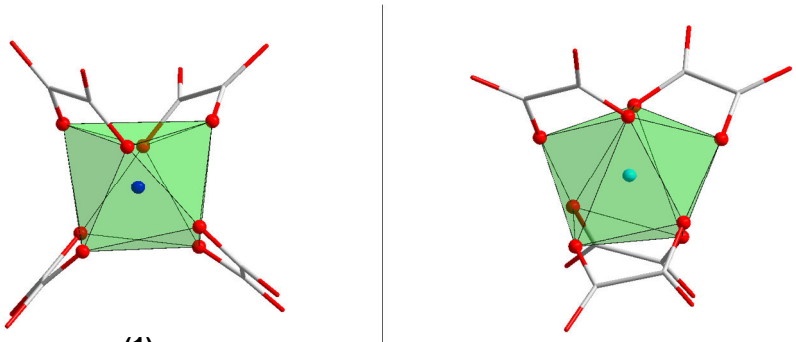

(1) **(2)**

Figure 2.19 Various examples of D_2-coordinated square antiprismatic compounds to Ta(IV) and Nb(IV) metal centres.(**(1)** *tetrakis*(oxalato)niobium(IV), **(2)** *tetrakis*(oxalato)tantalum(IV)).

[73] B. Ooi, T. Shihabara and G. Sakane, (1997). *Inorg. Chim. Acta*, **266**, 103-114.

[74] F. A. Cotton, M. P. Diebold and W. J. Roth, (1987). *Inorg. Chem.*, **26**, 2889-2901.

2.3.3.2 D_4-Square Antiprismatic Geometry (D_4-422/IIII)

This specific type of coordination geometry is hardly ever encountered in the $[M(Bid)_3(X)]$ type of compounds. D_4-422 geometry for *tetrakis*-structures are very easily identified and characterized by the fact that all four bidentate ligands are coordinated to the vertices of the *I*-symmetry edges of the square antiprism (see Figure 2.16). A general illustration of this geometry is illustrated in Figure 2.20. This scarcity could most likely be ascribed to the excessive strain of the ligand structures to accommodate the larger bite-angles required to attain this geometry. Interestingly, in the case of niobium metal centres *tetrakis*-compounds with D_4-geometry are not uncommon. Examples of these arrangements include the *tetrakis*(*tert*-butylacetylacetonato)niobium(V) cation and *tetrakis*(hexafluoroacetylacetonato) tantalum(V) and are illustrated in Figure 2.21.[75]

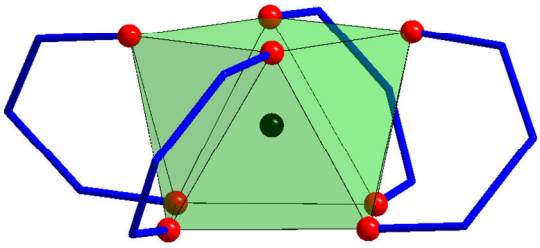

Figure 2.20 Illustration of the corner-bonded D_4-square antiprismatic geometry.

[75] T. J. Pannavaia, B. L. Barnett and G. Podolsky, (1975). *J. Am. Chem. Soc.*, **97**, 2712-2730.

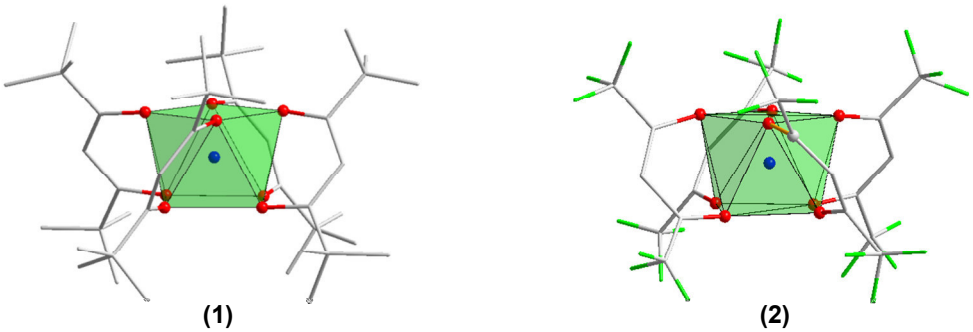

(1) **(2)**

Figure 2.21 Various examples of D_4-coordinated square antiprismatic compounds Nb(V) metal centres. (**(1)** *tetrakis*(*tert*-butylacetylacetonato)niobium(V) cation**, (2)** *tetrakis*(hexafluoro acetylacetonato)niobium(V) cation)

2.3.3.3 C_2-Square Antiprismatic Geometry (C_2-2/lss)

This specific type of coordination geometry is commonly encountered in these types of compounds. C_2-2 geometry for *tetrakis*-structures are very easily identified and characterized by the fact that two of the bidentate ligands are coordinated to the vertices of the *l*-symmetry edges and the remaining two ligands are coordinated to the vertices of the *s*-symmetry edges of the square antiprism. A general illustration of this isomer is illustrated in Figure 2.22. Various cases of these C_2-combined D_2/D_4 corner bonded structures are found in literature for a wide range of metal centres for both neutral and cationic compounds. Examples include the *tetrakis*(trifluorofurylacetylacetonato)europium(V) cation and *tetrakis*(hexa fluoroacetyl acetonato)zirconium(IV) which are depicted in Figure 2.23.[76,77] C_2-square antiprismatic has never been found in any *tetrakis-O,O'*-coordinated niobium complex and only one example, the *tetrakis*(*tert*-butylacetylacetonato)tantalum(V) cation.[78] This structure is illustrated in Figure 2.24.

[76] F. Wang, Z. Hu and J. Wu, (2011). *Chin. J. Synth. Chem.*, **19**, 328-341.

[77] U. K. Urs, M. S. Dharmaprakash and T. N. G. Row, (2003). *Acta Cryst.* **E59**, m83-m84.

[78] H. O. Davies, A. C. Jones and M. Motevalli, (1999). *Inorg. Chem. Commun.*, **8**, 585-597.

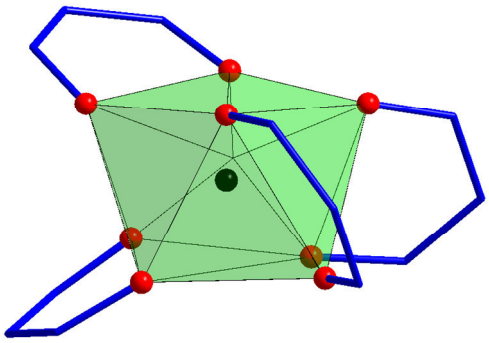

Figure 2.22 Illustration of the corner-bonded C_2-square antiprismatic geometry.

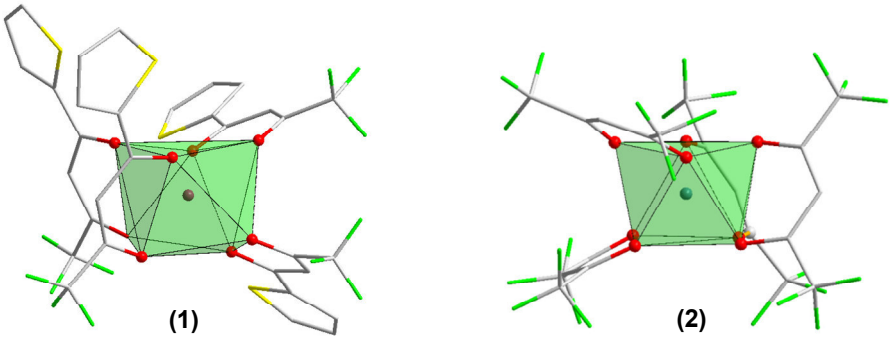

Figure 2.23 Various examples of C_2-coordinated square antiprismatic compounds of different metal centres. (**(1)** *tetrakis*(thenoyltrifluoroacetylacetonato)europium(V) cation, **(2)** *tetrakis*(hexafluoro acetylacetonato)zirconium(IV))

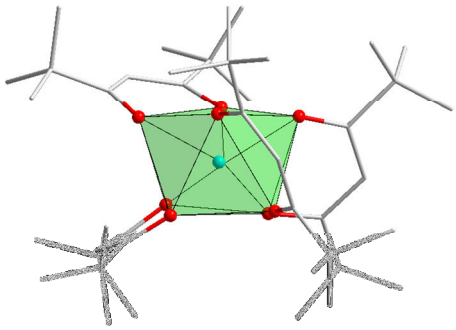

Figure 2.24 Illustration of C_2-coordination of the *tetrakis*(*tert*-butylacetylacetonato)tantalum(V) cation.

2.3.3.4 Other Eight Coordinate Geometries

Owing to steric and electronic effects of the ligands, the square antiprismatic (SAP) geometry may distort to the bicapped trigonal prism (BTP) geometry as illustrated in Figure 2.25. According to Burdett *et al.* BTP has three different ligand sites; a basal site (b), a capping site (c) and a site that lies in the vertical mirror plane (m) (Figure 2.25).[79] Additional distortion will lead to dodecahedral (DD) geometry; accordingly BTP is seen as a way point between SAP and DD structures. In a paper by Muetteries *et al.* it was noted that the idealized eight coordinate geometries can be divided into two groups; a low energy set of structures (SAP, BTP and DD) and a higher energy set (bicapped trigonal antiprismatic, cubic, hexagonal bipyrimidal and square prismatic).[80] These high energy conformations are not regularly observed with SAP and DD geometries being most common for these types of eight-coordinate $[M(Bid)_4]$ structures.

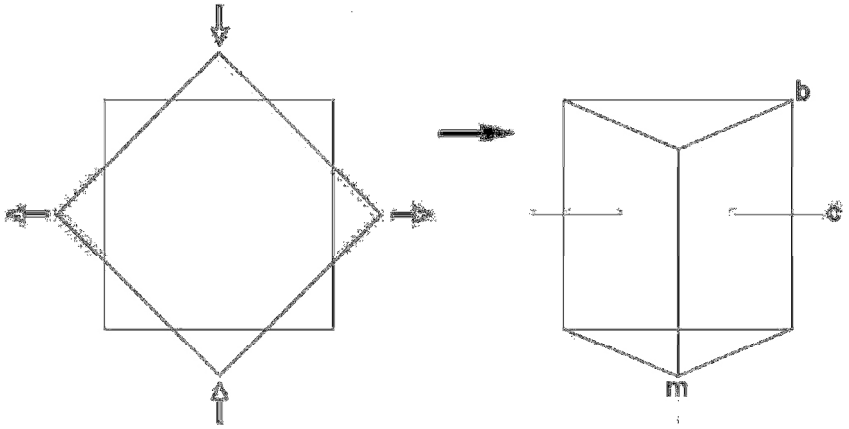

Figure 2.25 Illustration of the distortion required to obtain a bicapped trigonal prismatic geometry and the three different coordination sites according to Burdett *et al.*[79]

As has been noted throughout this section, many examples of the *tetrakis*-coordination of bidentate ligands of complexes with the various isomers of distorted SAP geometry exist in literature. Numerous investigations for a wide range of metal centres and analogous *N,O'*-bidentate ligands have been undertaken but no specific focus was placed on Ta(V) and Nb(V) metal centres. Examples of tantalum and

[79] J. K. Burdett, R. Hoffmann and R. C. Fay, (1978). *Inorg Chem.*, **17**, 2553-2568.

[80] E. L. Muetteries and C. M. Wright, (1967). *Q. Rev., Chem. Soc.,* **21**, 109-121.

niobium complexes have also been noted but definition of a preferential coordination mode of these metal centres does remain elusive. The overarching aim here is to identify certain ligands which may induce *tetrakis*-coordination that can manipulate solid state structural properties in such a way to induce different physical or chemical behaviours for Ta(V) and Nb(V). During the course of this project, a crystallographic solid state structural characterisation study will shed some light on this topic.

2.4 Sublimation Purification and Separation

Sublimation is the process of phase transition of a substance directly from the solid to the gaseous state.[81] This is an endothermic phase transition and occurs below the triple point on the phase diagram of a substance as is illustrated in Figure 2.6.[82]

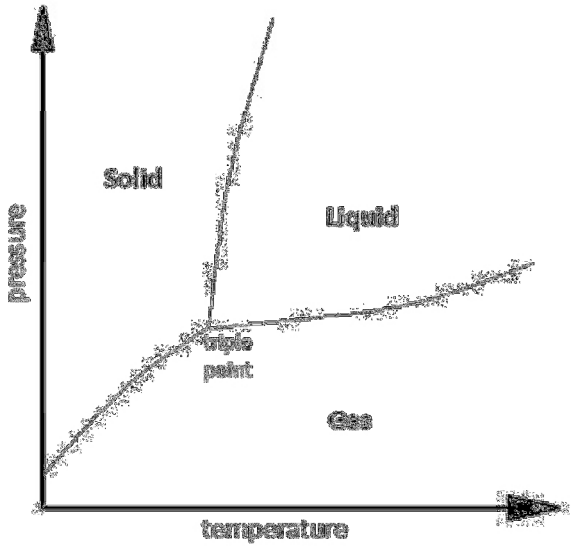

Figure 2.26 General example of a phase diagram of a substance.[83]

[81] A. Gavezzotti, (1997). *Theoretical Aspects and Computer Modeling of the Molecular Solid State*, Wiley and Sons, United Kingdom.

[82] R. B. King, (1965). *Organometallic Syntheses.* **1**, Academic Press, New York, United States of America.

[83] Picture adapted from: https://physichemist.files.wordpress.com/2012/01/phase_diag.png: Last accessed, 12/07/2015.

2.4.1 Sublimation Purification

Vacuum sublimation purification is a well-known technique used by chemists, which involves placing a solid in a sublimation apparatus and then heating under vacuum. Because of the higher temperature and reduced pressure, the solid passes its triple point and volatilizes directly into the gas phase. This gaseous product is then condensed onto a cooled surface (cold-finger) as a purified compound, while the non-volatile residue of impurities is left behind. The purified complex may then be collected from the cooling surface.[84] This setup is illustrated in Figure 2.27. Temperature gradients can also be used to further enhance efficiency of purification. Vacuum sublimation has been a method of choice of purification of compounds for use in the organic electronics industry where very high purities (> 99.9 %) of compounds are required.[85]

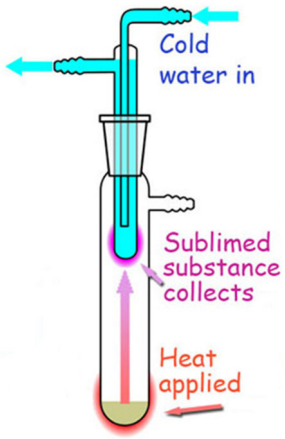

Figure 2.27 General setup for sublimation purification

2.4.2 Sublimation Separation of Mixtures

Vacuum sublimation can also be used to separate a mixture of solids. For example, if one of the solids sublimes while the others remain in the solid phase or melts, or if

[84] L. M. Harwood and C. J. Moody, (1989). *Experimental Organic Chemistry: Principles and Practice,* Wiley Blackwell, United Kingdom.

[85] J. Girard, (2011). *Criminalistics: Forensic Science, Crime and Terrorism,* Jones & Bartlett Learning, United Kingdom.

the substances have different sublimation temperatures, the complexes can be purified by fractional sublimation.[85] This is also applicable to the study at hand. An example of this is mentioned in Paragraph 2.1.3.4, where vacuum sublimation is identified as a possible separation method of Ta(V)- and Nb(V)-tropolonates if both complexes precipitate from solution simultaneously. Therefore, there is indeed some scope to further study in this field.

This technique has the ideal characteristics for a separation method that can be up scaled for industrial application as a separation method of solid state mixtures of Ta(V) and Nb(V) complexes. Some of these aspects which render sublimation as a more 'green' process are listed below.

- Owing to the fact that the separation is done at a lower pressure, the temperature that is required to volatilize the Ta(V) and Nb(V) complexes is much lower than what is currently seen as the industrial norm.
- The use of strong and corrosive acids is avoided which is advantageous because less hazardous waste is evolved.
- Less solvent waste is created because no solvent is required during the process.
- The technique is not as laborious or time consuming as the current methods. This is very cost efficient and profitable for the company.
- It is much less energy intensive than solvent extraction at elevated temperatures.
- And finally, it is a very inexpensive setup, not requiring specialized equipment and accordingly it is also much easier to maintain.

The advantages of the vacuum sublimation separation are numerous and must be investigated with relation to Ta(V)- and Nb(V)-bidentate complexes. Ideally, the aim of the construction of a sublimation prediction model is of cardinal importance and the 'magic bullet'. If it is possible to envisage at which temperatures certain complexes sublime or the properties influence rate or temperature of sublimation one should gain significant insight into these systems. With this enhanced knowledge base, the finding of idealized conditions for maximum separation of Ta(V)- and

Nb(V)-complexes should become more predictable. This solid state study combined with a solution state mechanistic investigation will significantly contribute to a better understanding of the intrinsic nature of the chemical and physical properties of these systems.

2.5 Solution-State Mechanistic Studies of Metal Ligand Coordination

Chemical or reaction kinetics comprises the study of the rates at which chemical reactions take place and involves the precise measurement of the variation of concentrations of the reacting species *vs*. time.[86] These measurements are conducted in such a way that the influence of a specific aspect, e.g. temperature, reaction time, pressure variation or reacting species' concentration may be studied for a reaction system.

2.5.1 Mechanistic Studies of Ligand Coordination to Tantalum(V) and Niobium(V) Centres

Research associated with the kinetic and associated mechanistic studies on tantalum(V) and niobium(V) complexes is very limited.[25] Most studies reported focussed specifically on the formation of coordination compounds with the aim to determine catalytic properties or catalytic conversion mechanisms.[87,88,89,90,91] Other solution state kinetic investigations e.g. bidentate ligand coordination to the metal centres have proven to be very scarce and results insufficient. In an attempt to rectify this, some related M.Sc. projects have previously been concluded.[92] The main aims

[86] K. J. Laidler, (1987). *Chem. Kinet.*, **3**, 33-39.

[87] B. J. Burger, B. D. Santarsiero, M. S. Trimmer and J. E. Bercaw, (1988). *J. Am. Chem. Soc.*, **110**, 3134-3146.

[88] P. J. Dyson, (2003). *Dalton Trans.*, **66**, 2964-2974.

[89] A. L. Reznichenko and K. C. Hultzsch, (2012). *J. Am. Chem. Soc.*, **134**, 3300-3311.

[90] K. A. Zemski, D. R. Justes, R. C. Bell and A. W. Castleman, (2001). *J. Phys. Chem. A.*, **105**, 4410-4417.

[91] F. Marchetti and G. Pampaloni, (2012). *Chem. Comm.*, **48**, 635-653.

of these studies were to investigate the solution behaviour of the formation of Nb(V)- and Ta(V)-acetylacetonato and related complexes under *pseudo* first-order conditions.[25,92]

2.5.1.1 Previous Mechanistic Studies

Analysis of the absorbance change vs. time data for the formation of *trans*-$[TaCl_2(OMe)_2$(acetylacetonato-κ^2-O,O')] and $[NbCl(OMe)_3$(acetylacetonato-κ^2-O,O')] complexes clearly indicated a similar, two-step reaction process in both cases. The mechanisms, as illustrated in Figures 2.8 and 2.9, describe an intricate and complex method of bidentate ligand coordination.[92] According to these schemes, the reactions involve a fast initial step where acetylacetone (acacH) substitutes a labile solvated MeOH group to form a mono-coordinated Ta(V)- or Nb(V)-species. In the second step, the intermediate undergoes a ring closure in a slower rate determining step, yielding the final product.

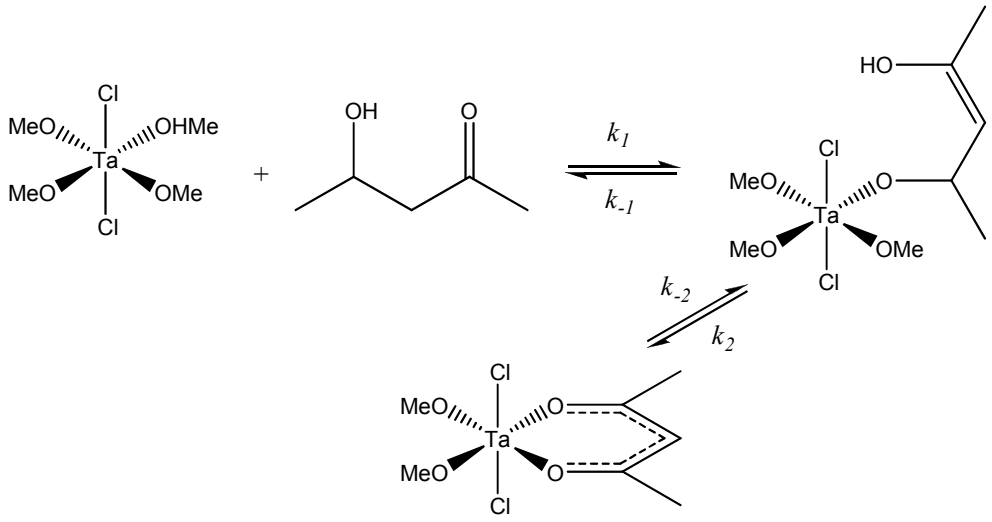

Figure 2.28 The proposed reaction scheme for the formation of $[TaCl_2(OMe)_2(acac)]$.

[92] R. Koen, (2012). *High Oxidation State Tantalum Coordination Chemistry: A Solution and Solid State Investigation,* M.Sc. Dissertation, University of the Free State, South Africa.

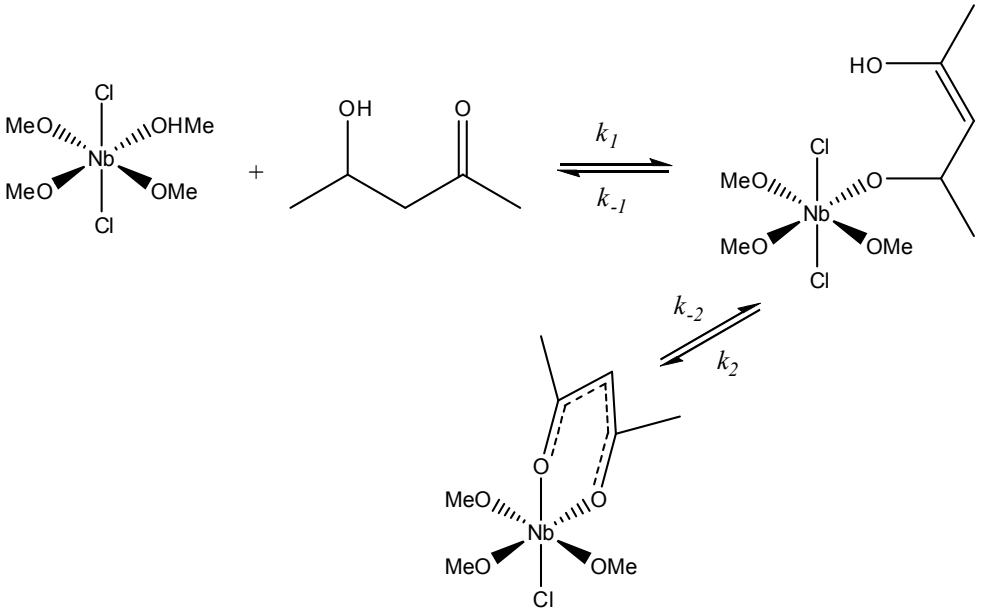

Figure 2.29 The proposed reaction scheme for the formation of $[NbCl(OMe)_3(acac)]$.[92]

When comparing the reaction rate constants (k_1, k_{-1}, k_2 and K_1) for both processes, it was found that these were of similar order, with k_{-2} being more prominent in Nb(V). In this case it was deemed that within experimental error, the tantalum(V) addition reaction does not show a conclusive k_{-2} step. Another prominent difference in coordination between the metal centres was noted during the ring-closure step. It was confirmed that in the case of Nb(V) a chloride group is liberated rather than a methoxy group as in the case of the Ta(V) complex. This was ascribed to the fact that Ta(V) is a much stronger Lewis acid. A graphical illustration of the products obtained from these two processes is shown in Figure 2.30.

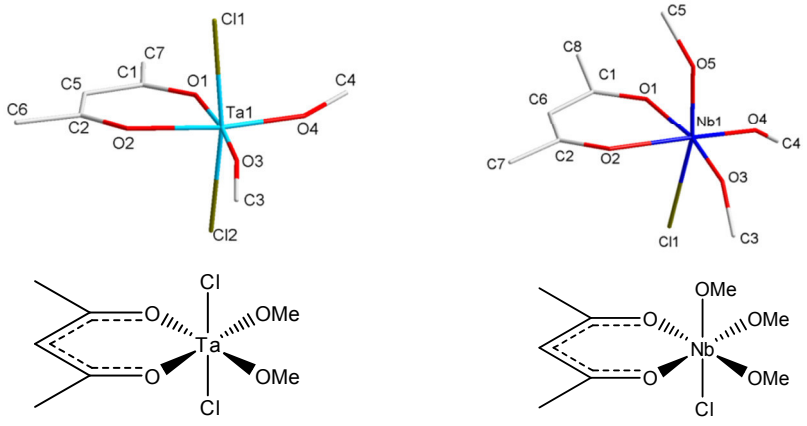

Figure 2.30 Illustration of different coordination modes of Ta(V) and Nb(V) obtained as facial products as a result of difference of Lewis acidity.

This difference in Lewis acidity between the metal centres can in principle be manipulated to provide an opportunity of a more effective separation method by using liquid-liquid extraction. In theory, the Nb(V) complex will extract into an organic phase at a lower acidity of the aqueous solution, whereas the Ta(V) complex is expected to require a higher level of acidity to be extracted.

Interestingly, knowledge that was acquired as a result from these kinetic studies combined with X-Ray diffraction data has yielded important insights into possible solvent extraction purification of niobium and tantalum. These examples underline the need to undertake detailed kinetic evaluations of these systems. Not only to solve the time-resolved behaviour of Ta(V)- and Nb(V)-bidentate ligand coordination but also to broaden the knowledge base of the effect of internal and external influences on these systems in solution.

2.6 Conclusion

The development of potentially improved industrial processes for separation for Nb(V) and Ta(V) from their mineral ores require clear definition of the investigative aims. Focus of a study which is targeted at applying ligand chelation characteristics for separation procedures would necessarily have to start with synthesizing novel compounds that are to be studied. However, it is of outmost importance for the development of such complexes, that adequate information exists regarding the basic principles of all contributing features in these coordination reactions.

All chemical processes involving metal complexes are largely governed by the coordinated ligands. Therefore it is of utmost importance that all properties (steric, electronic, etc.) of the ligands be clearly understood to enable an educated adjustment to the system to induce the desired effects. In addition, the time-resolved kinetic aspects combined with the general and stoichiometric mechanistic principles of these systems should constantly be incorporated into the argument.

Successful execution of this research endeavour necessitates full characterization of all Ta(V) and Nb(V) complexes obtained. This does not only include a full solid-state

structural analysis by crystallographic methods but also a solution behavioural quantification of product formation by means of kinetic rate evaluations via UV/Vis absorbance and NMR spectroscopies.

When all of these aspects are considered, it becomes quite obvious that this project constitutes a significant challenge of investigation of the effects of ligand coordination on the solution- and solid-state behaviour of tantalum(V) and niobium(V) complexes.

Chapter 3:
Synthesis of Various Nb(V)- and Ta(V) Compounds

The synthesis of tantalum(V) and niobium(V) complexes form a fundamental part of this project, focusing on the study of solid state characterization of these types of compounds. Furthermore, without specific synthetic aims as far as the intended Ta(V) and Nb(V) products are concerned, a detailed solution kinetic study would be futile, owing to lack of structural definition of the final products.

As mentioned in Chapter 2, only a small number of *O,O'*- and *N,O*-bidentate ligands have successfully been coordinated to Ta(V)- and Nb(V) metal centres and characterized by X-Ray crystallography.[1,2,3,4] Most relevant references report only random synthetic methods without fully discussing choice or effectiveness of method used for intended aims of respective projects. Accordingly, a main objective of this study is to investigate a range of organic, bidentate ligands that were subjected to chelation with Ta(V)- and Nb(V) metal centres. This was done not only to expand the knowledge base of these types of complexes but also to conduct a comparative identification study for the behavioural trends of these systems. Any subtle nuances relating to the Ta(V) and Nb(V) crystallization tendencies could be potentially exploited for separation studies.

A large number of successful syntheses are reported in this chapter and the compounds characterized by UV/Vis-, IR- and ^{1}H-, ^{13}C- and ^{19}F NMR spectroscopy. In this Ph.D. study, only complexes that yielded crystalline products are described, as they could be utilized for structural investigations by means of single crystal XRD,

[1] G. J. Bullen, R. Mason and P. Pauling, (1965). *Inorg. Chem.*, **4**, 456-465.

[2] F. Preuss, G. Lamding and S. Mueller-Becker, (1994). *Z. Anorg. Allg. Chem.*, **620**, 1812-1821.

[3] H. Funk, (1934). *Ber. Dtsch. Chem. Ges.*, **62**, 1801-1816.

[4] H. O. Davies, T. J. Leedlam and A. C. Jones, (1999). *Polyhedron*, **18**, 3165-3180.

thus contributing significantly to the solid state data of the coordination chemistry of Ta(V) and Nb(V).

3.1 General Chemicals, Solvent and Analysis Techniques

3.1.1 Reagents and Solvents

All chemicals used for the synthesis and preparation of the complexes were of analytical grade and were purchased from Sigma-Aldrich, South Africa. Reaction solvents were of analytical grade and mostly used as received. In cases where anhydrous conditions were required, solvents were purified and dried according to literature procedures.[5]

3.1.2 Infrared Spectroscopy

Solid state FT-IR spectra of samples were recorded on a Bruker Tensor 27 Fourier transform spectrometer (ATR), utilizing a He-Ne laser at 632.6 nm, in the range of 3000 to 600 cm^{-1}.

3.1.3 Nuclear Magnetic Resonance Spectroscopy

The ^{1}H-, ^{13}C- and ^{19}F FT-NMR solution-state spectra were recorded on a Bruker AVANCE II 600 MHz (^{1}H: 600.28 MHz; ^{13}C: 150.96 MHz; ^{19}F: 564.83 MHz) or Bruker DPX 300 MHz (^{1}H: 300.13 MHz; ^{13}C: 75.47 MHz; ^{19}F: 282.40 MHz) nuclear magnetic resonance spectrometer using the appropriate deuterated solvent. Chemical shifts, δ, are reported in ppm. ^{1}H NMR spectra were referenced internally using residual protons in the deuterated solvents, Acetonitrile-d_3 [CD_3CN = 1.94(5) ppm]. ^{13}C NMR spectra were similarly referenced internally to the solvent resonance [CD_3CN = 1.39(4) ppm and 118.69(8) ppm] with values reported relative to tetramethylsilane (δ

[5] D. D. Perrin and W. L. F. Armarego, (1988). *Purification of Laboratory Chemicals*, Pergamon Press, Oxford, Great Britian.

0.0 ppm). In the case of ^{19}F NMR the values were reported relative to the hexafluorobenzene peak (-127.6 ppm).

3.1.4 UV/Vis Spectroscopy

UV/Vis absorbance spectra were collected in a 1.000(1) cm tandem quartz cuvette on a Varian Cary 50 Conc. spectrophotometer, which was equipped with a Julabo F12-mV temperature cell regulator accurate within 0.1 °C. All λ_{max} values reported in this chapter were collected at 25.0 °C.

3.2 Synthesis of Tantalum(V) and Niobium(V) Synthons

Most of the recorded literature indicates that tantalum(V) and niobium(V) bidentate complexes can only be synthesized under inert and anhydrous conditions. This can be attributed to the $[MCl_5]_2$ (M = Ta(V), Nb(V)) starting material hydrolizing to various unreactive oxido-metal species.[6] In an attempt to overcome this problem, a more robust synthon is required for application in atmospheric conditions.

The synthesis of this semi-stable Ta(V)/Nb(V)-synthon involves a simple, atmospheric condition, addition of $[MCl_5]_2$ (M = Ta(V), Nb(V)) and a quaternary ammonium counter-ion in acetonitrile at reflux for 12 hours. Removal of solvent yields the more stable ionic synthon, $(NEt_4)[MCl_6]$. Specific quantities of reagents, other reaction conditions and rates of crystallization are described below.

[6] R. Koen, (2012). *High Oxidation State Tantalum Coordination Chemistry: A Solution and Solid State Investigation*, M.Sc. Dissertation, University of the Free State, South Africa.

3.2.1 Synthesis of Tetraethylammonium hexachloridotantalate(V), $(NEt_4)[TaCl_6]$

Tetraethylammonium hexachloridotantalate(V) was prepared by modifying the known literature synthesis of bis-(tetraethylammonium) aqua-tetrachlorido-oxido-niobate(V).[7,8] $[TaCl_5]_2$ (0.500 g, 0.954 mmol) and tetraethylammonium chloride monohydrate (0.157 g, 0.954 mmol) were dissolved in acetonitrile. The colourless solution was refluxed for 12 hours while fumes of hydrogen chloride were relieved and the colour of the solution disappeared. After vacuum evaporation of excess solvent, colourless crystals suitable for X-Ray diffraction were obtained. (0.388 g, yield 69 %). Structural characterization using X-Ray diffraction methods of $(NEt_4)[NbCl_6]$ is discussed in Chapter 4.4.

IR (ATR, cm^{-1}): υ = 781, 948, 999, 1172, 1366, 1395, 1437, 1483. UV/Vis: λ_{max} = 305 nm, ε = 1.051 x 10^3 $M^{-1}.cm^{-1}$. ^{1}H NMR (300.13 MHz, Acetonitrile-d_3, *ppm*): δ = 1.22 (t, 12H), 3.21 (q, 8H). ^{13}C NMR (150.96 MHz, Acetonitrile-d_3, *ppm*): δ = 6.80, 52.1.

3.2.2 Synthesis of Tetraethylammonium hexachloridoniobate(V), $(NEt_4)[NbCl_6]$

Tetraethylammonium hexachloridoniobate(V) was prepared by modifying the known literature synthesis of bis-(tetraethylammonium) aqua-tetrachlorido-oxido-niobate(V)[7,8]. $[NbCl_5]_2$ (0.500 g, 1.115 mmol) and tetraethylammonium chloride monohydrate (0.340 g, 1.115 mmol) were dissolved in acetonitrile. The faintly yellow solution was refluxed for eight hours while fumes of hydrogen chloride were relieved and the colour of the solution disappeared. After vacuum evaporation of excess solvent, colourless crystals suitable for X-Ray diffraction were obtained (0.678 g, yield 74 %). Structural characterization using X-Ray diffraction methods of $(NEt_4)[NbCl_6]$ is discussed in Chapter 4.3.

[7] R. Kergoat and J. Guerchais, (1975). *J. Less Common Met*., **39**, 91-99.

[8] J. Daran, Y. Jeanin, R. Kergoat and J. Guerchais, (1979). *Inorg. Chim. Acta*., **33**, 81-90.

IR (ATR, cm^{-1}): υ = 779, 866, 949, 997, 1028, 1171, 1363, 1437, 1480. UV/Vis: λ_{max} = 294 nm, ε = 991 $M^{-1}.cm^{-1}$. ^{1}H NMR (300.13 MHz, Acetonitrile-d_3, *ppm*): δ = 1.31 (t, 12H), 3.18 (q, 8H). ^{13}C NMR (150.96 MHz, Acetonitrile-d_3, *ppm*): δ = 7.35, 53.62.

3.3 Metal Complex Synthesis: New synthon approach

Due to the favourable properties of the $[MCl_6]^-$ core (M = Nb(V) or Ta(V)) in combination with the promising, yet largely unexplored, *O,O'*-bidentate ligand systems, it was decided to investigate the coordinative ability of various bidentate ligands to the $[MCl_6]^-$ anion and to establish the solid state coordination modes as well as solution state kinetic behaviour towards the incoming bidentate ligands at the M^{5+} metal centres.

A range of *O,O'*-mono-negative, *β*-diketone ligands were used of which the substituents in the R_1, R_2 and R_3 positions were varied with respect to different electron-donating and electron-withdrawing groups. Figure 3.1 gives the general *β*-diketone structure, see also Chapter 2.3.1.

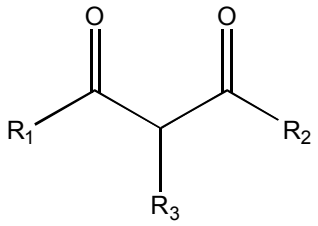

Figure 3.1 General *β*-diketones structure indicating positions where functionalities can be altered.

The synthesis of the M(V)-*β*-diketone complexes involved a simple method under atmospheric conditions: 1:1 molar addition of $(NEt_4)[MCl_6]$ (M = Ta(V), Nb(V)) and the *β*-diketone while stirring for 10 minutes at 50 ºC. Removal of solvent yields the moderately-stable complex, $(NEt_4)[MOCl_3(\beta\text{-diket})]$. Specific quantities of reagents, other reaction conditions and rates of crystallization are described below.

3.3.1 *β*-diketonate Ligands Utilized with Niobium(V) - (NEt_4)[$NbOCl_3$(*β*-diket)]

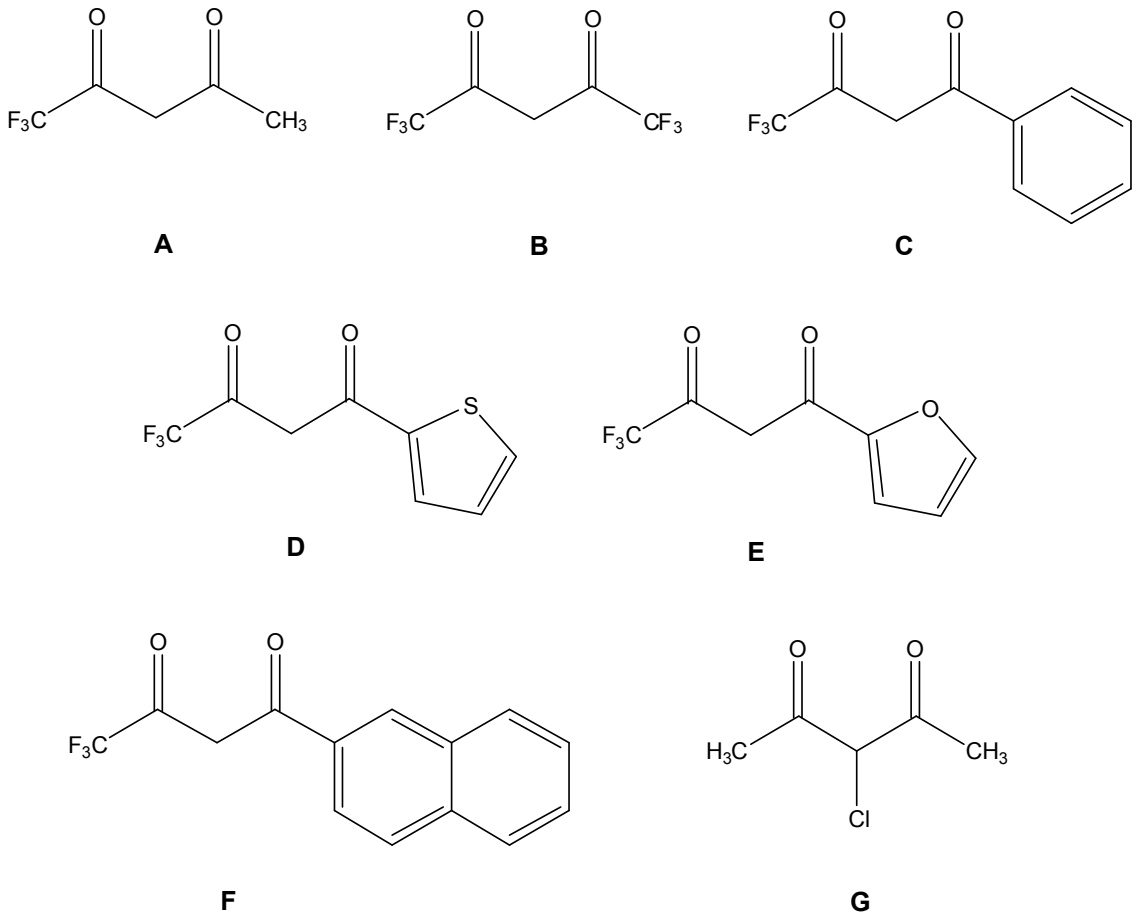

Figure 3.2 Graphical representation of the *β*-diketone ligands employed in both the synthesis of niobium(V) and tantalum(V) complexes. **A** *1,1,1*-Trifluoro-*2,4*-pentanedione (tfaaH), **B** *1,1,1,5,5,5*-Hexafluoro-*2,4*-pentanedione (hfaaH), **C** *4,4,4*-Trifluoro-*1*-phenyl-*1,3*-butanedione (btfaH), **D** *4,4,4*-Trifluoro-*1*(*2*-thienyl)-*1,3*-butanedione (ttfaH), **E** *4,4,4*-Trifluoro-*1*(*2*-furyl)-*1,3*-butanedione (tffaH), **F** *4,4,4*-Trifluoro-*1*(*2*-naphtyl)-*1,3*-butanedione (ntfaH), **G** *3*-Chloro-*2,4*-pentanedione (3-ClacacH).

3.3.1.1 Tetraethylammonium *mer*-trichloridooxido(trifluoroacetylacetonato-κ^2*O,O'*)niobate(V) ($(NEt_4)[NbOCl_3(tfaa)]$)

$(Et_4N)[NbCl_6]$ (0.500 g, 1.147 mmol) was added to **A** - *1,1,1*-Trifluoro-*2,4*-pentanedione (tfaaH) (0.176 g, 1.147 mmol) in acetonitrile (20 cm^3). The resulting solution was heated to 50 ºC and stirred for 10 minutes. The excess solvent was evaporated on a rotary evaporator and dark yellow plate-like crystals were immediately obtained (0.613 g, yield 86 %). These crystals were found to be very unstable and unsuitable for crystallographic structural characterization.

IR (ATR, cm^{-1}): $\upsilon_{(Nb=O)}$ = 931. UV/Vis: λ_{max} = 356 nm, ε = 3.323 x 10^3 $M^{-1}.cm^{-1}$. ^{1}H NMR (300.13 MHz, Acetonitrile-d_3, *ppm*): δ = 2.12 (s, 3H), 7.10 (s, 1H). ^{13}C NMR (75.47 MHz, Acetonitrile-d_3, *ppm*): δ = 20.0 124.2 141.3 142.8, 179.7. ^{19}F NMR (282.40 MHz, Acetonitrile-d_3, *ppm*): δ = -73.22.

3.3.1.2 Tetraethylammonium *mer*-trichlorido(hexafluoroacetylacetonato-κ^2*O,O'*) oxidoniobate(V) ($(NEt_4)[NbOCl_3(hfaa)]$)

$(Et_4N)[NbCl_6]$ (0.500 g, 1.147 mmol) was added to **B** - *1,1,1,5,5,5*-Hexafluoro-*2,4*-pentanedione (hfaaH) (0.305 g, 1.147 mmol) in acetonitrile (20 cm^3). The resulting solution was heated to 50 ºC and stirred for 10 minutes. The excess solvent was evaporated on a rotary evaporator and dark yellow plate-like crystals, suitable for single X-Ray diffraction were immediately obtained (0.214 g, yield 59 %). The crystallographic structural characterization of $(NEt_4)[NbOCl_3(hfaa)]$ is discussed in Chapter 6.4 and kinetics of formation in solution in Sections 8.3 and 8.4.

IR (ATR, cm^{-1}): $\upsilon_{(Nb=O)}$ = 949. λ_{max} = 358 nm, ε = 3.411 x 10^3 $M^{-1}.cm^{-1}$. ^{1}H NMR (300.13 MHz, Acetonitrile-d_3, *ppm*): δ = 7.54 (s, 1H). ^{13}C NMR (75.47 MHz, Acetonitrile-d_3, *ppm*): δ = 124.5, 143.0, 185.7. ^{19}F NMR (282.40 MHz, Acetonitrile-d_3, *ppm*): δ = -76.34, -77.96.

3.3.1.3 Tetraethylammonium *mer*-(benzoyltrifluoroacetylacetonato-κ^2*O,O'*) trichloridooxidoniobate(V) ($(NEt_4)[NbOCl_3(btfa)]$)

$(Et_4N)[NbCl_6]$ (0.500 g, 1.147 mmol) was added to **C** – *4,4,4*-Trifluoro-*1*-benzoyl-*1,3*-butanedione (btfaH) (0.317 g, 1.147 mmol) in acetonitrile (20 cm^3). The resulting solution was heated to 50 ºC and stirred for 10 minutes. The excess solvent was evaporated on rotary evaporator and dark yellow needle-like crystals, suitable for single X-Ray diffraction were immediately obtained (0.508 g, yield 81 %). Crystallographic structural characterization of $(NEt_4)[NbOCl_3(btfa)]$ is discussed in Chapter 5.6.

IR (ATR, cm^{-1}): $\upsilon_{(Nb=O)}$ = 935. λ_{max}= 371 nm, ε = 3.552 x 10^3 $M^{-1}.cm^{-1}$. ^{1}H NMR (300.13 MHz, Acetonitrile-d_3, *ppm*): δ = 7.33 (t, 1H), 2.61 (q, 4H), 7.37 (s, 1H), 7.40 (t, 2H), 7.71 (d, 2H). ^{13}C NMR (75.47 MHz, Acetonitrile-d_3, *ppm*): δ = 125.3, 127.5, 128.1, 128.8, 130.3, 144.5 149.8, 178.9. ^{19}F NMR (282.40 MHz, Acetonitrile-d_3, *ppm*): δ = -73.66.

3.3.1.4 Tetraethylammonium *mer*-trichloridooxido(thenoyltrifluoroacetyl acetonato-κ^2*O,O'*)niobate(V) ($(NEt_4)[NbOCl_3(ttfa)]$)

$(Et_4N)[NbCl_6]$ (0.500 g, 1.147 mmol) was added to **D** – *4,4,4*-Trifluoro-*1*(*2*-thienyl)-*1,3*-butanedione (ttfaH) (0.327 g, 1.147 mmol) in acetonitrile (20 cm^3). The resulting solution was heated to 50 ºC and stirred for 10 minutes. The excess solvent was evaporated on a rotary evaporator and dark yellow plate-like crystals, suitable for X-Ray diffraction were immediately obtained (0.565 g, yield 89 %). Crystallographic structural characterization of $(NEt_4)[NbOCl_3(ttfa)]$ is discussed in Chapter 5.4 and kinetics of formation in solution in Section 8.3 and 8.4.

IR (ATR, cm^{-1}): $\upsilon_{(Nb=O)}$ = 936. λ_{max} = 362 nm, ε = 3.478 x 10^3 $M^{-1}.cm^{-1}$. ^{1}H NMR (300.13 MHz, Acetonitrile-d_3, *ppm*): δ = 7.22 (t, 1H), 7.36 (d, 1H), 7.56 (s, 1H), 7.69 (d, 1H). ^{13}C NMR (75.47 MHz, Acetonitrile-d_3, *ppm*): δ = 126.3, 128.4, 128.7, 131.6, 135.9, 143.8, 148.7, 180.2. ^{19}F NMR (282.40 MHz, Acetonitrile-d_3, *ppm*): δ = -73.37.

3.3.1.5 Tetraethylammonium *mer*-trichlorido(furyltrifluoroacetylacetonato-κ^2*O,O'*)oxidoniobate(V) ($(NEt_4)[NbOCl_3(tffa)]$)

$(Et_4N)[NbCl_6]$ (0.500 g, 1.147 mmol) was added to **E** – *4,4,4*-Trifluoro-*1*(*2*-furyl)-*1,3*-butanedione (ttfaH) (0.236 g, 1.147 mmol) in acetonitrile (20 cm^3). The resulting solution was heated to 50 ºC and stirred for 10 minutes. The excess solvent was evaporated on a rotary evaporator and dark yellow plate-like crystals, suitable for single X-Ray diffraction were obtained (0.462 g, yield 75 %). Crystallographic structural characterization of $(NEt_4)[NbOCl_3(tffa)]$ is discussed in Chapter 5.5 and kinetics of formation in solution in Section 8.3 and 8.4.

IR (ATR, cm^{-1}): $\upsilon_{(Nb=O)}$ = 934. λ_{max} = 363 nm, ε = 3.499 x 10^3 $M^{-1}.cm^{-1}$. ^{1}H NMR (300.13 MHz, Acetonitrile-d_3, *ppm*): δ = 6.52 (t, 1H), 6.54 (d, 1H), 7.52 (s, 1H), 7.74 (d, 1H). ^{13}C NMR (75.47 MHz, Acetonitrile-d_3, *ppm*): δ = 110.1, 112.7, 123.6, 143.7, 144.5, 147.0, 149.2, 180.0. ^{19}F NMR (282.40 MHz, Acetonitrile-d_3, *ppm*): δ = -73.41.

3.3.1.6 Tetraethylammonium *mer*-trichlorido(naphtyltrifluoroacetylacetonato-κ^2*O,O'*)oxidoniobate(V) ($(NEt_4)[NbOCl_3(ntfa)]$)

$(Et_4N)[NbCl_6]$ (0.500 g, 1.147 mmol) was added to **F** – *4,4,4*-Trifluoro-*1*(*2*-naphtyl)-*1,3*-butanedione (ntfaH) (0.305 g, 1.147 mmol) in acetonitrile (20 cm^3). The resulting solution was heated to 50 ºC and stirred for 10 minutes. The excess solvent was evaporated on a rotary evaporator and dark yellow plate-like crystals, suitable for single X-Ray diffraction were immediately obtained (0.424 g, yield 62 %). Crystallographic structural characterization of $(NEt_4)[NbOCl_3(ntfa)]$ is discussed in Chapter 5.6 and kinetics of formation in solution in Section 8.3 and 8.4.

IR (ATR, cm^{-1}): $\upsilon_{(Nb=O)}$ = 942. λ_{max} = 375 nm, ε = 3.611 x 10^3 $M^{-1}.cm^{-1}$. ^{1}H NMR (300.13 MHz, Acetonitrile-d_3, *ppm*): δ = 7.41 (d, 1H), 7.46 (s, 1H), (d, 1H), 7.59 (t, 2H), 7.76 (s, 1H), 7.83 (s, 1H), 8.02 (t, 2H). ^{13}C NMR (75.47 MHz, Acetonitrile-d_3, *ppm*): δ = 123.5, 124.2, 126.0, 126.4, 127.7, 128.1, 128.6, 133.2, 133.6, 134.8, 144.5, 149.2, 181.6. ^{19}F NMR (282.40 MHz, Acetonitrile-d_3, *ppm*): δ = -73.25.

3.3.1.7 Tetraethylammonium *mer*-(3-chloroacetylacetonato-κ^2*O,O'*)trichlorido oxidoniobate(V) ($(NEt_4)[NbOCl_3(3\text{-}Clacac)]$)

$(Et_4N)[NbCl_6]$ (0.500 g, 1.147 mmol) was added to **G** – *3*-Chloro-*2,4*-pentanedione (3-ClacacH) (0.147 g, 1.147 mmol) in acetonitrile (20 cm^3). The resulting solution was heated to 50 ºC and stirred for 10 minutes. The excess solvent was evaporated on a rotary evaporator and dark yellow plate-like crystals, suitable for single X-Ray diffraction were immediately obtained (0.353 g, yield 67 %). Crystallographic structural characterization of $(NEt_4)[NbOCl_3(3\text{-}Clacac)]$ is discussed in Chapter 6.3.

IR (ATR, cm^{-1}): $\upsilon_{(Nb=O)}$ = 929. λ_{max} = 355 nm, ε = 3.291 x 10^3 $M^{-1}.cm^{-1}$. ^{1}H NMR (300.13 MHz, Acetonitrile-d_3, *ppm*): δ = 2.69 (s, 6H). ^{13}C NMR (75.47 MHz, Acetonitrile-d_3, *ppm*): δ = 123.1, 149.4, 181.7.

3.3.2 *β*-diketonate Complexes of Tantalum(V) - $(NEt_4)[TaOCl_3(\beta\text{-diket})]$

The synthesis and successful characterization of $(NEt_4)[TaOCl_3(\beta\text{-diket})]$ complexes has proven to be elusive. In the case of the Nb(V) compounds, the $(Et_4N)[NbCl_6]$ synthon seems to be very robust and ideal to obtain solid state structures of the when coordinated to various *β*-diketones reproducibly. In contrast, no crystal structures could be obtained for the Ta(V) analogues. Some crystalline products have been obtained but decomposed too rapidly to be subjected to a successful single crystal data collection. From the shifts in the various IR, ^{13}C- and ^{1}H-NMR spectra it can be deducted that the *β*-diketone has coordinated to the metal. Without the crystallographic data of these complexes, no conclusive solid-state information about coordination geometry and intermolecular interactions could be obtained. As has been mentioned in Chapter 2, these characteristics have a large effect on properties such as anion acidity and volatility.

3.3.2.1 Tetraethylammonium *mer*-trichlorido(trifluoroacetylacetonato-κ^2*O,O'*)oxidotantalate(V) ($(NEt_4)[TaOCl_3(tfaa)]$)

$(Et_4N)[TaCl_6]$ (0.500 g, 0.954 mmol) was added to **A** - *1,1,1*-Trifluoro-*2,4*-pentanedione (tfaaH) (0.147 g, 0.954 mmol) in acetonitrile (20 cm^3). The resulting solution was heated to 50 ºC and stirred for 10 minutes. The excess solvent was evaporated on a rotary evaporator and pale-yellow needle-like crystals were immediately obtained (0.421 g, yield 69 %). These crystals were found to be very unstable and unsuitable for crystallographic structural characterization.

IR (ATR, cm^{-1}): $\upsilon_{(Ta=O)}$ = 921. λ_{max} = 321 nm, ε = 2.423 x 10^3 $M^{-1}.cm^{-1}$. ^{1}H NMR (300.13 MHz, Acetonitrile-d_3, *ppm*): δ = 2.23 (s, 3H), 7.41 (s, 1H). ^{13}C NMR (75.47 MHz, Acetonitrile-d_3, *ppm*): 108.1, 111.1, 121.7, 147.7, 149.6, 151.7, 153.6, 184.1. ^{19}F NMR (282.40 MHz, Acetonitrile-d_3, *ppm*): δ = -72.83.

3.3.2.2 Tetraethylammonium *mer*-trichlorido(hexafluoroacetylacetonato-κ^2*O,O'*)oxidotantalate(V) ($(NEt_4)[TaOCl_3(hfaa)]$)

$(Et_4N)[TaCl_6]$ (0.500 g, 0.954 mmol) was added to **B** - *1,1,1,5,5,5*-Hexafluoro-*2,4*-pentanedione (hfaaH) (0.198 g, 0.954 mmol) in acetonitrile (20 cm^3). The resulting solution was heated to 50 ºC and stirred for 10 minutes. The excess solvent was evaporated on a rotary evaporator and pale-yellow needle-like crystals were immediately obtained (0.289 g, yield 55 %).

IR (ATR, cm^{-1}): $\upsilon_{(Ta=O)}$ = 933. λ_{max} = 329 nm, ε = 2.511 x 10^3 $M^{-1}.cm^{-1}$. ^{1}H NMR (300.13 MHz, Acetonitrile-d_3, *ppm*): δ = 7.64 (s, 1H). ^{13}C NMR (75.47 MHz, Acetonitrile-d_3, *ppm*): δ = 128.6, 143.6, 180.9. ^{19}F NMR (282.40 MHz, Acetonitrile-d_3, *ppm*): δ = -75.01, 75.52.

3.3.2.3 Tetraethylammonium *mer*-(benzoyltrifluoroacetylacetonato-κ^2*O,O'*) trichloridooxidotantalate(V) ($(NEt_4)[TaOCl_3(btfa)]$)

$(Et_4N)[TaCl_6]$ (0.500 g, 0.954 mmol) was added to **C** – *4,4,4*-Trifluoro-*1*-phenyl-*1,3*-butanedione (btfaH) (0.206 g, 0.954 mmol) in acetonitrile (20 cm^3). The resulting solution was heated to 50 ºC and stirred for 30 minutes. The excess solvent was evaporated on a rotary evaporator and a white powder was obtained (0.458 g, yield 86 %).

IR (ATR, cm^{-1}): $\upsilon_{(Ta=O)}$ = 919. λ_{max} = 340 nm, ε = 2.755 x 10^3 $M^{-1}.cm^{-1}$. ^{1}H NMR (300.13 MHz, Acetonitrile-d_3, *ppm*): δ = 7.41 (t, 1H), 7.45 (s, 1H), 7.55 (t, 2H) 7.83 (d, 2H). ^{13}C NMR (75.47 MHz, Acetonitrile-d_3, *ppm*): δ = 126.8, 129.1, 130.3, 130.5, 133.0, 145.9, 151.0, 183.1 ^{19}F NMR (282.40 MHz, Acetonitrile-d_3, *ppm*): δ = -72.59.

3.3.2.4 Tetraethylammonium *mer*-trichloridooxido(thenoyltrifluoroacetyl acetonato-κ^2*O,O'*)tantalate(V) ($(NEt_4)[TaOCl_3(ttfa)]$)

$(Et_4N)[TaCl_6]$ (0.500 g, 0.954 mmol) was added to **D** – *4,4,4*-Trifluoro-1(2-thienyl)-1,3-butanedione (ttfaH) (0.211 g, 0.954 mmol) in acetonitrile (20 cm^3). The resulting solution was heated to 50 ºC and stirred for 30 minutes. The excess solvent was evaporated on a rotary evaporator and pale-yellow, unstable, plate-like crystals, were obtained (0.422 g, yield 78 %).

IR (ATR, cm^{-1}): $\upsilon_{(Ta=O)}$ = 917. λ_{max} = 339 nm, ε = 2.835 x 10^3 $M^{-1}.cm^{-1}$. ^{1}H NMR (300.13 MHz, Acetonitrile-d_3, *ppm*): δ = 7.21(s, 1H), 7.31 (t, 1H), 7.42 (d, 1H), 7.81 (d, 1H). ^{13}C NMR (75.47 MHz, Acetonitrile-d_3, *ppm*): δ = 121.1, 16.9, 19.3, 133.7, 136.5, 146.9, 152.0, 184.1. ^{19}F NMR (282.40 MHz, Acetonitrile-d_3, *ppm*): δ = -72.89.

3.3.2.5 Tetraethylammonium *mer*-trichlorido(furyltrifluoroacetylacetonato-κ^2*O,O'*)oxidotantalate(V) ($(NEt_4)[TaOCl_3(tffa)]$)

$(Et_4N)[TaCl_6]$ (0.500 g, 0.954 mmol) was added to **E** – *4,4,4*-Trifluoro-*1*(*2*-furyl)-*1,3*-butanedione (ttfaH) (0.196 g, 0.954 mmol) in acetonitrile (20 cm^3). The resulting solution was heated to 50 ºC and stirred for 30 minutes. The excess solvent was evaporated on a rotary evaporator and a white powder was obtained (0.341 g, yield 65 %).

IR (ATR, cm^{-1}): $\upsilon_{(Ta=O)}$ = 911. ^{1}H NMR (300.13 MHz, Acetonitrile-d_3, *ppm*): δ = 6.44 (t, 1H), 6.67 (d, 1H), 7.21 (s, 1H), 7.89 (d, 1H). ^{13}C NMR (75.47 MHz, Acetonitrile-d_3, *ppm*): δ = 108.1, 111.1, 121.7, 147.7, 149.6, 151.7, 153.6, 184.1. ^{19}F NMR (282.40 MHz, Acetonitrile-d_3, *ppm*): δ = -72.71.

3.3.2.6 Tetraethylammonium *mer*-trichlorido(naphtyltrifluoroacetylacetonato-κ^2*O,O'*)oxido tantalate(V) ($(NEt_4)[TaOCl_3(ntfa)]$)

$(Et_4N)[TaCl_6]$ (0.500 g, 0.954 mmol) was added to **F** – *4,4,4*-trifluoro-*1*(*2*-naphtyl)-*1,3*-butanedione (ntfaH) (0.253 g, 0.954 mmol) in acetonitrile (20 cm^3). The resulting solution was heated to 50 ºC and stirred for 30 minutes. The excess solvent was evaporated on a rotary evaporator and dark yellow, unstable, plate-like crystals were obtained (0.250 g, yield 43 %).

IR (ATR, cm^{-1}): $\upsilon_{(Ta=O)}$ = 927. λ_{max} = 344 nm, ε = 2.807 x 10^3 $M^{-1}.cm^{-1}$. ^{1}H NMR (300.13 MHz, Acetonitrile-d_3, *ppm*): δ = 7.33 (s, 1H), 7.50 (d, 1H), 7.63(t, 2H), 7.70 (d, 1H), 7.94 (s, 1H), 8.09 (t, 2H). ^{13}C NMR (75.47 MHz, Acetonitrile-d_3, *ppm*): δ = 119.6, 122.21, 124.6, 127.3, 128.9, 129.3, 135.6, 136.9, 138.2, 148.3, 154.2, 182.1. ^{19}F NMR (282.40 MHz, Acetonitrile-d_3, *ppm*): δ = -71.07.

3.3.2.7 Tetraethylammonium *mer*-(3-chloroacetylacetonato-κ^2*O,O'*)trichlorido oxido tantalate(V) ($(NEt_4)[NbOCl_3(3\text{-}Clacac)]$)

$(Et_4N)[TaCl_6]$ (0.500 g, 0.954 mmol) was added to **G** – 3-Chloro-2,4-pentanedione (3-ClacacH) (0.128 g, 0.954 mmol) in acetonitrile (20 cm^3). The resulting solution was heated to 50 ºC and stirred for 30 minutes. The excess solvent was evaporated on a rotary evaporator and dark yellow, unstable, plate-like crystals were obtained (0.283 g, yield 62 %).

IR (ATR, cm^{-1}): $\upsilon_{(Ta=O)}$ = 918. λ_{max} = 324 nm, ε = 2.577 x 10^3 $M^{-1}.cm^{-1}$. ^1H NMR (300.13 MHz, Acetonitrile-d_3, *ppm*): δ = 2.81 (s, 6H). ^{13}C NMR (75.47 MHz, Acetonitrile-d_3, *ppm*): δ = 130.1, 155.6, 187.3.

3.4 Tropolonato Complexes of Niobium(V) and Tantalum(V)

The *O,O'*-mono-negative, tropolone ligand is ideally suited to the formation of structures of high coordination number by virtue of the planarity and compactness of the ligand and the rigidity of the functionality.[9] Figure 3.3 gives the general tropolone (TropH) structure.

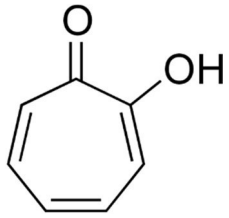

Figure 3.3 Illustration of the general tropolone (TropH) structure.

According to Muetteries *et al*., niobium and tantalum pentachlorides react with acidic aqueous solutions of tropolone to give the tetrakistropolono cations $[Nb(Trop)_4]^+$ and $[Ta(Trop)_4]^+$ respectively (Trop = tropolonato). With increasing pH or increasing temperature, the niobium chelate undergoes partial hydrolysis to $[NbO(Trop)_3]$ which

separates from solution.[9] Specific quantities of reagents, other reaction conditions and rate of crystallization for the formation of these products are described below.

3.4.1 *Tetrakis*(tropolonato-κ^2*O,O'*)niobate(V) chloride – $[Nb(Trop)_4]Cl$

A solution of $[NbCl_5]_2$ (0.270 g, 1.001 mmol) in a mixture of dichloromethane (200 cm^3) and of ether (30 cm^3) was added to a solution of tropolone (0.489 g, 4.004 mmol) in of dichloromethane (200 cm^3) to give an orange solution from which a solid slowly separated. The solvent was evaporated under reduced pressure, and acetonitrile (400 cm^3) was added to the residue. This was heated until reaction was complete. On cooling, bright orange crystals separated. The solid was recrystallized from hot acetonitrile and vacuum dried at 120 ºC for 3 hr (0.409 g, yield 76 %). Crystallographic structural characterization of $[Nb(Trop)_4]Cl$ is discussed in Chapter 7.5.

IR (ATR, cm^{-1}): υ = 723, 876, 965, 1078, 1221, 1265, 1331, 1426, 1530, 1584. ^1H NMR (300.13 MHz, Acetonitrile-d_3, *ppm*): δ = 7.11 (d, 2H), 7.18 (t, 2H), 7.55 (t, 1H)). ^{13}C NMR (75.47 MHz, Acetonitrile-d_3, *ppm*): δ = 87.8, 91.6, 101.3, 133.8.

3.4.2 *Tetrakis*(tropolonato-κ^2*O,O'*)tantalate(V) chloride – $[Ta(Trop)_4]Cl$

A solution of $[TaCl_5]_2$ (1.433 g, 4.000 mmol) in concentrated hydrochloric acid (40 cm^3) and methanol (40 cm^3) was added to a solution of tropolone (0.244 g, 20.001 mmol) in of concentrated hydrochloric acid (20 cm^3) and of methanol (320 cm^3). A yellow precipitate formed during the addition. The slurry was heated to reflux for 15 min until a clear yellow solution was obtained. This solution on cooling yielded yellow crystalline $[Ta(Trop)_4]Cl$. The compound was recrystallized from a hot water-methanol mixture and vacuum dried for 3 hr (0.394 g, yield 63 %). Crystallographic structural characterization of $[Ta(Trop)_4]Cl$ is discussed in Chapter 7.6.

[9] E. L. Muetterties and C. M. Wright, (1965). *J. Am. Chem. Soc.*, **87**, 21, 4706-4721.

IR (ATR, cm^{-1}): υ = 721, 830, 1225, 1353, 1431, 1534, 1591, 1633, 3349. ^{1}H NMR (300.13 MHz, Acetonitrile-d_3, *ppm*): δ = 7.18 (d, 2H), 7.32 (t, 2H), 7.87 (t, 1H)). ^{13}C NMR (75.47 MHz, Acetonitrile-d_3, *ppm*): δ = 89.2, 94.3, 103.6, 127.2.

3.4.3. *Tris*(tropolonato-κ^2*O,O'*)oxido niobate(V) – [NbO(Trop)$_3$]

$[NbCl_5]_2$ (4.351 g, 0.01 mol) was dissolved in concentrated hydrochloric acid (10 cm^3) and methanol (10 cm^3). This was added to a solution of tropolone (6.106 g, 0.05 mol) in concentrated hydrochloric acid (5 cm^3) and methanol (80 cm^3). Water (50 cm^3) was added to the reaction mixture and the solution heated until a solid separated. The reaction mixture was refluxed for 15 min and then cooled to room temperature. The solid was collected by filtration and recrystallized from a hot acetonitrile-water mixture to give orange-yellow needle-like crystals, suitable for X-ray diffraction (0.392 g, yield 83 %). Crystallographic structural characterization of [NbO(Trop)$_3$] is discussed in Chapter 7.4.

IR (ATR, cm^{-1}): υ = 711, 811, 1199, 1341, 1481, 1534, 1591, 1616. ^{1}H NMR (300.13 MHz, Acetonitrile-d_3, *ppm*): δ = 7.21 (d, 2H), 7.34 (t, 2H), 7.51 (t, 1H)). ^{13}C NMR (75.47 MHz, Acetonitrile-d_3, *ppm*): δ = 91.2, 91.8, 111.1, 130.1.

3.5 Discussion and Conclusions

During the course of this synthetic investigation, some novel and re-synthesised synthons and complexes of tantalum(V) and niobium(V) were prepared and characterized. The more significant focal area revolved around the *O,O'*-type bidentate ligand family (e.g. tropolones and *β*-diketones), of which very few examples of Ta(V) and Nb(V)-compounds were available in literature.[1,2,3,4] Each of the preceding sections have had an overarching topic which has helped in gaining knowledge about these systems.

The focus of Section 3.2 has mainly been placed on developing more stable Nb(V)/Ta(V) synthons for bidentate ligand coordination. In the past, the coordination

of these ligands to Ta(V) and Nb(V) metal centres has mostly been found to be very laborious, requiring anhydrous and inert reaction conditions. This has been ascribed to the fact that M(V) synthons are readily hydrolysed under these unfavourable conditions.[10,11,12] The hydrolysed specie is very unreactive and seemingly not very useful in coordination chemistry.[13] Accordingly attempts have been made to create synthons which are much more durable in atmospheric conditions. These synthons could be more useful in understanding the chemical characteristics of bidentate ligand coordination to the Nb(V) and Ta(V) metal centres.

In this study, the use of an ammonium-type counter-ion has led to the development of two synthons $(NEt_4)[NbCl_6]$ and $(NEt_4)[TaCl_6]$. The simplicity and efficiency (90+ % yields) of the syntheses in atmospheric conditions is exactly what is required when creating a new synthon. In addition, the stability of the obtained $(NEt_4)[MCl_6]$ is noteworthy. These compounds, even when stored under atmospheric conditions, have been found to be functional for coordination reactions to *β*-diketones weeks after synthesis.

One of the aims set out in Chapter 1 was to obtain a reproducible method to synthesize Ta(V)/Nb(V) - *β*-diketonate complexes. Reproducibility of the synthesis would simplify reaction system manipulation when separation studies are furthered. Ideally this method should also be very simple, inexpensive and practicable in atmospheric as it could be up scaled to industrial application.

[10] H. O. Davies, T. J. Leedham, A. C. Jones, P. O'Brien, A. J. P. White and D. J. Williams, (1999). *Polyhedron*, **18**, 3165-3172.

[11] H. O. Davies, A. C. Jones, M. A. Motevalli, E. A. McKinnell and P. O'Brien, (2005). *Inorg. Chem. Comm.*, **8**, 585-588.

[12] P. A. Williams, A. C. Jones, P. J. Wright, M. J. Crosbie, J. F. Bickley, A. Steiner, H. O. Davies and T. J. Leedham, (2002). *Chem. Vap. Dep.*, **8**, 110-116.

[13] L. G. Hubert-Pfalzgraf, M. Postel and J. G. Riess, (1987). *Niobium and Tantalum, Comprehensive Coordination Chemistry*, **3**, London, United Kingdom.

In Section 3.3, such a method discussed, where *β*-diketones were coordinated to these newly obtained synthons discussed in Section 3.2. A range of *β*-diketone ligands with various functionalities was employed in a 1:1 molar addition to $(NEt_4)[NbCl_6]$, at slightly elevated temperatures. In all cases, by simply utilizing acetonitrile as reaction solvent and without enforcing any special precautions on reaction environment (i.e. standard bench-top, aerobic conditions), several niobium(V) products could easily be obtained. In this chapter, 6 examples of a mono-coordinated Nb(V)-*β*-diketonate complexes have been described that yielded crystalline material, within seconds after reaching saturation point, without any elaborate crystallization technique. Furthermore, these complexes tend to favour crystalline products in most cases observed and described here. Several attempts were made to determine which physical aspects of a reaction system control the extent of coordination, i.e. mono-, bis- or tetrakis- ligand coordination, with no success. It seems that niobium(V) coordination reactions, favour singular bidentate coordination, suggesting that the crystallization energy of the mono-coordinated complex is quite low in this system.[14]

Unfortunately a similar method to obtain crystalline products could not be conclusively developed for the Ta(V) counterpart. By comparing the ^{1}H-, ^{13}C- and ^{19}F NMR spectra of the free ligand to that obtained after *β*-diketone addition to $(NEt_4)[TaCl_6]$, some peak shifts are observed for some of the ligands, all in accordance with what would be expected for singular *β*-diketonate coordination to the metal centre. Regrettably, no crystals suitable for X-Ray diffraction studies were obtained to confirm the solid-state structure. A comparison of the δ (^{19}F), υ (M=O) and λ_{max} values of the various Nb(V) and Ta(V) *β*-diketonate complexes is illustrated in Tables 3.1 and 3.2.

[14] J. E. Huheey, E. A. Keiter and R. L. Keiter, (1993). *Inorganic Chemistry: Principles of Structure and Reactivity*, **4**, New York, United States of America.

Table 3.1 Comparison of pK_a values with δ (^{19}F), υ (M=O) and λ_{max} values of the various Nb(V)-*β*-diketonate complexes discussed in this chapter.

Nb(V) Complex	*pK_a* of *β*-diketonate[15]	δ (^{19}F) (ppm)	υ (M=O) (cm^{-1})	λ_{max} (nm)
$(NEt_4)[NbOCl_3(hfaa)]$	4.60	-76.34, -77.96	949	358
$(NEt_4)[NbOCl_3(btfa)]$	6.30	-73.66	935	371
$(NEt_4)[NbOCl_3(tfaa)]$	6.30	-73.22	931	356
$(NEt_4)[NbOCl_3(tffa)]$	6.48	-73.41	934	363
$(NEt_4)[NbOCl_3(ttfa)]$	6.50	-73.37	936	362
$(NEt_4)[NbOCl_3(ntfa)]$	unknown	-73.25	942	375
$(NEt_4)[NbOCl_3(3\text{-}Clacac)]$	6.77	n/a	929	355

Table 3.2 Comparison pK_a values of δ (^{19}F), υ (M=O) and λ_{max} values of the various Ta(V)-*β*-diketonate complexes discussed in this chapter.

Ta(V) Complex	*pK_a* of *β*-diketonate[16]	δ (^{19}F) (ppm)	υ (M=O) (cm^{-1})	λ_{max} (nm)
$(NEt_4)[TaOCl_3(hfaa)]$	4.60	-75.01, 75.52	933	329
$(NEt_4)[TaOCl_3(btfa)]$	6.30	-72.59	919	340
$(NEt_4)[TaOCl_3(tfaa)]$	6.30	-72.83	921	321
$(NEt_4)[TaOCl_3(tffa)]$	6.48	-72.71	911	341
$(NEt_4)[TaOCl_3(ttfa)]$	6.50	-72.89	917	339
$(NEt_4)[TaOCl_3(ntfa)]$	unknown	-71.07	927	344
$(NEt_4)[TaOCl_3(3\text{-}Clacac)]$	6.77	n/a	918	324

From Tables 3.1 and 3.2, various overarching trends can be noticed when comparing the δ (^{19}F), υ (M=O) and λ_{max} values of the Nb(V) and Ta(V) *β*-diketonate complexes. An increase of pK_a value of the free ligand generally relates to an upfield shift of the peak in the ^{19}F NMR spectra, whereas it causes a decrease of the M=O stretching frequency value. Interestingly, the λ_{max} seems to be influenced by the aromaticity of the substituent on the acac backbone. As the substituent/ring becomes larger, the λ_{max} also increases. This trend becomes obvious when comparing $(NEt_4)[NbOCl_3(ntfa)]$ (344 nm), $(NEt_4)[NbOCl_3(btfa)]$ (340 nm) and

[15] H. Watarai and I. Takahashi, (1998). *Anal. Commun.*, **38**, 289-292.

[16] H. Watarai and I. Takahashi, (1998). *Anal. Commun.*, **38**, 289-292.

$(NEt_4)[NbOCl_3(tfaa)]$ (321 nm). A more thorough comparison of these and other additional properties of these compounds will be undertaken in Chapter 9.

In Section 3.3, tropolone (TropH) was coordinated to Ta(V) and Nb(V) metal centres, while studying the influence of pH on the coordination geometry of these systems. It was mentioned in earlier sections that in most cases, the $[TaCl_5]_2$ and $[NbCl_5]_2$ synthons do not yield stable complexes when coordinated to bidentate ligands in atmospheric conditions. Interestingly, in this case, it was found that the metal-tropolonato complexes form quite readily with very high yields, in hydrous conditions and were found to remain stable for weeks after synthesis.

The influence of pH on the metal-tropolonato complex formation and the resulting coordination modes has also become evident during the study. The pentachlorides react with acidic aqueous solutions (pH < 3) of tropolone to afford the *tetrakis*-tropolono cations, $[Ta(Trop)_4]Cl$ and $[Nb(Trop)_4]Cl$ respectively (T = tropolone), as described in Section 3.4.1 and 3.4.2. With increasing pH or increasing temperature, the niobium chelate undergoes partial hydrolysis to $[NbO(Trop)_3]$ which separates from solution. The crystal structures of these predicted compounds were successfully obtained. This difference in charge around the metal centre between the two metals, offers an ideal point to further Ta(V)/Nb(V) separation in future studies.

A single crystal X-Ray diffraction study, focusing on complex structure, intra-/inter molecular interactions and crystal packing of the crystals obtained from the preceding sections is discussed in the following chapters (Chapter 4 – 7). Furthermore, in Chapter 8, a solution behavioural kinetic study of selected *β*-diketones in complex formation reactions with niobium(V) and tantalum(V) are also evaluated.

Chapter 4: Chrystallographic Evaluation of New Nb(V)- and Ta(V) Synthons

4.1 Introduction

An extensive literature review revealed that some Ta(V)- and Nb(V)-*β*-diketonato complexes have been synthesized in the past.[1,2,3,4] In a vast majority of the cases, these compounds were synthesized under an inert atmosphere and favoured a *mono*- chelated moiety.[1,2,3,4,5,6,7,8] This instability in atmospheric conditions has been attributed to the hydrolysis of the various metal chloride precursors, e.g. $[NbCl_5]_2$ or $[TaCl_5]_2$.[9] Improvement of stability of the various metal(V)-*β*-diketonato complexes is crucial to further investigation of the separation process to possibly be applied to an industrial level. Accordingly, more stable Ta(V) and Nb(V) synthons are required.

Synthesis and development of new starting materials for the group 5 elements is not a novel notion, being the focal point of several publications.[7,8] Examples of these investigations are quite diverse and with various research outcomes. These precursors find application in catalysis, investigation of the properties of photo-

[1] H. O. Davies, T. J. Leedlam and A. C. Jones, (1999). *Polyhedron.* **18**, 3165-3172.

[2] P. Wendrup and V. G. Kessler, (2001). *J. Chem. Soc., Dalton Trans*, **69**, 574-579.

[3] E. L. Lippert and M. R. Truter, (1960). *J. Chem. Soc. A.*, **33**, 309-311.

[4] G. J. Bullen, R. Mason and P. Pauling, (1965). *Inorg Chem.*, **4**, 456-461.

[5] F. Preuss, G. Lambing and S. Mueller-Becker, (1994). *Z. Anorg. Allg. Chem.,* **620**, 1812-1821.

[6] P. A. Williams, A. C. Jones, P. J. Wright and M. J. Crosbie, (2002). *Chem. Vap. Deposition*, **8**, 110-116.

[7] M. J. Crosbie, P. J. Wright, P. A. Lane, A. C. Jones and T. J. Leedham, (1999). *J. Phys. IV.* **9**, 8-935.

[8] H. Funk, (1934). *Ber. Dtsch. Chem. Ges.*, **62**, 1801-1805.

[9] C. K. Gupta and A. K. Suri, (1993). *Extractive Metallurgy of Niobium*, CRC Press, Boca Raton, United States of America.

excited states of group 5 compounds and anaerobic coordination chemistry.[10,11,12] Unfortunately, past studies have not revealed specific details that relate to the factors that govern air-stability or lability of the substituents on the precursors. Accordingly, it was concluded that a solid state crystallographic investigation will provide greater insight to the intra- and inter- molecular interactions that govern molecule stability and also shed light on the lability of various substituents by comparing bond lengths and -angles of the various compounds.

4.2 Experimental

The X-Ray intensity data was collected on a Bruker X8 ApexII 4K Kappa CCD area detector diffractometer, equipped with a graphite monochromator and Mo*Kα* fine-focus sealed tube (*λ* = 0.71069 Å, T = 100(2) K) operated at 2.0 kW (50 kV, 40 mA). The initial unit cell determinations and data collections were done by the SMART software package.[13] The collected frames were integrated using a narrow-frame integration algorithm and reduced with the Bruker SAINT-Plus and XPREP software packages respectively.[14] Analysis of the data showed no significant decay during the data collection. Data was corrected for absorption effects using the multi-scan technique SADABS, and the structure was solved by the direct methods package SIR97 and refined using the WinGX software incorporating SHELXL.[15,16,17,18] The

[10] S. Mishra, E. Jeanneau, S. Mangematin, H. Chermette and M. Poor-Kalhor, (2015). *Dalton Trans.*, **44**, 6848-6862.

[11] A. V. Korolev, A. L. Rheingold and D. S. Williams, (1997). *Inorg Chem.*, **36**, 2647-2655.

[12] N. Galesic, N. Brnicevic, B. Matkovic and M. Hercey, (1977). *J. Less-Common Met.*, **51**, 295-270.

[13] Bruker SMART-NT Version 5.050, (1998). *Bruker AXS Inc. Area-Detector Software Package*; Madison, Winconsin, United States of America**.**

[14] Bruker SAINT-Plus Version 6.02 (including XPREP), (1999). *Bruker AXS Inc. Area-Detector Integration Software*, Madison, Winconson, United States of America.

[15] Bruker SADABS Version 2004/1, (1998). *Bruker AXS Inc. Area Detector Absorption Correction Software*, Madison, Wisconsin, United States of America.

[16] A. Altomare, M. C. Burla, M. Camalli, G. L. Cascarano, C. Giacovazzo, A. Guagliardi, A. G. G. Moliterni, G. Polidori and R. Spagna, (1999). *J. Appl. Cryst.,* **32**, 115-119.

[17] L. J. Farrugia, (1999). *J. Appl. Cryst.* **32**, 837-838.

[18] G. M. Sheldrick; SHELXL97, (1997). *Program for Crystal Structure Refinement*, University of Göttingen, Germany.

final anisotropic full-matrix least-squares refinement was done on F^2. The methyl and aromatic protons were placed in geometrically idealized positions (C–H = 0.93 – 0.98 Å) and constrained to ride on their parent atoms with $U_{iso}(H) = 1.2U_{eq}(C)$. Non-hydrogen atoms were refined with anisotropic displacement parameters. The graphics were obtained with the DIAMOND program with 50% probability ellipsoids for all non-hydrogen atoms.[19]

Table 4.1 Crystallographic and refinement details for structures discussed in this chapter.

Crystal Formula	$(Et_4N)[NbCl_6]$	$(Et_4N)[TaCl_6]$
Empirical formula	$C_8H_{20}Cl_6N_1Nb$	$C_8H_{20}Cl_6N_1Ta$
Formula weight (g.mol^{-1})	435.9	523.9
Crystal system, Space Group	Monoclinic, $P2_1/c$	Monoclinic, $P2_1/c$
a, b, c (Å)	7.213(4), 10.157(3) 12.675(3),	7.155(1), 10.009(1) 11.629(1),
α, β, γ (°)	90, 114.166(4), 90	90, 98.487(3), 90
Volume (Å^3), Z	847.2(8), 2	823.7(8), 2
Density (calculated, Mg/m^3)	1.709	2.112
Crystal colour	Yellow	Colourless
Crystal size (mm^3)	0.31 x 0.24 x 0.14	0.46 x 0.14 x 0.10
Absorption coefficient μ (mm^{-1})	1.634	7.622
F(000)	436	500
Theta range	2.7 – 27.7°	2.7 - 28°
Index ranges	-9<=h<=9, -13<=k<=13, -17<=l<=16	-9<=h<=9, -13<=k<=13, -15<=l<=14
Reflections collected, Independent Reflections, R_{int}	2148, 1689, 0.0617	16031, 1985, 0.0567
Completeness to 2θ (°, %)	27.99, 99.9	27.99, 99.8
Max. and min. transmission	0.666 and 0.818	0.289 and 0.481
Data, restraints, parameters	1322, 0, 95	1556, 12, 100
Goodness-of-fit on F^2	1.019	1.026
Final R indices [I>2sigma(I)]	R_1 = 0.0326 wR_2 = 0.0481	R_1 = 0.0207 wR_2 = 0.0501
R indices (all data)	R_1 = 0.0782 wR_2 = 0.0848	R_1 = 0.0264 wR_2 = 0.0531
Largest diff. peak and hole (e.Å^{-3})	0.43, -0.50	1.03, -1.07

[19] K. Brandenburg and H. Putz; DIAMOND, (2006). *Release 3.0e, Crystal Impact GbR*, Bonn, Germany.

4.3 Crystal Structure of Tetraethylammonium hexachlorido niobate(V) ($(Et_4N)[NbCl_6]$, (Nb_1))

The crystal structure of tetraethylammonium hexachloridoniobate(V) ($(Et_4N)[NbCl_6]$, (**Nb_1**)) was obtained during an attempt to investigate new stable Nb(V) synthons to be used in coordination reactions to *β*-diketonate ligands. Synthesis of **Nb_1** and the resulting yellow crystals obtained was discussed in Section 3.2.2. This title compound was previously prepared by Stewart *et al.*, with X-Ray diffraction data collected at room temperature (298 K). For this current investigation, this structural data was recollected at 100 K.[20]

A summary of the general crystallographic data is given in Table 4.1, while the numbering scheme of the complex is shown in the perspective drawing in Figure 4.1. Table 4.2 presents selected bond lengths and angles of **Nb_1**. Atomic coordinates, anisotropic displacement parameters, bond distances and angles and hydrogen coordinates, are given in the supplementary data (Appendix 1). Hydrogen atoms are omitted for clarity.

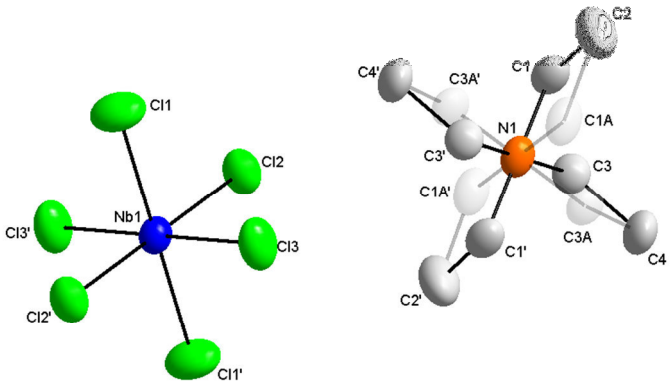

Figure 4.1: DIAMOND representation of the molecular structure of $(Et_4N)[NbCl_6]$ (**Nb_1**) displaying the atom numbering system. The two-position disorder (50 %:50 %) of the tetraethylammonium counter-ion is also illustrated. The displacement ellipsoids are drawn at a 50 % probability level. Hydrogen atoms omitted for clarity.

[20] B. Stewart, G. Koellner, K. Ruhlandt-Senge, F. Schmock and U. Muller, (1991). *Z. Anorg. Allg. Chem.* **593**, 160-168.

Nb_1 crystallizes in the monoclinic space group, $P2_1/c$ with Z = 2. The asymmetric unit of this structure consists of two moieties. A niobium(V) atom located on a crystallographic two-fold roto-inversion axis coordinated to three crystallographically independent chloride ligands (Cl1-Cl3) (Cl1'-Cl3' chloride ligands are generated by symmetry) and half a tetraethylammonium cation. This tetraethylammonium counter-ion is disordered over two positions in a 50 %:50 % ratio. The bond distances and angles are in accordance with similar structures.[20]

The coordination polyhedron around the niobium(V) metal centre has a minutely distorted octahedral geometry. *Cis*- Cl-Nb-Cl angles average 90.16 (1) º by symmetry and range from 89.75 (1) and 90.64 (1) º, while *trans*- Cl-Nb-Cl angles are at an ideal 180 º due to the symmetry. Nb-Cl distances vary between 2.343 (7) and 2.354 (7) Å. All bond distances and angles are in accordance with other relevant niobium(V) structures.[21,22]

Table 4.2 Selected geometric parameters for **Nb_1**.

Selected Bond Lengths (Å)			
Nb-Cl1	2.343(1)	Nb-Cl1'	2.343(1)
Nb-Cl2	2.348(1)	Nb-Cl2'	2.348(1)
Nb-Cl3	2.354(1)	Nb-Cl3'	2.354(1)
Selected Bond Angles (°)			
Cl1-Nb1-Cl2	89.75(1)	Cl1-Nb1-Cl1'	180.00
Cl1-Nb1-Cl3	90.14(1)	Cl2-Nb1-Cl2'	180.00
Cl2-Nb1-Cl3	90.64(1)	Cl3-Nb1-Cl3'	180.00

Figure 4.2 illustrates the crystal packing of **Nb_1**. When viewing the crystal structure along the a-axis a "head-to-tail" crystal packing structure can be observed. There are

[21] L. Herbst, R. Koen, A. Roodt and H. G. Visser, (2010). *Acta Cryst*., **E66**, m801-m802.

[22] D. B. Soria, J. Grundy, M. P. Coles and P. B. Hitchcock, (2005). *J. Organomet. Chem.,* **690**, 2278-2284.

no classical hydrogen bonds or intermolecular short contacts observed in the structure.

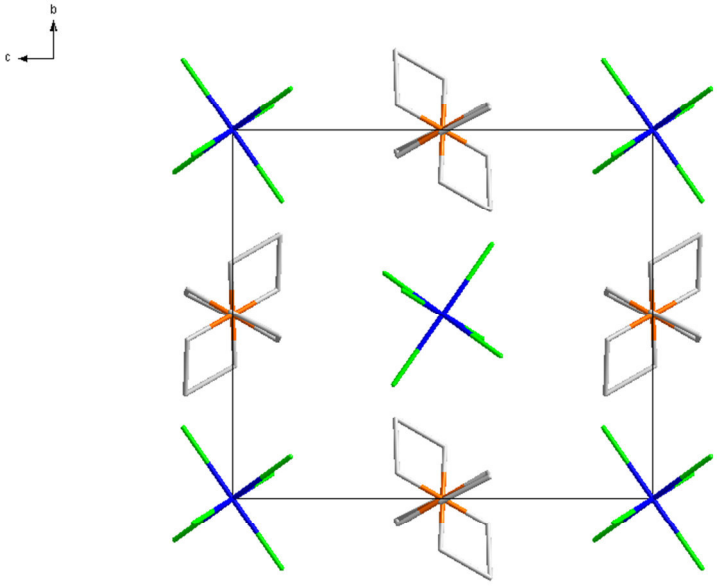

Figure 4.2 Packing of tetraethylammonium hexachloridoniobate(V) displaying the "head-to-tail" crystal packing when viewed along the a-axis. Hydrogen atoms have been omitted for clarity.

It has been mentioned that the crystal structure determination of the previously published complex $(NEt_4)[NbCl_6]$ was performed at room temperature (298 K) (**Nb_1A**), while the newly synthesized structure of **Nb_1** was determined at 100 K.[20] In addition, an analogous structure has been published by Cotton, *et al.* for a hexachloridoniobate(IV) compound ($(NEt_4)_2[NbCl_6]$, (**Nb_1B**)).[23] The crystallographic parameters of the various structures are compiled in Table 4.3. Tables 4.4 and 4.5 illustrate a comparison between bond angles and distances of the two published structures vs. the structure collected at 100 K.

[23] F. A. Cotton, M. P. Diebold and W. J. Roth, (1989). *Acta Cryst.,* **C46**, 1624-1627.

Table 4.3 Crystallographic details for the hexachloridoniobate(V) structures discussed in this section.

Crystal Formula	Nb_1 (100 K)	Nb_1A (298 K)[20]	Nb_1B (298 K)[23]
Empirical formula	$C_8H_{20}Cl_6N_1Nb$	$C_8H_{20}Cl_6N_1Nb$	$C_8H_{50}Cl_{14}N_2Nb$
Formula weight ($g.mol^{-1}$)	435.9	435.9	566.1
Crystal system, Space Group	Monoclinic, $P2_1/c$	Monoclinic, $P2_1/c$	Monoclinic, $P2_1/c$
a, b, c (Å)	7.213(4), 10.157(3) 12.675(3)	7.235(1), 10.180(2), 11.746(2)	13.206(3), 14.006(2), 14.366(4)
α, β, γ (°)	90, 114.166(4), 90	90, 100.07(4), 90	90, 90.67(2), 90
Volume ($Å^3$), Z	847.2(8), 2	851.7(3), 2	2657.2(2), 4
Density (calculated, Mg/m^3)	1.709	1.715	1.415

Table 4.4 Comparison of bond lengths for the hexachloridoniobate(V) structures discussed in this section

Nb_1 (100 K)		Nb_1A (298 K)[20]		Nb_1B (298 K)[23]	
Atoms	**Bond length (Å)**	**Atoms**	**Bond length (Å)**	**Atoms**	**Bond length (Å)**
Nb-Cl1	2.343(1)	Nb-Cl1	2.340(2)	Nb-Cl1	2.409(9)
Nb-Cl2	2.348(1)	Nb-Cl2	2.346(1)	Nb-Cl2	2.413(2)
Nb-Cl3	2.354(1)	Nb-Cl3	2.349(1)	Nb-Cl3	2.422(2)

Table 4.5 Comparison of bond angles for the hexachloridoniobate(V) structures discussed in this section

Nb_1 (100 K)		Nb_1A (298 K)[20]		Nb_1B (298 K)[23]	
Atoms	**Bond angle (°)**	**Atoms**	**Bond angle (°)**	**Atoms**	**Bond angle (°)**
Cl1-Nb1-Cl2	89.75(1)	Cl1-Nb1-Cl2	89.29(1)	Cl1-Nb1-Cl2	89.36(8)
Cl1-Nb1-Cl3	90.14(1)	Cl1-Nb1-Cl3	89.63(2)	Cl1-Nb1-Cl2	90.46(8)
Cl2-Nb1-Cl3	90.64(1)	Cl2-Nb1-Cl3	90.12(2)	Cl1-Nb1-Cl2	90.78(8)

Some very interesting observations can be made when comparing the crystallographic parameters of these structures. From the aforementioned data, it seems that **Nb_1** and **Nb_1A** correlate very well, barring some minor differences in

volume, density and bond lengths and angles. These anomalies could possibly be attributed to the lower thermal vibrations within the crystal lattice of **Nb_1**. The difference in volume strongly implies a crystallographic phase change has occurred as a result of temperature influence. In both cases the counter-ion is disordered over 2 positions in a 50 %:50 % ratio.

In the case of **Nb_1B**, more noticeable variances are observed when compared to the other structures. From this comparison it becomes obvious that that the chemical properties of the 4+ and 5+ oxidation states of niobium differ quite significantly. Structurally, a significant increase in Nb-Cl bond length is observed in the case of **Nb_1B**. This is indicative of a weaker Nb-Cl bond and a more labile chloride group. Theoretically this is an ideal property for a synthon to be used in coordination reactions as it simplifies chloride substitution. Unfortunately, as was mentioned in Chapter 2, naturally occurring niobium is predominately excavated in the 5+ oxidation state. Although it would seem favourable to investigate air-stable Nb(IV) synthons, this would be totally redundant for a separation study.

4.4 Crystal Structure of Tetraethylammonium hexachlorido tantalate(V) ($(Et_4N)[TaCl_6]$, (Ta_1))

The structure of tetraethylammonium hexachloridotantalate(V) ($(Et_4N)[TaCl_6]$, (**Ta_1**)) was obtained during an attempt to create new stable synthons to be used in bidentate ligand coordination reactions to Ta(V) metal centres. Synthesis of **Ta_1** and the resulting colourless crystals obtained was discussed in Section 3.2.1.

A summary of the general crystallographic data is given in Table 4.1, while the numbering scheme of the complex is shown in the perspective drawing in Figure 4.3. Table 4.5 presents selected bond lengths and angles of **Ta_1**. Atomic coordinates, anisotropic displacement parameters, bond distances and angles and hydrogen coordinates, are given in the supplementary data (Appendix 2). Hydrogen atoms are omitted for clarity.

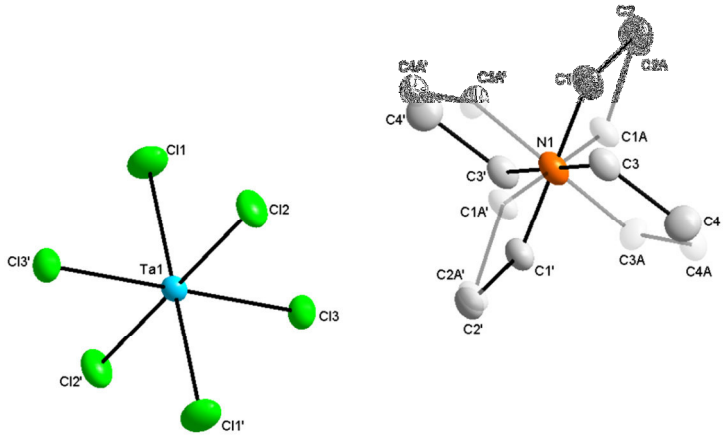

Figure 4.3 DIAMOND representation of the molecular structure of $(Et_4N)[TaCl_6]$ (**Ta_1**) displaying the atom numbering system. The two-position disorder (50 %:50 %) of the tetraethylammonium counter-ion is also illustrated. The displacement ellipsoids are drawn at a 50 % probability level. Hydrogen atoms omitted for clarity.

Ta_1 crystallizes in the monoclinic space group, $P2_1/c$ with Z = 2. The asymmetric unit of this structure consists of two moieties. A tantalum(V) atom located on a crystallographic two-fold roto-inversion axis coordinated to three crystallographically independent chloride ligands (Cl1-Cl3) (Cl1'-Cl3' chloride ligands are generated by symmetry) and half a tetraethylammonium cation disordered over two positions in a 50 %:50 % ratio.

The coordination polyhedron around the tantalum(V) metal centre shows a slightly distorted octahedral geometry. *Cis*- Cl-Ta-Cl angles average 90.31 (1) º by symmetry and range from 90.19 (1) and 90.56 (1) º, while *trans*- Cl-Ta-Cl angles are at 180 º as required by the symmetry. Ta-Cl distances vary between 2.343 (7) and 2.353 (7) Å.

Table 4.5 Selected geometric parameters for **Ta_1**.

Selected Bond Lengths (Å)			
Ta-Cl1	2.343(1)	Ta-Cl1'	2.343(1)
Ta-Cl2	2.345(1)	Ta-Cl2'	2.345(1)
Ta-Cl3	2.353(1)	Ta-Cl3'	2.353(1)
Selected Bond Angles (°)			
Cl1-Ta1-Cl2	90.19(1)	Cl1-Ta1-Cl1'	180.00
Cl1-Ta1-Cl3	90.19(1)	Cl2-Ta1-Cl2'	180.00
Cl2-Ta1-Cl3	90.56(1)	Cl3-Ta1-Cl3'	180.00

Figure 4.4 illustrates the crystal packing of **Ta_1**. When viewing the crystal structure along the a-axis a "head-to-tail" crystal packing structure can be observed. There are no classical hydrogen bonds or intermolecular short contacts observed in the structure.

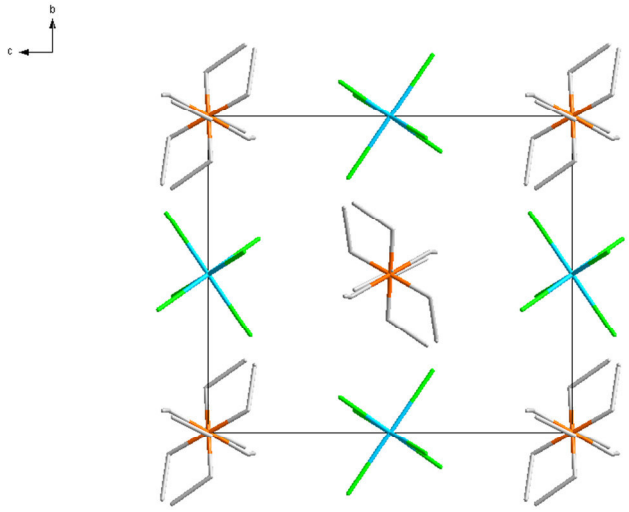

Figure 4.4 Packing of tetraethylammonium hexachloridotantalate(V) displaying the "head-to-tail" crystal packing when viewed along the a-axis. Hydrogen atoms have been omitted for clarity.

4.5 Discussion

Various aspects influence the efficiency of a new precursor which may be suitable for Nb(V)- and Ta(V)-*β*-diketonato complex formation. Factors such as synthon stability, longer (weaker) metal-chlorido bond interactions and cost effectiveness all contribute and must be evaluated individually to select the ideal synthon. For this comparative study various tetraalkylammonium counter-ions were selected as these compounds are relatively inexpensive and will be discussed. Examples include tetramethylammonium (TMA), tetraethylammonium (TEA), tetrapropylammonium (TPA), tetrabutylammonium (TBA) and trimethylbenzoylammounium (TMBA).[20,24,25] A systematic evaluation of all of the aforementioned synthon properties will follow and a selection made for the ideal Nb(V)- and Ta(V)-precursor to continue this separation study. The structures selected were obtained from this study, as well as the Cambridge Crystallographic Database.[26]

4.5.1 Stability of Synthon in Atmospheric Conditions

The air-stability of a precursor is a relative grey area as quantification of this property is very ambiguous. Some of the literature reports on tetraalkylammonium hexachloroniobate(V) (**(TAA)[$NbCl_6$]**) synthons mention that these compounds can remain stable for hours (TMBA) to days (TPA) to weeks (TBA). Even though this can give a general idea of stability, quantitative results are however required.[20,24,25]

Accordingly, a crystallographic comparison of the inter- and intra-molecular forces within the crystal lattice (stabilization forces) between the various compounds might shed some light on the problem. Table 4.6 illustrates a comparison of these forces for the various **(TAA)[$NbCl_6$]** compounds.

[24] K. Stumpf, R. Blachnik, H. Reuter and H. Eickmeier, (1998). *Z. Cryst. NCS*., **213**, 155-156.

[25] B. Tinant, D. Boyet and M. De Villiers, (2004). *Z. Cryst. NCS*., **219**, 381-382.

Table 4.6: Illustration of the intermolecular stabilization forces for **(Pr_4N)[$NbCl_6$]** (TPA), **(Bu_4N)[$NbCl_6$].** (TBA) and **(Me_3PhN)[$NbCl_6$]** (TMBA).[20,24,25]

(Pr_4N)[$NbCl_6$] (298K)			(Bu_4N)[$NbCl_6$] (298K)			(Me_3PhN)[$NbCl_6$] (298K)		
Atoms	**Symmetry code**	**Distance (Å)**	**Atoms**	**Symmetry code**	**Distance (Å)**	**Atoms**	**Symmetry code**	**Distance (Å)**
Cl3⋯H36	*x,y,z*	2.680(1)	Cl1⋯H2	*x,y,z*	2.883(1)	Cl1⋯H3	*1+x,y,z*	2.948(1)
Cl3'⋯H31	*x,y,z*	2.912(2)	Cl2⋯H23	*x,y,1+z*	2.860(2)	Cl3⋯H7A	*-x,-y,1-z*	2.927(1)
Cl1⋯H28	*x,1+y,z*	2.828(2)	Cl3'⋯H36	*1-x,1-y,1-z*	2.815(2)	Cl3⋯H15	*-x,-y,1-z*	3.416(1)
Cl3⋯H11	*1+x,y,z*	2.866(1)	Cl3⋯H15	*-½+x,½-y,½+z*	2.868(2)			
Cl3⋯H35	*1-x,1-y,1-z*	2.893(1)	Cl1'⋯H9	*½+x,½ -y,½ +z*	2.874(1)			

* CIF data obtained from Cambridge crystallographic database.[26]

Table 4.6 illustrates that the stabilization of the compact conformation of the cation/anion is found to be more pronounced as the length of the apolar TAA counter-ion chain increases.[27] These counter-ions fill the void between the $NbCl_6^-$ moieties effectively and the hydrophobic chains seemingly shield the metal centres against hydrolization. This would explain why these types of compounds are more stable than the dinuclear $[NbCl_5]_2$ counterpart, which has no intermolecular stabilization interactions.[25]

As was mentioned in Section 4.3, no significant inter-molecular forces were found in the structure of (NEt_4)[$NbCl_6$], yet it is still stable enough to form crystals and not decompose within seconds. This is assumed to be linked to the non-polar chain shielding of the metal centre. The lack of interactions also explains why (NEt_4)[$NbCl_6$] is not as air-stable as (Pr_4N)[$NbCl_6$], (Bu_4N)[$NbCl_6$] and (Me_3PhN)[$NbCl_6$]. In the case of (NMe_4)[$NbCl_6$] no crystal structure has ever been obtained. It thus seems that the hydrophobic arm lengths of the counter-ion do not sufficiently shield the metal centre against hydrolization.

[26] Cambridge Structural Database (CSD) Version 5.35, November 2013 update. F.H. Allen, (2002). *Acta Cryst.*, **B58**, 380-388.

[27] K. Jayant, H. N Singh, A. G. MacDiarmid and T. Sukant, (2002). *Handbook of Polyelectrolytes and Their Applications*, **3**, American Scientific Publishers, Washington, United States of America.

When considering all the data in this section it would seem that from a stability point of view that $(Bu_4N)[NbCl_6]$ would be precursor of choice closely followed by $(Pr_4N)[NbCl_6]$ and $(Et_4N)[NbCl_6]$.

4.5.2 Niobium-Chlorido Bond Length

In solution, the lability of the chlorido groups on the $NbCl_6^-$ moiety correlates directly to the ease with which and entering *β*-diketonate can substitute these groups.[28] In theory, the ideal precursor should have weaker metal chlorido interactions as less energy is required to break such a bond. A quantitative perspective of this property can be related to niobium-chloride bond distances in the solid state. Table 4.7 is a comparative table of the bond lengths of the synthons that are under investigation.

Table 4.7: Comparison of Nb-Cl bond distances for **$(NEt_4)[NbCl_6]$** (TEA), **$(Pr_4N)[NbCl_6]$** (TPA), **$(Bu_4N)[NbCl_6]$** (TBA) and **$(Me_3PhN)[NbCl_6]$** (TMBA).[20,24,25]

Atoms	**Nb_1**	**$(Pr_4N)[NbCl_6]$**	**$(But_4N)[NbCl_6]$**	**$(Me_3PhN)[NbCl_6]$**
Bond length (Å)	**(100 K)**	**(298K)**	**(298K)**	**(298K)**
Nb-Cl1	2.343(1)	2.336(1)	2.329(2)	2.344(1)
Nb-Cl2	2.348(1)	2.353(1)	2.356(2)	2.345(1)
Nb-Cl3	2.354(1)	2.358(1)	2.359(2)	2.346(1)

Ideally, longer metal-chlorido bond distances relate to a weaker interaction and thus a more effective synthon for the replacement of the Cl^- ligands. From Table 4.7 it becomes quite obvious that the selection of TAA-counter ion has no effect on the Nb-Cl bond lengths with all distances ranging within 2.329(2) – 2.359 (2) Å. Accordingly, it seems that the "lability" of a chlorido-group is independent from selected counter-ion.

[28] R. A. Scott and C. M. Lukehart, (2007). *Applications of Physical Methods to Inorganic and Bioinorganic Chemistry*, **1**, John Wiley & Sons, Sussex, United Kingdom.

4.6 Conclusion

When all the above mentioned aspects of this crystallographic and literature studies are systematically considered an effective selection of a good synthon for *β*-diketonate coordination can be made. In the case of the Nb(V) metal centre it seems that the three realistic options are $(Et_4N)[NbCl_6]$, $(Pr_4N)[NbCl_6]$ and $(Bu_4N)[NbCl_6]$.

From a stability point of view it indicates that $(Bu_4N)[NbCl_6]$ will be the preferred choice. However, an in-depth literature study revealed that no Nb(V)-*β*-diketonate complexes have ever been isolated as a tetrabutylammonium salt. In contrast, the tetraethylammonium counter-ion has yielded some success, with a *mer*-trichloridooxido(thenoyltrifluoroacetylacetonato-κ^2O,O')niobate(V) complex being obtained and characterized.[29] Therefore, in the case of these Nb(V) ionic systems it seems that the physical stability of $(Pr_4N)[NbCl_6]$ and $(Bu_4N)[NbCl_6]$ is found to be a slight hindrance during complex formation and $(Et_4N)[NbCl_6]$ is the synthon of choice.

Due to a lack of scientific information, the case of selection of the ideal Ta(V) analogue is more problematic. There is no crystallographic data in literature to structurally compare the compound as was investigated with the Nb(V) metal centre. Accordingly, for the sake of the comparative approach of this study, the $(Et_4N)[TaCl_6]$ synthon is selected by default.

As has been mentioned, the comparison of analogous Ta(V)- and Nb(V)-*β*-diketonate would give better insight into the solid state physical and electronic characteristics of these systems. Accordingly, the next two chapters will deal with crystallographic studies to investigate the influence of varying substituting groups on the *β*-diketone backbone on the complexes.

In the following chapter four niobium-*β*-diketonate complexes are reported, structurally evaluated and described. The results presented will be discussed later in a more overarching and detailed manner with regard formation kinetics a reported in in Chapter 8.

[29] J. Daran, Y. Jeanin, J. E. Guerchais and R. Kergoat, (1979). *Inorg Chim Acta*, **33**, 81-86.

Chapter 5: Crystallographic Evaluation of [$NbOCl_3$(*β*-diket)] Complexes (1)

5.1 Overview

β-diketone bidentate ligands are used widely as a type of conjugated ligand system in organometallic chemistry. These ligand systems are very useful because of its highly coordinative nature, good solubility but also due to the ability to be functionalized with various substituents on the carbonyl carbons.[1] Ability to 'tweak' these substituents could be very useful for enhancing small differences in coordination between tantalum and niobium complexes for separation purposes. When attempting to find a unique chemical state difference, it is crucial to investigate metal compounds with ligand types, which allow for effective and accurate characterization and evaluation of these metal complexes.[2]

An integral part of this project has been focused on employing different commercially available *β*-diketone ligands, with various substituents on the acetylacetone (acacH) back-bone and coordinating these systems to Nb(V) and Ta(V) metal centres. The substituents alter the electronic characteristics of the ligand as a whole, influencing the chelation and stabilization aspects of the final organometallic complex. *β*-diketones with fluorinated functionalities form a significant part of the interest in this

[1] J. A. Viljoen, (2009). *Speciation and Interconversion Mechanism of Mixed Halo O,O'- and N,O-Bidentate Ligand Complexes of Hafnium.* M.Sc. Dissertation, University of the Free State.

[2] A. Agulyansky, (2004). *The Chemistry of Tantalum and Niobium Fluoride Compounds*, CRC Press, Boca Raton, United States of America.

investigation and properties that govern ligand selection was be discussed in Section 2.3.1.3.[3,4,5,6,7,8]

Furthermore, when considering the limited database entries for these types of Nb(V) and Ta(V) complexes that have been structurally characterized, it becomes apparent that a crystallographic study of metal complexes containing this ligand family could shed considerable light on characteristics of complexes and thus on experimental design regarding possible separation studies utilizing such ligands.[9]

5.2 Introduction

The discussion in Chapter 2 underlined that fluorinated *β*-diketones exhibits or introduces potentially favourable properties for both sublimation separation as well as solvent extraction. Some of the characteristics that govern these properties (both intramolecular and intermolecular interactions, bond distances and bond angles) can be studied by a detailed crystallographic investigation of the various complexes. The coordinating ligands that were utilized for coordination to the stable Nb(V) synthon yielding appropriate complexes of which the solid state structures are reported in this chapter, are illustrated in Figure 5.1.

[3] A. Chauvin, F. Gumy, I. Matsubayashi, Y. Hasegawa and J. G. Bunzli, (2006). *Eur. J. Inorg.*, **2**, 473-480.

[4] A. C. du Preez and J. S. Preston, (2004). *S.A.I.M.M.*, **1**, 333-338.

[5] H. O. Davies, T. J. Leedlam and A. C. Jones, (1999). *Polyhedron*, **18**. 3165-3172.

[6] P. Wendrup and V. G. Kessler, (2001). *J. Chem. Soc., Dalton Trans*, 574-579.

[7] E. L. Lippert and M. R. Truter, (1960). *J. Chem. Soc. A.*, **33**, 309-311.

[8] G. J. Bullen, R. Mason and P. Pauling, (1965). *Inorg Chem.*, **4**, 456-461.

[9] Cambridge Structural Database (CSD) Version 5.35, November 2013 update. F.H. Allen, (2002). *Acta Cryst*., **B58**, 380-388.

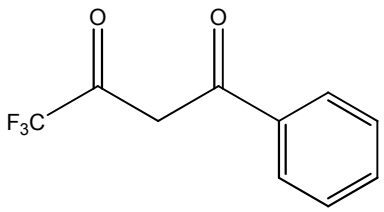

4,4,4-Trifluoro-1-phenyl-1,3-butanedione
(btfaH)

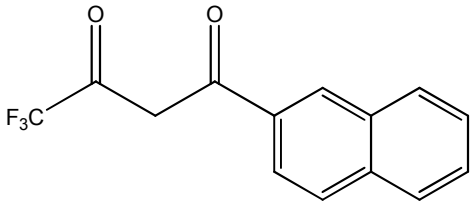

4,4,4-Trifluoro-1-(2-naphtyl)-1,3-butanedione
(ntfaH)

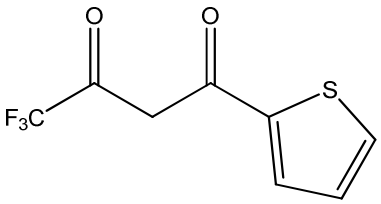

4,4,4-Trifluoro-1-(2-thienyl)-1,3-butanedione
(ttfaH)

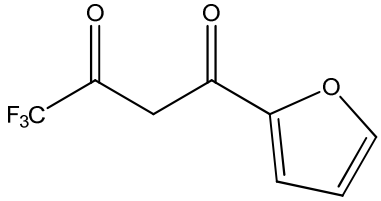

4,4,4-Trifluoro-1-(2-furyl)-1,3-butanedione
(tffaH)

Figure 5.1 An Illustration of the *β*-diketones coordinated to the Nb(V)-synthon in this chapter.

This chapter will focus on the crystal structures of four niobium(V) complexes obtained in the study; tetraethylammonium *mer*-trichloridooxido (thenoyltrifluoroacetylacetonato-κ^2O,O')niobate(V) ($(NEt_4)[NbOCl_3(ttfa)]$), (**Nb_2**)), tetraethylammonium *mer*-trichlorido(furyltrifluoroacetylacetonato-κ^2O,O')oxido niobate(V) ($(NEt_4)[NbOCl_3(tffa)]$), (**Nb_3**), tetraethylammonium *mer*-(benzoyltrifluoro acetylacetonato-κ^2O,O')trichloridooxidoniobate(V) ($(NEt_4)[NbOCl_3(btfa)]$), (**Nb_4**) and tetraethylammonium *mer*-trichlorido(naphtyltrifluoroacetylacetonato-κ^2O,O')oxido niobate(V) ($(NEt_4)[NbOCl_3(ntfa)]$), (**Nb_5**)). Emphasis will be placed on the solid state structural data of the above mentioned complexes with special attention given to general molecular geometry and intermolecular interactions that contribute to the stability of the crystal packing. Geometric parameters such as the bond distances and angles in the molecules will also be highlighted.

For this study, the dihedral angle within the ligand, where appropriate, is defined as the angle between the plane running through the aromatic ring of the *β*-diketonato substituent and the plane which runs through the O1-C2-C3-C4-O2 backbone of the *β*-diketonato ligand. This is illustrated in Figure 5.2.

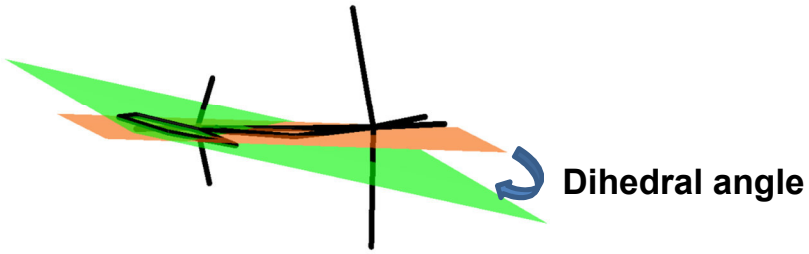

Figure 5.2 Illustration of the dihedral angle.

The out-of-plane *β*-diketonate ligand bend is defined as; the angle between the plane that runs through the O1, O2 and Nb1 atoms and the O1, C2, C3, C4 plane which runs through backbone of the *β*-diketonato ligand. This is illustrated in Figure 5.3.

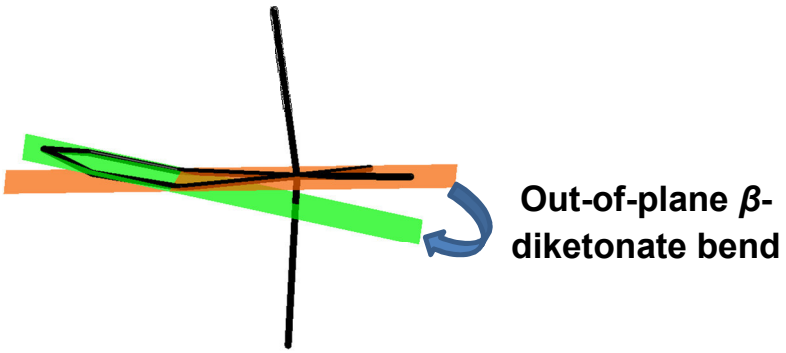

Figure 5.3 Illustration of the out-of-plane *β*-diketonate bend.

Finally, the axial plane illustrating the out-of-plane distortion is defined by; a coordination plane constructed through atoms, Cl1, Cl2, Cl3 and O1 and measuring the distance that the Nb(V) atom is shifted out of this plane.

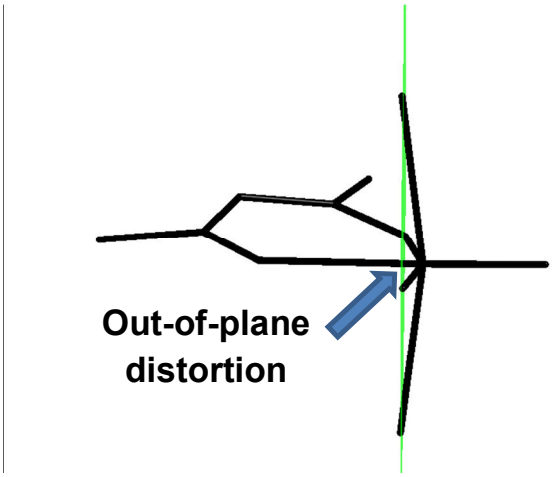

Figure 5.4 Side view of the axial plane illustrating the out-of-plane distortion.

5.3 Experimental

The X-Ray intensity data was collected on a Bruker X8 ApexII 4K Kappa CCD area detector diffractometer, equipped with a graphite monochromator and Mo*Kα* fine-focus sealed tube (*λ* = 0.71069 Å, T = 100(2) K) operated at 2.0 kW (50 kV, 40 mA). The initial unit cell determinations and data collections were done by the SMART software package.[10] The collected frames were integrated using a narrow-frame integration algorithm and reduced with the Bruker SAINT-Plus and XPREP software packages respectively.[11] Analysis of the data showed no significant decay during the data collection. Data was corrected for absorption effects using the multi-scan technique SADABS, and the structure was solved by the direct methods package SIR97 and refined using the WinGX software incorporating SHELXL.[12,13,14,15] The

[10] Bruker SMART-NT Version 5.050, (1998). *Bruker AXS Inc. Area-Detector Software Package*; Madison, Winconsin, United States of America**.**

[11] Bruker SAINT-Plus Version 6.02 (including XPREP), (1999). *Bruker AXS Inc. Area-Detector Integration Software*, Madison, Winconson, United States of America.

[12] Bruker SADABS Version 2004/1, (1998). *Bruker AXS Inc. Area Detector Absorption Correction Software*, Madison, Wisconsin, United States of America.

[13] A. Altomare, M. C. Burla, M. Camalli, G. L. Cascarano, C. Giacovazzo, A. Guagliardi, A. G. G. Moliterni, G. Polidori and R. Spagna, (1999). *J. Appl. Cryst.,* **32**, 115-119.

[14] L. J. Farrugia, (1999). *J. Appl. Cryst.* **32**, 837-838.

[15] G.M. Sheldrick; SHELXL97, (1997). *Program for crystal structure refinement*, University of Göttingen, Germany.

final anisotropic full-matrix least-squares refinement was done on F^2. The methyl and aromatic protons were placed in geometrically idealized positions (C–H = 0.93 – 0.98 Å) and constrained to ride on their respective parent atoms with $U_{iso}(H) = 1.2U_{eq}(C)$. Non-hydrogen atoms were refined with anisotropic displacement parameters. The graphics were obtained with the DIAMOND program with 50% probability ellipsoids for all non-hydrogen atoms.[16]

[16] K. Brandenburg and H. Putz; DIAMOND, (2006). *Release 3.0e, Crystal Impact GbR*, Bonn, Germany.

Table 5.1 Crystallographic and refinement details for structures discussed in this chapter.

Crystal Formula	$(NEt_4)[NbOCl_3(ttfa)]$ (Nb_2)	$(NEt_4)[NbOCl_3(tffa)]$ (Nb_3)	$(NEt_4)[NbOCl_3(btfa)]$ (Nb_4)	$(NEt_4)[NbOCl_3(ntfa)]$ (Nb_5)
Empirical formula	$C_{16}H_{24}Cl_3F_3N_1Nb_1O_3S$	$C_{16}H_{24}Cl_3F_3N_1Nb_1O_4$	$C_{18}H_{26}Cl_3F_3N_1Nb_1O_3$	$C_{22}H_{28}Cl_3F_3N_1Nb_1O_3$
Formula weight ($g.mol^{-1}$)	566.68	550.63	558.72	608.24
Crystal system, Space Group	Monoclinic, $P2_1/c$	Monoclinic, $P2_1/c$	Monoclinic, $P2_1/c$	Triclinic, $P\bar{1}$
***a, b, c* (Å)**	11.483(3), 12.563(3), 17.110(3)	11.132(3), 12.246(3), 17.003(3)	11.349(4), 12.468(3), 17.676(4)	8.234(3), 11.461(3), 14.350(4)
α, β, γ (°)	90, 100.83(1), 90	90, 101.55(1), 90	90, 101.40(1), 90	94.73(1), 103.14(1), 92.38(1)
Volume ($Å^3$), Z	2424.3(16), 4	2271.0(15), 4	2451.8(16), 4	1311.7(11), 2
Density (calculated, Mg/m^3)	1.553	1.610	1.509	1.540
Crystal colour	Yellow	Yellow	Yellow	Yellow
Crystal size (mm^3)	0.59 x 0.39 x 0.21	0.45 x 0.16 x 0.15	0.61 x 0.25 x 0.19	0.30 x 0.18 x 0.13
Absorption coefficient μ (mm^{-1}), F(000)	0.951, 1144	0.928, 1112	0.857,1131	0.808, 617
Theta range	2.66 – 27.99°	2.50 – 28.17°	2.45 – 27.99°	2.93 – 24.45°
Index ranges	-16<=h<=15, -15<=k<=15, -22<=l<=22	-16<=h<=15, -14<=k<=11, -22<=l<=22	-16<=h<=16, -14<=k<=14, -23<=l<=23	-10<=h<=10, -15<=k<=15, -18<=l<=18
Reflections collected, Independent Reflections, R_{int}	5834, 5209, 0.0574	5689, 4721, 0.0475	5912, 4248, 0.0474	6324, 3184, 0.0794
Completeness to 2θ (°, %)	27.99, 99.6	27.99, 99.9	27.99, 99.9	27.99, 97.7
Max. and min. transmission	0.750 and 0.412	0.777 and 0.442	0.848 and 0.772	0.803 and 0.667
Data, restraints, parameters	18884, 894, 501	20177, 0, 276	19971, 30, 260	22105, 0, 313
Goodness-of-fit on F^2	1.098	1.120	1.060	0.975
Final R indices [I>2sigma(I)]	R_1 = 0.0260 wR_2 = 0.0740	R_1 = 0.0510 wR_2 = 0.1304	R_1 = 0.0733 wR_2 = 0.1829	R_1 = 0.0924 wR_2 = 0.1707
R indices (all data)	R_1 = 0.0303 wR_2 = 0.0796	R_1 = 0.0641 wR_2 = 0.1516	R_1 = 0.0992 wR_2 = 0.2072	R_1 = 0.1585 wR_2 = 0.2274
Largest diff. peak and hole ($e.Å^{-3}$)	0.583, -0.583	1.010, -1.281	1.242, -1.202	0.880, -1.249

5.4 Crystal Structure of Tetraethylammonium *mer*-trichlorido oxido(thenoyltrifluoroacetylacetonato-κ^2*O,O'*)niobate(V) ($(NEt_4)[NbOCl_3(ttfa)]$), (Nb_2))

The crystal structure of tetraethylammonium *mer*-trichloridooxido(thenoyl trifluoroacetylacetonato-κ^2O,O')niobate(V) ($(NEt_4)[NbOCl_3(ttfa)]$ (**Nb_2**)) forms part of an investigation which focuses on studying applied ligand chelation effects on novel Ta(V)- and Nb(V)-compounds. Synthesis of **Nb_2** and the resulting yellow crystals obtained, were discussed in Section 3.3.1.1. The title compound was previously prepared by Daran *et al*., with X-ray diffraction data collected at room temperature. For this study, the reaction procedure was modified as described in above and the data collected at 100K.[17]

A summary of the general crystallographic data is given in Table 5.1, while the numbering scheme of the complex is shown in the perspective drawing in Figure 5.5. Tables 5.2 and 5.3 present selected bond lengths and angles of **Nb_2**. Atomic coordinates, anisotropic displacement parameters, bond distances and angles and hydrogen coordinates, are given in the supplementary data (Appendix 3). Counter-ions and hydrogen atoms are omitted for clarity.

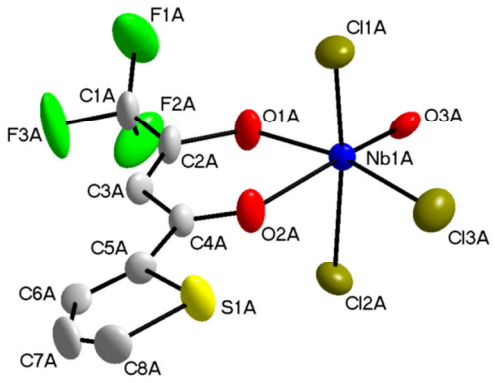

Figure 5.5 DIAMOND representation of the complex structure of $[NbOCl_3(ttfa)]^-$ (**Nb_2**) displaying the atom numbering system. The displacement ellipsoids are drawn at a 50 % probability level. Hydrogen atoms and counter-ion are omitted for clarity.

[17] J. Daran, Y. Jeanin, J. E. Guerchais and R. Kergoat, (1979). *Inorg Chim Acta*, **33**, 81-86.

Nb_2 crystallizes in the monoclinic space group, $P2_1/c$, with four $(NEt_4)[NbOCl_3(ttfa)]$ entities in the unit cell (Z = 4). The asymmetric unit consists of a Nb(V) metal centre coordinated to three crystallographically independent chlorido groups (Cl1A – Cl3A), an oxido group (O3A), one *O,O′*-bonded thenoyltrifluoroacetonato ligand and a tetraethylammonium cation. The complex molecule and the counter-ion are disordered over two positions in a 50 ***Nb^A*** *(red)*: 50 ***Nb^B*** *(blue)* ratio as shown in Figure 5.6.

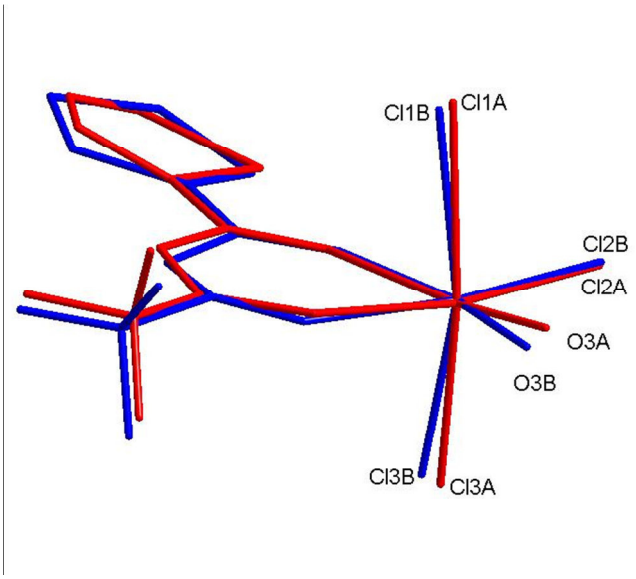

Figure 5.6 Graphic illustration of the *mer*-$[NbOCl_3(ttfa)]^-$ anion illustrating the disorder in an overlay. (**red**) ***Nb^A*** = 50.0%; (**blue**) ***Nb^B*** = 50.0%. Hydrogen atoms and counter-ion omitted for clarity.

The coordination polyhedron around the niobium(V) metal centre has a distorted octahedral geometry for both ***Nb^A*** and ***Nb^B*** structures. Several characteristics, including bond distances and angles, illustrate this inequality. Selected bond lengths and bond angles are for ***Nb^A*** and ***Nb^B*** are listed in Table 5.2 and 5.3.

Table 5.2 Selected bond lengths of the two disordered parts in the *mer*-$[NbOCl_3(ttfa)]^-$ anion, denoted by ***Nb^A*** **a**nd ***Nb^B***.

Nb^A		***Nb^B***	
Atoms	**Bond length (Å)**	**Atoms**	**Bond length (Å)**
Nb1A-Cl1A	2.507(1)	Nb1B-Cl1B	2.373(1)
Nb1A-Cl2A	2.390(1)	Nb1B-Cl2B	2.389(1)
Nb1A-Cl3A	2.428(1)	Nb1B-Cl3B	2.339(1)
Nb1A-O1A	2.037(1)	Nb1B-O1B	2.095(1)
Nb1A-O2A	2.357(1)	Nb1B-O2B	2.254(1)
Nb1A-O3A	1.733(1)	Nb1B-O3B	1.745(1)
O1···O2[a]	2.779(1)	O1···O2[a]	2.787(1)
Out-of-plane distortion[b]	0.275(1)	Out-of-plane distortion[b]	0.270(1)

[a] Bite atom distance; [b] Out-of-plane distortion illustrated in Figure 5.4.

Table 5.3 Selected bond angles of the two disordered parts in the title compound *mer*-$[NbOCl_3(ttfa)]$, denoted by ***Nb^A*** and ***Nb^B***.

Nb^A		***Nb^B***	
Atoms	**Bond angle (º)**	**Atoms**	**Bond angle (º)**
O1A-Nb1A-O2A	79.65(1)	O1B-Nb1B-O2B	76.82(1)
Cl2A-Nb1A-O3A	96.28(1)	Cl2B-Nb1B-O3B	103.50(2)
O2A-Nb1A-O3A	171.69(2)	O2B-Nb1B-O3B	166.36(2)
Cl1A-Nb1A-O2A	163.58(1)	Cl1B-Nb1B-O2B	166.38(1)
Cl2A-Nb1A-Cl3A	168.11(1)	Cl2B-Nb1B-Cl3B	160.12(1)
C2A-C3A-C4A	120.60(2)	C2B-C3B-C4B	120.99(2)
Dihedral Angle[a]	17.27(1)	Dihedral Angle[a]	17.68(1)

[a] Out-of-plane *β*-diketonate ligand bend illustrated in Figure 5.3.

i) Nb-Cl_{axial} distances for ***Nb^A*** are 2.428(1) and 2.507(1) Å, while the equatorial Nb1A-Cl3A and Nb1A-O3A bonds have distances of 2.390(1) and 1.733(1) Å respectively. Comparison of the Nb1A-O1A and Nb1A-O2A bond lengths of the coordinated *β*-diketone, revealed distances of 2.357(1) vs. 2.037(1) Å. The Nb1A-O2A bond (*trans* to the oxido) is thus more than 0.3 Å longer than the Nb1A-O1A (*trans* to the chlorido), underlining the trans influence of the oxido ligand. The corresponding influence in the ***Nb^B*** fragment is less significant, i.e. 2.095(1) Å *vs.* 2.254 (1) Å (Δ = 0.2 Å) between Nb1B-O2B and Nb1B-O1B. The difference in the ***Nb^A*** and ***Nb^B***

fragments in particular with respect to the linear O=Nb-O_B-moeities, cannot be explained currently. This also holds for the Nb-Cl distances, which vary significantly in the ***Nb^A*** and ***Nb^B*** fragments (see Table 5.2). Distortion from ideal octahedral geometry is further highlighted when considering the 0.275(1) Å out-of-plane distortion of the niobium metal centre.

ii) The *trans* Cl2-Nb1-Cl3 angle is 168.11(1) º, while the O1-Nb1-O2 bite angle is 79.65(1) º. Quantification of the out-of-plane bend was achieved by measuring the angle between the O1A, O2A and Nb1A plane and the O1A, C2A, C3A, C4A plane which revealed a 1.68(1) º out-of-plane bend of the coordinated ligand. The ***Nb^B*** fragment revealed a 1.55(1) º out-of-plane bend.

When constructing an equatorial plane through O1, O2, O3 and Cl3, it was observed that upon exclusion the thenoyl and CF_3 substituents, most of the atoms lie either in or just slightly off this plane. A dihedral angle of 15.53(1)° between the thenoyl ring and plane constructed through O3A-C3A-C4A-C5A-O4A atoms was noted.

Halogen interactions involving the Cl2 atom of **Nb_2** is encountered in the crystal lattice. This notion of intermolecular bonding was based on the theory that halogen bonds originate through the interactions of a positively charged σ-hole present on a halogen atom with negative sites of nucleophiles.[18] Halogen bonding is typically encountered bond angles of approximately 180° between donor and acceptor sites. This holds true except in cases where secondary interactions are found to disrupt this arrangement.[19]

The halogen bond between molecules of **Nb_2** is illustrated in Figure 5.7 and data related to the interaction given in Table 5.4. These interactions result in the formation

[18] J. P. M. Lommerse, A. J. Stone, R. Taylor and F. H. Allen, (1996). *J. Am. Chem. Soc.*, **118**, 3108-3116.

[19] P. Metrangola, J. S. Murray, T. Pilati, P. Politzer, G. Resnatti and G. Terraneo, (2011). *Cryst. Growth Des.*, **11**, 4238-4246.

of a pseudo-dimeric complex species. In particular if the fact that each Nb site is further occupied by a 50 % packing type as defined by ***Nb^A^*** and ***Nb^B^***. This tightly knit two-dimensional interaction network rigidly ties the crystal lattice together, influencing the overall packing in pairs of these two niobium molecules dispersed in a head-to-tail packing fashion throughout the system. Two soft contacts were also observed between Cl2A and H6A and Cl2A and H3A atoms which further ensure the stabilization of the crystal lattice. This interaction for ***Nb^A^*** is also illustrated in Figure 5.7 and data related to the non-classical hydrogen bonds is given in Table 5.5. A near identical set of interactions were observed for the ***Nb^B^*** fragment.

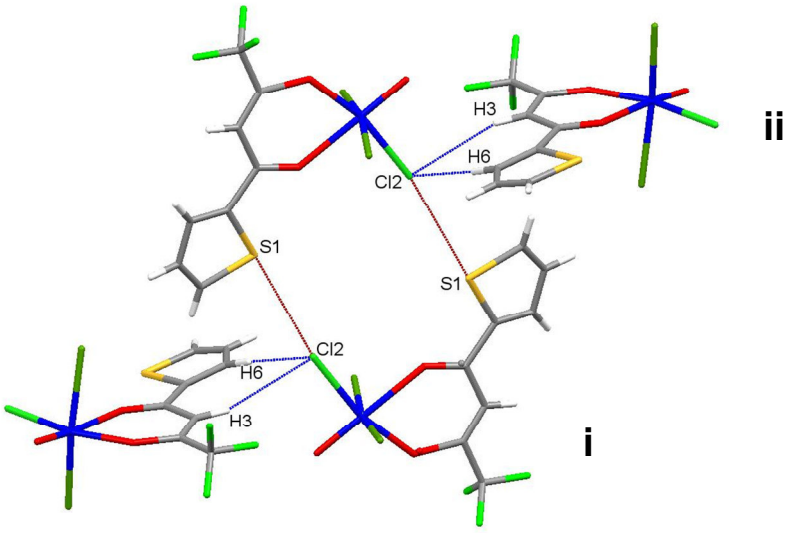

Figure 5.7 A graphic illustration of the halogen bond (indicated in red) connects neighbouring molecules of the ***Nb^A^*** fragment of **Nb_2** forming a pseudo-dimeric complex in a "head-to-tail" motif and the stabilizing hydrogen bonds (indicated in blue).

Table 5.4 Halogen bond geometry for **Nb_2** as depicted in Figure 5.7.

D-Cl···S	dNb-Cl (Å)	dCl···S (Å)	dNb···S (Å)	Angle Nb-Cl···S (°)
Nb1A-Cl2A···S1A^{i}	2.405(1)	3.457(1)	5.795(1)	162.33(1)

Symmetry code: i) *x, ½-y, ½-z.*

Table 5.5 Hydrogen bond geometry for **Nb_2** as depicted in Figure 5.7.

C-H···Cl	dC-H (Å)	dH···Cl (Å)	dC···Cl (Å)	Angle C-H···Cl (°)
C6A-H6A···Cl2A^{i}	0.930(1)	2.724(1)	3.652(1)	176.35(3)
C3A-H3A···Cl2A^{ii}	0.930(1)	2.942(1)	3.835(1)	131.41(2)

Symmetry code: i) *1-x, y, 1-z; ii) x, ½-y, ½+z.*

An illustration of the crystal lattice packing of **Nb_2** is given in Figure 5.8. When viewing the crystal structure along the c-axis the "head-to-tail" crystal packing structure due to the intermolecular interactions can be observed. It is also noticed that the cavities between the Nb(V) moieties are filled by the tetraethylammonium ($(NEt_4)^+$) counter ions. These cavities are relatively large with relation to the counter ion and leaves sufficient space for the disordered nature of the $(NEt_4)^+$ cation.

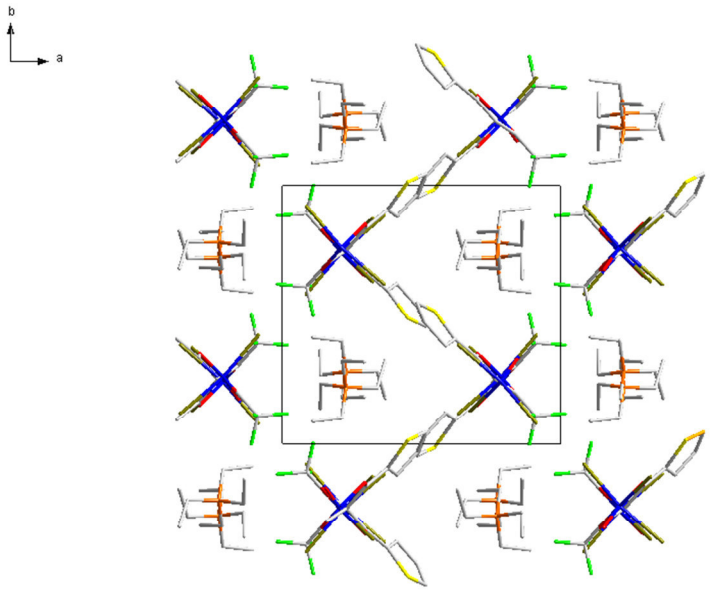

Figure 5.8 A graphic illustration highlighting to "head-to-tail" crystal packing as well as the voids filled by the tetraethylammonium cations of $(NEt_4)[NbOCl_3(ttfa)]$ (***Nb^A***) along the c-axis.

The structure of the previously published complex was performed at room temperature (298 K), while the synthesized analogue **(Nb_2)** was redetermined at 100(2) K.[17] Data obtained for the title compound **(Nb_2)**, correlates well with the previously published structure. The disordered part denoted by ***Nb^B*** differs less from the literature structure and is probably a better representation of the anionic complex. Table 5.7 illustrates a comparison between bond angles and distances of

the published structure vs. the structure collected at 100K. The most significant difference between the two complexes is the positional disorder observed in the newly synthesized product. Both counter-ions displayed a 50 %:50 % positional disorder. Repeated crystallization of the material did not improve the disorder nor eliminate it.

Table 5.6 Crystallographic details for $(NEt)_4[NbOCl_3(ttfa)]$ in the current as well as previous investigations.

Crystal Formula	Nb_2 (100 K)	$(NEt)_4[NbOCl_3(ttfa)]$ (298 K)[17]
Empirical formula	$C_{16}H_{24}Cl_3F_3N_1Nb_1O_3S$	$C_{16}H_{24}Cl_3F_3N_1Nb_1O_3S$
Formula weight ($g.mol^{-1}$)	566.68	566.21
Crystal system, Space Group	Monoclinic, $P2_1/c$	Monoclinic, $P2_1/c$
a, b, c (Å)	11.483(3), 12.563(3), 17.110(3)	11.392(2), 12.495(2), 16.940(3)
α, β, γ (°)	90, 100.83(1), 90	90, 101.00(1), 90
Volume ($Å^3$), Z	2424.3(16), 4	2366.9(10), 4
Density (calculated, Mg/m^3)	1.553	1522

Table 5.7 Comparison of bond lengths and bond angles of $(NEt_4)[NbOCl_3(ttfa)]$ collected at room temperature vs. $(NEt_4)[NbOCl_3(ttfa)]$ at 100 K.

$(NEt_4)[NbOCl_3(ttfa)]$-Nb^A (100 K)			$(NEt_4)[NbOCl_3(ttfa)]$ (298 K)[17]	
Atoms	**Bond length (Å)**		**Atoms**	**Bond length (Å)**
	Nb^A	Nb^B		
Nb1-Cl1	2.390(1)	2.389(1)	Nb1-Cl1	2.367(1)
Nb1-Cl2	2.507(1)	2.373(1)	Nb1-Cl2	2.365(2)
Nb1-Cl3	2.428(1)	2.339(1)	Nb1-Cl3	2.422(2)
Nb1-O1	2.357(1)	2.254(1)	Nb1-O1	2.285(3)
Nb1-O2	2.037(1)	2.095(1)	Nb1-O2	2.044(3)
Nb1-O3	1.733(1)	1.745(1)	Nb1-O3	1.704(3)
Atoms	**Bond angle (º)**		**Atoms**	**Bond angle (º)**
	Nb^A	Nb^B		
O1-Nb1-O2	79.65(1)	76.82(1)	O1-Nb1-O2	78.7(1)
Cl2-Nb1-Cl3	168.11(1)	160.12(1)	Cl2-Nb1-Cl3	165.0(1)
C2-C3-C4	120.60(2)	120.99(2)	C2-C3-C4	122.9(1)

5.5 Crystal Structure of Tetraethylammonium *mer*-trichlorido (furyltrifluoroacetylacetonato-κ^2O,O')oxidoniobate(V) ($(NEt_4)[NbOCl_3(tffa)]$), (Nb_3))

The novel crystal structure of tetraethylammonium *mer*-trichlorido(furyltrifluoro acetylacetonato-κ^2O,O')oxidoniobate(V) ($(NEt_4)[NbOCl_3(ttfa)]$ (**Nb_3**)) forms part of an investigation which focusses on studying applied ligand (*β*-diketone) chelation effects on novel Ta(V)- and Nb(V)-compounds in the solid state. Synthesis of **Nb_3** and the resulting yellow crystals obtained was discussed in Section 3.3.1.5.

The general crystallographic data of the structure is summarized in Table 5.1, while the numbering scheme of the complex is shown in the perspective drawing in Figure 5.9 (hydrogen atoms are omitted for clarity). An illustration of the two position CF_3 disorder is illustrated in Figure 5.10. Various selected bond lengths and angles of **Nb_3** are noted in Table 5.8. Atomic coordinates, anisotropic displacement parameters, bond distances and angles and hydrogen coordinates, are given in the supplementary data (Appendix 4).

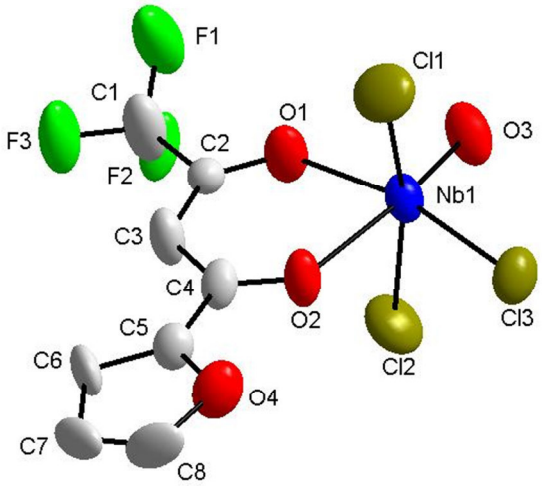

Figure 5.9 DIAMOND representation of the complex structure of *mer*-$[NbOCl_3(tffa)]^-$ (**Nb_3**) displaying the atom numbering system.

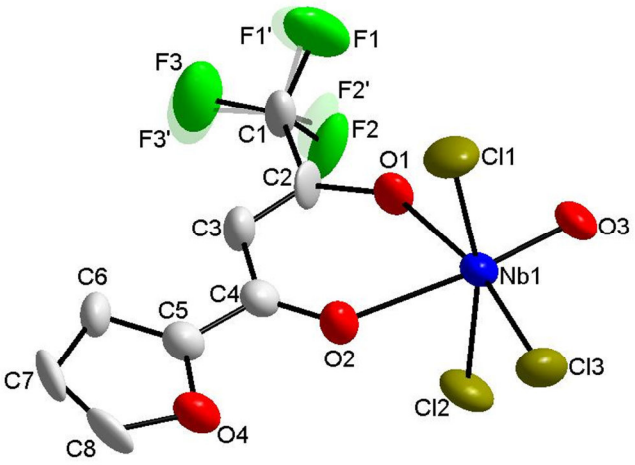

Figure 5.10 The two-position disorder (50 %:50 %) of the CF_3 group of **Nb_3** is illustrated. The displacement ellipsoids are drawn at a 50 % probability level. Hydrogen atoms and counter-ion are omitted for clarity.

The **Nb_3** compound crystallizes in the monoclinic space group, $P2_1/c$, with four $(NEt_4)[NbOCl_3(ttfa)]$ entities in the unit cell (Z = 4). For this asymmetric unit, a Nb(V) metal centre is surrounded by three crystallographically independent chloride atoms (axial; Cl1 and Cl2 and equatorial; Cl3), a terminal oxygen occupies an equatorial site, an equatorially *O,O'*-bonded furyltrifluoroacetonato ligand and finally a tetraethylammonium counter-ion. The CF_3 group of the ligand as well as the alkyl "arms" of the counter-ion display a disorder over two positions in a 50:50 ratio.

This type of arrangement is not very common for similar 8-coordinated structures as the terminal oxido is generally not found *trans* to a bidentate ligand donor atom.[3,4,17] In addition, it was found that the coordination polyhedron around the niobium(V) metal centre has a distorted octahedral geometry. Mostly this distortion can be attributed to the constraints of the oxido double bond, but several additional physical properties, illustrates this inequality.

Table 5.8 Selected bond lengths and angles of the *mer*-$[NbOCl_3(tffa)]^-$ (**Nb_3**) anion.

***mer*-$[NbOCl_3(tffa)]^-$**			
Atoms	**Bond length (Å)**	**Atoms**	**Bond length (Å)**
Nb1-Cl1	2.423(1)	Nb1-O1	2.069(1)
Nb1-Cl2	2.379(1)	Nb1-O2	2.295(1)
Nb1-Cl3	2.375(1)	Nb1-O3	1.715(1)
O1···O2[a]	2.788(2)	Out-of-plane distortion[b]	0.293(1)
Atoms	**Bond angle (º)**	**Atoms**	**Bond angle (º)**
O1-Nb1-O2	79.92(1)	O1-Nb1-O3	93.55(1)
Cl2-Nb1-Cl3	91.93(1)	O2-Nb1-O3	172.77(2)
Cl1-Nb1-O3	96.62(1)	C2-C3-C4	120.54(2)
Cl1-Nb1-Cl2	165.13(1)	Dihedral angle[d]	15.56(1)
Out-of-plane bend[c]	4.18(2)		

[a] Bite atom distance; [b] Out-of-plane distortion illustrated in Figure 5.4; [c] Out-of-plane *β*-diketonate ligand bend illustrated in Figure 5.3; [d] The torsion angle between the O1-C2-C3-C4-O2 plane and the furyl ring (see Figure 5.2).

i) Nb-Cl_{axial} distances for **Nb_3** are 2.423(1) and 2.379(1) Å, while the equatorial Nb1-Cl3 and Nb1-O3 bonds have distances of 2.375(1) and 1.715(1) Å. Comparison of the Nb1-O1 and Nb1-O2 bond lengths of the coordinated *β*-diketone, revealed distances of 2.069(1) *vs*. 2.295(1) Å. The Nb1-O2 (*trans* to the oxido) bond distance is more than 0.2 Å longer than the Nb1-O1 (*trans* to the chloride) distance underlining the *trans* influence of the oxido ligand. This distortion from ideal octahedral geometry is further highlighted when considering the 0.293(1) Å out-of-plane distortion of the niobium metal centre (see Figure 5.4).

ii) The *trans* Cl1-Nb1-Cl2 angle is 165.13(1) º, while the O1-Nb1-O2 bite angle is 79.92(1) º. Quantification of the out-of-plane bend was achieved by measuring the angle between the O1, O2 and Nb1 plane and the O1, C2, C3, C4 plane which revealed a 4.18(1) º out-of-plane bend of the coordinated ligand.

Construction of a plane through the O1, O2, O3 and Cl3 equatorial atoms, revealed that by ignoring the furyl and CF_3 substituents, all of the atoms lie either in or just slightly off this plane. Additionally, a dihedral angle of 15.56(1)° was noted between the furyl ring and plane constructed of O3-C3-C4-C5-O4 atoms.

A single halogen interaction, as defined in Section 5.4, involving the F2 atom of **Nb_3** and a carbon on the counter-ion is encountered within the crystal lattice. The halogen interaction between molecules of **Nb_3** is illustrated in red in Figure 5.11 and data related to the interaction given in Table 5.9. A hydrogen soft contact between H28C on the tetraethylammonium moeity and F1 is also observed. This interaction is illustrated in blue in Figure 5.11 and data related to the hydrogen bond given in Table 5.10.

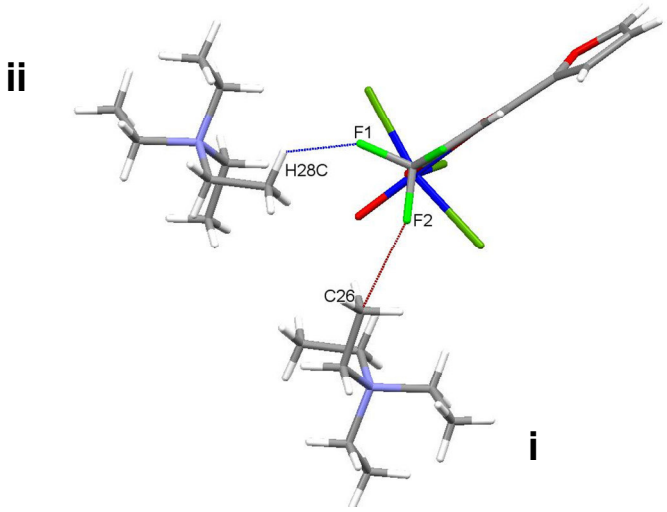

Figure 5.11 A graphic illustration of the halogen bond (indicated in red) connects neighbouring ions of **Nb_3** and the stabilizing hydrogen bonds (indicated in blue).

Table 5.9 Halogen bond geometry for **Nb_3** as depicted in Figure 5.11.

C-F···C	dC-F (Å)	dF···C (Å)	dC···C (Å)	Angle C-F···C (°)
C1-F2···C26^{i}	1.337(1)	3.063(1)	4.083(1)	132.35(3)

Symmetry code: i) *x, y, z*.

Table 5.10 Hydrogen bond geometry for **Nb_3** as depicted in Figures 5.11-5.15.

D-H···A	dD-H (Å)	dH···A (Å)	dD···A (Å)	Angle D-H···A (°)
Fluorine	(Figure 5.11)			
C26-H28C···F1^{ii}	0.970(1)	2.587(1)	3.196(1)	121.51(2)
Oxygen	(Figure 5.12)			
C25-H25B···O3^{i}	0.970(1)	2.646(1)	3.522(1)	150.46(2)
C28-H28B···O3^{i}	0.960(1)	2.682(1)	3.606(1)	161.73(2)
C27-H27B···O3^{ii}	0.970(1)	2.526(1)	3.336(1)	140.97(3)
Chlorine (Inter-anion)	(Figure 5.12)			
C7-H7···Cl2^{iii}	0.930(1)	2.650(1)	3.546(1)	161.77(1)
C6-H6···Cl3^{iv}	0.930(1)	2.720(1)	3.617(1)	162.15(1)
Chlorine (Counter-ion)	(Figure 5.13)			
C21-H21B···Cl3^{v}	0.970(1)	2.837(1)	3.659(1)	143.18(3)
Carbon	(Figure 5.14)			
C27-H27A···C6^{vi}	0.930(1)	2.650(1)	3.546(1)	161.77(1)
C27-H27A···C7^{vi}	0.930(1)	2.720(1)	3.617(1)	162.15(1)

Symmetry code: i) *x, y, z*; ii) *1-x, 1-y, -z*; iii) *-x, ½+y, ½-z;* iv) *x, ½-y, -½+z;* v) *1-x, -y, -z*; vi) *1-x, -½-y, ½-z.*

Various additional intermolecular hydrogen soft contacts contribute to the stabilization of the crystal lattice. Due to the fact that this intrinsic network will be difficult to graphically illustrate, the various interactions will be illustated atomic groups (carbon, chloride, oxido and fluoride) to highlight the complexity of the crystal structure. These interactions occur extensively and can be observed as either counter ion-anion or anion-anion connections and are illustrated in blue in Figures 5.12, 5.13, 5.14 and 5.15. The data related to the hydrogen soft contacts are given in Table 5.10.

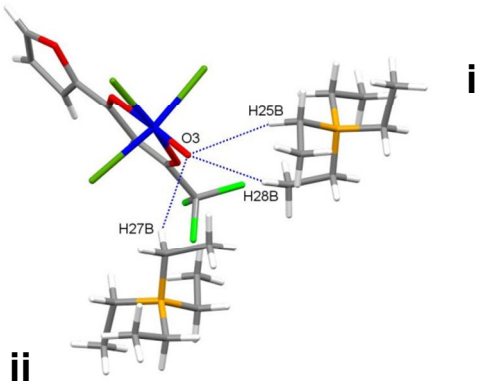

Figure 5.12 A graphic illustration of the stabilizing hydrogen bonding (indicated in blue) of selected oxygen substituents connecting neighbouring anion-counter-ion moeities of **Nb_3**.

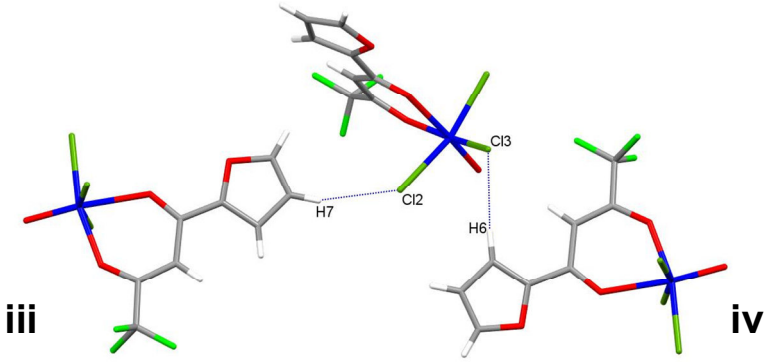

Figure 5.13 A graphic illustration of the hydrogen bonding (indicated in blue) of selected chloride substituents connecting neighbouring anion units of **Nb_3**.

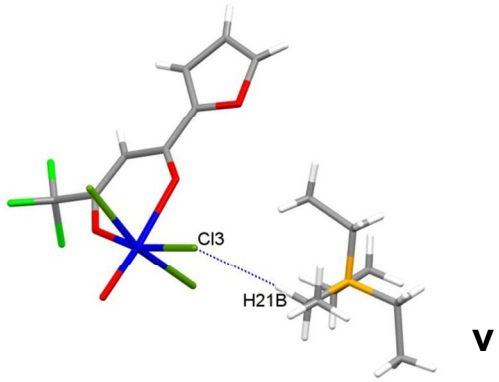

Figure 5.14 A graphic illustration of the hydrogen bonding (indicated in blue) of selected chloride substituents connecting neighbouring anion-counter-ion moeities of **Nb_3**.

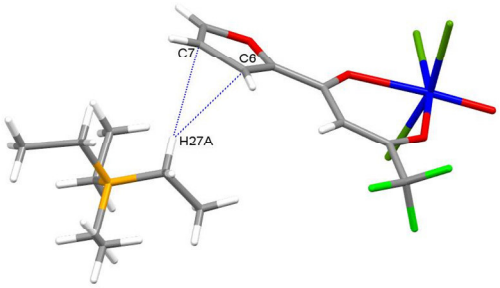

vi

Figure 5.15 A graphic illustration of the stabilizing hydrogen bonding (indicated in blue) of selected carbon atoms connecting neighbouring anion-counter-ion moeities of **Nb_3**.

Several other short contacts were observed in the **Nb_3** structure with O···H interactions being the most prominent. The illustrated hydrogen bonding, rigidly ties the crystal lattice together influencing the overall packing in pairs of these niobium molecules, as illustrated in the "head-to-tail" packing structure in Figure 5.16. A view along the c-axis reveals that between the Nb(V) units are large cavities filled by the tetraethylammonium (NEt_4^+) counter-ions. These large cavities allow for the disorder nature of the NEt_4^+ cation.

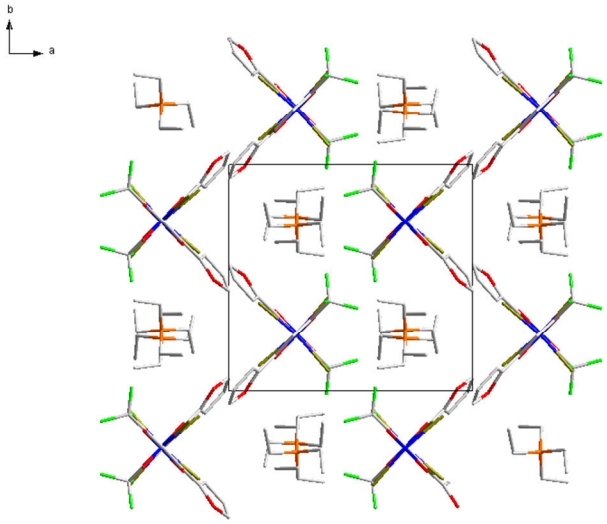

Figure 5.16 A graphic illustration highlighting to "head-to-tail" crystal packing as well as the voids filled by the tetraethylammonium cations of $(NEt_4)[NbOCl_3(tffa)]$ (**Nb_3**) along the c-axis.

5.6 Crystal Structure of Tetraethylammonium *mer*-(benzoyltrifluoroacetylacetonato-κ^2*O,O'*)trichloridooxidoniobate(V) ($(NEt_4)[NbOCl_3(btfa)]$), (Nb_4))

The complex, tetraethylammonium *mer*-(benzoyltrifluoroacetylacetonato-κ^2*O,O'*) trichloridooxido niobate(V) ($(NEt_4)[NbOCl_3(btfa)]$ (**Nb_4**)), has been synthesized as described in Section 3.3.1.3 and yellow plate-like crystals were obtained from an acetonitrile solution of the product.

The **Nb_4** compound crystallizes in the monoclinic space group, $P2_1/c$, with four $(NEt_4)[NbOCl_3(btfa)]$ entities in the unit cell (Z = 4). The crystal structure as well as the numbering scheme of the complex is represented in Figure 5.17 (hydrogen bonds are omitted for clarity). General crystallographic information pertaining to the crystal structure is referred to in Table 5.1 and selected bond lengths and angles are given in Table 5.11. For comprehensive information regarding bond distances, angles, atomic coordinates and anisotropic displacement parameters related to the structure, refer to Appendix 5.

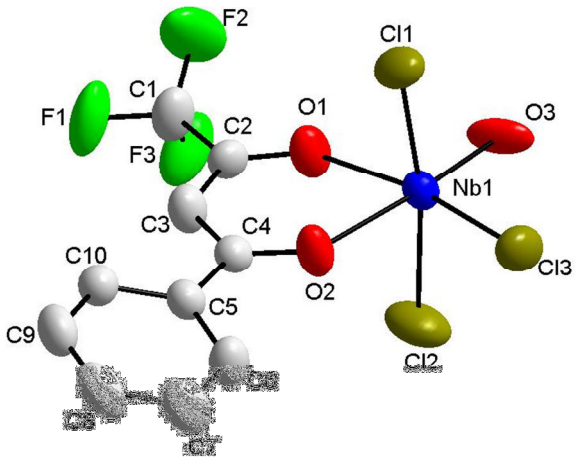

Figure 5.17 DIAMOND representation of the complex structure of *mer*-$[NbOCl_3(btfa)]^-$ (**Nb_4**) displaying the atom numbering system.

The asymmetric unit of this compound consists of a Nb(V) metal centre surrounded by an equatorial oxido (O3), three independent chlorido groups (Cl1 – Cl3), one *O,O'*-bonded benzoyltrifluoroacetonato ligand and a tetraethylammonium cation. The fluoro substituents of the CF_3 entity and the ethyl groups on the counter-ion display a two position disorder in a 50:50 ratio. The disorder on the anion is illustrated in Figure 5.18.

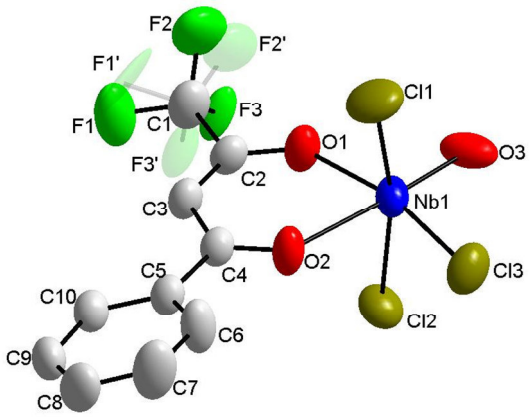

Figure 5.18 The two position disorder (50 %:50 %) of the CF_3 group is also illustrated. The displacement ellipsoids are drawn at a 50 % probability level. Hydrogen atoms and counter-ion are omitted for clarity.

All of the aforementioned groups are arranged in a distorted octahedral geometry around the metal centre. This occurrence can be attributed to several physical properties (steric bulk, electronic parameters, etc.) and can be described in terms of both complex bond lengths and angles.

Table 5.11 Selected bond lengths and angles of the *mer*-$[NbOCl_3(btfa)]^-$ (**Nb_4**) anion.

***mer*-$[NbOCl_3(btfa)]^-$**			
Atoms	**Bond length (Å)**	**Atoms**	**Bond length (Å)**
Nb1-Cl1	2.417(1)	Nb1-O1	2.046(1)
Nb1-Cl2	2.368(1)	Nb1-O2	2.266(1)
Nb1-Cl3	2.324(1)	Nb1-O3	1.806(1)
O1···O2[a]	2.733(4)	Out-of-plane distortion[b]	0.265(1)
Atoms	**Bond angle (º)**	**Atoms**	**Bond angle (º)**
O1-Nb1-O2	78.17(1)	Cl1-Nb1-Cl2	165.09(1)
Cl2-Nb1-Cl3	89.86(2)	O2-Nb1-O3	174.91(2)
Cl1-Nb1-O3	97.77(2)	C2-C3-C4	122.97(2)
O1-Nb1-O3	96.75(1)	Dihedral angle[d]	16.92(1)
Out-of-plane bend[c]	1.73(1)		

[a] Bite atom distance; [b] Out-of-plane distortion illustrated in Figure 5.4; [c] Out-of-plane *β*-diketonate ligand bend illustrated in Figure 5.3; [d] The torsion angle between the O1-C2-C3-C4-O2 plane and the phenyl ring (see Figure 5.2).

i) From Table 5.11 it is noted that the Nb-Cl_{axial} distances for **Nb_4** are 2.368(1) and 2.417(1) Å, while the equatorial Nb1-Cl3 and Nb1-O3 bonds have distances of 2.324(1) and 1.806(1) Å. The Nb-O bond distances to the *β*-diketone, Nb1-O1 and Nb1-O2, have distances of 2.046(1) and 2.226(1) Å respectively. When comparing these distances an obvious 0.18 Å difference is noted, again underlined the *trans* influence of the oxido ligand. The out-of-plane distortion, as described in Figure 5.4, is equal to 0.27(1) Å.

ii) Visually, a more obvious distortion is noted when considering the *trans* Cl1-Nb1-Cl2 angle (165.09(1) º vs. ideal 180 º) and the O1-Nb1-O2 bidentate bite angle (78.17(1) º vs. ideal 90 º). Quantification of the out-of-plane bend was achieved by measuring the angle between the O1, O2 and Nb1 plane and the O1, C2, C3, C4 plane which revealed a 1.73(1) º out-of-plane bend of the coordinated ligand.

The significance of intermolecular stabilzation interactions has been described in detail for these Nb(V) systems and the case **Nb_4** is no different. This structure displays different examples of intermolecular hydrogen bonding which contribute to the rigidity of crystal lattice. Due to the fact that this intrinsic network is difficult to illustrate graphically, the various interactions will be illustated by atomic group to highlight the complexity of the crystal structure.

Once again, as is in the previous structures, halogen bonding interactions are observed involving the F2 and F3 atoms of **Nb_4**. The halogen bonds between molecules of **Nb_4** are illustrated in red in Figure 5.19 and data related to the interaction given in Table 5.12. Hydrogen bonds between the hydrogen molecule on the tetraethylammonium moeity (H26A, H26B and H28A) and F2 and F3 atoms are also observed. These interactions are illustrated in blue in Figure 5.19 and data related to the hydrogen bond is also given in Table 5.13.

Table 5.12 Halogen bond geometry for **Nb_4** as depicted in Figure 5.19.

C-F···C	dC-F (Å)	dF···C (Å)	dC···C (Å)	Angle C-F···C (°)
C1-F2···C26^{i}	1.275(1)	2.958(1)	4.051(1)	143.19(3)
C1-F3···C28^{ii}	1.296(1)	3.112(1)	4.353(1)	160.00(2)

Symmetry code: i) *1-x, -y, -z;* ii) *x, ½-y, ½+z.*

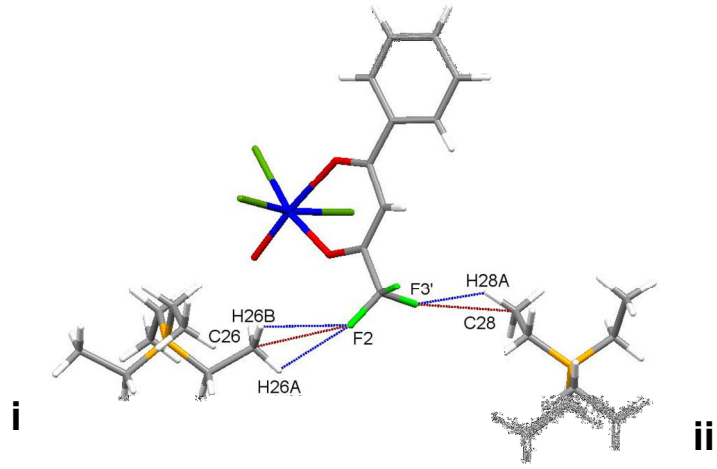

Figure 5.19 A graphic illustration of the halogen bond (indicated in red) connects neighbouring ions of **Nb_4** and the stabilizing hydrogen bonds (indicated in blue).

Additional intermolecular hydrogen bonds contribute to the stabilization of the crystal lattice. These interactions occur extensively and can be observed as either counter ion-anion or anion-anion connections. Hydrogen bonding for selected carbon, chlorine and oxygen atomic groups are noted for this structure. These interactions are illustrated in blue in Figures 5.20, 5.21 and 5.22 and data related to the hydrogen bonds given in Table 5.13.

Table 5.13 Hydrogen bond geometry for **Nb_4** as depicted in Figure 5.20-5.22.

D-H···A	dD-H (Å)	dH···A (Å)	dD···A (Å)	Angle D-H···A (°)
Fluorine	(Figure 5.17)			
C26-H26A···F2^{i}	0.980(1)	2.585(1)	2.598(1)	102.06(3)
C26-H26B···F2^{i}	0.980(1)	2.579(1)	2.598(1)	102.56(3)
C28-H28A···F3^{ii}	0.981(1)	2.335(1)	3.112(1)	135.68(2)
Oxygen	(Figure 5.18)			
C25-H25B···O3^{iii}	0.9910(1)	2.624(1)	3.460(1)	142.07(2)
C21-H21B···O3^{i}	0.990(1)	2.715(1)	3.608(1)	150.23(2)
C26-H26C···O3^{i}	0.980(1)	2.870(1)	3.640(1)	162.92(2)
Chlorine	(Figure 5.19)			
C8-H8···Cl1^{iv}	0.951(1)	2.846(1)	3.573(1)	132.71(3)
C10-H10···Cl3^{ii}	0.949(1)	2.870(1)	3.778(1)	160.48(2)
C9-H9···Cl1^{ii}	0.990(1)	2.920(1)	3.808(1)	149.75(2)
C27-H27A···Cl3^{v}	0.951(1)	2.949(1)	3.960(1)	135.62(3)
Carbon	(Figure 5.20)			
C6-H6···C24A^{vi}	0.989(1)	2.847(1)	3.623(1)	136.91(3)
C25-H25A···C9^{vii}	0.950(1)	2.837(1)	3.701(1)	150.10(2)

Symmetry code: i) *1-x, -y, -z;* ii) *x, ½-y, ½+z*; iii) *x, 1+y, z;* iv) *-x, ½+y, ½- z;* v) *x, -y, z*; vi) *x, y, z;* vii) *x, -½-y, ½+z.*

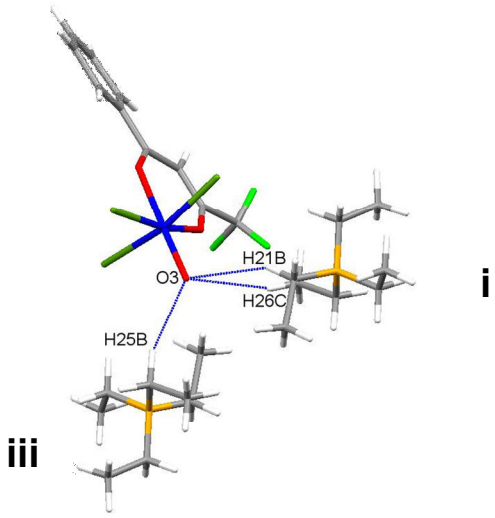

Figure 5.20 A graphic illustration of the stabilizing hydrogen bonding (indicated in blue) of selected oxygen substituents connecting neighbouring anion-counter-ion moeities of **Nb_4**.

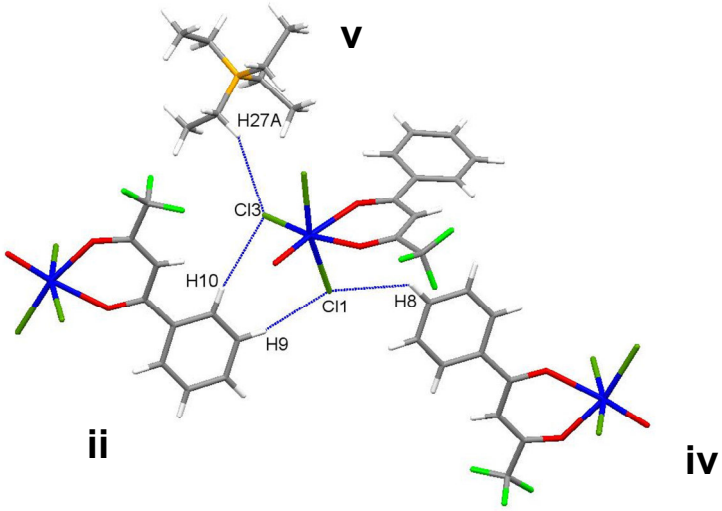

Figure 5.21 A graphic illustration of the stabilizing hydrogen bonding (indicated in blue) of selected chloride substituents connecting neighbouring anions of **Nb_4**.

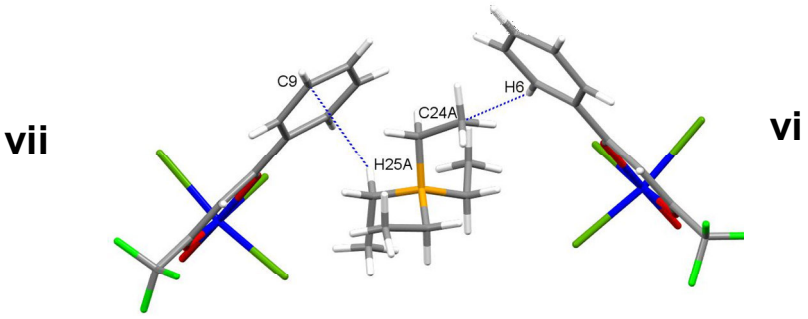

Figure 5.22 A graphic illustration of the stabilizing hydrogen bonding (indicated in blue) of selected carbon atoms connecting neighbouring anion-counter-ion moeities of **Nb_4**.

All of these intermolecular interactions contribute to the stability of the crystal lattice and causes the niobium units to be dispersed in a “head-to-tail” packing fashion throughout the system. An illustration of the crystal lattice packing of **Nb_4** is illustrated in Figure 5.23. When viewing the crystal structure along the c-axis it is again noticed that the cavities between the Nb(V) moieties are filled by the tetraethylammonium ($(NEt_4)^+$) counter ions.

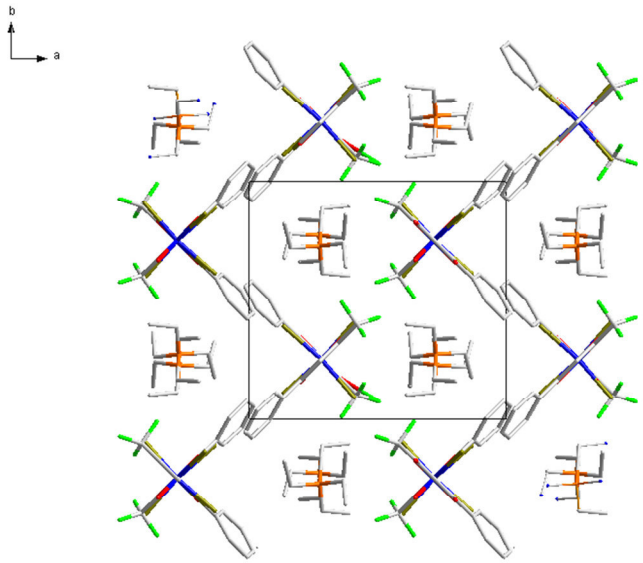

Figure 5.23 A graphic illustration highlighting to “head-to-tail” crystal packing as well as the voids filled by the tetraethylammonium cations of $(NEt_4)[NbOCl_3(btfa)]$ (**Nb_4**) along the c-axis.

5.7 Crystal Structure of Tetraethylammonium *mer*-oxidotrichlorido(naphtyltrifluoroacetylacetonato-κ^2O,O')niobate(V) ($(NEt_4)[NbOCl_3(ntfa)]$), (Nb_5))

As was mentioned in Chapters 2 and 3 it was difficult to obtain crystals for the different niobium complexes. In the case of the $[(NEt_4)[NbOCl_3(ntfa)]$ complex only crystals of relatively lower quality could be obtained from various recrystallization attempts. As a result, these crystals afforded crystallographic data with a lower completeness (97.7 %) as well as the high R_{int} and Goodness-of-Fit values (see Table 5.1). With respect to this study, the data collection however still yielded sufficient quality data to determine the structure and intermolecular stabilization interactions of **Nb_5**, which will be discussed in this section.

The crystal structure of tetraethylammonium *mer*-trichlorido(naphtyltrifluoro acetylacetonato-κ^2O,O')oxidoniobate(V) ($(NEt_4)[NbOCl_3(ntfa)]$ (**Nb_5**)) forms part of an investigation which focuses on studying applied ligand chelation effects (steric bulk, electronic properties, etc.) on novel Ta(V)- and Nb(V)-compounds. Synthesis of **Nb_5** and the resulting yellow crystals obtained was discussed in Section 3.3.1.6.

A summary of the general crystallographic data is given in Table 5.1, while the numbering scheme of the complex is shown in the perspective drawing in Figure 5.24. Table 5.14 presents selected bond lengths and angles of **Nb_5**. Atomic coordinates, anisotropic displacement parameters, bond distances and angles and hydrogen coordinates, are given in the supplementary data (Appendix 6). Hydrogen atoms are omitted for clarity.

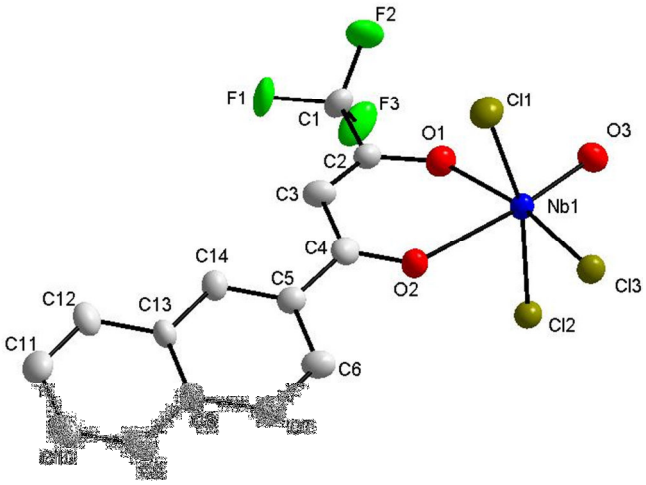

Figure 5.24 DIAMOND representation of the charged complex structure of $[NbOCl_3(ntfa)]^-$ (**Nb_5**) displaying the atom numbering system.

Nb_5 crystallizes in the monoclinic space group, $P2_1/c$, with four molecules in the unit cell ($Z = 4$). The asymmetric unit consists of a Nb(V) metal centre surrounded by three crystallographically independent chlorido groups (Cl1 – Cl3), an oxido (O3), one *O,O′*-bonded naphtyltrifluoroacetonato ligand and a tetraethylammonium cation. No positional disorder was observed on the CF_3 group in this structure which can probably be attributed to the slightly poorer quality of crystal.

The coordination polyhedron around the niobium(V) metal centre has a distorted octahedral geometry. Several physical properties, including bond distances and angles, contribute to this inequality.

Table 5.14 Selected bond lengths and angles of the *mer*-$[NbOCl_3(ntfa)]^-$ (**Nb_5**) anion.

***mer*-$[NbOCl_3(ntfa)]^-$**			
Atoms	**Bond length (Å)**	**Atoms**	**Bond length (Å)**
Nb1-Cl1	2.412(1)	Nb1-O1	2.046(1)
Nb1-Cl2	2.415(1)	Nb1-O2	2.314(1)
Nb1-Cl3	2.396(1)	Nb1-O3	1.711(1)
O1···O2[a]	2.746(4)	Out-of-plane distortion[b]	0.285(1)
Atoms	**Bond angle (º)**	**Atoms**	**Bond angle (º)**
O1-Nb1-O2	77.98(2)	O1-Nb1-O3	93.30(1)
Cl2-Nb1-Cl3	89.23(2)	O2-Nb1-O3	174.91(2)
Cl1-Nb1-O3	96.75(1)	C2-C3-C4	122.51(3)
Cl1-Nb1-Cl2	165.30(1)	Dihedral angle[d]	8.01(1)
Out-of-plane bend[c]	-14.34(1)		

[a] Bite atom distance; [b] Out-of-plane distortion illustrated in Figure 5.4; [c] Out-of-plane *β*-diketonate ligand bend illustrated in Figure 5.3; [d] The torsion angle between the O1-C2-C3-C4-O2 plane and the naphtyl ring system (see Figure 5.2).

i) Nb-Cl_{axial} distances for **Nb_5** are 2.412(1) and 2.415(1) Å, while the equatorial Nb1-Cl3 and Nb1-O3 bonds have distances of 2.396(1) and 1.711(1) Å. Comparison of the Nb1-O1 and Nb1-O2 bond lengths of the coordinated *β*-diketone, revealed distances of 2.046(1) vs. 2.314(1) Å. The Nb1-O2 bond (*trans* to the oxido) is thus more than 0.25 Å longer than the Nb1-O1 (*trans* to the chlorido), underlining the trans influence of the oxido ligand. This distortion from ideal octahedral geometry is further highlighted when considering the 0.29(1) Å out-of-plane distortion of the niobium metal centre.

ii) The *trans* Cl1-Nb1-Cl2 angle is 165.30(1) º, while the O1-Nb1-O2 bite angle is 77.98(2) º. Quantification of the out-of-plane bend was achieved by measuring the angle between the O1, O2 and Nb1 plane and the O1, C2, C3, C4 plane which revealed a -14.34(1) º out-of-plane bend of the coordinated ligand.

When constructing an equatorial plane through O1, O2, O3 and Cl3, it was observed that upon exclusion of the naphtyl and CF_3 substituents most of the atoms lie either in or just slightly off this plane. A dihedral angle of 8.01(1)° between the naphtyl ring and plane constructed of O3-C3-C4-C5-O4 atoms was noted.

There are numerous intermolecular hydrogen bonding stabilzation interactions within this molecule. These interactions are very complex, occur extensively and can be observed as either counter ion-anion or anion-anion connections. Hydrogen bonding for selected carbon, chlorine (anion-anion and anion-counter ion) and oxygen atomic groups are noted for this structure. These interactions are illustrated in blue in Figures 5.25, 5.26, 5.27 and 5.28 and data related to the hydrogen bonds given in Tables 5.15.

Table 5.15 Hydrogen bond geometry for **Nb_5** as depicted in Figure 5.25-5.28.

D-H···A	dD-H (Å)	dH···A (Å)	dD···A (Å)	Angle D-H···A (°)
Fluorine	(Figure 5.23)			
C25-H25B···F1^{i}	0.970(1)	2.650(1)	3.328(1)	127.25(3)
C28-H28B···F1^{ii}	0.960(1)	2.638(1)	3.307(1)	127.21(3)
C26-H26B···F1^{iii}	0.961(1)	2.644(1)	3.499(1)	141.59(2)
Oxygen	(Figure 5.24)			
C24-H24A···O1^{i}	0.960(1)	2.575(1)	3.528(1)	172.00(2)
C25-H25A···O1^{i}	0.970(1)	2.712(1)	3.584(1)	149.90(3)
C25-H25A···O3^{i}	0.970(1)	2.492(1)	3.331(1)	144.76(2)
C26-H26C···O3^{iv}	0.960(1)	2.511(1)	3.308(1)	140.51(3)
Chlorine (Inter-anion)	(Figure 5.25)			
C6-H6···Cl1^{v}	0.930(1)	2.892(1)	3.645(1)	119.00(3)
C6-H6···Cl3^{v}	0.930(1)	2.906(1)	3.681(1)	151.34(2)
Chlorine (Counter-ion)	(Figure 5.26)			
C21-H21B···Cl3^{vi}	0.970(1)	2.749(1)	3.645(1)	159.75(2)
C27-H27B···Cl2^{iv}	0.969(1)	2.929(1)	3.681(1)	135.25(2)
C21-H21A···Cl3^{iv}	0.970(1)	2.945(1)	3.904(1)	170.55(2)
C22-H22A···Cl2^{iii}	0.961(1)	2.922(1)	3.967(1)	172.60(3)

Symmetry code: i) *x, 1+y, z;* ii) *1+x,1+y, z*; iii) *2-x, -y, 2-z*; iv) *1-x, -y, 2-z*; v) *-1+x, y, z.*

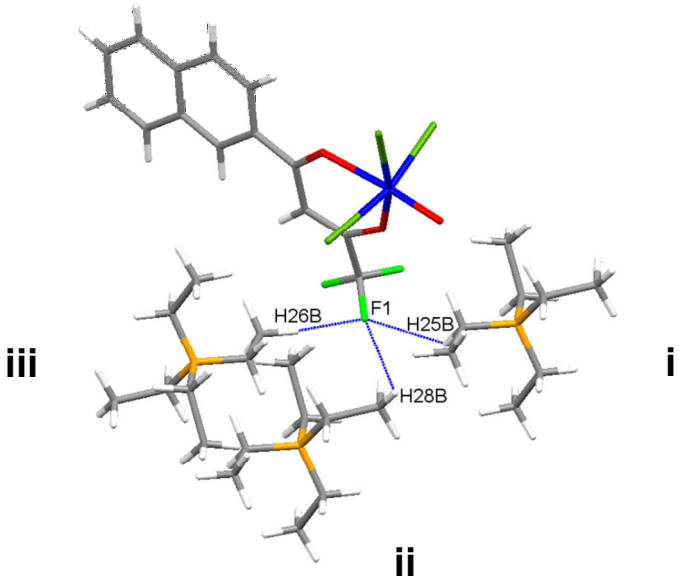

Figure 5.25 A graphic illustration of the stabilizing hydrogen bonding (indicated in blue) of selected fluorine substituents connecting neighbouring anion-counter-ion moeities of **Nb_5**.

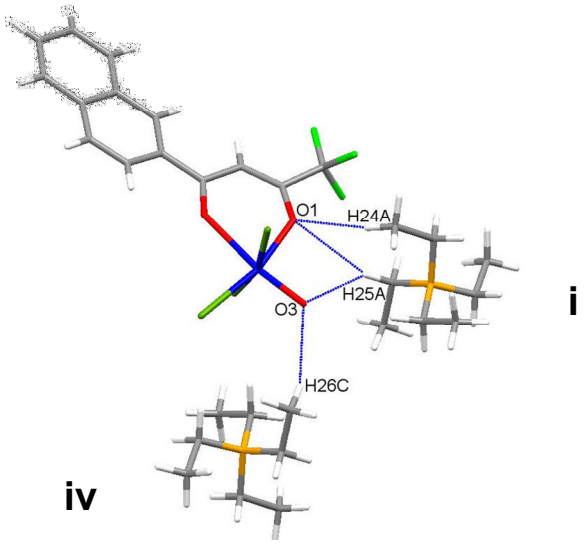

Figure 5.26 A graphic illustration of the stabilizing hydrogen bonding (indicated in blue) of selected oxygen substituents connecting neighbouring anion-counter-ion moeities of **Nb_5**.

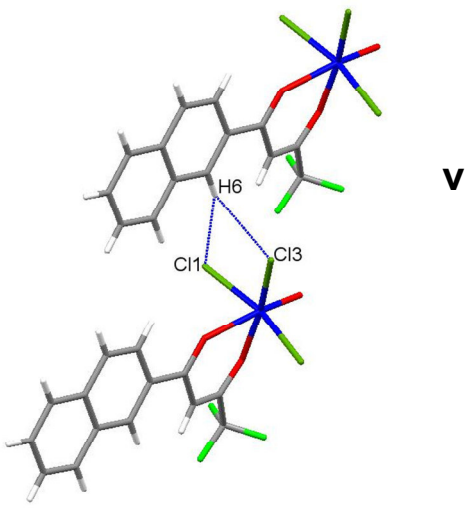

Figure 5.27 A graphic illustration of the stabilizing hydrogen bonding (indicated in blue) of selected chloride substituents connecting neighbouring anion units of **Nb_5**.

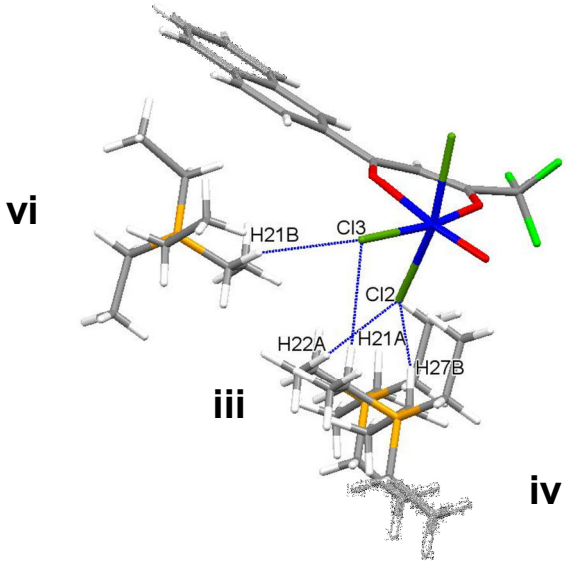

Figure 5.28 A graphic illustration of the stabilizing hydrogen bonding (indicated in blue) of selected chloride substituents connecting neighbouring anion-counter-ion moeities of **Nb_5**.

Furthermore, the two-dimensional supra-molecular network is additionally stabilized by intermolecular π-π interactions between the overlapping ntfa-ligands within the structure as illustrated in Figure 5.27. This type of π-π-stacking is defined as an interaction between two aromatic rings in which the angle of communication is less

than 30 º between the ring planes with a distance between ring centroids shorter than 4.4 Å (face-to-face).[20] Aromatic molecules attract one another when the π-system on one arene interacts more powerfully with the σ-system of the other than the π-π repulsion destabilizes the complex.[21] In this structure the centroid-to-centroid distances for the intermolecular π-π interactions are 3.777(3) Å and 3.791(3) Å, respectively. This tightly knit two-dimensional interaction network rigidly ties the crystal lattice together, influencing the overall packing in pairs of these two niobium molecules dispersed in a “head-to-tail” packing fashion throughout the system.

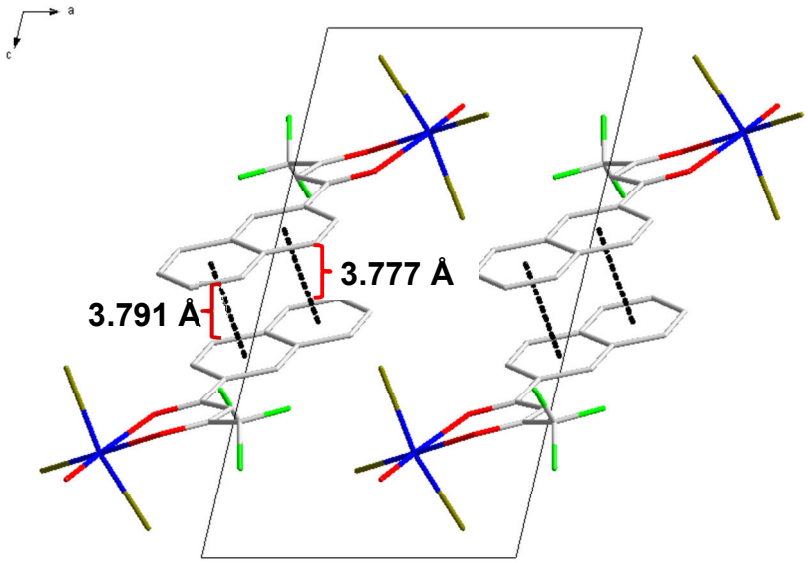

Figure 5.29 The crystal packing of **Nb_5** when viewed along the b-axis. The intermolecular π-π stacking is illustrated in black.

[20] C. A. Hunter and J. K. M. Sanders, (1990). *J. Am. Chem. Soc.*, **112**, 5525-5534.

[21] G. B. McGaughey, M. Gagne and A. K. Rappe, (1998). *J. Biol. Chem.*, **273**, 15458-15463.

5.8 Correlation of Structural Parameters of the Compounds Discussed in this Chapter

The crystal structures of four Nb(V)-*β*-diketonate complexes containing chlorido and oxido substituents were analyzed and discussed in this chapter. The steric and electronic properties of these ligands were investigated to evaluate the effect induced when systematically changing the aryl substituent on the C5 atom from one ligand to another.

The unit cell parameters for all these structures are within a similar range with a maximum difference between the highest and lowest values of 0.306 Å for *a*-axis, 0.317 Å for *b*-axis and 0.673 Å for *c*-axis for the monoclinic systems. In general, it is observed that these Nb(V) complexes appear to favour a monoclinic solid state crystal packing system, excluding the triclinic **Nb_5** compound. It seems that the larger naphtyl substituent influenced the crystal packing in such a way that some of the crystallographic symmetry had been lost. This conformational distortion from monoclinic to triclinic geometry (decrease of symmetry) with increase of steric bulk of aryl substituent has been noticed in similar investigations.[22,23,24]

Herbst *et al*. focused on comparable Nb(V) acetyacetonate type structures as illustrated in Figure 5.30.[22,23,24] From this research it was found that the steric bulk from a simple benzoyl substituent on the acac backbone of the complex was sufficient to induce this distortion of crystallographic symmetry of the Nb(V) complex. In contrast, Davies *et al.* found that for Ta(V) acetyacetonates type structures as illustrated in Figure 5.31, a larger dibenzoyl substituent on the acac back bone was required to induce distortion.[5] Tables 5.16 and 5.17 document the unit cell parameters of the aforementioned compounds. The differences of the effect of the steric bulk of a ligand on the symmetry of the solid state packing for both Ta(V) and Nb(V) complexes seem to be very useful in manipulating conformational order and

[22] L. Herbst, H. G. Visser, A. Roodt and C. Pretorius, (2012). *Acta Cryst.*, **E68**, m1392-1394

[23] L. Herbst, H. G. Visser and A. Roodt, (2015). *Z. Cryst. NCS.*, **228**, 451-456.

[24] L. Herbst, H. G. Visser and A. Roodt, (2015). *Z. Cryst. NCS.*, **228**, 397-402.

stabilization interactions within the crystal lattice. Accordingly, this crystallographic study then goes a long way into allowing for the prediction of solid state behaviour of niobium(V) acetylacetonato complexes.

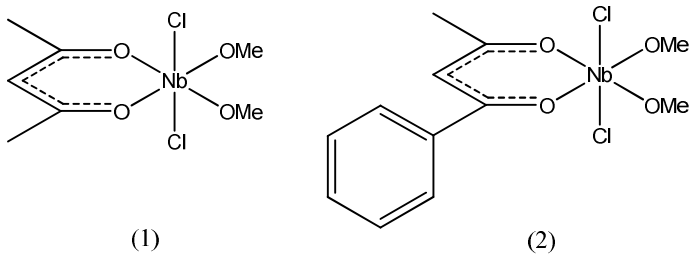

Figure 5.30 Graphic illustrations of the Nb(V) compounds discussed in the preceding section.
(1) *(Acetylacetonato-κ²O,O')dichlorobis(methanolato-κO)niobium(V)*[22]
(2) *(Benzoylacetylacetonato-κ²O,O')dichlorobis(methanolato-κO)niobium(V)*[23]

Table 5.16 Unit cell parameters of the Nb(V) compounds discussed in the preceding section.

Crystal Complex	**(1)**[22]	**(2)**[23]
Crystal system	Monoclinic	Triclinic
Space Group	$P2_1/c$	$P\bar{1}$
***a* (Å)**	7.798(1)	7.899(2)
***b* (Å)**	11.603(3)	9.774(1)
***c* (Å)**	14.682(2)	10.780(2)
α (°)	90	89.51(2)
β (°)	111.28(3)	72.98(2)
γ (°)	90	71.45(3)

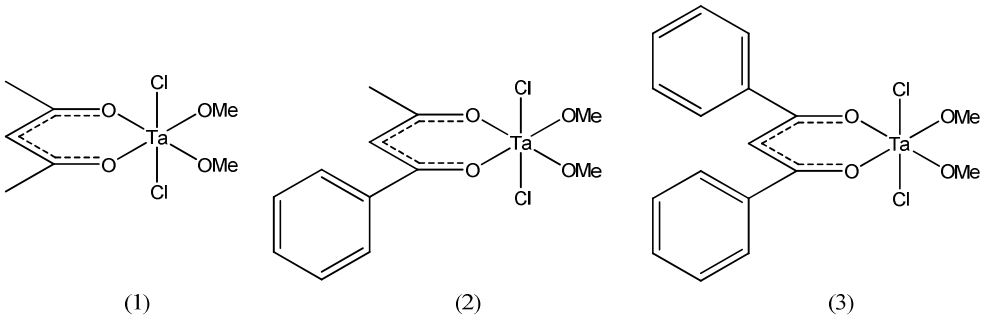

Figure 5.31 Graphic illustrations of the Ta(V) compounds discussed in the preceding section.
(1) *(Acetylacetonato-κ²O,O')dichlorobis(methanolato-κO)tantalum(V)*[5]
(2) *(Benzoylacetylacetonato-κ²O,O')dichlorobis(methanolato-κO)tantalum(V)*[24]
(3) *(Dibenzoylacetylacetonato-κ²O,O')dichlorobis(methanolato-κO)tantalum(V)*[5]

Table 5.17 Unit cell parameters of the Ta(V) compounds discussed in the preceding section.

Crystal Complex	(1)[5]	(2)[24]	(3)[5]
Crystal system	Monoclinic	Monoclinic	Triclinic
Space Group	$P2_1/c$	$P2_1/c$	$P\bar{1}$
***a* (Å)**	7.764(2)	7.982(5)	8.215(5)
***b* (Å)**	11.604(2)	12.194(4)	10.540(3)
***c* (Å)**	13.396(3)	15.318(5)	11.462(2)
α (°)	90	90	82.31(1)
β (°)	99.41(3)	93.89(3)	76.15(1)
γ (°)	90	90	77.44(5)

The coordination environment around the metal centre for these complexes tends to favour the octahedral polyhedron with noticeable distortion. In all of the cases mentioned in this chapter the Nb-O2 bond distance (*trans* to the oxo-group) is considerably longer than the Nb-O1 counterpart. This phenomenon is comparable with the lengthening of niobium-nitrogen bond *trans* to the multiple bond Nb=O in the $NbOCl_3(CH_3CN)_2$ complex.[25] Differences in these bond lengths are likely related to the valence shell electron pair repulsions between Cl and O atoms.[17]

The general structural parameters, bond distances and angles from the various Nb(V)-*β*-diketonate complexes as described above are given in Tables 5.27. When comparing these bond distances and angles to structures from literature it was found that they correlate very well.[5,6,7,22,23,24,25] In this regard, a more detailed comparative study of these four Nb(V)-*β*-diketonate complexes as well as two additional structures, discussed in the following chapter, will be undertaken in Chapter 9. Properties such as steric bulk and electronic properties of the *β*-diketonate complex of the will be correlated to various aspects such as complex stability and structural effects.

[25] C. Chavant, J. C. Daran, Y. Jeannin and G. Constant, (1975). *Acta Cryst.* **B31**, 1828-1830.

Table 5.28 Cell dimension overview of presented Nb(V)-*β*-diketonate complexes.

Crystal Formula	$(NEt_4)[NbOCl_3(ttfa)]$		$(NEt_4)[NbOCl_3(tffa)]$	$(NEt_4)[NbOCl_3(btfa)]$	$(NEt_4)[NbOCl_3(ntfa)]$
Bond Distances (Å)					
Nb1-O1	2.037(1)	2.095(1)*	2.069(1)	2.046(1)	2.046(1)
Nb1-O2	2.357(1)	2.254(1)*	2.295(1)	2.266(1)	2.314(1)
Nb1-O3	1.733(1)	1.745(1)*	1.715(1)	1.806(1)	1.711(1)
Nb1-Cl1	2.507(1)	2.373(1)*	2.423(1)	2.417(1)	2.412(1)
Nb1-Cl2	2.390(1)	2.389(1)*	2.379(1)	2.368(1)	2.415(1)
Nb1-Cl3	2.428(1)	2.339(1)*	2.375(1)	2.324(1)	2.396(1)
O1···O2	2.779(1)	2.787(1)*	2.788(2)	2.733(4)	2.746(4)
Out-of-plane distortion	0.275(1)	0.270(1)*	0.293(1)	0.265(1)	0.285(1)
Bond Angles (°)					
O1-Nb1-O2	79.65(1)	76.82(1)*	79.92(1)	78.17(1)	77.98(2)
Cl2-Nb1-Cl3	88.39(1)	92.40(1)*	91.93(1)	89.86(2)	89.23(2)
Cl1-Nb1-O3	96.57(1)	98.41(1)*	96.62(1)	97.77(2)	96.75(1)
Cl1-Nb1-Cl2	166.03(2)	164.55(1)*	165.13(1)	165.09(1)	165.30(1)
O1-Nb1-O3	96.98(1)	92.82(1)*	93.55(1)	96.75(1)	93.30(1)
O2-Nb1-O3	171.69(2)	166.36(2)*	172.77(2)	174.91(2)	174.91(2)
C2-C3-C4	120.60(2)	120.99(2)*	120.54(2)	122.97(2)	122.51(3)
Out-of-plane bend[c]	6.23(1)	5.55(1)*	4.18(2)	1.73(1)	-14.34(1)
Dihedral angle	17.27(1)	17.68(1)*	15.56(1)	16.92(1)	8.01(1)

* Disordered structure

Each of these anionic compounds is stabilized by a tetraethylammonium counter-ion that displays a 50:50 positional disorder. In all of the aforementioned examples, the crystal packing diagrams revealed that these counter-ions are located periodically within large voids between the anionic complexes in the lattice. The ample space within the voids allow for the disordered nature of this moiety which is often found in systems containing tetraethylammonium ions.[26,27] Figure 5.28 illustrates an example of this phenomenon.

[26] R. Van Deun, P. Van der Voort, I. Van Driessche and K. Van Hecke, (2012). *Acta Cryst.*, **E68**, m111-112.

[27] S. J. Hibble, S. G. Eversfield and A. M. Chippindale, (2002). *Acta Cryst.*, **E58**, m366-368.

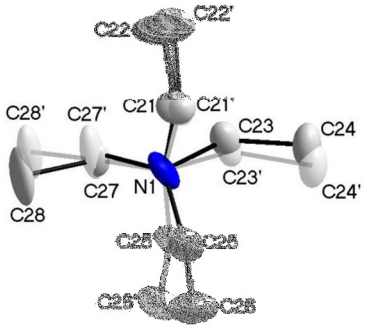

Figure 5.30 An illustrative example of the 50:50 ratio postional disorder of the tetraethylammonium cation observed within the crystal structures.

5.9 Conclusion

In this chapter four Nb(V) complex structures with different coordinated *β*-diketonato ligands were presented. These structures were very similar with relation to bond lengths and angles, packing modes and all of the complexes displayed intermolecular interactions to some extent with the intermolecular hydrogen bonding being most frequent within the crystal lattices.

This chapter forms part of an overarching crystallographic investigation on *β*-diketonate ligand coordination to Nb(V) metal centres. A comprehensive discussion of all the complexes evaluated during this crystallographic study will be presented in Chapter 9 including an overview of the four structures presented in this chapter. The comparative nature of this subdivision will allow for a better evaluation of the effect that subtle changes on the coordinating *β*-diketonato ligands may have on the solid and solution state properties of the compounds.

In the following chapter, two additional Nb(V)-*β*-diketonato type complexes are structurally evaluated and described. The introduction of other electronic and steric changes to the coordinating ligands to allow for the manipulation of the intermolecular interactions, the packing of the crystal lattice and other physical properties associated with the crystal structures will be included.

Chapter 6: Chrystallographic Evaluation of [$NbOCl_3$(*β*-diket)] Complexes (2)

6.1 Overview

This chapter forms part of the over-arching crystallographic study relating to the coordination of different *β*-diketone ligands, with various substituents on the diketonato back-bone, to niobium(V) metal centres. As has been mentioned in previous sections, these varying substituents alter the electronic characteristics of the ligand as a whole, thereby influencing the chelation and stabilization aspects of the final coordination complex. *β*-diketones with fluorinated functionalities form a significant part of the focus in this investigation. The properties that govern ligand selection were noted in the discussions in Chapters 2 and 5. From these considerations it seems that fluorinated metal-*β*-diketonate complexes are favourable candidates for both potential sublimation separation as well as solvent extraction.[1,2,3,4,5,6] Some of the characteristics that govern these characteristics (intramolecular interactions, intermolecular interactions, bond distances and bond angles) can be studied and hopefully quantified to some extent by a detailed crystallographic investigation of the various complexes.

The focus of Chapter 5 was mainly on the utilization of unsymmetrical, acetylacetone-type ligands with a bulky aromatic substituents on the C5 atom in coordination to Nb(V) metal centres. These aryl substituents on the ligands are

[1] A. Chauvin, F. Gumy, I. Matsubayashi, Y. Hasegawa and J. G. Bunzli, (2006). *Eur. J. Inorg.*, **2**, 473-480.

[2] A. C. du Preez and J. S. Preston, (2004). *J. S.A.I.M.M.*, **1**, 333-338.

[3] H. O. Davies, T. J. Leedlam and A. C. Jones, (1999). *Polyhedron*, **18**. 3165-3172.

[4] P. Wendrup and V. G. Kessler, (2001). *J. Chem. Soc., Dalton Trans*, 574-579.

[5] E. L. Lippert and M. R. Truter, (1960). *J. Chem. Soc. A.*, **33**, 309-311.

[6] G. J. Bullen, R. Mason and P. Pauling, (1965). *Inorg Chem.*, **4**, 456-461.

sterically bulky and slightly electron-donating in nature.[7] Accordingly the emphasis may be shifted to gain greater insight into the electron and steric effects of other types of substituents. For this study, the large aryl group will be removed from the systems and smaller, more symmetrical *β*-diketones with electron-withdrawing groups on both the C3 and C5 carbons, will be considered. These ligands are illustrated in Figure 6.1.

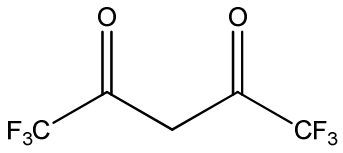

1,1,1-Hexafluoro-2,4-pentanedione
(HfaaH)

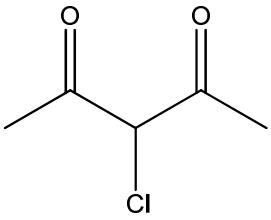

3-Chloro-2,4-pentanedione
(3Cl-acacH)

Figure 6.1 An Illustration of the symmetrical *β*-diketones coordinated to the Nb(V) synthon in this chapter.

The effect of fluorination on acetylacetonates has been discussed extensively in Section 2.3.1.3. The extent of the fluoride substituents influence both intermolecular interactions within the crystal structure but also increase the acidity of the complex due to the electron-withdrawing effect. However, in the case of the hfaaH ligand and the corresponding complexes, the electron-withdrawing effect is symmetrically enhanced throughout the metal complex. These significant aspects could be favourable in finding the ideal complex to be used in the solid and solution state separation of Nb(V) and Ta(V).

Even though the class of 3-substituted *β*-diketones coordination complexes has much application potential, there is an obvious shortage of current literature data on their complexing capability and the stability of resulting compounds. Lack of research interest in 3-substituted *β*-diketonates is seemingly mostly due to the difficulties in the isolation of pure ligand products of the hydrogen substitution of the acetylacetone

[7] H. Neuvonen, K. Neuvonen and P. Pasanen, (2004). *J. Org. Chem.*, **69**, 3794-3800.

methylene group.[8] Some successful investigations indicated that the substitution of the acidic hydrogen atom in the 3 position of the *β*-diketone with groups able to increase conjugation and/or steric effects improves the power of the hydrogen bridge, as evidenced by the shortening of the O···O distance.[9,10,11] 3-chloroacetylacetone is characterized by a 3-substituent with minimal steric hindrance but which has a chlorido group able to provide an electron-withdrawing effect. This is very interesting from a conformational point of view, because it can supply further information on the intramolecular forces governing the relative stabilities of such conformers.

This chapter will thus focus on the crystal structures of two addtional niobium(V) complexes obtained in the study; tetraethylammonium *mer*-(3-chloroacetylacetonato-κ^2O,O')trichloridooxidoniobate(V) ($(NEt_4)[NbOCl_3(3\text{-}Clacac)]$), (**Nb_6**)) and tetra ethylammonium *mer*-trichlorido(hexafluoroacetylacetonato-κ^2O,O')oxidoniobate(V) ($(NEt_4)[NbOCl_3(hfaa)]$), (**Nb_7**)). Emphasis will be placed on the solid state structural data of the above mentioned complexes with special attention given to general molecular geometry and intermolecular interactions that contribute to the stability of the crystal packing. Geometric parameters such as the bond distances and angles in the molecules will also be highlighted.

[8] J. L. Ault, H. J. Harries and J. Burgess, (1977). *Inorg. Chim. Acta*, **25**, 65-69.

[9] J. Emsley, (1984). *Struct. Bonding*, **57**, 147-155.

[10] J. Emsley, L. Y. Y. Ma, S. C. Nyburg and A. W. Parkins, (1990). *J. Mol. Struct.*, **240**, 59-66.

[11] Z. Yoshida, H. Ogoshi and T. Tokumitsu, (1970). *Tetrahedron*, **26**, 5691-5697.

6.2 Experimental

The X-Ray intensity data was collected on a Bruker X8 ApexII 4K Kappa CCD area detector diffractometer, equipped with a graphite monochromator and Mo$K\alpha$ fine-focus sealed tube (λ = 0.71069 Å, T = 100(2) K) operated at 2.0 kW (50 kV, 40 mA). The initial unit cell determinations and data collections were done by the SMART software package.[12] The collected frames were integrated using a narrow-frame integration algorithm and reduced with the Bruker SAINT-Plus and XPREP software packages respectively.[13] Analysis of the data showed no significant decay during the data collection. Data was corrected for absorption effects using the multi-scan technique SADABS, and the structure was solved by the direct methods package SIR97 and refined using the WinGX software incorporating SHELXL.[14,15,16,17] The final anisotropic full-matrix least-squares refinement was done on F^2. The methyl and aromatic protons were placed in geometrically idealized positions (C–H = 0.93 – 0.98 Å) and constrained to ride on their parent atoms with $U_{iso}(H) = 1.2U_{eq}(C)$. Non-hydrogen atoms were refined with anisotropic displacement parameters. The graphics were obtained with the DIAMOND program with 50% probability ellipsoids for all non-hydrogen atoms.[18]

---

[12] Bruker SMART-NT Version 5.050, (1998). *Bruker AXS Inc. Area-Detector Software Package*; Madison, Winconsin, USA**.**

[13] Bruker SAINT-Plus Version 6.02 (including XPREP), (1999). *Bruker AXS Inc. Area-Detector Integration Software*, Madison, Winconson, USA.

[14] Bruker SADABS Version 2004/1, (1998). *Bruker AXS Inc. Area Detector Absorption Correction Software*, Madison, Wisconsin, USA.

[15] A. Altomare, M. C. Burla, M. Camalli, G. L. Cascarano, C. Giacovazzo, A. Guagliardi, A. G. G. Moliterni, G. Polidori and R. Spagna, (1999). *J. Appl. Cryst.,* **32**, 115-119.

[16] L. J. Farrugia, (1999). *J. Appl. Cryst.* **32**, 837-838.

[17] G. M. Sheldrick; SHELXL97, (1997). *Program for Crystal Structure Refinement*, University of Göttingen, Germany.

[18] K. Brandenburg and H. Putz; DIAMOND, (2006). *Release 3.0e, Crystal Impact GbR*, Bonn, Germany.

Table 6.1 Crystallographic and refinement details for structures discussed in this chapter.

Crystal Formula	$(NEt_4)[NbOCl_3(3\text{-Clacac})]$	$(NEt_4)[NbOCl_3(hfaa)]$
Empirical formula	$C_{13}H_{26}Cl_4N_1NbO_3$	$C_{13}H_{21}Cl_3F_6N_1NbO_3$
Formula weight ($g.mol^{-1}$)	479.10	552.57
Crystal system, Space Group	Monoclinic, $P2_1/c$	Tetragonal, $P4_2/ncm$
a, b, c (Å)	15.273(4), 7.315(3) 18.276(3),	11.282(2), 11.282(2) 17.438(2),
α, β, γ (°)	90, 100.27(4), 90	90, 90, 90
Volume ($Å^3$), Z	2009.2(16), 4	2220.0(2), 4
Density (calculated, Mg/m^3)	1.584	1.653
Crystal colour	Yellow	White
Crystal size (mm^3)	0.34 x 0.16 x 0.15	0.44 x 0.30 x 0.25
Absorption coefficient μ (mm^{-1})	1.140	0.964
F(000)	976	1104
Theta range	2.7 – 26.6°	2.3 – 28.4°
Index ranges	-20<=h<=20, -9<=k<=9, -24<=l<=24	-9<=h<=9, -13<=k<=13, -15<=l<=14
Reflections collected, Independent Reflections, R_{int}	17399, 2967, 0.1121	16031, 727, 0.0617
Completeness to 2θ (°, %)	27.99, 99.9	28.38, 99.5
Max. and min. transmission	0.553 and 0.713	0.414 and 0.651
Data, restraints, parameters	5039, 0, 201	1485, 13, 99
Goodness-of-fit on F^2	0.983	1.053
Final R indices [I>2sigma(I)]	R_1 = 0.0512 wR_2 = 0.1390	R_1 = 0.0596 wR_2 = 0.1639
R indices (all data)	R_1 = 0.1043 wR_2 = 0.1888	R_1 = 0.1488 wR_2 = 0.2408
Largest diff. peak and hole ($e.Å^{-3}$)	0.89, -1.23	0.56, -1.30

6.3 Crystal Structure of Tetraethylammonium *mer*-(3-chloroacetylacetonato-κ^2O,O')trichloridooxidoniobate(V) ($(NEt_4)[NbOCl_3(3Cl\text{-}acac)]$), (Nb_6))

The complex, tetraethylammonium *mer*-(3-chloroacetylacetonato-κ^2O,O') trichloridooxidoniobate(V) ($(NEt_4)[NbOCl_3(3\text{-}Clacac)]$ (**Nb_6**)), has been synthesized as described in Section 3.3.1.6 and yellow plate-like crystals were obtained from an acetonitrile solution of the product.

The **Nb_6** compound crystallizes in the monoclinic space group, $P2_1/c$, with four $(NEt_4)[NbOCl_3(3\text{-}Clacac)]$ entities in the unit cell (Z = 4). The crystal structure as well as the numbering scheme of the complex is represented in Figure 6.4 (hydrogen bonds are omitted for clarity). General crystallographic information pertaining to the crystal structure is referred to in Table 6.1 and selected bond lengths and angles are given in Table 6.2. For comprehensive information regarding bond distances, angles, atomic coordinates and anisotropic displacement parameters related to the structure, refer to Appendix 7.

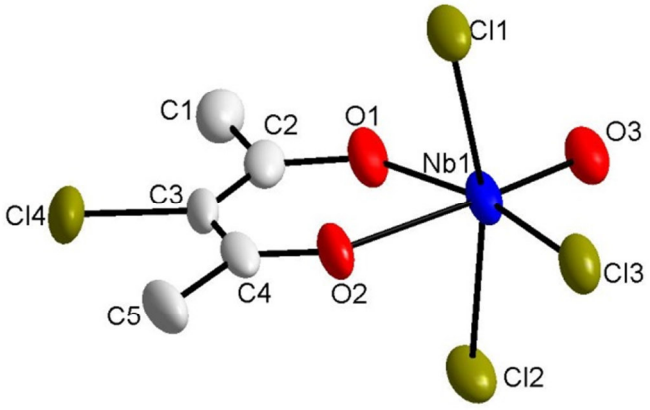

Figure 6.4 DIAMOND representation of the complex structure of $[NbOCl_3(3\text{-}Clacac)]^-$ (**Nb_6**) displaying the atom numbering system. The displacement ellipsoids are drawn at a 50 % probability level. Hydrogen atoms and counter-ion are omitted for clarity.

Nb_6 crystallizes in the monoclinic space group, $P2_1/c$, with four $(NEt_4)[NbOCl_3(3\text{-}Clacac)]$ entities in the unit cell (Z = 4). The asymmetric unit is built up of a Nb(V) metal centre, coordinated to three crystallographically independant chlorine atoms, the chelating *β*-diketone, an oxido oxygen atom and a tetraethylammonium counter-ion. The crystal comprises of isolated tetraethylammonium cations and *mer*-(3-chloroacetylacetonato-κ^2O,O')trichloridooxidoniobate(V) anions, with the niobium and nitrogen atoms on general positions within the crystal lattice. The niobium atom within the anion is at the centre of a distorted coordination octahedron. The tetraethylammonium counter-ion displays a disorder over two positions in 50:50 ratio.

The octahedral distortion can mostly be attributed the constraints of the oxido double bond, but several additional physical properties (steric and electronic), contribute to this inequality. This disparity can be described in terms of both complex bond lengths and angles.

Table 6.2 Selected bond lengths and angles of the *mer*-$[NbOCl_3(3\text{-}Clacac)]^-$ (**Nb_6**) anion.

***mer*-$[NbOCl_3(3\text{-}Clacac)]^-$**			
Atoms	**Bond length (Å)**	**Atoms**	**Bond length (Å)**
Nb1-Cl1	2.419(1)	Nb1-O1	2.023(1)
Nb1-Cl2	2.413(1)	Nb1-O2	2.280(1)
Nb1-Cl3	2.382(1)	Nb1-O3	1.704(1)
O1···O2[a]	2.721(2)	Out-of-plane distortion[b]	0.312(1)
Atoms	**Bond angle (º)**	**Atoms**	**Bond angle (º)**
O1-Nb1-O2	78.21(1)	O1-Nb1-O3	95.97(2)
Cl2-Nb1-Cl3	90.75(1)	O2-Nb1-O3	174.14(2)
Cl1-Nb1-O3	98.01(1)	C2-C3-C4	125.54(2)
Cl1-Nb1-Cl2	164.29(1)	Out-of-plane bend[c]	-3.33(2)

[a] Bite distance; [b] Out-of-plane distortion illustrated in Figure 6.3; [c] Out-of-plane *β*-diketonate ligand bend illustrated in Figure 6.2.

i) Table 6.2 notes that the Nb-Cl_{axial} distances for **Nb_6** are 2.419(1) and 2.413(1) Å, while the equatorial Nb1-Cl3 and Nb1-O3 bonds have distances of 2.382(1) and 1.715(1) Å. Comparison of the Nb1-O1 and Nb1-O2 bond lengths of the coordinated *β*-diketone, revealed distances of 2.023(1) vs. 2.280(1) Å. The Nb1-O2 bond (*trans* to the oxido) is thus more than 0.2 Å longer than the Nb1-O1 (*trans* to the chlorido), underlining the trans influence of the oxido ligand. This distortion from ideal octahedral geometry is further highlighted when considering the 0.312(1) Å out-of-plane distortion of the niobium metal centre as illustrated in Figure 6.3.

ii) The *trans* Cl1-Nb1-Cl2 angle is 164.29(1) º, while the O1-Nb1-O2 bite angle is 78.21(1) º. Out-of-plane bend determination was achieved by measuring the angle between the O1, O2 and Nb1 plane and the O1, C2, C3, C4 plane which revealed a -3.33(1) º out-of-plane bend of the coordinated ligand. When constructing an equatorial plane through O1, O2, O3 and Cl3, it was observed that all of the atoms lie in this plane.

There are abundant intermolecular hydrogen bonding stabilzation interactions within this molecule. A hydrogen bond interaction is defined as a type of dipole-dipole interaction which is the electromagnetic attraction between a partially positively charged hydrogen atom attached to an electronegative atom and another nearby electronegative atom.[19] These interactions are very complex, occur extensively and can be observed as either counter-ion-anion or anion-anion connections. Hydrogen bonding for selected carbon, chlorine (anion-anion and anion-counter-ion) and oxygen atomic groups are noted for this structure. These interactions are illustrated in blue in Figures 6.5, 6.6, 6.7 and 6.8 and data related to the hydrogen bonds given in Table 6.3.

[19] T. K. Harris and A. S. Mildvan, (1999). *Proteins*, **35**, 275-282.

Table 6.3 Hydrogen bond geometry for **Nb_6** as depicted in Figure 6.5-6.8.

D-H···A	dD-H (Å)	dH···A (Å)	dD···A (Å)	Angle D-H···A (°)
Oxygen	(Figure 6.5)			
C21-H21C···O3^{i}	0.960(1)	2.664(1)	3.498(1)	145.40(2)
C21-H21B···O3^{ii}	0.960(1)	2.673(1)	3.620(1)	168.82(2)
C26-H26B···O3^{ii}	0.969(1)	2.624(1)	3.421(1)	139.66(3)
Chlorine (Inter-anion)	(Figure 6.6)			
C1-H1B···Cl3^{iii}	0.960(1)	2.778(1)	3.661(1)	153.29(2)
C5-H5C···Cl4^{iv}	0.959(1)	2.823(1)	3.575(1)	135.86(3)
C1-H1C···Cl4^{v}	0.961(1)	2.690(1)	3.543(1)	148.20(3)
Chlorine (Counter-ion)	(Figure 6.7)			
C20-H20A···Cl1^{vi}	0.971(1)	2.813(1)	3.775(1)	170.88(1)
C24-H24B···Cl2^{vii}	0.959(1)	2.924(1)	3.743(1)	151.95(2)
C27-H27A···Cl2^{iii}	0.970(1)	2.869(1)	3.875(1)	166.87(2)
Carbon	(Figure 6.8)			
C5-H5C···H27C^{i}	0.960(1)	2.664(1)	3.498(1)	145.40(2)

Symmetry code: i) *-x, ½+y, 3/2-z;* ii) *x, ½-y, ½+z*; iii) *x, -1+y, z;* iv) *1-x, ½+y, 3/2-z*; v) *1-x, 1-y, 2-z;* vi) *x, y, z;* vii) *x, -½-y, ½+z.*

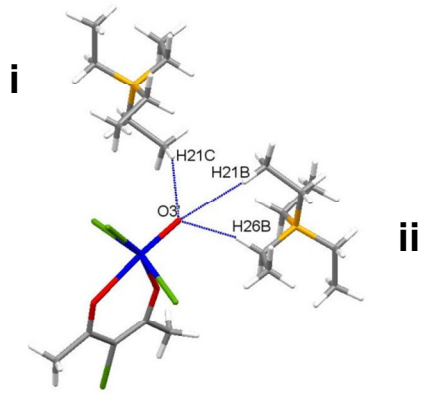

Figure 6.5 A graphic illustration of the stabilizing hydrogen bonding (indicated in blue) of selected oxygen substituents connecting neighbouring anion-counter-ion moeities of **Nb_6**.

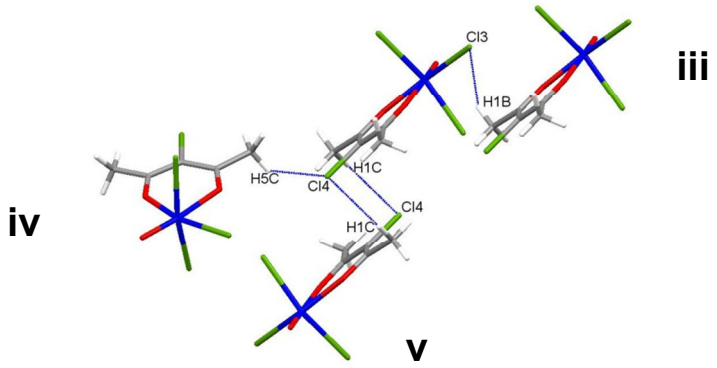

Figure 6.6 A graphic illustration of the stabilizing hydrogen bonding (indicated in blue) of selected chloride substituents connecting neighbouring anion moeities of **Nb_7**.

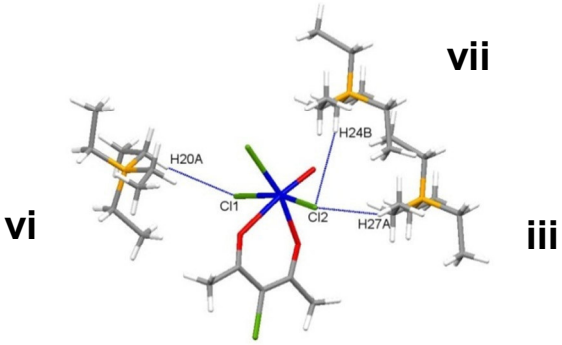

Figure 6.7 A graphic illustration of the stabilizing hydrogen bonding (indicated in blue) of selected chloride substituents connecting neighbouring anion-counter-ion moeities of **Nb_6**.

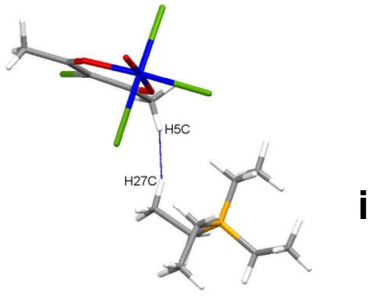

Figure 6.8 A graphic illustration of the stabilizing hydrogen bonding (indicated in blue) of selected carbon atoms connecting neighbouring anion-counter-ion moeities of **Nb_6**.

The array of hydrogen bonds observed seems to enhance the solid state ordering of the compound. This tightly knit two-dimensional interaction network rigidly ties the crystal lattice together in a “head-to-tail” packing fashion throughout the system. An illustration of the crystal lattice packing of **Nb_6** is illustrated in Figure 6.9. When viewing the crystal structure along the c-axis this “head-to-tail” crystal packing structure can be observed. It is also noticed that the cavities between the Nb(V) moieties are filled by the tetraethylammonium ($(NEt_4)^+$) counter ions. These cavities are quite large with relation to the counter ion and leaves sufficient space for the disordered nature of the $(NEt_4)^+$ cation.

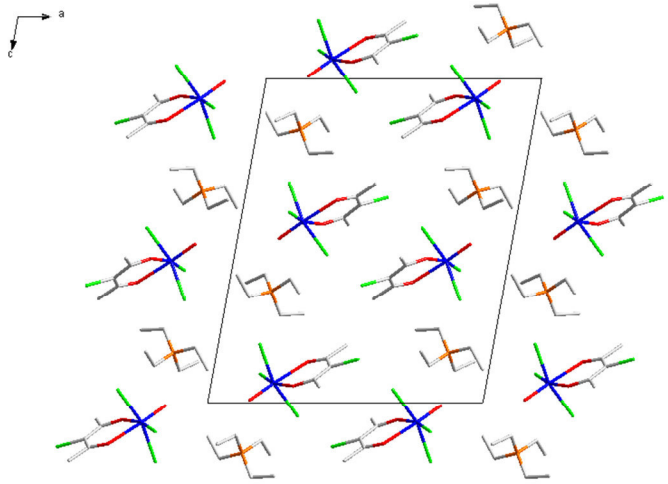

Figure 6.9 A graphic illustration highlighting to “head-to-tail” crystal packing as well as the voids filled by the tetraethylammonium cations of $(NEt_4)[NbOCl_3(3\text{-}Clacac)]$ (**Nb_6**) along the b-axis.

6.4 Crystal Structure of Tetraethylammonium *mer*-trichlorido (hexafluoroacetylacetonato-κ^2O,O')oxidoniobate(V) ($(NEt_4)[NbOCl_3(hffa)]$), (Nb_7))

The crystal structure of tetraethylammonium *mer*-trichlorido (hexafluoro acetylacetonato-κ^2O,O')oxido niobate(V) ($(NEt_4)[NbOCl_3(hfaa)]$ (**Nb_7**)) forms part of an investigation which focuses on studying applied ligand chelation effects with varying substituents on novel Ta(V)- and Nb(V)-compounds. Synthesis of **Nb_7** and the resulting yellow crystals obtained was discussed in Section 3.3.1.2.

A summary of the general crystallographic data is given in Table 6.1, while the numbering scheme of the complex is shown in the perspective drawing in Figure 6.10. Table 6.4 presents selected bond lengths and angles of **Nb_7**. Atomic coordinates, anisotropic displacement parameters, bond distances and angles and hydrogen coordinates, are given in the supplementary data (Appendix 8). Hydrogen atoms are omitted for clarity.

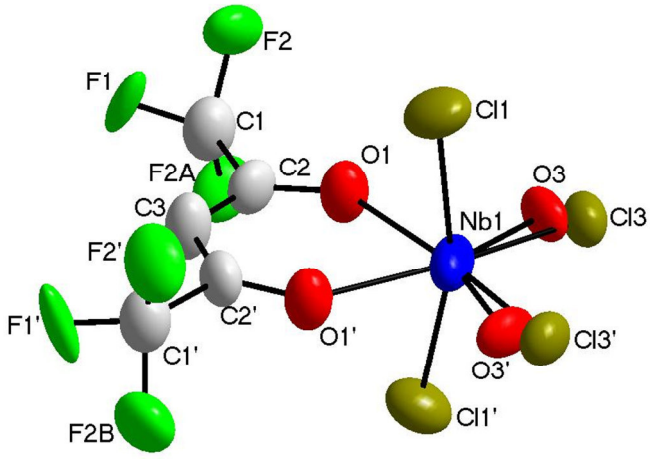

Figure 6.10 DIAMOND representation of the complex structure of $[NbOCl_3(hfaa)]^-$ (**Nb_7**) displaying the atom numbering system. The displacement ellipsoids are drawn at a 50 % probability level. Hydrogen atoms and counter-ion are omitted for clarity.

Nb_7 crystallizes in the tetragonal space group, $P4_2/ncm$, with four $(NEt_4)[NbOCl_3(hfaa)]$ entities in the unit cell ($Z = 4$). The crystal is built up of isolated tetraethylammonium cations and *mer*-trichlorido(hexafluoroacetylacetonato-κ^2O,O') oxidoniobate(V) anions, with the niobium and nitrogen atoms on special positions within the crystal lattice. The asymmetric unit consists of half a Nb(V) metal centre surrounded by three crystallographically independent groups; an axial chlorido group (Cl1), an equatorial oxido group (O3), one half of the *O,O'*-bonded thenoyltrifluoroacetonato ligand (O1) and a quarter of a tetraethylammonium counter-ion. The rest of the molecule is symmetrically generated through the various mirror planes. Accordingly, the complete anion is at the centre of a distorted coordination octahedron of three chlorine atoms, the chelating *β*-diketone and an oxido oxygen atom. The complex molecule displays an oxido/chlorido disorder over two positions in a 50 ***Nb^A*** *(red)*: 50 ***Nb^B*** *(blue)* ratio as shown in Figure 6.11. The tetraethylammonium counter-ion also displays a disorder over two positions in 50:50 ratio.

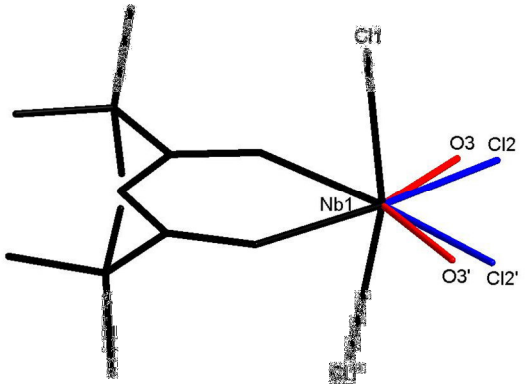

Figure 6.11 Graphic illustration of the *mer*-$[NbOCl_3(hfaa)]^-$ anion illustrating the disorder in an overlay (**red**) ***Nb^A*** = 50.0%; (**blue**) ***Nb^B*** = 50.0%. Hydrogen atoms and counter-ion omitted for clarity.

This chlorido/oxido disorder averages out the effect caused by the valence shell electron pair repulsions between Cl and O atoms that caused the lengthening of the in the Nb-O2(O1') bond distance noticed in the previous structures. Interestingly, the coordination polyhedron around the niobium(V) metal centre still has a distorted octahedral geometry. This inequality can be described in terms of both complex bond lengths and angles.

Table 6.4 Selected bond lengths and angles of the *mer*-$[NbOCl_3(hfaa)]^-$ anion.

***mer*-$[NbOCl_3(hfaa)]^-$**			
Atoms	**Bond length (Å)**	**Atoms**	**Bond length (Å)**
Nb1-Cl1	2.374(1)	Nb1-O1	2.223(1)
Nb1-Cl1'	2.374(1)	Nb1-O1'	2.223(1)
Nb1-Cl3	2.198(1)	Nb1-O3	1.836(1)
O1···O2[a]	2.800(2)	Out-of-plane distortion[b]	0.168(1)
Atoms	**Bond angle (º)**	**Atoms**	**Bond angle (º)**
O1-Nb1-O1'	78.08(1)	O1-Nb1-O3	89.04(2)
Cl1'-Nb1-Cl3	95.62(1)	O1'-Nb1-O3	162.10(1)
Cl1-Nb1-O3	94.34(1)	C2-C3-C2'	122.09(2)
Cl1-Nb1-Cl1'	164.06(1)	Out-of-plane bend[c]	0

[a] Bite atom distance; [b] Out-of-plane distortion illustrated in Figure 6.3; [c] Out-of-plane *β*-diketonate ligand bend illustrated in Figure 6.2.

i) The Nb-Cl_{axial} distance for **Nb_7** is 2.374(1) Å, while the equatorial Nb1-Cl3 and Nb1-O3 bonds have distances of 2.198(1) and 1.836(1) Å. The Nb1-O1 bond lengths of the coordinated *β*-diketone, revealed distances of 2.223(1) Å. In contrast to all the aforementioned structures, the *trans* influence of the oxido group in averaged out due to the chloride/oxido disorder. This distortion from ideal octahedral geometry is further highlighted when considering the 0.168(1) Å out-of-plane distortion of the niobium metal centre.

ii) According to Table 6.4, the *trans* Cl1-Nb1-Cl1' angle is 164.06(1) º, while the O1-Nb1-O1' bite angle is 78.08(1) º. When constructing an equatorial plane through O1, O2, O3 and Cl3, it was observed that all of the atoms lie exactly in this plane.

Restricted intermolecular hydrogen bonds contribute to the stabilization of the crystal lattice. For this symmetric structure these interactions can be observed as a counter-ion-anion connection. These interactions are illustrated in blue in Figure 6.12 and data related to the hydrogen bonds given in Table 6.5.

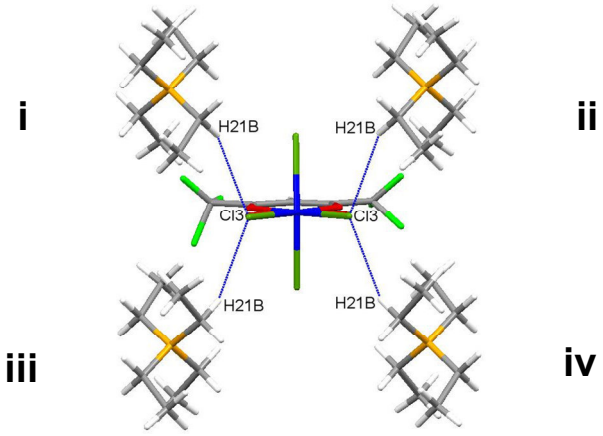

Figure 6.12 A graphic illustration of the stabilizing hydrogen bonding (indicated in blue) of selected chloride substituents connecting neighbouring anion-counter-ion moeities of **Nb_7**.

Table 6.8 Hydrogen bond geometry for **Nb_7** as depicted in Figure 6.12.

C-H···Cl	dC-H (Å)	dH···Cl (Å)	dC···Cl (Å)	Angle C-H···Cl (°)
C21-H21B···Cl3^{i}	0.970(1)	2.765(1)	3.518(1)	134.95(3)
C21-H21B···Cl3^{ii}	0.970(1)	2.765(1)	3.518(1)	134.95(3)
C21-H21B···Cl3^{iii}	0.970(1)	2.765(1)	3.518(1)	134.95(3)
C21-H21B···Cl3^{iv}	0.970(1)	2.765(1)	3.518(1)	134.95(3)

Symmetry code: i) *1-y, 1-x, -z;* ii) *½+y, ½+x, -z*; iii) *1-x, 1-y, -z;* iv) *½+x, ½+y, -z.*

This tightly knit two-dimensional interaction network rigidly ties the crystal lattice together, influencing the overall packing of these niobium anions dispersed in a "head-to-tail" packing fashion throughout the system. An illustration of the crystal lattice packing of **Nb_7** is illustrated in Figure 6.13. When viewing the crystal structure along the c-axis this "head-to-tail" crystal packing structure can be observed.

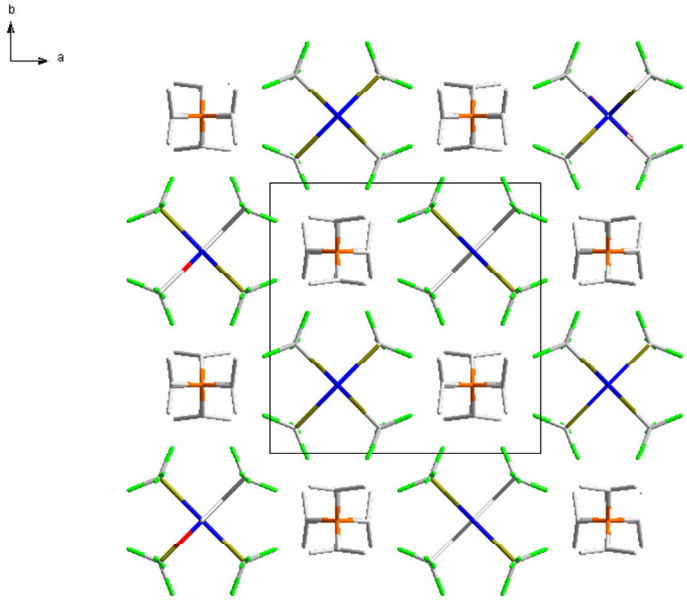

Figure 6.13 A graphic illustration highlighting to “head-to-tail” crystal packing as well as the voids filled by the tetraethylammonium cations of $(NEt_4)[NbOCl_3(hfaa)]$ (**Nb_7**) along the c-axis.

6.5 Discussion

Two additional Nb(V)-*β*-diketonate complexes have been investigated and described thus far in the preceding sections. The general structural parameters, bond distances and angles from the various complexes as in are given in Table 6.9. Synthesis of these complexes as described in Chapter 3 seems to afford these types of compounds with relative ease, reproducibly and with very high yields. The success of this approach can be attributed to the more stable $(Et_4N)[NbCl_6]$ synthon, described in Chapter 4. An added advantage is that these complexes form rapidly, without any special manipulations, minimal solvent waste is evolved and forms in 85+ % yields. This approach is much more cost effective, environmentally friendly and accordingly ideal to further a separation study.

Table 6.9 Cell dimension overview of presented Nb(V)-*β*-diketonate complexes.

Crystal Formula	$(NEt_4)[NbOCl_3(3\text{-}Clacac)]$	$(NEt_4)[NbOCl_3(hfaa)]$
Bond Distances (Å)		
Nb1-O1	2.023(1)	2.223(1)
Nb1-O2	2.280(1)	2.223(1)
Nb1-O3	1.704(1)	1.836(1)
Nb1-Cl1	2.419(1)	2.223(1)
Nb1-Cl2	2.413(1)	2.223(1)
Nb1-Cl3	2.382(1)	2.198(1)
O1···O2	2.721(2)	2.800(2)
Out-of-plane distortion	0.312(1)	0.168(1)
Bond Angles (°)		
O1-Nb1-O2	78.21(1)	78.08(1)
Cl2-Nb1-Cl3	90.75(1)	95.62(1)
Cl1-Nb1-O3	98.01(1)	94.34(1)
Cl1-Nb1-Cl2	164.29(1)	164.06(1)
O1-Nb1-O3	95.97(2)	89.04(2)
O2-Nb1-O3	174.14(2)	162.10(1)
C2-C3-C4	125.54(2)	122.09(2)
Out-of-plane bend[c]	-3.33(2)	0

As was found for the compounds in Chapter 5, the coordination environment around the Nb(V) metal centre for both of the complexes tends to favour the octahedral polyhedron with noticeable distortion. This was discussed in Sections 6.3 and 6.4. When comparing these bond distances and angles to structures from literature it was found that they correlate very well.[4,5,20,21,22] In this regard, a more detailed comparative relation study of these Nb(V)-*β*-diketonate complexes as well as the four additional structures, discussed in the previous chapter, will be undertaken in Chapter 9. Properties such as steric bulk and electronic properties of the *β*-diketonate complex of the will be correlated to various aspects such as complex stability and structural effects.

[20] L. Herbst, H. G. Visser, A. Roodt and C. Pretorius, (2012). *Acta Cryst.*, **E68**, m1392-1394.

[21] L. Herbst, H. G. Visser and A. Roodt, (2015). *Z. Cryst. NCS.*, **228**, 451-456.

[22] L. Herbst, H. G. Visser and A. Roodt, (2015). *Z. Cryst. NCS.*, **228**, 397-402.

6.6 Conclusion

In this chapter two additional Nb(V) complex structures with different coordinated *β*-diketonate ligands were presented. Both of these structures were very similar with relation to bond lengths and angles to the structures previously investigated, with the noticeable exception being the identical niobium-oxygen bond distances of the *β*-diketonate ligands of the $[NbOCl_3(hfaa)]^-$ anion. This was caused by the oxido/chlorido disorder and illustrated in Figure 6.11. All of the complexes displayed varying degrees of intermolecular interactions such as halogen···halogen interactions and hydrogen bonding within the crystal lattices. It was obvious that the fluoride substituents on the hfaa backbone markedly reduced the extent of the intermolecular interactions vs. the non-fluorinated 3-Clacac counterpart.

This chapter forms part of an overarching crystallographic investigation on *β*-diketonate ligand coordination to Nb(V) metal centres. A comprehensive discussion of all the complexes evaluated during this crystallographic study will be presented in Chapter 9 including the two structures presented in this chapter. The comparative nature of this subdivision will allow for a better evaluation of the effect that subtle changes on the coordinating *β*-diketonato ligands may have on the solid and solution state properties of the compounds.

In the following chapter, various Nb(V)-tropolonato type complexes are structurally evaluated and described. The main focus will be placed on the influence of pH of reaction solution on the coordination modes and coordination geometry of the obtained solid-state structures.

Chapter 7: Chrystallographic Evaluation of Nb(V)- and Ta(V) Tropolonato Complexes

7.1 Overview

In the three preceding chapters focus was placed on identifying the ideal Nb(V) synthon and coordination of this compound to various functionalized *β*-diketone type ligands. The logic behind this was that a more stable synthon would afford more easily accessible and hopefully more stable products. It was noted that the cause of instability of the unmodified $[NbCl_5]_2$ and $[TaCl_5]_2$ starting materials has been ascribed to the hydrolysis of the metal synthon under atmospheric conditions.[1] Even though significant success was achieved using the more robust $(NEt_4)[NbCl_6]$ synthon, the use of an unmodified synthon in a separation method would be advantageous as this would lower costs.

On conducting a background literature review, a singular unique study revealed that bidentate ligands have successfully been coordinated to Ta(V)- and Nb(V)- metal centres using the unmodified synthons in atmospheric conditions.[2] According to Muetteries *et al*., niobium(V) and tantalum(V) pentachlorides react with acidic aqueous solutions of tropolone to form the tetrakistropolonato cations $[Nb(Trop)_4]^+$ and $[Ta(Trop)_4]^+$, with near quantitative yields.[2] The focus of their investigation was to determine the effect of pH on the hydrolytic stabilities of the Ta(V)- and Nb(V)-tropolonato analogues. From the ^{1}H-NMR kinetic investigation, it was found that in strongly acidic media both $[Nb(Trop)_4]^+$ and $[Ta(Trop)_4]^+$ species were found to be stable. With increasing temperature or pH, the niobium chelate undergoes partial

[1] C. K. Gupta and A. K. Suri, (1993). *Extractive Metallurgy of Niobium*. **1**, New York, United States of America.

[2] E. L. Muetteries and C. M. Wright, (1965). *J. Am. Chem. Soc.*, **87**, 4706-4717.

hydrolysis to the neutral [$NbO(Trop)_3$] which separates from solution. This type of chemical difference in coordinative behaviour is an ideal starting point to be potentially used in a separation strategy.

The solution state investigation of the formation of these compounds was very thorough but not much attention was given to the solid state characteristics of the compounds.[2] With this in mind, a crystallographic investigation of the coordination modes and intermolecular interactions could shed even more light on this nuance between Ta(V) and Nb(V) behaviour. Accordingly, the crystal structures of [$NbO(Trop)_3$], [$Ta(Trop)_4$]Cl and [$Nb(Trop)_4$]Cl as obtained following the above strategy will be discussed in this chapter. These compounds have either a *tris*-Trop-oxido (seven) or *tetrakis*-Trop (eight) coordination mode. The different modes of coordination have various subdivisions and are characterized according to specific properties depending on the type of ligand coordination.

For [$M(Bid)_3(X)$] complexes (M = Nb; Bid = Trop; X = O), like [$NbO(Trop)_3$], as discussed in Section 2.3.1.4, a seven-coordinate geometry is expected. An idealized representation of this seven-coordinate structure can be obtained by adding a supplementary vertex (ligand) to a regular octahedron as was illustrated in Figure 2.6. From this vertex addition, 3 types of complex geometries could be obtained, namely; a pentagonal bipyramidal geometry (D_5h), a capped octahedron (C_3v) or capped trigonal prism (C_2) and are shown in Figure 7.1. There are various examples of each coordination mode found in published structures for a wide variety of metal centres, but in the case of Nb(V) and Ta(V) the data is very limited.[3] Accordingly, a crystallographic investigation of these compounds was proposed to provide additional insight of the coordination preferences and modes.

[3] Cambridge Structural Database (CSD) Version 5.35, November 2013 update. F.H. Allen, (2002). *Acta Cryst*., **B58**, 380-388.

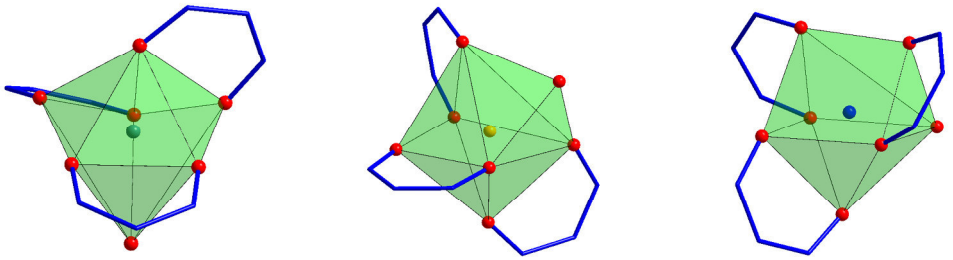

Pentagonal bipyramidal (D_5h) **Capped octahedron (C_3v)** **Capped trigonal prism (C_2)**

Figure 7.1 Illustration of the various seven-coordinate crystallographic geometries.

For $[M(Bid)_4]^+$ complexes, like $[Ta(Trop)_4]Cl$ and $[Nb(Trop)_4]Cl$, as discussed in Section 2.3.1.4, an eight-coordinate geometry is expected. This *tetrakis*-coordination is also well-known to favour a square anti-prismatic (SAP) type of polyhedron or geometry.[4,5] From the discussion on eight-coordinated and square antiprismatic geometry found in metal complexes included in Section 2.3.3, three possible isomers are observed and classified. For complexes with four *O,O*-donating bidentate ligands chelated to the metal centre, the specific position of these groups on the square antiprism dictates the named isomer. These isomers are defined according to that shown in Figure 7.2.

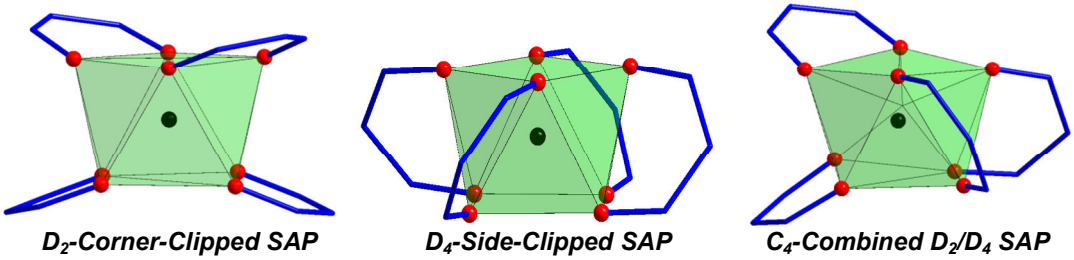

D_2-Corner-Clipped SAP ***D_4-Side-Clipped SAP*** ***C_4-Combined D_2/D_4 SAP***

Figure 7.2 Illustration of different eight-coordinate SAP isomers.

Owing to steric and electronic effects of the ligands, the square antiprismatic (SAP) geometry may distort to the bicapped trigonal prism (BTP) geometry as illustrated in Figure 2.25, while additional distortion will lead to dodecahedral (DD) geometry.

[4] J. V. Silverton and J. L. Hoard, (1963). *Inorg. Chem.*, **2**, 243-249.

[5] J. L. Hoard and J. V. Silverton, (1963). *Inorg. Chem.*, **2**, 235-242.

Limited knowledge relating to eight-coordinate Nb(V) and Ta(V) is found in literature sources.[3] Thus, the overarching aim in this study is to investigate tropolonato ligands which induce *tetrakis*-coordination to see if it is possible to manipulate the solid state structural properties in such a way to induce different physical or chemical behaviours for Ta(V) and Nb(V). In particular, since O-M-O bite angle in tropolonato complexes are typically about 10 º smaller since a five coordinate chelate is formed, compared to the six-membered bonding mode in the *β*-diketone type ligands.

7.2 Introduction

Tropolone (TropH) is a very effective chelating agent and has a wide range of applications in chemistry. In coordination compounds, the tropolonato ion forms a five-membered chelating ring with a bite distance and angle smaller than that of a *β*-diketonate.[6] Metal-tropolonato complexes have a duplicitious nature in that the molecule can either behave as an allylic or aromatic functionality.[7] Several general characteristic intermolecular properties of tropolonato compounds are observed in the solid state packing and can potentially be most revealing in unlocking the mysteries of the molecule's behaviour.[8] These properties include; hydrogen bonding and π-π stacking.

Various aspects of hydrogen bonding in solid state complexes have been discussed extensively in Chapters 5 and 6 (see Sections 5.4 and 6.3). Intermolecular π-π stacking is a secondary aspect of solid state interactions in most tropolonato compounds.[9] This effect is caused by the delocalization of electron density on the cycloheptatriene ring system over the entire molecule.[10] In general the intermolecular

[6] M. J. S. Dewar, (1950). *Science*, **166**, 790-791.

[7] V. R. Sastri and J. R. Ramachandra, (2001). *Modern Aspects of Rare Earths and their Complexes*, Netherlands.

[8] J. C. A. Booyens and J. F. Oglvie, (2008). *Models, Mysteries, and Magic of Molecules*, Netherlands.

[9] M. J. Rashkin and M. L. Waters, (2002). *J. Am. Chem. Soc.*, **124**, 1860–1861.

[10] G. B. McGaughey and M. Gagne, (1998). *J. Biol. Chem.*, **273**, 15458-15463.

interaction is of order *c.a.* 3.7(3) Å with an inter-planar dihedral angle of only 0.7(8) ° between the rings.[11] An example is illustrated in Figure 7.3.

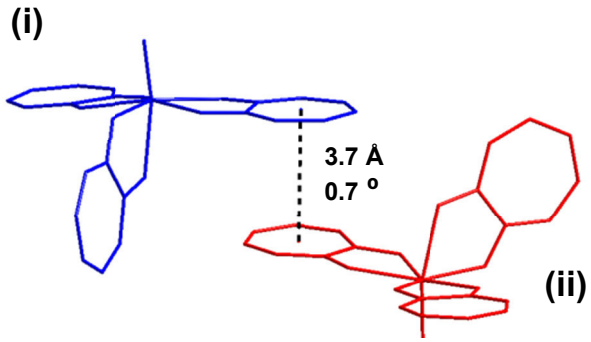

Figure 7.3 Depiction of general intermolecular π-π stacking.[11]

7.3 Experimental

The X-Ray intensity data was collected on a Bruker X8 ApexII 4K Kappa CCD area detector diffractometer, equipped with a graphite monochromator and Mo*Kα* fine-focus sealed tube (*λ* = 0.71069 Å, T = 100(2) K) operated at 2.0 kW (50 kV, 40 mA). The initial unit cell determinations and data collections were done by the SMART software package.[12] The collected frames were integrated using a narrow-frame integration algorithm and reduced with the Bruker SAINT-Plus and XPREP software packages respectively.[13] Analysis of the data showed no significant decay during the data collection. Data was corrected for absorption effects using the multi-scan technique SADABS, and the structure was solved by the direct methods package

[11] S. Grimme, (2008). *Angew. Chem. Int. Ed.*, **47**, 3430-3434.

[12] Bruker SMART-NT Version 5.050, (1998). *Bruker AXS Inc. Area-Detector Software Package*; Madison, Winconsin, USA.

[13] Bruker SAINT-Plus Version 6.02 (including XPREP), (1999). *Bruker AXS Inc. Area-Detector Integration Software*, Madison, Winconson, USA.

SIR97 and refined using the WinGX software incorporating SHELXL.[14,15,16,17] The final anisotropic full-matrix least-squares refinement was done on F^2. The methyl and aromatic protons were placed in geometrically idealized positions (C–H = 0.93 – 0.98 Å) and constrained to ride on their respective parent atoms with $U_{iso}(H) = 1.2U_{eq}(C)$. Non-hydrogen atoms were refined with anisotropic displacement parameters. The graphics were obtained with the DIAMOND program with 50% probability ellipsoids for all non-hydrogen atoms.[18]

[14] Bruker SADABS Version 2004/1, (1998). *Bruker AXS Inc. Area Detector Absorption Correction Software*, Madison, Wisconsin, USA.

[15] A. Altomare, M. C. Burla, M. Camalli, G. L. Cascarano, C. Giacovazzo, A. Guagliardi, A. G. G. Moliterni, G. Polidori and R. Spagna, (1999). *J. Appl. Cryst.,* **32**, 115-119.

[16] L. J. Farrugia, (1999). *J. Appl. Cryst.* **32**, 837-838.

[17] G. M. Sheldrick; SHELXL97, (1997). *Program for crystal structure refinement*, University of Göttingen, Germany.

[18] K. Brandenburg and H. Putz; DIAMOND, (2006). *Release 3.0e, Crystal Impact GbR*, Bonn, Germany.

Table 7.1 Crystallographic and refinement details for structures discussed in this chapter.

Crystal Formula	$[NbO(Trop)_3]$ (Nb_8)	$[Nb(Trop)_4]Cl$ (Nb_9)	$[Ta(Trop_4)]Cl$ (Ta_2)
Empirical formula	$C_{21}H_{15}NbO_7$	$C_{28}H_{20}NbO_8$	$C_{28}H_{20}O_8Ta$
Formula weight ($g.mol^{-1}$)	472.24	537.80	625.55
Crystal system, Space Group	Monoclinic, $P2_1/c$	Triclinic, $P\bar{1}$	Monoclinic, $C2/c$
a, b, c (Å)	7.399(1), 16.520(2) 16.801(2)	10.027(3), 12.907(3), 14.750(4)	19.626(3), 20.360(3) 22.446(3)
α, β, γ (°)	90, 100.85(2), 90	68.776(4), 78.141(3), 81.860(4)	90, 96.050(3), 90
Volume ($Å^3$), Z	2017.1(4), 4	1778.3(1), 2	2919.3(4), 4
Density (calculated, Mg/m^3)	1.555	1.371	1.506
Crystal colour	Orange	Orange	Yellow
Crystal size (mm^3)	0.23, 0.18, 0.08	0.53 x 0.13 x 0.09	0.25 x 0.18 x 0.10
Absorption coefficient μ (mm^{-1})	0.636	0.399	3.802
F(000)	952	583	3828
Theta range	1.75 - 28.37°	2.45 - 27.70°	1.35 - 28.00°
Index ranges	-9<=h<=9, -20<=k<=22, -21<=l<=21	-12<=h<=12, -15<=k<=15, -17<=l<=17	-29<=h<=29, -26<=k<=26, -25<=l<=25
Reflections collected, Independent Reflections, R_{int}	4961, 1893, 0.1697	6119, 3518, 0.1556	4792, 6477, 0.1617
Completeness to 2θ (°, %)	28.4, 98.4	28.00, 97.6	28.00, 100
Max. and min. transmission	0.424 and 0.756	0.333 and 0.838	0.278 and 0.687
Data, restraints, parameters	27842, 0, 262	20299, 0, 370	10753, 0, 240
Goodness-of-fit on F^2	0.996	1.296	1.152
Final R indices [I>2sigma(I)]	R_1 = 0.0779 wR_2 = 0.1810	R_1 = 0.1995 wR_2 = 0.2956	R_1 = 0.1131 wR_2 = 0.3584
R indices (all data)	R_1 = 0.2059 wR_2 = 0.2781	R_1 = 0.2586 wR_2 = 0.3470	R_1 = 0.1803 wR_2 = 0.4097
Largest diff. peak and hole ($e.Å^{-3}$)	0.92, -0.84	0.40, -1.04	3.31, -2.15

7.4 Crystal Structure of Oxido-*tris*(tropolonato-κ^2*O,O'*)niobium(V) ([NbO(Trop)$_3$]), (Nb_8))

The crystal structure of oxido-*tris*(tropolonato-κ^2*O,O'*)niobium(V) ([NbO(Trop)$_3$]), (**Nb_8**)) forms part of an investigation which focuses on studying applied ligand chelation effects on the coordination geometry of Ta(V)- and Nb(V)-compounds. Synthesis of **Nb_8** and the resulting orange crystals obtained were discussed in Section 3.4.3. The title compound was previously prepared by Drew *et al*., with X-ray diffraction data collected at room temperature.[19] It has to be pointed out that the absence of a water of hydration in the current structure highlights the difference between that reported by Drew *et al*. For this study, the reaction was modified as described above and the data collected at 100 K.

The complex crystallizes in the monoclinic $P2_1/c$ space group, in discrete [NbO(Trop)$_3$] entities. The sub-standard Goodness-of-fit (0.996) and R_{int} (0.1697) is indicative of the twinned nature of these crystals and adversely effects data quality. A summary of the general crystallographic data is given in Table 7.1, while the numbering scheme of the complex is shown in the perspective drawing in Figure 7.4. Table 7.2 presents selected bond lengths and angles of **Nb_8**. Atomic coordinates, anisotropic displacement parameters, bond distances and angles and hydrogen coordinates, are given in the supplementary data (Appendix 9). Hydrogen atoms are omitted for clarity.

[19] M. G. Drew, D. A. Rice and D. M. Williams, (1986). *Inorg. Chim. Acta*, **118**, 165-168.

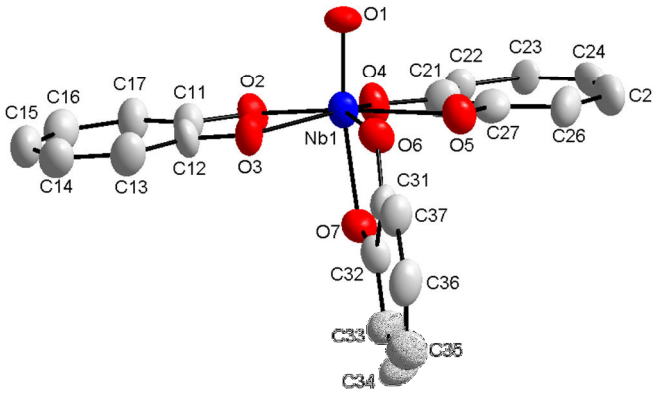

Figure 7.4 DIAMOND representation of the complex structure of $[NbO(Trop)_3]$ (**Nb_8**) displaying the atom numbering system. The displacement ellipsoids are drawn at a 50 % probability level. Hydrogen atoms are omitted for clarity.

Table 7.2 Selected bond lengths and angles of the $[NbO(Trop)_3]$ (**Nb_8**).

$[NbO(Trop)_3]$ (Nb_8)			
Atoms	**Bond length (Å)**	**Atoms**	**Bond length (Å)**
Nb-O1	1.754(3)	Nb-O5	2.186(2)
Nb-O2	2.126(2)	Nb-O6	2.125(2)
Nb-O3	2.152(2)	Nb-O7	2.216(2)
Nb-O4	2.113(2)	Out-of-plane distortion[a]	0.206(1)
Atoms	**Bond angle (º)**	**Atoms**	**Bond angle (º)**
O2-Nb1-O3	69.69(2)	O1-Nb1-O4	100.51(3)
O4-Nb1-O5	71.59(2)	O1-Nb1-O7	162.10(3)
O6-Nb1-O7	72.37(2)	O4-Nb1-O6	144.94(3)

[a] Out-of-plane distortion of the Nb(V) atom illustrated in Figure 7.6.

The coordination polyhedron around the niobium(V) metal centre for **Nb_8** has a distorted pentagonal bipyramidal geometry. The general pentagonal bipyramidal geometry has a sp^3d^3 hybridization, where one *s*, three *p*, and three *d* (d_{xy}, d_{yz} and d_{zx}) orbitals combine and give a set of seven hybrid orbitals.[20] These orbitals are orientated to the seven corners of a regular pentagonal bipyramid. Five of these orbitals (basal hybrid planes) lie in the pentagonal plane while the remaining orbitals

[20] R. Hoffmann, B. F. Beier, E. L. Muetteries and A. R. Rossi, (1977). *Inorg. Chem.*, **3**, 511-522.

(axial hybrid orbitals) are found above and below this plane or on the approximate vertices of the polyhedron.

In the case of the title compound, **Nb_8**, the terminal oxygen occupies the axial site, two chelating tropolone ligands are in the equatorial plane while the oxygen atoms of the remaining tropolone ligand fill the available axial and equatorial positions. This type of arrangement is very common for these 7-coordinated structures and is illustrated in Figure 7.5.[21,22] The distortion from ideal geometry can be attributed to constraints and the strength of the double bond and the limitations caused by the three chelate rings. The 0.206(1) Å, out-of-plane distortion from the pentagonal plane (O2-O3-O4-O5-O6) of the Nb-atom is illustrated in Figure 7.6.

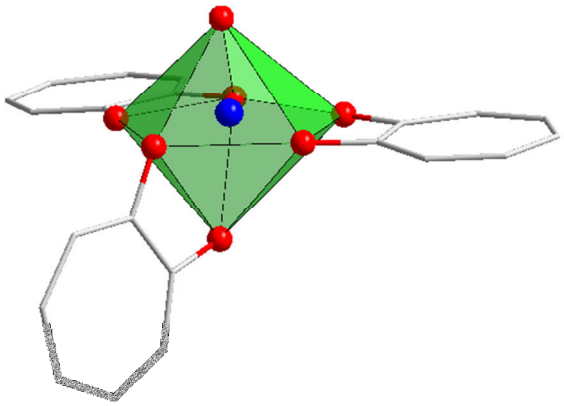

Figure 7.5 DIAMOND representation of the distorted pentagonal bipyramidal coordination geometry of $[NbO(Trop)_3]$ (**Nb_8**). Hydrogen atoms are omitted for clarity.

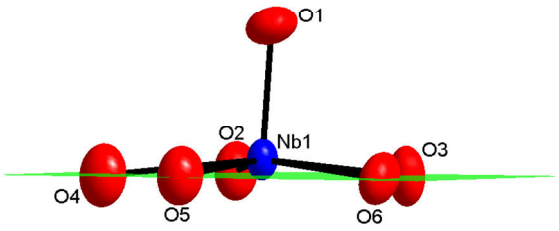

Figure 7.6 Out-of-plane pentagonal plane (O2-O3-O4-O5-O6) distortion of the Nb-atom of $[NbO(Trop)_3]$.

[21] M. G. D. Drew, (1977). *Prog. Inorg. Chem.*, **23**, 72-79.

[22] D. A. Rice, (1978). *Coord. Chem. Rev.*, **25**, 199-208.

Various intermolecular hydrogen bonds contribute to the stabilization of the crystal lattice and occur extensively within the crystal lattice. Hydrogen bonding to selected oxygen atoms is noted for this structure. These interactions are illustrated in blue in Figure 7.7 and data related to the hydrogen bonds given in Table 7.3. Furthermore, the two-dimensional supra-molecular network is further stabilized by intermolecular π-π interactions between the overlapping tropolonato ligands within the structure as illustrated in Figure 7.8. The centroids and plane distances relating to these interactions are defined in Table 7.4. This tightly knit two-dimensional interaction network rigidly ties the crystal lattice together, influencing the overall packing in pairs of these two niobium molecules dispersed in a “head-to-tail” packing fashion throughout the system. This mode is quite evident when viewing the crystal packing along the c-axis as seen in Figure 7.9 and is assumed to contribute to the crystallization of the complex and the ease with which it crystallizes.

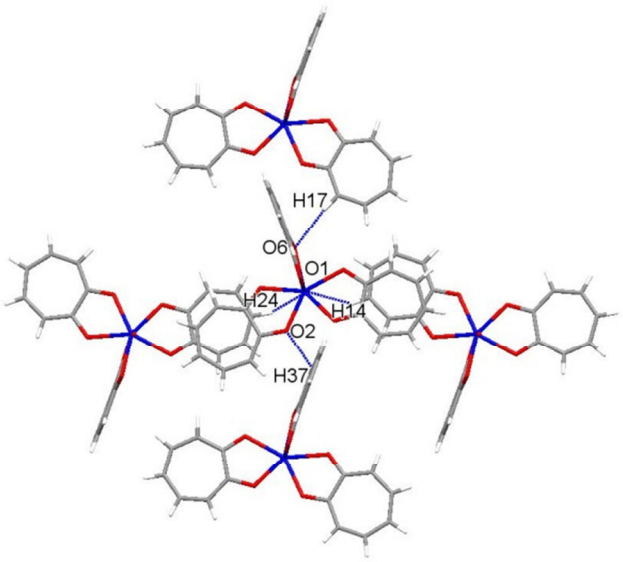

Figure 7.7 Graphic illustration of the intermolecular stabilizing hydrogen bonding (indicated in blue) of selected oxygen substituents connecting neighbouring molecules of **Nb_8**.

Table 7.3 Hydrogen bond geometry of oxygen acceptors for **Nb_8** as depicted in Figure 7.7.

C-H···O	dC-H (Å)	dH···O (Å)	dC···O (Å)	Angle C-H···O (°)
C24-H24···O1^{i}	0.951(1)	2.715(1)	3.414(1)	132.57(3)
C14-H14···O1^{ii}	0.949(1)	2.577(1)	3.310(1)	136.05(3)
C17-H17···O6^{iii}	0.990(1)	2.645(1)	3.540(1)	160.65(1)
C37-H37···O2^{iv}	0.951(1)	2.590(1)	3.297(1)	133.13(3)

Symmetry code: i) *2-x, -½+y, ½-z;* ii) *2-x, ½+y, ½-z;* iii) *x, ½-y, -½+z;* iv) *x, ½-y, ½+z*.

Table 7.4 Intermolecular π-π interactions for **Nb_8** as depicted in Figure 7.8.

Centroid-to-Centroid	Symmetry code of counterpart	π-π Interaction distance (Å)
Cg1···Cg2^{i}	*1-x, ½+y, ½-z*	3.774(8)
Cg2···Cg1^{ii}	*2-x, -½+y, ½-z*	3.838(8)

Note: *Cg1* (seven-membered ring) = C11-C12-C13-C14-C15-C16-C17.
Cg2 (seven-membered ring) = C21-C22-C23-C24-C25-C26-C27.

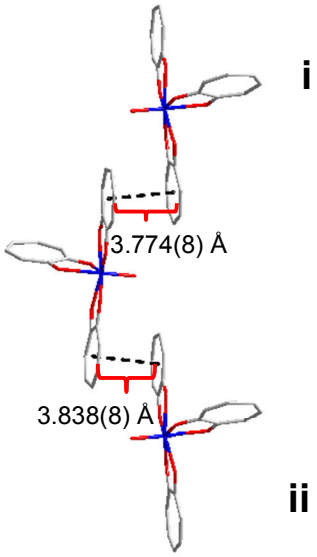

Figure 7.8 Illustration of the intermolecular π-π interactions causing the "head-to-tail" packing of **Nb_8**.

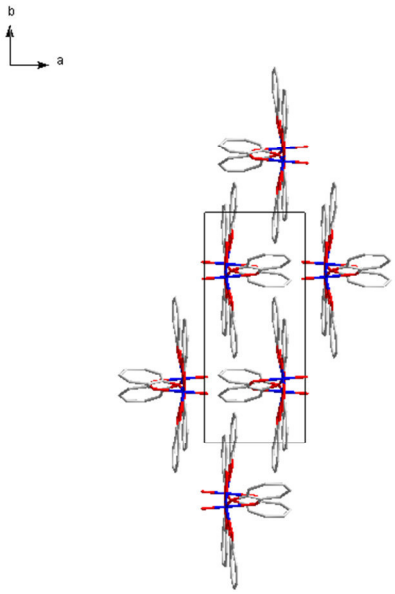

Figure 7.9 A graphic illustration highlighting the "head-to-tail" crystal packing in [NbO(Trop)$_3$] along the c-axis.

It has been mentioned that the crystal structure determination of the previously published complex [NbO(Trop)$_3$]·H$_2$O, was performed at room temperature (298 K) (**Nb_8A**), while the newly synthesized structure of **Nb_8** was collected at 100 K.[19] The crystallographic parameters of the both structures are given in Table 7.4. Tables 7.5 and 7.6 illustrate a comparison between bond angles and distances of the two published structures *vs*. the structure collected at 100 K. It has to be noted again that the current structure (**Nb_8**) represents a polymorph from the published one by Drew *et al.*[19]

Table 7.4 Crystallographic details for the niobium(V) *tris*-tropolonato structures discussed in this section.

Crystal Formula	Nb_8 (100 K)	Nb_8A (298 K)[19]
Empirical formula	$C_{21}H_{15}NbO_7$	$C_{21}H_{17}NbO_8$
Formula weight (g.mol^{-1})	472.24	491.10
Crystal system, Space Group	Monoclinic, $P2_1/c$	Monoclinic, $P2_1/c$
a, b, c (Å)	7.399(1), 16.520(2) 16.801(2)	7.328(7), 16.373(13), 16.669(13)
α, β, γ (°)	90, 100.85(2), 90	90, 99.50(10), 90
Volume (Å^3), Z	2017(4), 4	1972(5), 4
Density (calculated, Mg/m^3)	1.555	1.630

Table 7.5 Comparison of bond lengths for the niobium(V)-*tris*-tropolonato structures discussed in this section.

Nb_8 (100 K)		Nb_8A (298 K)[19]	
Atoms	**Bond length (Å)**	**Atoms**	**Bond length (Å)**
Nb-O1	1.754(3)	Nb-O1	1.711(14)
Nb-O2	2.126(2)	Nb-O2	2.188(15)
Nb-O3	2.152(2)	Nb-O3	2.070(16)
Nb-O4	2.113(2)	Nb-O4	2.087(16)
Nb-O5	2.186(2)	Nb-O5	2.195(15)
Nb-O6	2.125(2)	Nb-O6	2.119(13)
Nb-O7	2.216(2)	Nb-O7	2.197(14)
Out-of-plane distortion[a]	0.206(1)	Out-of-plane distortion[a]	0.218(1)

[a] Out-of-plane distortion illustrated in Figure 7.6.

Table 7.6 Comparison of bond angles for the niobium(V)-*tris*-tropolonato structures discussed in this section.

Nb_8 (100 K)		Nb_8A (298 K)[19]	
Atoms	**Bond angle (°)**	**Atoms**	**Bond angle (°)**
O2-Nb1-O3	69.69(2)	O2-Nb1-O3	70.40(65)
O4-Nb1-O5	71.59(2)	O4-Nb1-O5	69.54(60)
O6-Nb1-O7	72.37(2)	O6-Nb1-O7	70.17(53)
O1-Nb1-O4	100.51(3)	O1-Nb1-O4	99.08(69)
O1-Nb1-O7	162.10(3)	O1-Nb1-O7	161.64(63)
O4-Nb1-O6	144.94(3)	O4-Nb1-O6	143.63(54)

When considering Table 7.4, it must be noted that some of the more obvious differences in solid state properties of the compounds such as formula weight, density and volume can be attributed to the presence of the H_2O moiety in the **Nb_8A** structure. Tables 7.5 and 7.6 highlight the fact that these complexes correlate very well with each other, excluding some minor differences which could be attributed to the lower thermal vibrations within the crystal lattice of **Nb_8**. All the noted bite angles and Nb-O bond distances are in accordance with similar

structures.[23,24,25,26,27,28,29,30] The coordination polyhedron around $[NbO(Trop)_3]\cdot H_2O$ also displayed a distorted pentagonal bipyramidal geometry with the Nb(V) metal centre exhibiting a similar out-of-plane distortion (0.218(1) Å) as was found for $[NbO(Trop)_3]$.

Interestingly, in both cases it was noted that obtaining a suitable single crystal for XRD analysis was an arduous process. During the course of this synthetic part of this investigation, stable crystals of the compound were easily obtained, but in most cases significant twinning within the crystal lattice was noted. Various recrystallization methods were attempted to resolve this problem with the ultimate method for **Nb_8** synthesis highlighted in Chapter 3.4.3. Even though this substantially improved crystal quality, some inherent problems with **Nb_8** are still observed when considering the high R_{int} (0.1697) and unsatisfactory completeness (98.4 %) values. These characteristic deficiencies of the systems are noted through all the metal-tropolonato structures in this chapter. Nevertheless, the higher than room temperature crystallization of the product most likely is the reason for obtaining the non-hydrated form **Nb_8**.

[23] H. O. Davies, T. J. Leedlam and A. C. Jones, (1999). *Polyhedron*, **18**. 3165-3172.

[24] P. Wendrup and V. G. Kessler, (2001). *J. Chem. Soc., Dalton Trans*, 574-579.

[25] E. L. Lippert and M. R. Truter, (1960). *J. Chem. Soc. A.*, **33**, 309-311.

[26] G. J. Bullen, R. Mason and P. Pauling, (1965). *Inorg Chem.*, **4**, 456-461.

[27] F. Preuss, G. Lambing and S. Mueller-Becker, (1994). *Z. Anorg. Allg. Chem.,* **620**, 1812-1821.

[28] P. A. Williams, A. C. Jones, P. J. Wright and M. J. Crosbie, (2002). *Chem. Vap. Deposition*, **8**, 110-116.

[29] M. J. Crosbie, P. J. Wright, P. A. Lane, A. C. Jones and T. J. Leedham, (1999). *J. Phys. IV.*, **9**, 918-935.

[30] H. Funk, (1934). *Ber. Dtsch. Chem. Ges.*, **62**, 1801-1805.

7.5 Crystal Structure of *Tetrakis*(tropolonato-κ^2*O,O'*)niobium(V) chloride ([Nb(Trop)$_4$]Cl), (Nb_9))

The novel crystal structure of *tetrakis*(tropolonato-κ^2*O,O'*)niobium(V) ([Nb(Trop)$_4$]Cl]), (**Nb_9**)) forms part of an investigation which focuses on highlighting the solid state chelation effects on the coordination geometry of Ta(V) and Nb(V) compounds. Due to the obvious absence of literature sources of *tetrakis*- Nb(V) and Ta(V) compounds, this study forms an ideal opportunity to broaden the knowledge base around the aforementioned structure types.

As has also been mentioned in Chapters 2 and 3 and in Section 7.4, many challenges were faced in the process of obtaining crystals for the different tantalum(V) and niobium(V) tropolonato complexes. In the case of the [Nb(Trop)$_4$]Cl complex only crystals of relatively poor quality could be obtained from various recrystallization attempts. As a result, the inferior quality of the crystals is reflected in the low completeness of 97.7 % for the subsequent data collection as well as the high R_{int} (0.1556) and Goodness-of-Fit values (1.296) (see Table 7.1). With respect to this study the data collection still yielded sufficient data to determine the structure coordination geometry and the intermolecular interactions of [Nb(Trop)$_4$]Cl with good accuracy which will be discussed in this section.

A summary of the general crystal data of **Nb_9** is given in Table 7.7, while the numbering scheme of the complex is shown in the perspective drawing in Figure 7.10. Table 7.8 presents selected bond lengths and angles of the title compound. Atomic coordinates, anisotropic displacement parameters, bond distances and angles and hydrogen coordinates, are given in the supplementary data (Appendix 10). Hydrogen atoms and the chloride counter-ion are omitted in some figures for clarity.

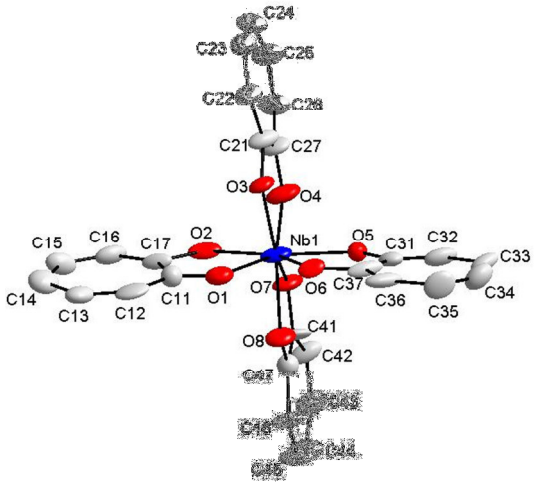

Figure 7.10 DIAMOND representation of the cationic complex structure of $[Nb(Trop)_4]^+$ (**Nb_9**) displaying the atom numbering system. The displacement ellipsoids are drawn at a 50 % probability level. Hydrogen atoms and chloride counter-ion are omitted for clarity.

Table 7.7 Selected bond lengths and angles of the $[Nb(Trop)_4]^+$ (**Nb_9**) anion.

$[Nb(Trop)_4]^+$			
Atoms	**Bond length (Å)**	**Atoms**	**Bond length (Å)**
Nb1-O1	2.094(1)	Nb1-O5	2.021(1)
Nb1-O2	2.099(1)	Nb1-O6	2.096(1)
Nb1-O3	2.092(1)	Nb1-O7	2.085(1)
Nb1-O4	2.087(1)	Nb1-O8	2.089(1)
O1···O2[a]	2.454(1)	O5···O6[a]	2.401(1)
O3···O4[a]	2.426(1)	O7···O8[a]	2.442(1)
Atoms	**Bond angle (º)**	**Atoms**	**Bond angle (º)**
O1-Nb1-O2	71.34(1)	O5-Nb1-O6	71.63(1)
O3-Nb1-O4	70.96(2)	O7-Nb1-O8	71.60(2)
Out-of-plane distortion[b] (O1-O2-O3-O4 plane)	28.46(3)	Out-of-plane distortion[b] (O5-O6-O7-O8 plane)	27.47(2)
Dihedral Ligand Plane Angles			
Ligands	**Angle (º)**	**Ligand**	**Angle (º)**
Trop1/Trop2	80.38(1)	Trop3/Trop4	87.50(1)
Trop2/Trop3	82.22(1)	Trop4/Trop1	85.64(1)
Trop2/Trop4	174.71(3)	Trop1/Trop3	174.34(2)

[a] Bite atom distance; [b] Out-of-plane distortion illustrated in Figure 7.12. Note: Trop 1 = C11-C17, Trop2 = C21-C27, Trop 3 = C31-C37 and Trop 4 = C41-C47.

The **Nb_9** compound crystallizes in the triclinic space group, $P\bar{1}$, with one independent molecule in the asymmetric unit. For this molecule, a Nb(V) metal centre is coordinated to four independent tropolonato ligands arranged in a distorted D_2-square anti-prismatic geometry. This type of arrangement is extremely rare and has hardly ever been observed for 8-coordinated Nb(V)-complexes.[3]

The *O,O'*-donating $Trop^-$ ligands surrounding the metal centre, are coordinated in a space filling, fan-like arrangement to give the D_2-corner-clipped SAP coordination polyhedron, with a strong outward distortion towards dodecahedral geometry (Figure 7.11). This distortion from the ideal square antiprism is associated with an outward bend of 28.46(2) ° in the O1-O2-O3-O4 plane and 27.47(2) ° in the O5-O6-O7-O8 plane, as illustrated in Figure 7.12. Distortion can be attributed to the limitations caused by the four chelate rings.

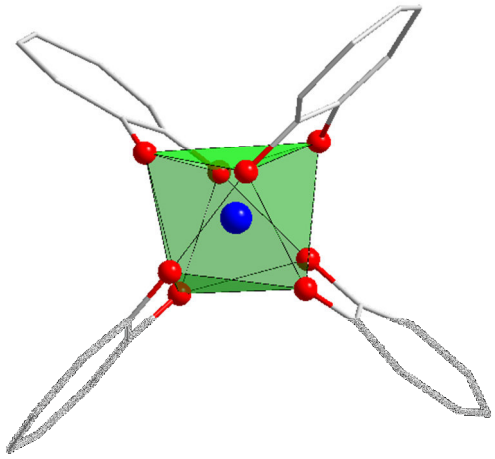

Figure 7.11 DIAMOND representation of the distorted D_2-corner-clipped square anti-prismatic coordination geometry of $[Nb(Trop)_4]^+$ (**Nb_9**). Hydrogen atoms and chloride counter-ion are omitted for clarity.

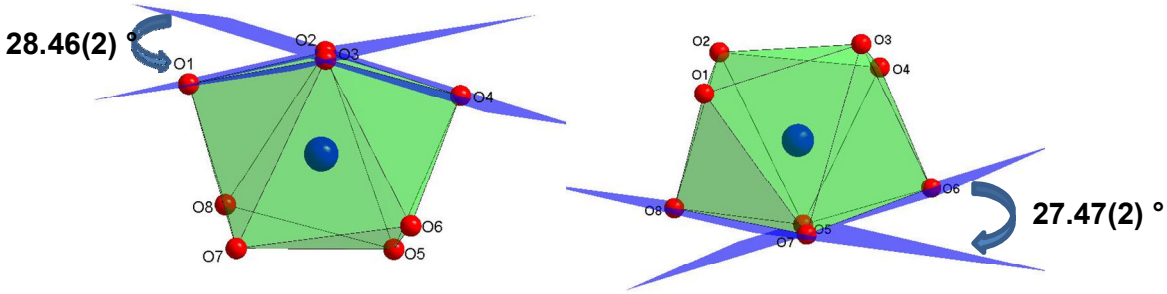

Figure 7.12 Illustration of the distortion of the square-antiprismatic coordination polyhedron found in $[Nb(Trop)_4]^+$ (**Nb_9**), showing (**Left**) the outward bend of the top-most atoms at an angle of 28.46(2) ° and (**Right**) 27.47(2) ° bend for the bottom plane.

In this structure the average Nb-O bond distance is 2.083 Å, and the average O-Nb-O bite angle is found to be 69.77 ° (Table 7.7). The coordinating ligands are characterized by both “opposite” and “adjacent” ligand pairs. The planes defined by each individual ligand appear flat, with no deviation of any one atom out of the plane. These "ligand-planes" lie across the metal centre at angles of 174.34(2) ° (Trop1/Trop3) and 174.71(4) ° (Trop2/Trop4) for each opposite facing pair and accentuate the distortion to dodecahedral geometry of the complex. An illustration of this is shown in Figure 7.13. The dihedral angles between adjacent ligand planes range from 80.38(1) ° at the smallest (Trop1/ Trop2) to 87.50(1) ° at the largest (Trop3/Trop4) value as reported in Table 7.7.

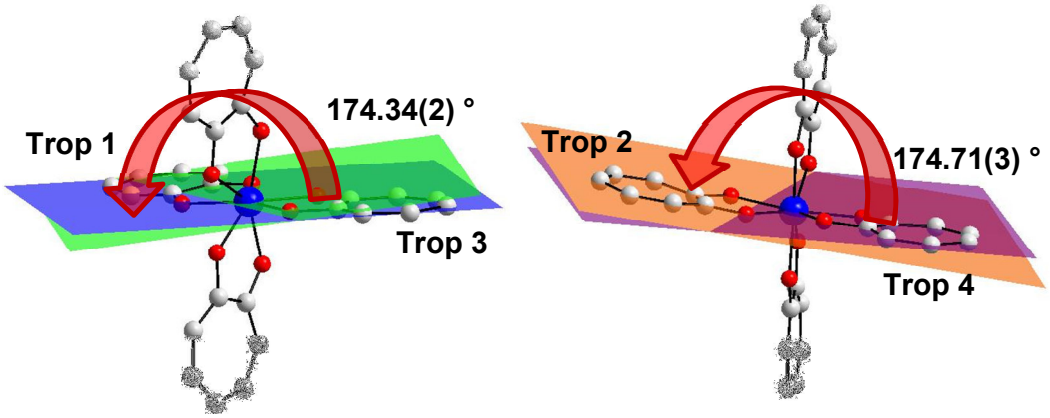

Figure 7.13 Illustration of the different ligand planes measured across the Nb metal centre. (**Left**) Trop1/Trop3 at an angle of 174.34(2) ° and (**Right**) Trop2/Trop4 at an angle of 174.71(3) °.

An array of C-H···O hydrogen-bonding interactions between neighbouring molecules stabilizes the crystal packing. The hydrogen bonds observed in **Nb_9** are illustrated in Figure 7.14 with the symmetry operations, distances and angles summarized in Table 7.8. These soft contacts, tightly tie the crystal lattice together and afford the "head-to-tail" packing mode within the crystal, these interactions are illustrated in the packing structure in Figure 7.14.

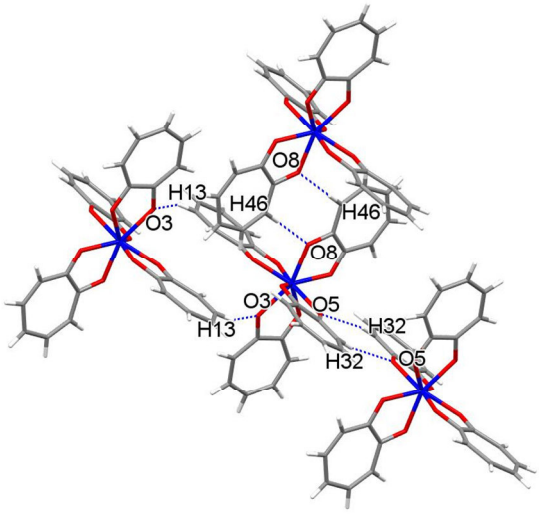

Figure 7.14 A graphic illustration of the stabilizing hydrogen bonding (indicated in blue) of selected oxygen substituents connecting neighbouring **Nb_9** molecules.

Table 7.8 Hydrogen bond geometry for **Nb_9** as depicted in Figure 7.14.

C-H···O	dC-H (Å)	dH···O (Å)	dC···O (Å)	Angle C-H···O (°)
C46-H46···O8^{i}	0.930(1)	2.465(1)	3.395(1)	178.31(1)
C32-H32···O5^{ii}	0.930(1)	2.562(1)	3.479(1)	168.55(1)
C13-H13···O3^{iii}	0.930(1)	2.598(1)	3.350(1)	138.29(3)

Symmetry code: i) *1-x, -y, 2-z;* ii) *1-x, 1-y, 2-z;* iii) *2-x, -y, 2-z*.

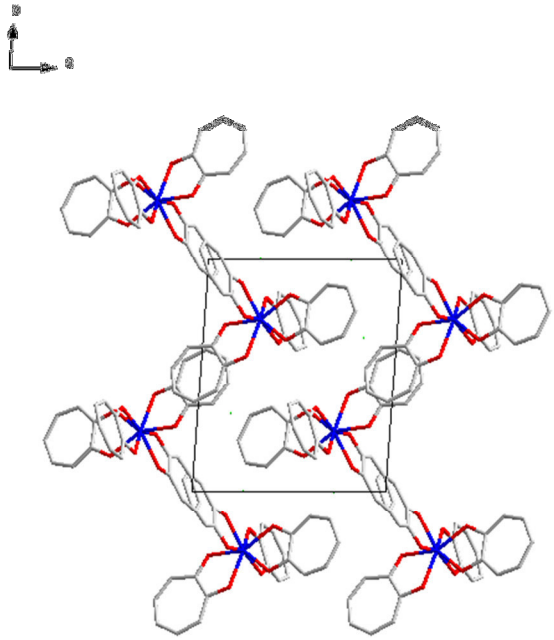

Figure 7.15 A graphic illustration highlighting to "head-to-tail" crystal packing of $[Nb(Trop)_4]Cl$ along the c-axis.

No intermolecular π-π interactions between the overlapping tropolonato ligands were noted in this structure. A basic visual evaluation was undertaken using DIAMOND to calculate the various distances between ring planes to verify that there were no possible π-π interactions that were missed due to poor crystal quality.[31] This investigation confirmed that no inter-planar ring distance was observed within the 3.7 Å – 4.0 Å range. This unexpected observation is quite infrequent for metal-tropolonato systems.[32]

[31] K. Brandenburg and H. Putz; DIAMOND, (2006). *Release 3.0e, Crystal Impact GbR*, Bonn, Germany.

[32] M. Steyn, (2014). *A Solid State and Mechanistic Study of Multidentate Ligand Zirconium(IV) Halido Complexes.* Ph.D. Thesis, University of the Free State, South Africa.

7.6 Crystal Structure of *Tetrakis*(tropolonato-κ^2*O,O'*)tantalum(V) chloride ([Ta(Trop)$_4$]Cl), (Ta_2))

The novel crystal structure of *tetrakis*(tropolonato-κ^2*O,O'*)tantalum(V) ([Ta(Trop)$_4$]Cl]), (**Ta_2**)) forms part of an investigation which focuses on studying applied bidentate ligand chelation effects on the coordination geometry of Ta(V)- and Nb(V)-compounds. Investigation of this structure is of cardinal importance, since the obtaining of Ta(V)-bidentate compounds is a trying prospect and not many examples are found in literature.[3]

As has been mentioned on several occasions during the course of this study, many challenges were faced in obtaining single crystal suitable for X-Ray diffraction studies. The difficulty in isolation of the crystal structure of the [Ta(Trop)$_4$]Cl complex highlights quite a few of these problems;

i) Even though the $[TaCl_5]_2$ is stored under vacuum, some degree of synthon hydrolization takes placed. This adversely affects solubility, yields and reproducibility of synthesis.

ii) Due to the fact that Ta(V) complexes hydrolyse quite readily, selection, collection and harvesting of an ideal crystal for X-ray diffraction studies is nearly impossible. Accordingly, the best crystals were of less than ideal quality, and since these were the only ones available they had to be used for data collection.

iii) These inherent flaws obviously adversely affected the information obtained from the data collection. Information regarding intermolecular hydrogen bonding and π-π interactions could be lost.

The synthesis of the [Ta(Trop)$_4$]Cl complex (Section 3.4.2) yielded only unstable crystals of relatively low quality from various recrystallization attempts. As a result, the reduced quality of the crystals is reflected in the high R_{int} (0.1617) and Goodness-of-Fit values (1.152) (see Table 7.1). A large residual electron density of

3.31 was located at a distance of 3.48 Å from C14. Although this value is very significant it is isolated from the coordination sphere and need not be assigned for this investigation as it has minimal effect with relation coordination geometry around the metal centre. With all this in mind data collection could still yield sufficient data to determine the structure and coordination geometry of $[Ta(Trop)_4]Cl$ which will be discussed in this section.

A summary of the general crystal data of **Ta_2** is given in Table 7.1, while the numbering scheme of the complex is shown in the perspective drawing in Figure 7.16. Table 7.9 presents selected bond lengths and angles of the title compound. Atomic coordinates, anisotropic displacement parameters, bond distances and angles and hydrogen coordinates, are given in the supplementary data (Appendix 11). Hydrogen atoms are omitted in some figures for clarity.

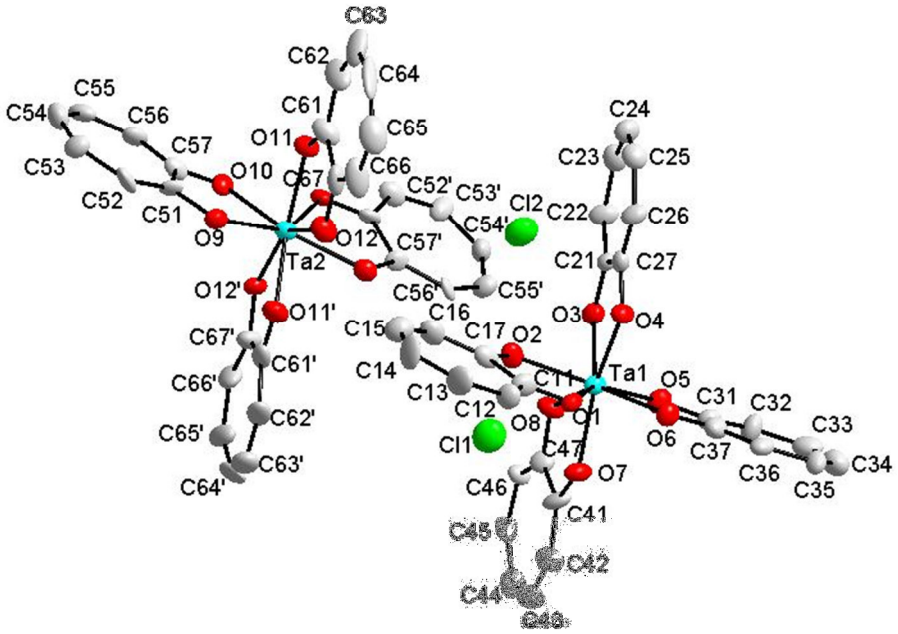

Figure 7.16 DIAMOND representation of the molecular structure of $[Ta(Trop)_4]Cl$ (**Ta_2**) displaying the atom numbering system. The displacement ellipsoids are drawn at a 50 % probability level. Hydrogen atoms are omitted for clarity.

Table 7.9 Selected bond lengths and angles of the $[Ta(Trop)_4]^+$ (**Ta_2**) anion.

$[Ta(Trop)_4]^+$ (Ta_2.1) Bond Distances			
Atoms	**Bond length (Å)**	**Atoms**	**Bond length (Å)**
Ta1-O1	2.098(1)	Ta1-O5	2.088(1)
Ta1-O2	2.068(1)	Ta1-O6	2.091(1)
Ta1-O3	2.098(1)	Ta1-O7	2.063(1)
Ta1-O4	2.093(1)	Ta1-O8	2.134(1)
O1···O2[a]	2.459(1)	O5···O6[a]	2.439(1)
O3···O4[a]	2.456(1)	O7···O8[a]	2.452(1)
$[Ta(Trop)_4]^+$ (Ta_2.2) Bond Distances			
Atoms	**Bond length (Å)**	**Atoms**	**Bond length (Å)**
Ta2-O9	2.087(1)	Ta2-O11	2.076(1)
Ta2-O10	2.095(1)	Ta2-O12	2.073(1)
O9···O10[a]	2.431(1)	O11···O12[a]	2.445(1)
$[Ta(Trop)_4]^+$ (Ta_2.1) Bond Angles			
Atoms	**Bond angle (º)**	**Atoms**	**Bond angle (º)**
O1-Ta1-O2	72.34(2)	O5-Ta1-O6	71.40(2)
O3-Ta1-O4	71.74(1)	O7-Ta1-O8	71.69(1)
Out-of-plane distortion[b] (O1-O2-O3-O4 plane)	31.01(1)	Out-of-plane distortion[b] (O5-O6-O7-O8 plane)	27.61(2)
$[Ta(Trop)_4]^+$ (Ta_2.2) Bond Angles			
Atoms	**Bond angle (º)**	**Atoms**	**Bond angle (º)**
O9-Ta2-O10	71.09(2)	O11-Ta2-O12	72.22(1)
Out-of-plane distortion[b] (O9'-O10'-O11'-O12' plane)	27.51(2)	Out-of-plane distortion[b] (O9-O10-O11-O12 plane)	26.99(2)
Ligand Plane Angles (Ta_2.1)			
Ligands	**Angle (º)**	**Ligand**	**Angle (º)**
Trop1/Trop2	77.26(1)	Trop3/Trop4	79.86(1)
Trop2/Trop3	80.13(1)	Trop4/Trop1	75.45(1)
Trop2/Trop4	169.05(1)	Trop1/Trop3	171.54(1)
Ligand Plane Angles (Ta_2.2)			
Ligands	**Angle (º)**	**Ligand**	**Angle (º)**
Trop5'/Trop6	74.32(1)	Trop5/Trop6'	74.32(2)
Trop5/Trop6	75.04(1)	Trop5'/Trop6'	75.04(1)
Trop5/Trop5'	167.06(1)	Trop6/Trop6'	173.81(1)

[a] Bite distance; [b] Out-of-plane distortion illustrated in Figure 7.19. Note: Trop 1 = C11-C17, Trop2 = C21-C27, Trop 3 = C31-C37, Trop 4 = C41-C47, Trop 5 = C51-C57 and Trop 6 = C61-C67.

The **Ta_2** compound crystallizes in the monoclinic space group, *C*2/*c*, with one full $[Ta(Trop)_4]^+$ cation (**Ta_2.1**) and half of another $[Ta(Trop)_4]^+$ (**Ta_2.2**) moiety in the asymmetric unit. In the case of **Ta_2.1**, a Ta(V) metal centre is surrounded by four independent tropolonato ligands arranged in a distorted D_2-square anti-prismatic geometry. In contrast, for **Ta_2.2**, the Ta 2 atom is located on a special position and is coordinated to two tropolonato ligands with the other half of the cation being generated through the mirror plane. **Ta_2.2** also illustrates a distorted D_2-square anti-prismatic coordination geometry. This type of arrangement has never been noted for a Ta(V) structure and only on one occasion in the structure of *tetrakis*(oxalato)tantalum(IV) for the Ta(IV) species.[33]

In both cations it was found that this D_2-corner-clipped SAP coordination polyhedron had a strong outward distortion towards dodecahedral geometry created by the *O,O'*-donating ligands surrounding the metal centre (Figure 7.17).

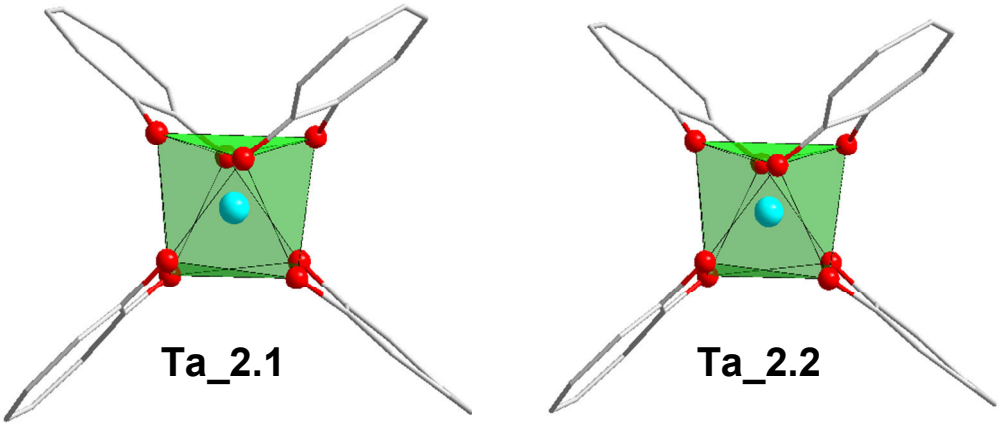

Figure 7.17 DIAMOND representation of the distorted D_2-corner-clipped square anti-prismatic coordination geometry of **Ta_2.1** and Ta**_2.2**. Hydrogen atoms and chloride counter-ion are omitted for clarity.

This distortion from the ideal square antiprism is associated with an outward bend of 31.01(1) ° in the O1-O2-O3-O4 plane and 17.61(2) ° in the O5-O6-O7-O8 plane for **Ta_2.1** (Figure 7.18) and 19.99(2) ° in the O9-O10-O11-O12 plane and 22.51(2) ° in the O9'-O10'-O11'-O12' plane for **Ta_2.2** (Figure 7.18). Distortion can be attributed to the limitations caused by the four chelate rings.

[33] F. A. Cotton, M. P. Diebold and W. J. Roth, (1987). *Inorg. Chem.*, **26**, 2889-2901.

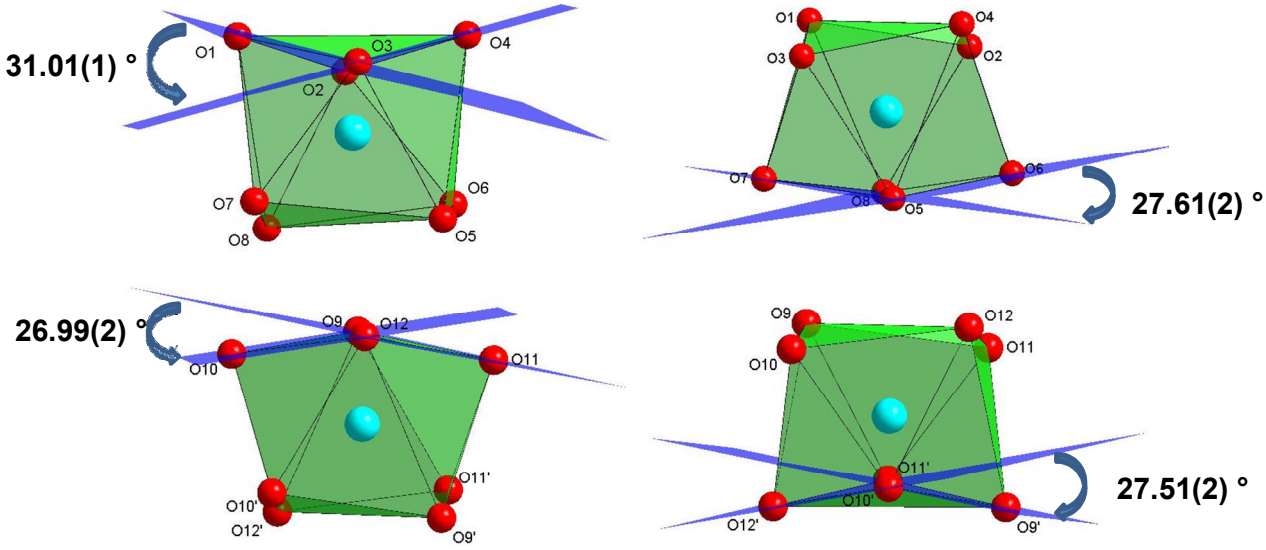

Figure 7.18 Illustration of the distortion of the square-antiprismatic coordination polyhedron found in **Ta_2.1** and **Ta_2.2**.

Ta_2.1: Outward bend of the top-most plane of 31.01(1) ° and 17.61(2) ° for the bottom plane.

Ta_2.2: Outward bend of the top-most plane of 17.61(2) ° and 22.51(2) ° for the bottom plane.

The **Ta_2** structure exhibits an average Ta-O bond distance is 2.092(1) Å and an average O-Ta-O bite angle of 71.75(7) ° (Table 7.9). Once again, the coordinating ligands are characterized by both “opposite” and “adjacent” ligand pairs. The planes defined by each individual ligand appear flat, with no deviation of any one atom out of the plane. These "ligand-planes" lie across both metal centres at angles of; 169.05(2) ° (Trop1/Trop3) and 171.54(1) ° (Trop2/Trop4) for **Ta_2.1** and 167.06(1) ° (Trop5/Trop5’) and 173.81(1) ° (Trop6/Trop6’) for **Ta_2.2**, for each opposite facing pair and accentuate the distortion to dodecahedral geometry of the complex. An illustration of this is shown in Figure 7.19. The dihedral angles between adjacent ligand planes range from 74.32(1) ° at the smallest (Trop5/Trop6) to 75.04(1) ° at the largest (Trop5’/Trop6’) value as reported in Table 7.9.

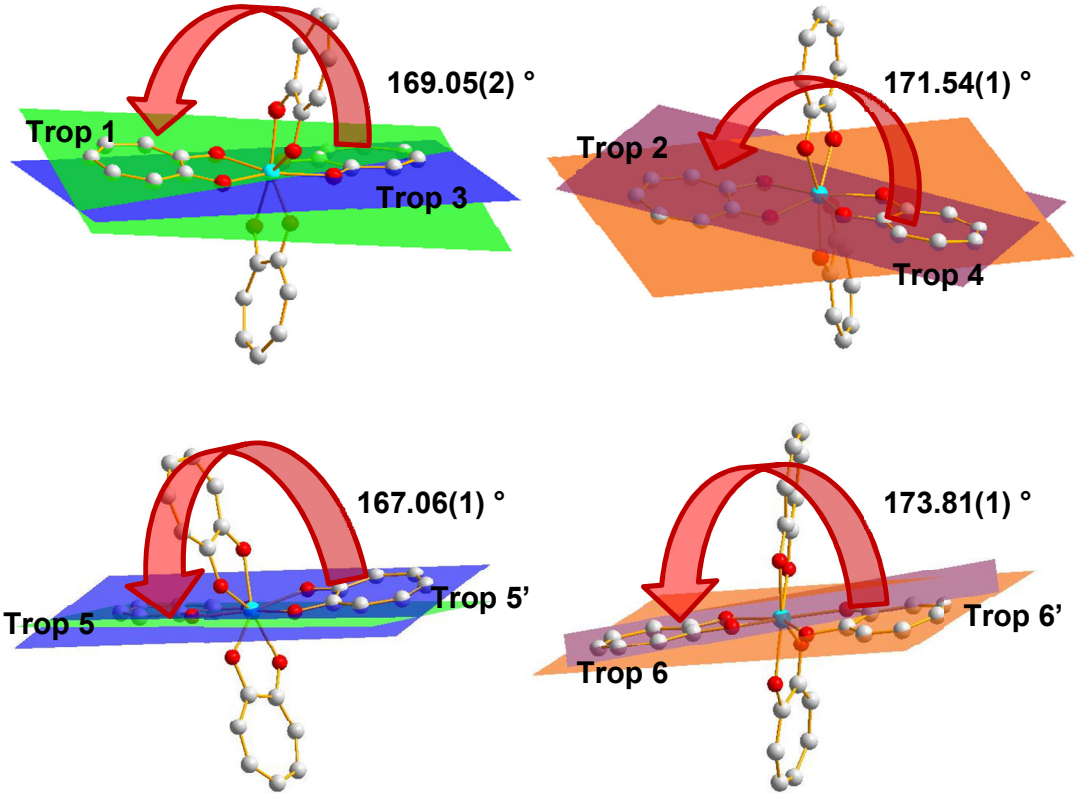

Figure 7.19 Illustration of the different ligand planes measured across the Ta metal centre for **Ta_2.1** and **Ta_2.2**.

Ta_2.1: Trop1/Trop3 at an angle of 169.05(2) ° and Trop2/Trop4 at an angle of 171.54(1) °.

Ta_2.2: Trop5/Trop5' at an angle of 167.06(2) ° and Trop6/Trop6' at an angle of 173.81(1) °.

The hydrogen bonds observed in **Ta_2** are illustrated in Figure 7.20 with the symmetry operations, distances and angles summarized in Table 7.10. These interactions afford the most effective "head-to-tail" crystal packing motif for this structure and are illustrated in Figure 7.21.

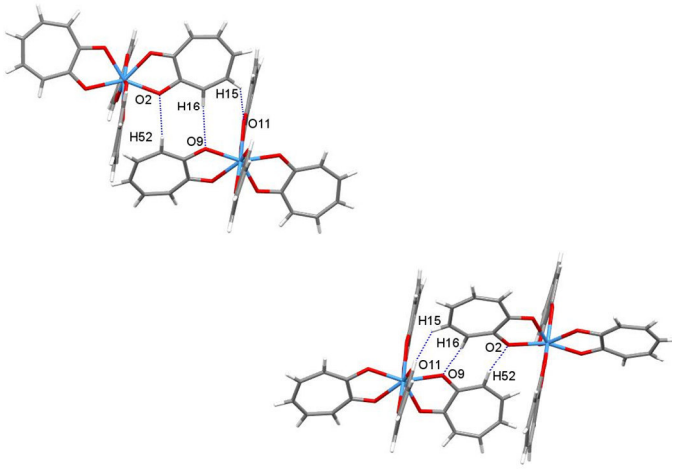

Figure 7.20 A graphic illustration of the stabilizing hydrogen bonding (indicated in blue) of selected oxygen substituents connecting neighbouring **Ta_2** molecules.

Table 7.10 Hydrogen bond geometry for **Ta_2** as depicted in Figure 7.20.

C-H···O	dC-H (Å)	dH···O (Å)	dC···O (Å)	Angle C-H···O (°)
C52-H52···O2^{i}	0.930(1)	2.605(1)	3.535(1)	163.07(2)
C15-H15···O11^{i}	0.930(1)	2.670(1)	3.395(1)	135.41(3)
C16-H16···O9^{i}	0.930(1)	2.607(1)	3.395(1)	175.63(1)

Symmetry code: i) *½-x, ½+y, 3/2-z*.

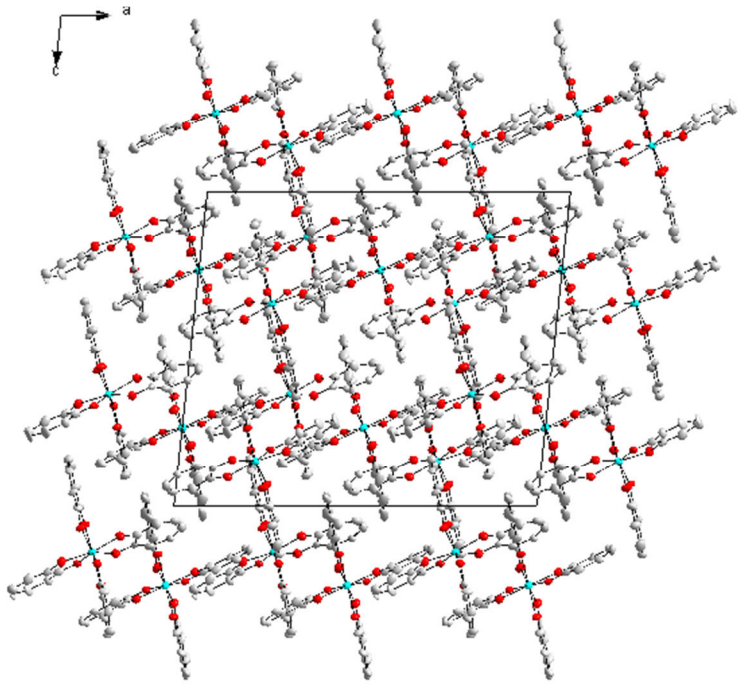

Figure 7.21 A graphic illustration highlighting to "head-to-tail" crystal packing of $[Ta(Trop)_4]^+$ along the c-axis. Chloride counter-ion omitted for clarity.

No intermolecular π-π interactions between the overlapping tropolonato ligands were noted in this structure. A basic visual evaluation was undertaken using DIAMOND to calculate the various distances between ring planes to verify that there were no possible π-π interactions that were missed due to poor crystal quality.[29] This investigation showed that no border rings systems were observed within the 3.7 Å – 4.0 Å range. As was found in the case of **Ta_2**, this unexpected observation is quite for metal-tropolonato systems.

7.7 Discussion

As was discussed in Chapter 2, the difference in properties of tantalum(V) and niobium(V) chemical behaviour when reacted with tropolone in a slightly acidic to a near neutral pH range could be crucial in obtaining adequate separation conditions for solutions containing both metals. The comprehensive investigation undertaken by Muetteries *et al*. on these compounds was extremely thorough and gave much insight of the properties of these compounds in solution. Interestingly, no focus was placed on the solid state structures of the compounds as well as the scope of these results for industrial scale separation purposes.

Similar investigations on extraction of other metal centres such as Eu^{3+} have been undertaken in the past. Noro *et al.* noticed that the solvent extraction of Eu^{3+} benzoyltrifluoroacetylacetone into carbon tetrachloride was enhanced by the addition of bulky cations such as the tetrabutylammonium ion.[34] This was attributed to the fact that the tetrakis complex, $[Eu(btfa)_4]^-$, is extracted as an ion pair with tetrabutylammonium and is more easily extracted than the tris $[Eu(btfa)_3]$ complex. Similar results were also obtained for the extraction of Pr^{3+} and Nd^{3+} with thenoyltrifluoroacetone.[35] With these successes in mind, the importance of understanding all chemical and physical properties of the metal-tropolonates becomes quite evident.

[34] J. Noro and T. Sekine, (1993). *Bul. Chem. Soc. Japan*, **66**, 804-809.

[35] J. Noro, (1999). *Anal. Sci.*, **15**, 1265-1268.

Comparison of the $[Nb(Trop)_4]Cl$ and $[Ta(Trop)_4]Cl$ structures is the main focal point of this chapter. The solid state structures of these compounds could give a clue as to why the coordination of tropolone is influenced so significantly as a result of pH alteration or add additional chemical variances into the equation. Table 7.11 compares the general crystallographic parameters of the two compounds.

Table 7.11 Crystallographic details for the metal-tropolonato structures discussed in this section.

Crystal Formula	Nb_9	Ta_2
Empirical formula	$C_{28}H_{20}NbO_8$	$C_{28}H_{20}O_8Ta$
Formula weight ($g.mol^{-1}$)	537.80	625.55
Crystal system, Space Group	Triclinic, $P\bar{1}$	Monoclinic, *C*2/*c*
a, b, c (Å)	10.027(3), 12.907(3), 14.750(4)	19.626(3), 20.360(3) 22.446(3)
α, β, γ (°)	68.776(4), 78.141(3), 81.860(4)	90, 96.050(3), 90
Volume ($Å^3$), Z	1778.3(1), 2	2919.3(4), 4
Density (calculated, Mg/m^3)	1.371	1.506

An obvious difference is immediately noted with relation to crystal system. As was observed in Chapter 5, loss of crystal lattice symmetry is seemingly much more readily obtained for Nb(V) structures than in the Ta(V) counterparts. This phenomenon now seems to hold true for both the troplonato and acetlacetonato ligands.

When comparing the various bond lengths, bite distances and bond angles listed in Tables 7.7 and 7.9 several trends are noticed. These tendencies will be discussed and compared systematically;

7.7.1 Nb-O and Ta-O Bond Distances

As expected, the average Nb-O (2.083(1) Å) and Ta-O (2.092(1) Å) bond distances correlate very well with each other. Similar average metal-oxido distances have been noted on several occasions in past studies, for both metal centres; *tetrakis*(2,2,6,6-tetramethylheptane-3,5-dione)tantalum(V) cation (2.078(2) Å), *tetrakis*(oxalato) tantalum(V) cation (2.089(3) Å) and *tetrakis*(hexafluoroacetylacetonato)niobium(V)

cation (2.095 Å).[36,37,38] This phenomenon can probably be attributed to the near identical covalent radii of both Ta and Nb. Although not much with relation to separation studies can be derived from this, it indicates that the assumption made that the inferior crystal quality would not influence coordinative crystal data is a fair assumption.

7.7.2 O-Metal-O Bond Angles and O···O Bite Distances

From a search conducted on the Cambridge crystallographic database (CSD), it was noted that the only example of a crystal structure of a Nb(V)- or Ta(V)-tropolonate, is that of $[NbO(Trop)_3]\cdot H_2O$, discussed in Section 7.4.[3] Accordingly, average tropolonato bite angles for *tetrakis* coordinated structures such as $[Ta(Trop)_4]Cl$ (71.75(7) °) and $[Nb(Trop)_4]Cl$ (69.77(7) °) was never been reported before. No examples of *tetrakis*-tropolonato coordination compounds for the other group 5 element, vanadium(V), have been observed. The only other examples are noted for Zr(IV) and Hf(IV) compounds; *tetrakis*(tropolonato)hafnium(IV) (69.66(7) °) and *tetrakis* (tropolonato)zirconium(IV) (68.53(7) °).[39,40] These bite angles were all found to be in accordance with **Nb_9** and **Ta_2**, with the smaller values of the Zr(IV) and Hf(IV) compounds ascribed to a smaller atomic radius.

Interestingly, a substantial difference (1.98(1) °) in bidentate bite angle is noted between **Nb_9** vs. **Ta_2**. From this it can be concluded that the chelate ring of the Nb(V) compound is significantly more strained. This could also give a clue as to why a decrease in pH has a different effect for both metals. As the solution becomes less acidic conditions becomes less and less advantageous for the *tetrakis*-coordination mode, preferring the more stable *tris*-coordinated oxido species especially if an oxygen donor is avaliable. Due to the fact that the chelate ring in the Nb(V) compound is more strained (71.28 º *vs.* 71.85 º) it could more readily offer up one of its tropolone ligands for the sake of obtaining greater stability.

---

[36] H. O. Davies, A. C. Jones and M. A. Motevalli, (2005). *Inorg. Chem. Commun.*, **8**, 585-592.

[37] B. Peric, N. Brnicevic and M. Juric, (2009). *Struct. Chem.*, **20**, 933-941.

[38] F. Calderazzo and U. Englert, (1998). *Inorg. Chim. Acta*, **270**, 177-191.

[39] D. Tranqui, A. Tissier and J. Laugier, (1977). *Acta Cryst B.*, **33**, 392-396.

[40] A. R. Jones, (1978). *Acta Cryst. B.*, **34**, 2110-2116.

In past investigations some emphasis has been placed on the bite distances of the ligands and modification of these distances to selectively remove various atoms from solution. Bite distances are very much related to ligand bite angle and as expected the average distance for **Ta_2** (2.447(1) Å) and **Nb_9** (2.431(1) Å) differ by a small amount yet quite significantly.

From this subsection it can be concluded that by varying bite distances and angles various properties of a compound can be influenced in such a way to induce significant chemical and physical differences. Modification of the tropolone backbone by addition of electron-donating of withdrawing groups would be the next step in refining this possible separation method.

7.7.3 Coordination Geometry

Tables 7.7 and 7.9 highlight the fact that the degree of distortion form D_2-SAP geometry towards dodecahedral geometry is much more pronounced for **Ta_2**. For ideal SAP geometry the ligand planes would have to lie opposite each other at an ideal 180 ° angle. When considering the "ligand planes" as described in Figures 7.13 and 7.19, it is obvious that the distortion from ideal 180 ° is much more pronounced in the case of the **Ta_2** compound although a significant distortion is also noted for **Nb_9**. The same trend was noted when observing the dihedral angles between adjacent ligand planes. These angles range from 80.38(1) ° and 87.50(1) ° for **Nb_9** and 74.32(1) ° to 75.04(1) ° for **Ta_2**.

Some correlation can be drawn to what was observed by Muetteries *et al.* in solution vs. this distortion noted in the solid state.[2] From basic crystallography it is known that dodecahedral geometry is an energetically favourable coordination mode, affording a more stable compound.[41] It might then seem that the robustness of **Ta_2** vs **Nb_9** in solution could also be ascribed to the more energetically favourable (stable) coordination mode. Accordingly, an argument can be made that the **Ta_2** has

[41] A. Hutchings, F. Habib, R. J. Holmberg and I. Korobkov, (2014). *Inorg. Chem.*, **53**, 2102-2112.

dodecahedral geometry and is significantly distorted towards the D_2-SAP geometry. Although this notion is not irrefutably conclusive it cannot be ignored.

7.8 Conclusion

In this chapter three group 5 metal complexes coordinated by the tropolone (TropH) ligand were presented. As has been mentioned throughout, this crystallographic investigation was undertaken to better understand and further contribute to the thorough solution state work done by Muetteries *et al*. from a solid state point of view.[2] Various aspects of these structures, such as coordination modes, bite angles and bond distances were evaluated and compared in an attempt to understand why these compounds have such different characteristics in solution.

Many obstacles were encountered throughout this study but isolation of good quality crystals for X-Ray diffraction studies was the most challenging. Due to a very high degree of twinning within the crystal and these compounds amenability towards hydrolization, obtaining good quality crystals was found to be very difficult. Although this obviously has an adverse effect on crystal data, the crystallographic information regarding ligand coordination was still acceptable and was actually found to be comparable with similar compounds.

Some very interesting observations and conclusions could be drawn from the comparison of the $[Ta(Trop)_4]Cl$ and $[Nb(Trop)_4]Cl$ solid-state crystal structures. The bite angles of both compounds revealed that the $[Nb(Trop)_4]Cl$ compound experiences a higher degree of stain within the chelate ring. This could have very interestingly implications with relation to complex stability. According to Muetteries *et al.*, in slightly acidic solutions, the preferred coordination mode of these compounds was noted to be *tetrakis*.[2] With increasing temperature or pH, the niobium chelate undergoes partial hydrolysis to $[NbO(Trop)_3]$ which separates from solution. As the solution becomes more basic, the niobium cation is rapidly and actually completely hydrolysed. In contrast the tantalum cation is resistant to hydrolysis provided the pH is not appreciably above 7 and is seemingly the more stable compound. When considering the higher degree of strain (less energetically favourable) within the

Nb(V) chelate ring, this complex could more readily offer up one of its tropolone ligands for the sake of obtaining the more stable [$NbO(Trop)_3$] (average bite angle 71.22(7) °).

Secondly, the $[Ta(Trop)_4]^+$ cation exhibits a more distorted square antiprismatic geometry when compared with $[Nb(Trop)_4]^+$. In fact the coordination geometry is so distorted that could be deemed that $[Ta(Trop)_4]Cl$ in more inclined towards the more energetically favourable dodecahedral geometry. This might also contribute to the Ta(V) complex stability.

Although comparison of reaction properties in solution with solid state crystal structures should be done with care, this crystallographic investigation has already shed some more light as to why the properties of the Nb(V) and Ta(V) compounds might differ so significantly. Unfortunately, due to the substandard crystal data much information relating to intermolecular interactions, π-π- stacking and solvent species influence might have been lost.

In Chapter 1 it was mentioned that a robust and well-structured separation method will be required for industrial application. The use of the tropolone ligand has many obvious advantages but due to the fact that all of the solid state properties could not be investigated in depth during this study, the robustness of this approach has to deemed more as a hypothetical notion and more research will be required on these systems. Accordingly, in the following chapters, focus will be shifted back to the Ta(V)- and Nb(V)-*β*-diketonate compounds. Chapter 8 will focus on the properties of these systems in solution, while Chapter 9 will compare and correlate all data relating to these compounds.

Chapter 8: Kinetic/Mechanistic Study of the Coordination of β-diketones to Nb(V)- and Ta(V) Metal Centres

8.1 Overview

Much of the focus of this Ph.D. investigation thus far has been placed on the evaluation of the chemical and physical properties of various Nb(V) and Ta(V) complexes, as described in Chapters 4 - 7. However, a fundamental question featured in the aims of the project, revolves around the elucidation of the step-wise formation processes of these compounds in solution. Accordingly, in this chapter, emphasis will be placed on the kinetics of coordination of various functionalized β-diketonate ligands to the $(Et_4N)[NbCl_6]$ and $(Et_4N)[TaCl_6]$ synthons described in Chapter 4.

One of the primary observations from the results describing the synthons (Chapters 5 and 6) was that only one β-diketone ligand coordinates to the metal centre in spite of adding an excess. A generalized depiction of this phenomenon is illustrated in Figure 8.1.

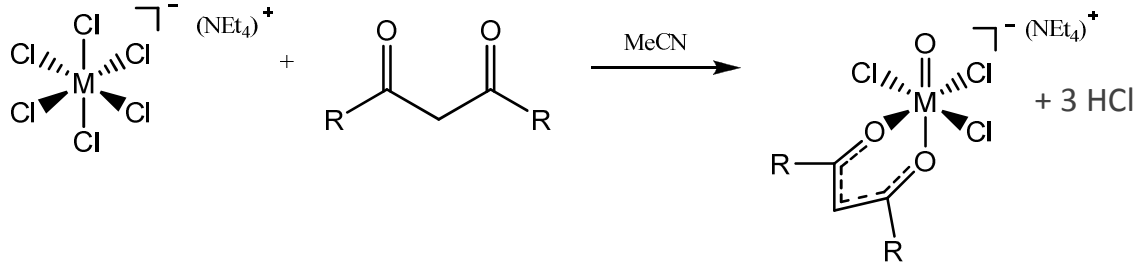

Figure 8.1 Illustration of general β-diketone ligand coordination to $(Et_4N)[NbCl_6]$ and $(Et_4N)[TaCl_6]$.

In this chapter, a reaction mechanism for the *β*-diketone coordination to Nb(V) and Ta(V) metal centres will be proposed and discussed with relation to reaction rates. Knowledge of the intimate mechanism will be very useful in identifying potential differences in Nb(V) and Ta(V) coordination behaviour. These nuances, if any, could then be used to develop a possible separation method for these metals.

In the related M.Sc. study, a preliminary solution investigation, utilizing a UV/Vis time resolved kinetic study, was performed on the formation reaction of the *trans*-$[TaCl_2(OMe)_2(acac)]$ complex and a rudimentary mechanism was postulated from these results.[1] Ignoring a few minor anomalies, these reaction rates and the corresponding coordination mechanism was found to be relatively analogous with those obtained for the formation of *trans*-$[NbCl(OMe)_3(acac)]$.[1] This comparative study shed considerable light on various aspects of the solution state characteristics of Nb(V) and Ta(V) systems, making a broader investigation more important.

A specialized literature review revealed a similar investigation conducted by Steyn *et al.* on Zr(IV)-quinolato complexes.[2] This study focused on the utilization of varying functionalities on the ligand backbone and determining the influence thereof on reaction rates, etc. Similarly, in the current study, a systematic variation of the functionalities on the acetylacetone (acacH) backbone is expected to yield better insight of the kinetic effects of ligand size (steric) and pK_a (electronic) on the Ta(V) and Nb(V) complexes. In this chapter the coordination kinetics of five different functionalized acacH-type ligands with $(Et_4N)[NbCl_6]$ and $(Et_4N)[TaCl_6]$ will be discussed. The ligands utilized are illustrated in Figure 8.2.

[1] R. Koen, (2012). *High Oxidation State Tantalum Coordination Chemistry: A Solution and Solid State Investigation,* M.Sc. Dissertation, University of the Free State, South Africa.

[2] M. Steyn, (2014). *A Solid State and Mechanistic Study of Multidentate Ligand Zirconium(IV) Halido Complexes.* Ph.D. Thesis, University of the Free State, South Africa.

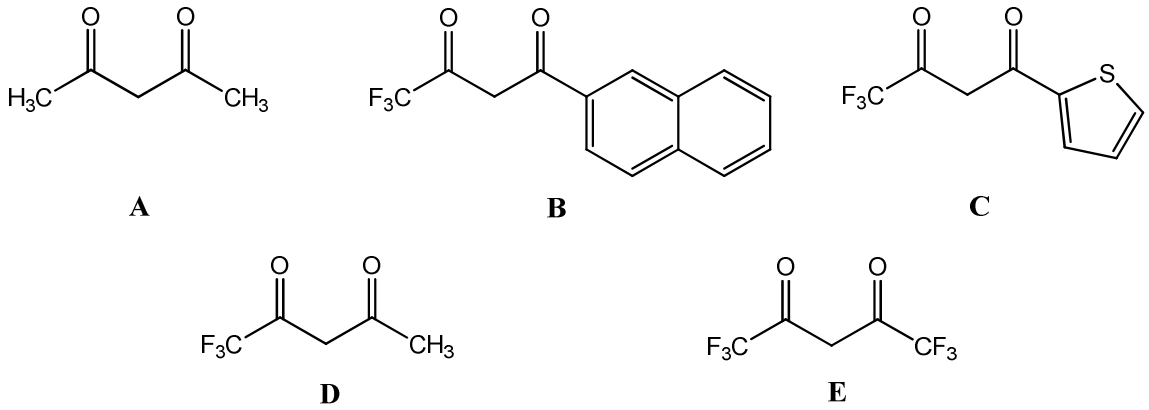

Figure 8.2 Graphical representation of the *β*-diketone ligands employed in synthesis of niobium(V) and tantalum(V) complexes. **A)** *2,4*-pentanedione (acetylacetone, acacH), **B)** *4,4,4*-Trifluoro-*1*(*2*-naphtyl)-*1,3*-butanedione (trifluoronaphylacetylaceone, ntfaH), **C)** *4,4,4*-Trifluoro-*1*(*2*-thienyl)-*1,3*-butanedione (thenoyltrifluoroacetylacetone, ttfaH), **D)** *1,1,1*-Trifluoro-*2,4*-pentanedione (trifluoroacetylacetone, tfaaH), **E)** *1,1,1,5,5,5*-Hexafluoro-*2,4*-pentanedione (hexafluoroacetylacetone, hfaaH).

The ligands illustrated in Figure 8.2 were selected to include a series of substituents which influence the electron donating and -withdrawing ability of the *β*-diketones, with the main focus being placed on fluorinated *β*-diketones. The electron-withdrawing nature of the fluorinated substituents is known to increase the acidity of extracting agents, making these agents more effective in acidic aqueous solutions. From literature it has been noted that fluorinated substituents have often been encountered in extractants.[3]

An interesting example of the practicality of this influence can be noted when considering extraction of rare earths with thenoyltrifluoroacetylacetone (ttfaH, p*Ka* = 6.50) *vs*. acetylacetone (acacH, pK_a = 8.95).[4] It has been well documented that ttfaH is a very popular and extremely effective ligand for rare earth element extraction. This efficacy has been ascribed to the fact that the metal ions can be extracted at lower pH values as opposed to acacH. For the current investigation, increased effectiveness at lower pH values is of paramount importance, especially in the case Ta(V) and Nb(V) since the metal ions are easily hydrolyzed. Table 8.1 illustrates a comparison of various functionalized acac-type ligands and highlights the effect of

[3] K. Nakashima, T. Maruyama, F. Kubota and M. Goto, (2009). *Anal. Sci.*, **25**, 77-82.

[4] J. Alstad, J. H. Augustson and L. Farbu, (1974). *J. Inorg. Nuc. Chem.*, **36**, 899-903.

the various substituents on the pK_a. For the selected ligands these values range from 8.95 for acetylacetone (acacH) to 4.60 for hexafluoroacetylacetone (hfaaH). This represents more than a four order-of-magnitude in proton concentration or around ten thousand times variation.

Table 8.1 Comparison of acetylacetone-type substrates and their pK_a values.

Acac-type ligand	pK_a
Dibenzoylacetylacetone (dbaaH)	9.35[5]
Acetylacetone* (acacH)	8.95[5]
Benzoylacetylacetone (bzaaH)	8.70[6]
Naphtyltrifluoroacetone* (ntfaH)	>6.60
Thenoyltrifluoroacetone* (ttfaH)	6.50[7]
Trifluoroacetylacetone* (tfaaH)	6.30[7]
Benzoyltrifluoroacetylacetone (btfaH)	6.30[6]
Hexafluoroacetylacetone* (hfaaH)	4.60[7]

* Ligands used in this investigation

The main purpose here is to obtain a general reaction mechanism for the coordination of *β*-diketone ligands to Ta(V) and Nb(V) metal centres. Following this mechanism elucidation, a comparison between the different metals will be undertaken. The ligands that have been identified differ significantly in terms of electronic and steric properties; accordingly, by investigating the influence of these intricacies a better understanding of both systems is envisaged. Additionally, the study is also intended to compare the influence on the reaction equilibria by either suppression of the forward equilibrium by the presence of excess leaving chlorido ligand in solution or by inciting the reaction rates, by forming a more reactive Ta(V) or Nb(V) species due to H_2O addition.

[5] P. Ebenebe, (1998). *A Mechanistic and Structural Study of Carbonyl Substitution in Square-Planar Rh(I)-β-diketone Complexes*. M.Sc. Dissertation, University of the Free State, Bloemfontein, South Africa.

[6] H. Watarai and I. Takahashi, (1998). *Anal. Commun.* **38**, 289-292.

[7] A. Kuhn, (2008). *O,O'-Chelated Titanium (IV) Complexes. A Synthetic, Kinetic, Electrochemical and Structural study*. Ph.D. Thesis, University of the Free State, Bloemfontein, South Africa.

8.2 General Experimental Considerations

8.2.1 Reagents

The synthesis of the $(Et_4N)[NbCl_6]$ and $(Et_4N)[TaCl_6]$ synthons were described in Chapter 4 (Section 4.3 and 4.4). All additional reagents including the various functionalized acetylacetone ligands used for reaction solutions were of analytical grade and were purchased from Sigma-Aldrich, South Africa. Reagents were used as received, without further purification and the acetonitrile (MeCN) dried and distilled prior to use. The tetraphenylphosphonium chloride, used in equilibrium alteration experiments was dried at ca. 90.0 °C under vacuum for two hours before use.

8.2.2 Equipment

Kinetic measurements were performed on a Varian Cary 50 Conc. UV/Visible spectrophotometer. Temperature control of the reaction solutions was maintained within ± 0.1 °C range by means of a Julabo F12-mV temperature cell regulator in a 1.000 ± 0.001 cm tandem quartz cuvette cell. The Scientist Micromath program, version 2.01 was used to fit all of the data to selected functions.[8] The *pseudo* first-order rate constants were determined from least-squares fits of the absorbance versus time data. The solid lines in the figures represent computer least-squares fits of data, while experimental values are represented as individual points, denoted by selected symbols.

8.2.3 Treatment of Data

The Beer-Lambert law incorporated with the first-order exponential yields the following equation for the evaluation of absorbance change *vs.* time in simple-first order reactions.

$$A_t = A_\infty - (A_\infty - A_0)e^{k_{obs}t} \qquad \text{Eq. 8.1}$$

[8] Micromath Scientist for Windows, Version 2.01, Copyright © 1986 – 1995, MicroMath, Inc.

Where A_t = the observed absorbance, A_0 = initial absorbance, A_∞ = final absorbance, k_{obs} = observed *pseudo* first-order rate constant.

The *pseudo* first-order rate constant (k_{obs}) is then determined by a least-squares fit of the absorbance *vs.* time data for the reaction. This equation was used in all the kinetic runs that were monitored in this study. All the observed rate constants that were calculated for the chemical reactions are reported in the supplementary material, if not documented in the text.

8.2.4 Reaction Solutions

All the kinetic runs were performed under *pseudo* first-order reaction conditions with the ligand reagent in excess. Ligand stability in the reaction solvent, acetonitrile (MeCN), was confirmed for a *ca.* 48 hour period, for each of the five functionalized acetylacetone ligands studied. Fresh reaction solutions were prepared for separate days of kinetic experiments, even though stability of solutions was confirmed.

The metal solution was maintained throughout this study at a final concentration of 5.00×10^{-4} M ($(Et_4N)[NbCl_6]$: 43.62 mg, 1.00×10^{-4} mol; $(Et_4N)[TaCl_6]$: 52.41 mg, 1.00×10^{-4} mol, dissolved in 100 cm^3 MeCN stock solution), from which reaction solutions were prepared. Ligand solutions were prepared from stock solutions of 1.00×10^{-1} M and dilution was carried out across a series of 5 solutions with minimum final concentration of 5.00×10^{-3} M (acacH: 1.021 cm^3, 1.00×10^{-2} mol; tfaaH: 1.54 g, 1.00×10^{-2} mol; hfaaH: 1.42 cm^3, 1.00×10^{-2} mol; ttfaH: 2.22 g, 1.00×10^{-2} mol each in 100 cm^3 MeCN total volume). For the equilibrium suppression experiments, tetraphenylphosphonium chloride (3.74 g, 1.00×10^{-2} mol, dissolved in $(Et_4N)[NbCl_6]$/$(Et_4N)[TaCl_6]$ reaction solution) was added to the metal reaction solution to maintain a 10^2 excess of free Cl^- ([Nb] : $[Cl^-]$ = 5×10^{-4} M : 5×10^{-2} M). In contrast, in an attempt to ascertain the effect of H_2O addition on the systems, a 10^3 excess of the liquid was added to the metal solution (1.051 cm^3, 1.00×10^{-1} mol).

8.2.5 Preliminary Experiments to Construct the Reaction Mechanism of the Formation of $[MOCl_3(\beta\text{-diket})]^-$ (M = Ta(V), Nb(V)).

As indicated by the respective study aims in Chapter 1, this investigation aims to give a better insight as to how the reaction occurs. Fortunately, as described in Chapter 3, the addition of the bidentate ligand to the metal yields a clear and definite colour change of solution, making it an ideal candidate for a UV/Vis kinetic evaluation. It has been noted throughout the text that various functionalized acetylacetone ligands were coordinated to the Ta(V) and Nb(V) metal centres, but in an attempt to gain preliminary insight into the solution state properties of these reaction systems. It was therefore decided to start with acacH since it is symmetrical (Figure 8.2) and should therefore in principle simplify the initial investigation since it gives only one possible initial attack mode, and thus not two as expected for the unsymmetrical ligands utilized.

8.2.5.1 Reaction of $(Et_4N)[NbCl_6]$ with Acetylacetone (acacH)

The reaction of acetylacetone (acacH) with $(Et_4N)[NbCl_6]$ in acetonitrile (MeCN) was investigated at 25.0 °C using standard UV/Vis techniques over the 300 to 475 nm range to determine the best wavelength at which to monitor product formation. Figure 8.3 illustrates the progress of the reaction, and as illustrated therein, the wavelength selected to evaluate the reaction in this case was chosen to be 365 nm.

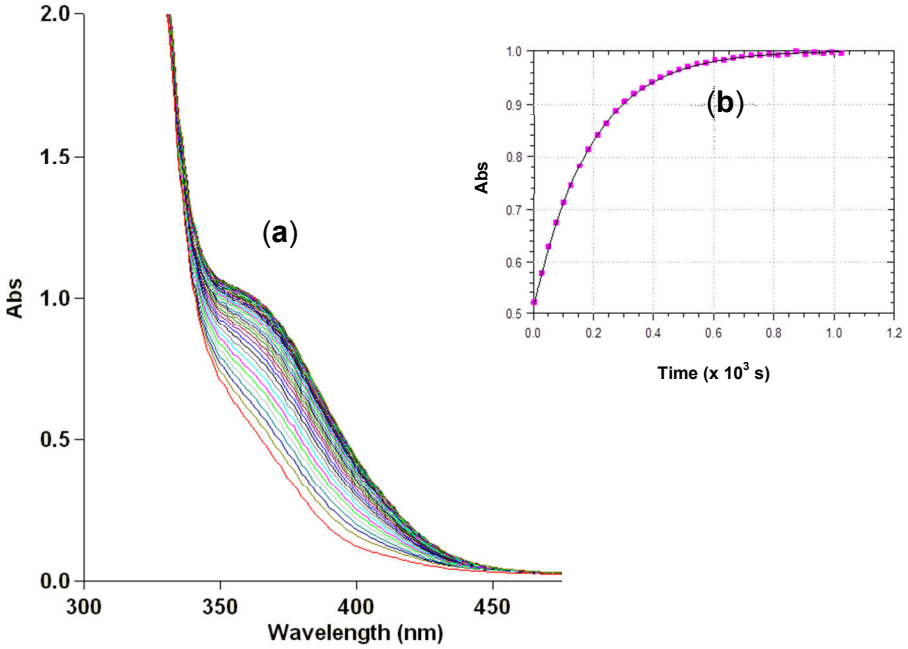

Figure 8.3 Graphical representation of data obtained from UV/Vis spectroscopic kinetics for the formation of $(Et_4N)[NbOCl_3(acac)]$: (**a**) Wavelengths scans over time (~3h); (**b**) Absorbance vs. time trace at 365 nm (25 s intervals between scans, insert illustrates initial 20 minutes) illustrating a fit for a first-order reaction (k_{obs} = 0.0072(1) s^{-1}). $[(NEt_4)[NbCl_6]]$ = 5.00 x 10^{-4} M, [acacH] = 1.00 x 10^{-2} M, Solvent: MeCN, 25 °C.

The example above confirms that the reaction reaches completion in less than 20 minutes. This is a convenient time-frame for typical UV/Vis spectroscopic analysis. Insert (**b**) illustrates a very good fit of experimental *vs.* calculated data to the *pseudo* first-order model for a one step reaction (Eq. 8.1).

8.2.5.2 Reaction of $(Et_4N)[NbCl_6]$ with Acetylacetone (acacH) in the Presence of Excess $[Cl^-]$

In another set of experiments, the influence of the excess Cl^- ions was tested by means of artificially manipulating the free $[Cl^-]$ in solution. By addition of a large excess of Cl^- ions, a suppression of the reaction rates is in principle possible. A similar investigation was performed on the formation kinetics of Zr(IV) bidentate complexes by Steyn *et al.*[2] In their study, the addition of excess $[Cl^-]$ had a substantial retarding effect on the reaction rate. This observation was ascribed to

equilibrium effects suppressing the liberation of the chlorido substituents from the Zr(IV) metal centre required for the bidentate quinolato ligand coordination.

For the Steyn *et al.* study, the organic salt, tetraphenylphosphonium chloride, was introduced into the solution as a 10^2-fold molar excess *vs.* $[(Et_4N)[NbCl_6]]$ ([Nb] : $[Cl^-]$ = 5 x 10^{-4} M : 5 x 10^{-2} M), in an attempt to investigate whether it would suppress the rate of complex formation.[2] Likewise, this procedure was followed for the current Ph.D. study.

The reaction process of acetylacetone (acacH) with $(Et_4N)[NbCl_6]$ (with excess Cl^- concentration) in acetonitrile (MeCN) was investigated at 25.0 °C using standard UV/Vis techniques over the 300 to 450 nm range to determine the ideal wavelength to follow product formation and the process illustrated in Figure 8.4. As illustrated, the wavelength selected is this case was 372 nm.

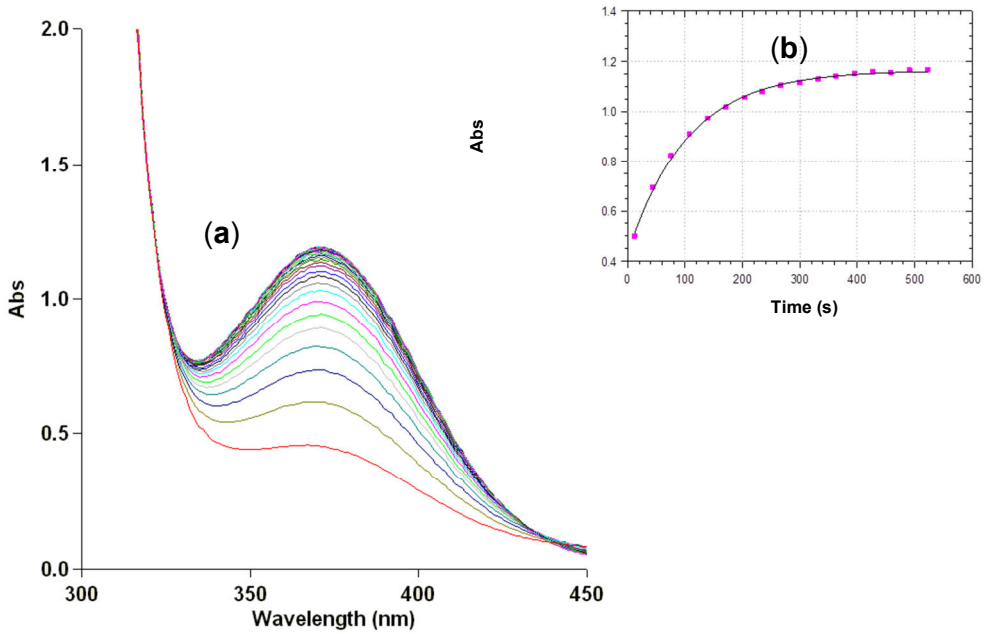

Figure 8.4 Graphical representation of data obtained from UV/Vis spectroscopic kinetics for the formation of $(Et_4N)[NbOCl_3(acac)]$: (**a**) Wavelengths scans over time (~3h); (**b**) Absorbance vs. time trace at 372 nm ((25 s intervals between scans, insert illustrates initial 10 minutes) illustrating a fit for a first-order reaction (k_{obs} = 0.0130(1) s^{-1}). $[(NEt_4)[NbCl_6]]$ = 5.00 x 10^{-4} M, $[Cl^-]$ = 5.00 x 10^{-2} M, [acacH] = 1.00 x 10^{-2} M, Solvent: MeCN, 25 °C.

The effectiveness of these types of chloride suppression experiments have been well documented in past investigations.[2,9] Ideally, when comparing the trace of the solution spiked with chloride *vs*. the unmodified system, it is expected that the spectra would be identical but that a slower coordination rate noted for the aforementioned if the same mechanism is followed. However, when comparing Figures 8.3 and 8.4 various anomalies are noted in the two traces.

- The most obvious difference is that the starting spectra in Figures 8.3 and Figure 8.4 differ substantially; indicating that the addition of Cl^- ions has a clear effect on the starting complex, possibly indicating that a new species is forming under low [Cl^-] conditions.

- Secondly, the final trace shapes of the two figures differ substantially. In the case of Figure 8.3, the final peak is observed at *ca.* 365 nm whereas Figure 8.4 illustrates the formation of a peak at *ca.* 372 nm. This is an indication that two different products have most likely formed.

- Thirdly, it also seems that the addition of Cl^- ions speeds up the rate of ligand coordination. From the insert in Figure 8.3 the reaction reaches completion in ± 750 s (k_{obs} = 0.0072(1) s^{-1}) whereas Figure 8.4 illustrates that the reaction reaches completion in less than ± 400 s (k_{obs} = 0.0130(1) s^{-1}). This is potentially counter intuitive with what would be expected for these types of suppression experiments.

The increase in reaction rate as a result of adding extra Cl^- ions into solution seems highly unlikely and considering the solid state structure of the synthon ($(Et_4N)[NbCl_6]$) (see Section 4.3, Figure 4.1), the excess of chloride ions should not influence the structure of the Nb(V) complex in solution. Accordingly, there must be another reason for this irregularity.

[9] J. A. Viljoen, (2009). *Speciation and Interconversion Mechanism of Mixed Halo O,O'- and N,O-Bidentate Ligand Complexes of Hafnium*, M.Sc. Dissertation, University of the Free State, South Africa.

From closer investigation it was realized that tetraphenylphosphonium chloride is a very hygroscopic compound and effectively extracts molecular water from the atmosphere.[10] In Section 8.2.1 it was mentioned that this compound was dried at 90.0 ºC for two hours, but it clearly remains possible that some water could still remain trapped within the powder or abstracted from atmosphere during sample preparation. To prove that H_2O actually has an influence on the coordination sphere around Nb, the addition of acacH to $(Et_4N)[NbCl_6]$ with a fixed excess of water was consequently investigated.

8.2.5.3 Reaction of $(Et_4N)[NbCl_6]$ with Acetylacetone (acacH) in the Presence of Excess $[H_2O]$

When attempting to follow the reaction of $(Et_4N)[NbCl_6]$ and acacH with a 10^3 molar excess of $[H_2O]$ ($[Nb] : [H_2O] = 5 \times 10^{-4}$ M : 5×10^{-1} M) in the MeCN, no reaction could be observed. In contrast, when tfaaH was added to $(Et_4N)[NbCl_6]$ under identical conditions, a clear reaction was detected. This observation is an indication that the acacH has not been deprotonated under the modified reaction conditions (decreased pH due to hydrolysis and H^+ release as a result of H_2O addition) in other words, under "wet" conditions acacH does seemingly not react with $[NbCl_6^-]$ in MeCN. Due to this observation, the study was further continued by rather using tfaaH, since it was important to also investigate the kinetics under excess of H_2O present. The tfaaH has a much lower pK_a value than acacH (see Table 8.1), thus it was postulated (and confirmed) that the former's kinetics will be possible to study under both anhydrous and excess H_2O conditions.

The reaction process of trifluoroacetylacetone (tfaaH) with $(Et_4N)[NbCl_6]$ in acetonitrile (MeCN) was thus investigated at 25.0 °C using standard UV/Vis techniques over the 300 to 600 nm range. The resulting spectra as illustrated in Figure 8.5, indicates that the reaction is easily monitored in both anhydrous conditions and upon addition of H_2O.

[10] Tetraphenylphosphonium chloride, (CAS: 2001-45-8). *TCI America MSDS*, Accessed 03-01-2016.

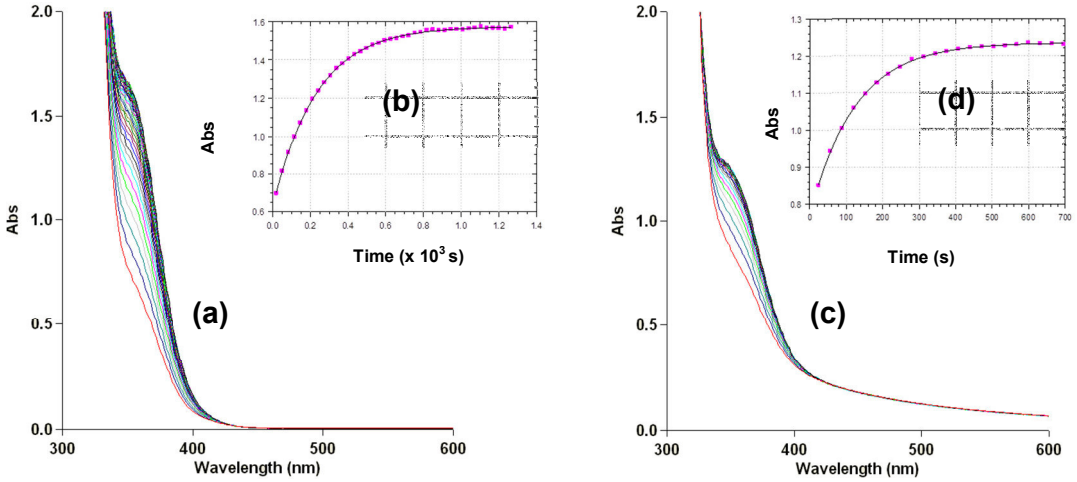

Figure 8.5 Graphical representation of data obtained from UV/Vis spectroscopic kinetics for the formation of $(Et_4N)[NbOCl_3(tfaa)]$: (**a**) Wavelengths scans over time: no $[H_2O]$ added (~2h); (**b**) Absorbance vs. time trace at 385 nm (k_{obs} = 0.0024(1) s^{-1}) (25 s intervals between scans, insert illustrates initial 23 minutes); (**c**) Wavelengths scans over time: excess $[H_2O]$ added (~2h); (**d**) Absorbance vs. time trace at 375 nm (k_{obs} = 0.0051(10 s^{-1}) (25 s intervals between scans, insert illustrates initial 12 minutes). $[(NEt_4)[NbCl_6]]$ = 5.00 x 10^{-4} M, [tfaaH] = 5.00 x 10^{-3} M, $[H_2O]$ = 5.00 x 10^{-1} M, Solvent: MeCN, 25 °C.

By comparing the trace in Figure 8.5 with Figures 8.3 and 8.4 it is clear that the addition of H_2O to the reaction solution has a similar effect as the Cl^- addition described Section 8.2.5.2. In other words, water shows a definite influence on the coordination and the products forming. This also means that the tetraphenylphosphonium chloride utilized was most probably not completely anhydrous in spite of being in an oven for two hours. With this in mind, it was decided to first study influence of H_2O on the reaction system.

8.2.5.4 The Effect of Additional H_2O on the Reaction of $(NEt_4)[NbCl_6]$ with tfaaH

In an attempt to understand what happens when water is added to these Nb(V) and Ta(V) solutions, three additional experiments were done. For this investigation the effect of varying both the $[Cl^-]$ and $[H_2O]$ on the reaction of $(Et_4N)[NbCl_6]$ (5.00 x 10^{-4} M) to tfaaH (2.50 x 10^{-2} M) (1:50 ratio) was examined.

a) The effect of [H_2O] on the rate of coordination; [tfaaH] = constant, no [Cl^-] added

For this investigation, five (Et_4N)[$NbCl_6$] (5.00 x 10^{-4} M) solutions were prepared by adding varying amounts of H_2O (5.00 x 10^{-4} M to 5.00 x 10^{-2} M) to the respective solutions. Figure 8.6 illustrates the effect on the observed rate (k_{obs}) of the reaction as a result of additional H_2O.

b) The effect of [Cl^-] on the rate of coordination; [tfaaH] = constant, no [H_2O] added

To determine the influence of additional Cl^- ions in these solutions, five (Et_4N)[$NbCl_6$] (5.00 x 10^{-4} M) solutions were prepared by adding varying amounts of tetraphenylphosphonium chloride (5.00 x 10^{-4} M to 5.00 x 10^{-2} M) to the respective solutions. Figure 8.6 illustrates the effect on the observed (k_{obs}) of the reaction as a result of additional Cl^-.

c) The effect of [H_2O] and [Cl^-] on the rate of coordination; [tfaaH] = constant

Finally, to determine the collective effect of additional [Cl^-] and [H_2O] on these systems, five (Et_4N)[$NbCl_6$] (5.00 x 10^{-4} M) solutions were prepared by adding varying amounts of H_2O (5.00 x 10^{-4} M to 5.00 x 10^{-2} M) and tetra phenylphosphonium chloride (5.00 x 10^{-4} M to 5.00 x 10^{-2} M) to the respective solutions. Figure 8.6 illustrates the effect on the observed rate (k_{obs}) of the reaction as a result of additional H_2O and Cl^-.

The relationships of k_{obs} on added [Cl^-], [H_2O] and [Cl^-/H_2O] are shown in Figure 8.6 which follows a non-linear relationship. This will be discussed further below.

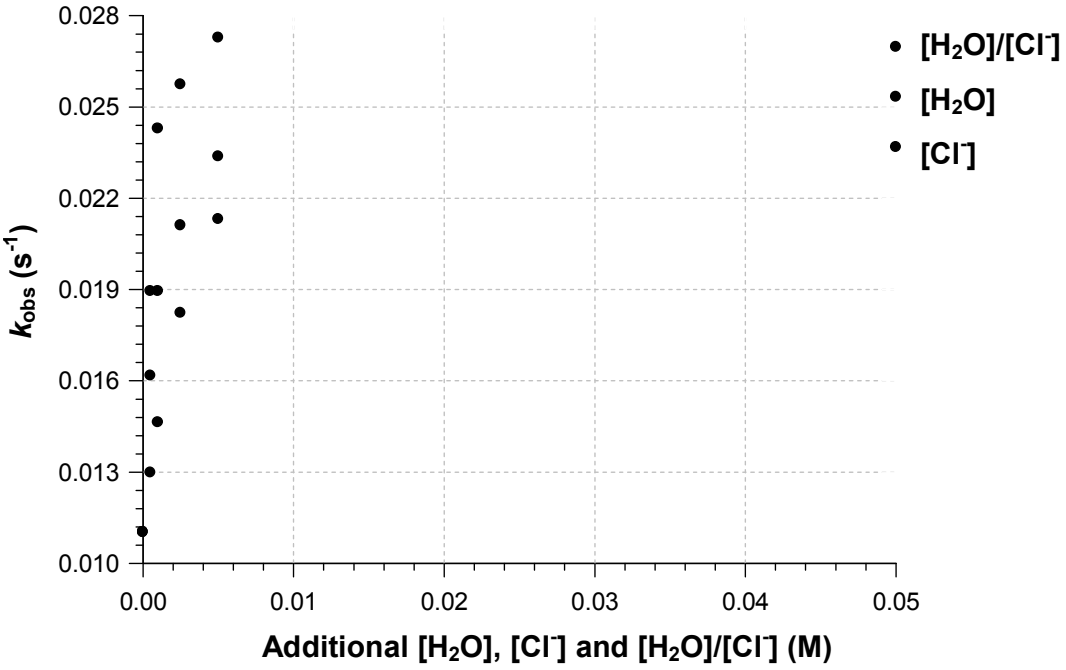

Figure 8.6 k_{obs} *vs.* [H_2O], [Cl^-] and [H_2O/Cl^-] addition plot for the reaction of (Et_4N)[$NbCl_6$] (5.00 x 10^{-4} M) and trifluoroacetylacetone (tffaH) (2.50 x 10^{-2} M).

8.2.6 Identification of Niobium(V) and Tantalum(V) Species in Solution

To more precisely predict the mechanism of any reaction, an accurate molecular structure, i.e. a well characterized species, of the solubilized starting material is important. A crystal structure of a synthon gives the precise structure in the solid state but the same compound in solution, could differ significantly. Both the solid state crystal structures of (Et_4N)[$NbCl_6$] and (Et_4N)[$TaCl_6$] were discussed in detail in Chapter 4 (Sections 4.3 and 4.4). A graphic illustration of these compounds is depicted in Figure 8.7.

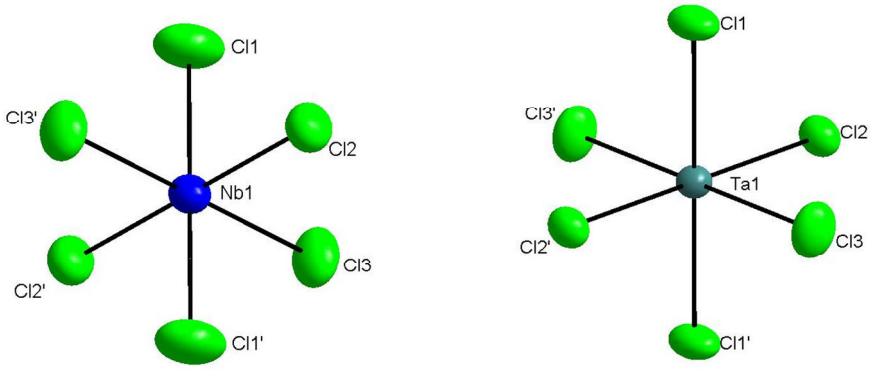

Figure 8.7 Crystallographic representations of $[NbCl_6]^-$ and $[TaCl_6]^-$.

Although these solid state structures have been well defined, their coordination sphere could alter significantly in solution and should be investigated. Solvated $(Et_4N)[NbCl_6]$ seems to have a different structure in anhydrous ("dry") *vs.* hydrous ("wet") MeCN, as was discussed in Section 8.2.5. Due to this observation, a minimum of three reactant species can be identified for the varying reaction conditions and will be defined in the following sections. Not much literature relating to the Ta(V) analogues has been reported; accordingly focus will be placed on the formation of Nb(V) complexes with the assumption that the Ta(V) systems have similar solution state behaviour.[1]

8.2.6.1 Identification of a Preliminary Nb(V) Complex: Anhydrous Acetonitrile

It has been well documented that niobium(V) halides have a common dimeric halogen-bridged structure and are soluble in Lewis donor solvents such as alkyl cyanides.[11] These types of addition reactions, afford mononuclear (six-coordinate) adducts that may be utilized as suitable precursors for a wide range of metal(V) complexes *via* ligand exchange.[11,12,13] Although mononuclear $(Et_4N)[NbCl_6]$ is used in this kinetic investigation, the $[NbCl_5(MeCN)]$ analogue should also be able to similarly react with *β*-diketone ligands.

[11] F. A. Cotton and G. Wilkinson, (1988). *Advanced Inorganic Chemistry*, **5**, Oxford, Great Britian.

[12] K. Feenan and G. W. A. Fowles, (1964). *J. Chem. Soc.*, **43**, 2842-2901.

[13] J. D. Wilkins, (1975). *J. Inorg. Nucl. Chem.*, **37**, 2095-2107.

A structural characterization of the $[NbCl_5(MeCN)]$ complex is noted, in a paper by Willey *et al.*[14] This product was obtained by dissolving $[NbCl_5]_2$ in an excess of anhydrous MeCN. The crystal structure of this compound is illustrated in Figure 8.8.

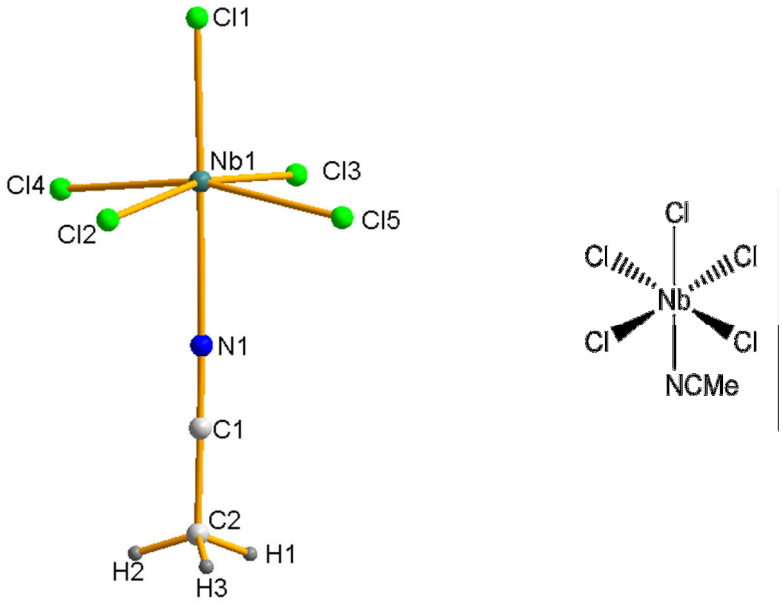

Figure 8.8 Crystal structure of $[NbCl_5(MeCN)]$ as characterized by Willey *et al.*[14,15]

The molecular structure of the six-coordinate, mono-solvated $[NbCl_5(MeCN)]$ complex has a distorted octahedral geometry. For this structure the observed metal-chlorido bond distances are in a the 2.249(2) - 2.319(2) Å range, with the Nb-Cl_{axial} distance being the shortest, due to the weaker σ–donating properties of the acetonitrile substituent as compared to Cl^-. The four equatorial chlorine atoms are co-planar within experimental error and are bent back towards the coordinated acetonitrile. This is might be due to steric requirements and reflects the larger steric bulk of Cl_{axial} *vs*. N_{axial}, especially since the axial chlorine has the shortest metal-chlorine bond distance.

It should however be possible that, an equatorial chloride functionality could additionally be substituted by a second MeCN group, forming the $[NbCl_4(MeCN)_2]^+$ in

[14] G. R. Willey, T. J. Woodman and M. G. B. Drew, (1996). *Polyhedron*, **16**, 351-353.

[15] L. Herbst, (2011). *A Solution and Solid State Study of Niobium Complexes*, M.Sc. Dissertation, University of the Free State, South Africa.

solution, in excess acetonitrile. This reversible substitution is illustrated in Figure 8.9. The substitution of the Cl_{axial} seems highly unlikely as this chlorido group is the most tightly bound to the metal centre as exemplified by the shortest Nb-Cl bond distance.

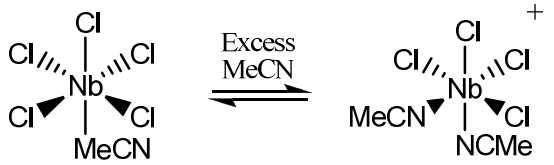

Figure 8.9 Illustration of MeCN addition solvation of Nb(V) synthon in anhydrous solution.[16]

We therefore postulate that there are at least two $[NbCl_x(MeCN)_y]$ species in solution that can react with *β*-diketones under our reaction conditions.

8.2.6.2 Identification of Possible Nb(V) Complexes in MeCN Containing H_2O

In an attempt to more accurately describe the structure of the Nb(V) reactant in MeCN containing H_2O, a study conducted by Levason *et al.* needs to be considered.[16] This paper was aimed at analyzing the synthesis and properties of $[NbOCl_3]$ complexes. The existence of $[NbOCl_3]$ complexes have been well documented in past investigations and have been obtained by adventitious hydrolysis, or O-abstraction from the solvent in reaction of $NbCl_5$.[17,18] In the investigation by Levason *et al*. a convenient alternative route to $[NbOCl_3]$ complexes was postulated. The mechanism described a Cl/O exchange from the corresponding $NbCl_5$ adducts, using hexamethyldisiloxane (HMDSO) as an oxygen donor.[16] This is illustrated in Figure 8.10.

[16] W. Levason, G. Reid, J. Trayer and W. Zhang, (2014). *Dalton Trans.*, **43**, 3649-3659.

[17] G. Wilkinson, R. D. Gillard and J. A. McCleverty, (1987). *Comprehensive Coordination Chemistry*, **3**, Oxford, Great Britain.

[18] W. A. Herrmann, W. R. Thiel and E. Herdtweck, (1990). *Chem Ber.*, **123**, 271-276.

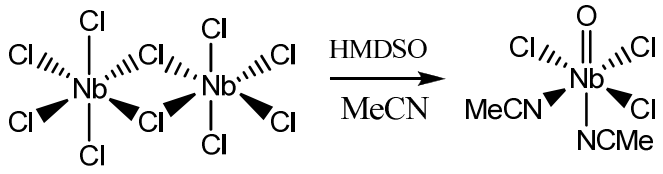

Figure 8.10 Depiction of the formation of $[NbOCl_3(MeCN)_2)]$ by means of O-abstraction as postulated by Levason *et al.*[16]

However, when considering the investigation at hand it is considered very likely that H_2O can act as the oxygen donating substance, especially since all the crystal structures obtained in this current investigation included an oxido ligand bound to a Nb(V) centre (Chapters 5 and 6). An argument can be made for the formation of $[NbCl_5(H_2O)]$ in the MeCN solution. Previous studies have shown that this aqua group may undergo various rapid proton exchange equilibria (hydroxido and oxido equilibrium) as a result of simple solution pH.[19,20,21]

Evidence to this effect exists for the middle transition metal cyanide complexes and over the past few decades various investigations have shown that the pH has a substantial effect on the proton exchange of *trans*-dioxidootetracyanido complexes of tungsten(IV), technetium(V), rhenium(V) and molybdenum(IV).[19,20,21] As the pH of the reaction solution decreases, this group can be protonated, resulting in the formation of the hydroxidooxido- and aquaoxido complexes.[22,23] These protonated species can undergo substitution reactions with mono- (aqua ligand substitution) and bidentate (aqua and cyanido ligand substitution) nucleophiles.[24,25,26,27,28] In other relevant studies, the protonation behaviour of these systems have been subject of ^{13}C- and ^{17}O-NMR investigations in order to examine the proton exchange within

[19] A. Roodt, J. G. Leipoldt, E. A. Deutsch and J. C. Sullivan, (1992). *Inorg Chem.*, **31**, 1080-1085.

[20] W. Purcell, A. Roodt, S. S. Basson and J. G. Leipoldt, (1991). *Trans. Met. Chem.*, **16**, 60-61.

[21] A. Roodt, J. G. Leipoldt, S. S. Basson and I. M. Potgieter, (1988). *Trans. Met. Chem.*, **13**, 336-339.

[22] J. P. Smit, W. Purcell, A. Roodt and J. G. Leipoldt, (1993). *Polyhedron*, **12**, 2271-2277.

[23] P. R. Robinson, E. O. Schlemper and R. K. Murmann, (1975). *Inorg. Chem.*, **14**, 2035-2040.

[24] J. G. Leipoldt, R. Van Eldik, S. S. Basson and A. Roodt, (1986). *Inorg. Chem.*, **25**, 4639-4642.

[25] J. G. Leipoldt, S. S. Basson, I. M. Potgieter and A. Roodt, (1987). *Inorg. Chem.*, **26**, 57-59.

[26] W. Purcell, A. Roodt and J. G. Leipoldt, (1991), *Trans. Met. Chem.*, **16**, 339-343.

[27] A. Samotus, A. Kanas, W. Glug and J. Szklarzewicz, (1991). *Trans. Met. Chem.*, **16**, 614-617.

[28] A. Roodt, S. S. Basson and J. G. Leipoldt, (1994). *Polyhedron*, **13**, 599-607.

these complexes.[29] This occurrence was extremely well documented in an investigation of the influence of pH on tungsten(IV)tetracyanido systems by means of ^{17}O-NMR spectroscopy.[30]

Roodt *et* al. noted that in a pH range of roughly of 6 - 7 only the oxidoaqua species $[WO(OH_2)(CN)_4]^{2-}$ of the W(IV) complex was present in reaction solution.[30,31] As the pH value increased to *c.a.* 9, past the first pK_a value of protonation, the aqua substituent is deprotonated and the hydroxidooxido species, $[WO(OH)(CN)_4]^-$, of the complex was noted. Thus, in a small pH range of two units, substitution can be activated or completely shut down.

This principle of proton exchange as a result of pH influence could also apply to the impending topic. Accordingly, the formation of $[NbOCl_5(H_2O)]$ is postulated, due to the fact that H_2O acts as an oxygen donor in hydrous MeCN solutions. As was found with the W(IV)-tetracyanido complexes this $[NbOCl_5(H_2O)]$ could be in equilibrium with the hydroxido- ($[NbCl_5(OH)]^-$) and the oxido- ($[NbOCl_5]^{2-}$) complexes. Due to the pH of the reaction mixture the equilibrium is strongly shifted towards ($[NbOCl_5]^{2-}$ formation.

Levason *et al.* further mentions that if this type of oxygen scavenging occurs in an excess in a MeCN solution, $[NbOCl_3(MeCN)_2]$ is formed *in situ*. The formation of this solvated species was also reported in various other publications.[15,32,33] It is important to note the probable existence of this species, but due to the fact that in this current study it could not be accurately defined the actuality of the structure as well as the fact that it would substantially complicate the postulated rate law, focus will only be placed the $[NbOCl_5]^{2-}$ synthon for the aqueous pathway.

---

[29] A. Roodt, J. G. Leipoldt, L. Helm, A. Abou-Hamdann and A. E. Merbach, (1995). *Inorg. Chem.*, **34**, 560-568.

[30] A. Roodt, J. G. Leipoldt, L. Helm, A. and A. E. Merbach, (1994). *Inorg. Chem.*, **34**, 140-147.

[31] A. Roodt, A. Abou-Hamdan, H. P. Engelbrecht and A. E. Merbach, (1999). *Advances in Inorganic Chemistry*, **47**, Academic Press, London, United Kingdom.

[32] V. C. Gibson and T. P. Kee, (1993). *Dalton Trans.*, **21**, 1657-1667.

[33] V. S. Sergienko, M. A. Porai-Koshits, A. A. Konovalova and V. V. Kovalev, (1984). *Koord. Khim.*, **10**, 1116-1121.

8.2.7 Reaction of $(Et_4N)[MCl_6]$ with Thenoyltrifluoroacetone (ttfaH)

From the previous section, six potential Nb(V) species in solution have been defined. In an attempt to further elucidate the reaction mechanism, focus now shifts to obtaining the coordination model for the reaction of other *β*-diketones with the Nb(V) and Ta(V) synthons described in Chapter 4. To obtain a generalized idea of the preferred coordinative modes, the reaction of thenoyltrifluoroacetylacetone (ttfaH) with $(Et_4N)[NbCl_6]$ in acetonitrile is considered.

8.2.7.1 Reaction of $(Et_4N)[NbCl_6]$ with Thenoyltrifluoroacetone (ttfaH) in both "Wet" and "Dry" MeCN

A kinetic investigation of the coordination of trifluorothenoylacetylacetone (ttfaH) to $(Et_4N)[NbCl_6]$ was performed as a generalized example of a substituted acetylacetone ligand chelation process in both anhydrous ("dry") and hydrous ("wet") MeCN. The synthesis and preliminary characterization of the anhydrous niobium(V) complex has been reported in Section 3.3.1.4 and the crystalline properties induced by ttfaH to the Nb(V), allowed a detailed crystallographic structural characterization of the solid state product obtained, as described in Section 5.4. As with other *β*-diketone ligands, ttfaH further yields a clear and definite colour change to a reaction solution when coordinated to Nb(V), making it an ideal candidate for a UV/Vis kinetic evaluation.

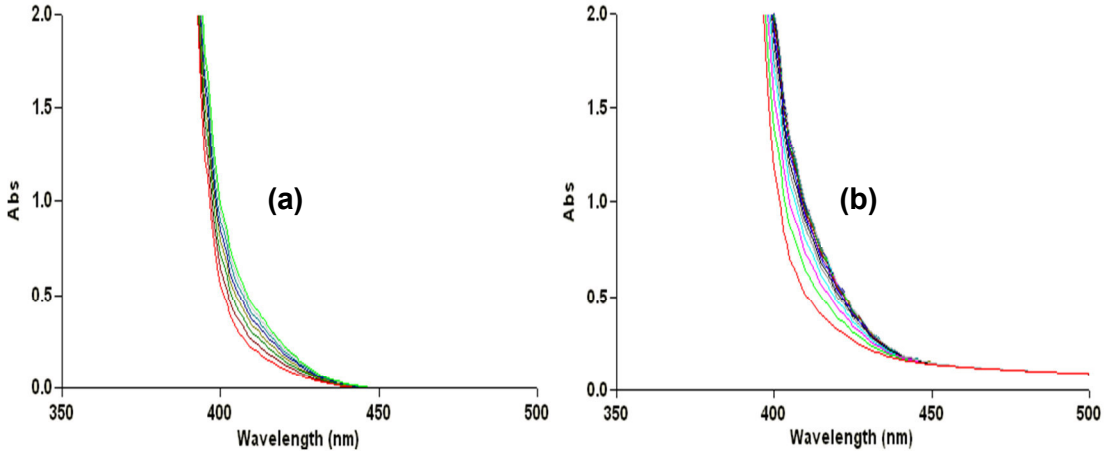

Figure 8.11 Graphical representation of data obtained from UV/Vis spectroscopic kinetics for the formation of $(Et_4N)[NbOCl_3(ttfa)]$ in (**a**) "dry" MeCN and (**b**) "wet" MeCN. Wavelengths scans over time (~2h), with 25s intervals between scans;
$[(NEt_4)[NbCl_6]] = 5.00 \times 10^{-4}$ M, [ttfaH] = 1.00×10^{-2} M, Solvent: MeCN, 25 °C.

Figure 8.11 illustrates the reaction process of ttfaH with $(Et_4N)[NbCl_6]$ over the 350-500 nm range. From this figure, the ideal wavelength to follow the rate of product formation is 410 nm for anhydrous and 418 nm for hydrous solutions of MeCN. The *pseudo* first-order rate constants (k_{obs}) were then determined by a least-squares fit of the absorbance *vs.* time data for the reaction by using Eq. 8.1. Figure 8.12 illustrates the good correlation of experimentally obtained data with the calculated data for a *pseudo* first order kinetic model for both solvent systems.

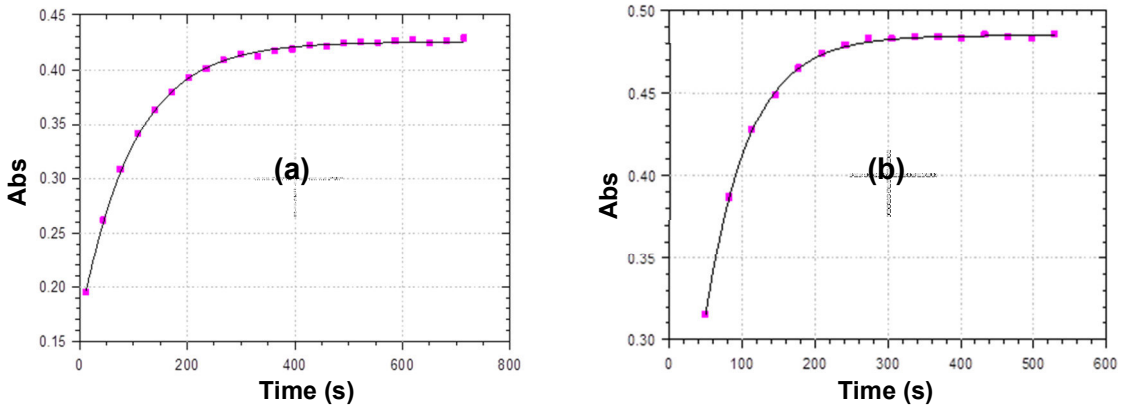

Figure 8.12 Absorbance vs. time trace of the formation $(Et_4N)[NbOCl_3(ttfa)]$ ((25 s intervals between scans) illustrating a fit for a first-order reaction in (**a**) anhydrous MeCN at 410 nm and (**b**) hydrous MeCN at 418 nm. $[(NEt_4)[NbCl_6]] = 5.00 \times 10^{-4}$ M, [ttfaH] = 1.00×10^{-2} M, Solvent: MeCN, 25 °C.

From the fits of these traces it seems that even though the *β*-diketone was reacted with different synthons it seems that the mode of this coordination is similar in both cases.

8.2.8 Identification of Reaction Products

Section 8.2.6 described the six possible Nb(V) reactant species in solution, whereas in Section 8.2.7 a *pseudo* first-order rate model for both solvent pathways was confirmed. In the final step to elucidate the reaction mechanism, the structures of final reaction products also need to be confirmed. Since, in any mechanistic study it is imperative that the final products that are proposed in the reaction mechanism are supported by the same physical evidence. This section describes clear evidence for the existence of $(NEt_4)[NbOCl_3(ttfa)]$ and $(NEt_4)[NbCl_4(ttfa)]$.

8.2.8.1 $(NEt_4)[NbOCl_3(ttfa)]$

The crystal structure of tetraethylammonium *mer*-trichloridooxido(thenoyl trifluoroacetylacetonato-κ^2O,O')niobate(V) ($(NEt_4)[NbOCl_3(ttfa)]$) was reported in Section 5.4 and the bench top synthesis in Section 3.3.1.4. A UV/Vis spectrum of the solution of $(NEt_4)[NbOCl_3(ttfa)]$ crystals dissolved in MeCN gives a λ_{max} of 370 nm which is similar to the spectra obtained for reaction solutions (kinetic studies) in “wet” MeCN. Similarly, the corresponding ^{19}F-NMR spectra yielded single peak at -73.37 ppm for both types of sets. Due to these similarities, it is safe to assume that $(NEt_4)[NbOCl_3(ttfa)]$ is the final product from the hydrous pathway.

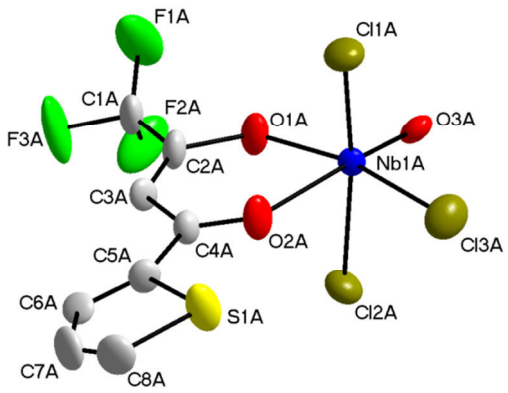

Figure 8.13 DIAMOND representation of the complex structure of *mer*-$[NbOCl_3(ttfa)]^-$ (**Nb_2**) (see Section 5.4) displaying the atom numbering system. The displacement ellipsoids are drawn at a 50 % probability level. Hydrogen atoms and counter ion are omitted for clarity.

8.2.8.2 $(NEt_4)[NbCl_4(ttfa)]$

The formation of $(NEt_4)[NbCl_4(ttfa)]$ from the anhydrous pathway is also postulated. Owing to the fact that no solid state structure could be obtained for this complex, additional experimentation was required to corroborate this assumption.

When a solution of $[NbCl_6]^-$ in dry MeCN is reacted with ttfaH, a UV-Vis spectrum can be obtained (Trace (**A**) in Figure 8.15). The addition of water to this solution results in a spectrum shift to Trace (**B**) in Figure 8.15, which corresponds to the UV-Vis spectrum of $(NEt_4)[NbOCl_3(ttfa)]$. It was therefore concluded that the first spectrum (**A**) is that of $(NEt_4)[NbCl_4(ttfa)]$.

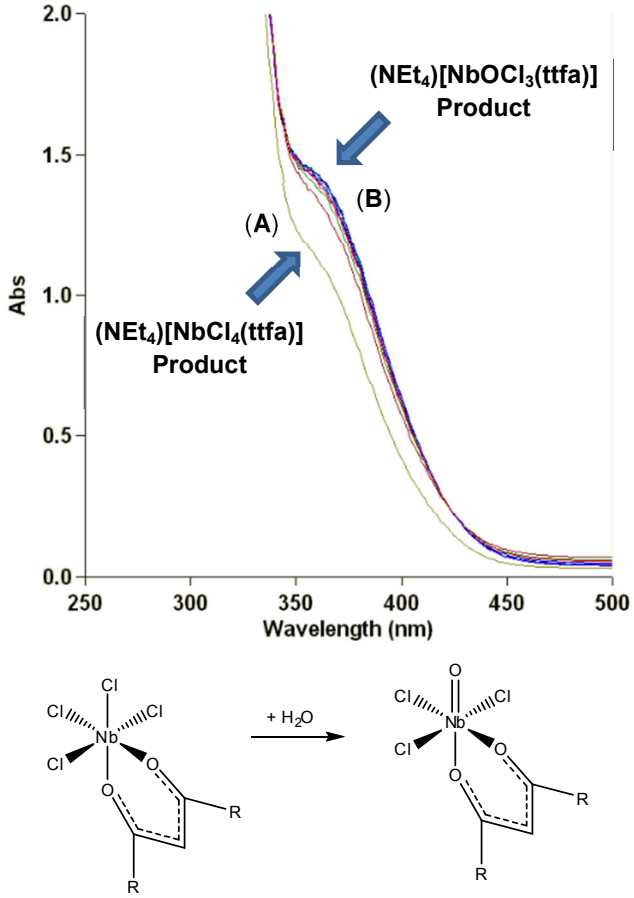

Figure 8.14 Illustration of the formation of $(NEt_4)[NbOCl_3(ttfa)]$ due to advantageous hydrolysis of $(NEt_4)[NbCl_4(ttfa)]$

The influence of the addition of H_2O to the $(NEt_4)[NbCl_4(ttfa)]$ product affords a noticeable peak shift, while the final trace from this investigation compares extremely well to the UV-Vis trace of the $(NEt_4)[NbOCl_3(ttfa)]$ product. This observation substantiates the postulation of advantageous hydrolysis of $(NEt_4)[NbCl_4(ttfa)]$ to form the $(NEt_4)[NbOCl_3(ttfa)]$ product.

From the three preceding sections, all of the reacting species within the postulated reaction have been identified. Accordingly, it can be deemed that a general reaction mechanism, to be noted in Section 8.3, for functionalized acetylacetone addition to $(Et_4N)[NbCl_6]$ can be constructed.

8.3 Proposed Reaction Mechanism

As was outlined in the introduction of this chapter, the prediction of a reaction mechanism is crucial in understanding the intricacies of bidentate ligand addition to Ta(V) and Nb(V) metal centres. In an attempt to obtain an accurate representation thereof, a systematic analysis of the various aspects of the reaction has been undertaken. When all of this data is considered as discussed above in Section 8.2.5, it could be utilized to produce a complete scheme as discussed below.

8.3.1 Reaction Scheme

In Figure 8.15 a proposed reaction scheme is presented, taking into account Section 8.2.5, for the general reaction between acacH-type ligands with both $(Et_4N)[NbCl_6]$ and $(Et_4N)[TaCl_6]$. An explanation of this proposed mechanism will be done in a step-wise and systematic manner in the following paragraphs. This scheme considers all the currently identified reacting species, as well as the dependence on; (i) entering [ligand], (ii) excess added $[Cl^-]$ as well as, (iii) excess H_2O as highlighted above.

The mechanism identifies three potential reacting species, i.e. $[NbCl_5(MeCN)]$; $[NbCl_4(MeCN)_2]^+$ as well as the aqueous hydrolysis product $[NbOCl_5]^-$, as depicted by (I), (II) and (III) below. The latter oxido species is expected to further undergo solvolysis, forming chloridooxido acetonitrile species as discussed above, which can react further with *β*-diketone entering ligands.

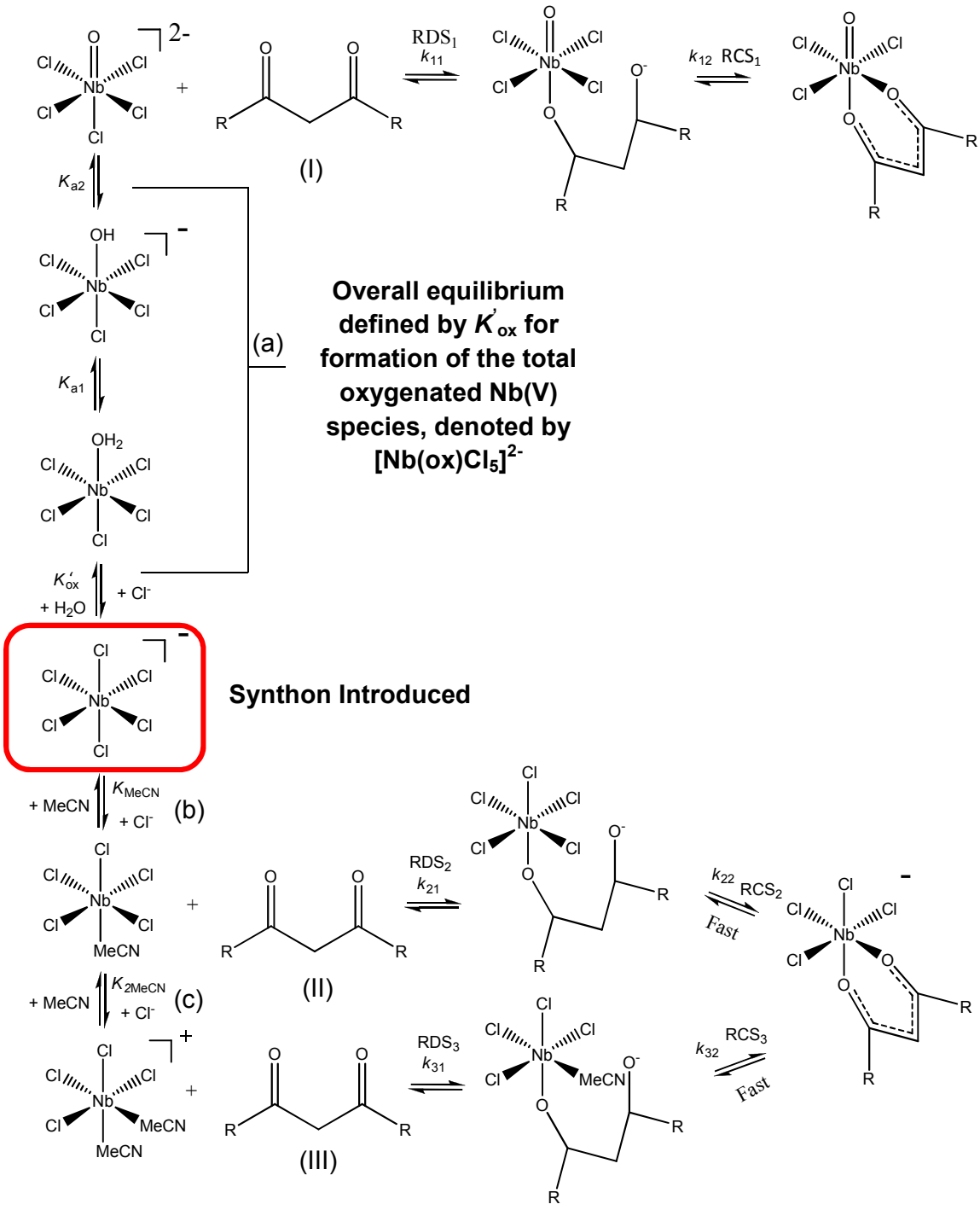

Figure 8.15 Generalized proposed reaction mechanism for the addition of *β*-diketone ligands to the $[MCl_6]^-$ anion. (M = Nb(V), Ta(V)). (RDS = Rate determining step; RCS = Ring closing step, fast step for reaction steps (I), (II) and (III))

The presence of oxygen (H_2O) and the fact that the final products containing the oxido ligand were obtained, means that at least three types of Nb(V)-oxido species, $[NbCl_5(H_2O)]$, $[NbCl_5(OH)]^-$ and $[NbOCl_5]^{2-}$ are possible, as indicated. Evidence for this was provided in Section 2.6.2.

As noted above, the formation of the solvated Nb-oxido species, $[NbOCl_x(MeCN)_y]^n$ is excluded for simplicity from the above scheme since it is obviously already an extremely complicated reaction mechanism. Overall, such solvated species most probably exists (see Section 8.2.6.1) but should not affect the general investigation.

According to the mechanism, three Nb(V) species react with the ligand in respective rate determining steps (k_{11}, k_{21} *and* k_{31}) after which fast ring closure (RCS) occurs.

It is also proposed that the bidentate entering ligands are deprotonated under the reaction conditions utilized, therefore allowing the acid dissociation equilibria in the derived rate equation to be ignored.

Owing to the fact that Ta(V)-*β*-diketonates to date did not afford any accurate crystallographic structural data, and keeping in mind that there is a marked shortage of literature relating to the structural properties/characterization of Ta(V) halides in solution, the postulation of the reaction mechanism of functionalized acetylacetones to Ta(V) was significantly complicated.

Fortunately, certain observations were noted during *β*-diketone addition to Ta(V) which clearly relates to the behaviour of the analogous Nb(V) systems.

- All of the ^1H, ^{13}C, ^{19}F, IR and UV-Vis characterization noted in Chapter 3 for the Ta(V)-*β*-diketonates relates extremely well to their Nb(V) counterparts. Accordingly only one *β*-diketone is expected to coordinate to the Ta(V) metal centre.

- When considering UV/Vis kinetic investigation, the addition of acetylacetone to Ta(V) shows similar influences on peak shapes as well as comparable rates of coordination to the Nb(V) systems.

- The addition of H_2O to the Ta(V) solution has a similar enhancing effect on reaction rates *vs*. that which was observed for the anhydrous systems. And finally, by adding H_2O to the anhydrous solubilized Ta(V) product a similar trend is noted to what was observed in Figure 8.14.

During the course of the related M.Sc. investigation, it was deemed that by ignoring a few minor anomalies the reaction rates and coordination mechanism of the formation of *trans*-$[TaCl_2(OMe)_2(acac)]$ and *trans*-$[NbCl(OMe)_3(acac)]$ were found to be relatively similar.[1] Accordingly, owing to the well-documented comparable coordinative nature of Nb(V) and Ta(V) systems, it is safe to assume that the reaction mechanism for the formation of the metal(V)-*β*-diketonates are nearly identical.

8.3.2 Derivation of Rate Law

In Figure 8.15 six possible species in solution are available for ligand coordination were identified. The various equilibria between four of these species are illustrated in Figure 8.16. When considering the K'_{ox} equilibrium depiction in Figure 8.16 between $[NbOCl_5]^{2-}$ and $[NbCl_6^-]$, it indicates an overarching representation of the total of $[NbCl_6]^-$ – $[NbCl_5(H_2O)]$ – $[NbCl_5(OH)]^-$ – $[NbOCl_5]^{2-}$ equilibria.

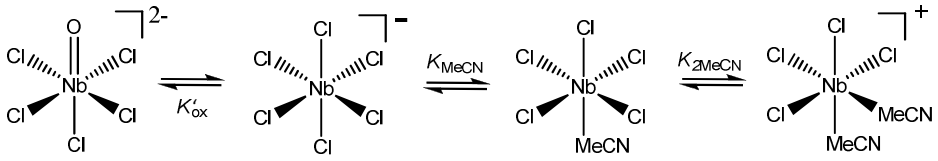

Figure 8.16 Illustration of kinetic equilibriums between the various synthons in solution.

8.3.2.1 Complete Rate Law

From the definition of the three equilibrium constants shown in the mechanism in Figures 8.15 and 8.16, K'_{ox}, K_{MeCN} and K_{2MeCN}, the following equations can be written from simple mass balance for (a), (b) and (c) (charges of complexes ions are omitted for clarity):

$$K'_{ox} = \frac{[M(ox)Cl_5][Cl^-]}{[MCl_6][H_2O]} \quad \text{Eq. 8.2}$$

$$K_{MeCN} = \frac{[M(MeCN)Cl_5][Cl^-]}{[MCl_6]} \quad \text{Eq. 8.3}$$

$$K_{2MeCN} = \frac{[M(MeCN)_2Cl_4][Cl^-]}{[M(MeCN)Cl_5]} \quad \text{Eq. 8.4}$$

To accurately define the total metal species available for coordination, the $[M(ox)Cl_5]^{2-}$, $[M(MeCN)Cl_5]$ and $[M(MeCN)_2Cl_4]^+$ concentrations are expressed in terms of $[M]_{tot}$, (the total [Nb] introduced). The total metal(V) concentration in solution ($[M]_{tot}$) at any time, is defined by:

$$[M]_{tot} = [MCl_6] + [M(ox)Cl_5] + [M(MeCN)Cl_5] + [M(MeCN)_2Cl_4] \quad \text{Eq. 8.5}$$

By substituting Eq. 8.2, Eq. 8.3 and Eq. 8.4 into Eq. 8.5 three expressions for $[M(ox)Cl_5]$, $[M(MeCN)Cl_5]$ and $[M(MeCN)_2Cl_5]$ are obtained:

$$[M(ox)Cl_5] = \frac{[M]_{tot}[H_2O]K_{ox}[Cl^-]}{[Cl^-]^2+[Cl^-]K_{ox}[H_2O]+[Cl^-]K_{MeCN}+K_{2MeCN}K_{MeCN}} \quad \text{Eq. 8.6}$$

$$[M(MeCN)Cl_5] = \frac{[M]_{tot}K_{MeCN}[Cl^-]}{[Cl^-]^2+[Cl^-]K_{ox}[H_2O]+[Cl^-]K_{MeCN}+K_{2MeCN}K_{MeCN}} \quad \text{Eq. 8.7}$$

$$[M(MeCN)_2Cl_4] = \frac{[M]_{tot}K_{MeCN}K_{2MeCN}}{[Cl^-]^2+[Cl^-]K_{ox}[H_2O]+[Cl^-]K_{MeCN}+K_{2MeCN}K_{MeCN}} \quad \text{Eq. 8.8}$$

These three equations define the total amount of reacting M(V) species in solution, i.e. $[M(ox)Cl_5]^{2-}$, $[M(MeCN)Cl_5]$ and $[M(MeCN)_2Cl_4]^+$ for which a complex rate law involving these reactants for the forward reaction, may be written. Thus, an expression for the total rate of the reaction is defined by:

$$\text{Rate}^{\text{tot}} = \text{Rate}^{[\text{M(ox)Cl}_5]} + \text{Rate}^{[\text{M(MeCN)Cl}_5]} + \text{Rate}^{[\text{M(MeCN)}_2\text{Cl}_4]} \quad \text{Eq. 8.9}$$

The main focus of this investigation was on the formation of the metal(V) products and for the sake of simplicity, the effect of the reverse steps weren't considered in great detail. However, for the final rate law it is imperative a reverse step is considered as defined by k_{rev}[M(β-diket)$_{product}$] .

$$\text{Rate}^{\text{tot}} = k_{11}[\text{M(ox)Cl}_5][\beta - \text{diket}] + k_{21}[\text{M(MeCN)Cl}_5][\beta - \text{diket}] + k_{31}[\text{M(MeCN)}_2\text{Cl}_4][\beta - \text{diket}] + k_{\text{rev}}[\text{M}(\beta - \text{diket})_{\text{product}}] \quad \text{Eq. 8.10}$$

By substituting Eq. 8.6, Eq. 8.7 and Eq. 8.8 into Eq. 8.10, the total rate law is obtained under conditions where [β-diket] >> [M_{tot}], yielding the *pseudo* first-order rate constant:

$$k_{\text{obs}}{}^{\text{tot}} = \frac{k_{11}[\text{H}_2\text{O}]K_{\text{ox}}[\text{Cl}^-] + k_{21}K_{\text{MeCN}}[\text{Cl}^-] + k_{31}K_{2\text{MeCN}}K_{\text{MeCN}}}{[\text{Cl}^-]^2 + [\text{Cl}^-]K_{\text{ox}}[\text{H}_2\text{O}] + [\text{Cl}^-]K_{\text{MeCN}} + K_{2\text{MeCN}}K_{\text{MeCN}}}\ [\beta - \text{diket}] + k_{\text{reverse}} \quad \text{Eq. 8.11}$$

8.3.2.1 Least Squares Fits Using Complete Rate Law

The preliminary results provided earlier, and in particular Figure 8.6 confirmed the non-linear relationship of the k_{obs} on [Cl^-] and [H_2O], reaching a plateau after larger amounts of [Cl^-] and [H_2O]. The complete rate law in Eq. 8.11 could be used *via* least-squares fits of the data to the complete equation. This is illustrated below.

For Figure 8.17, Eq. 8.11 was fitted to the listed data given in Figure 8.6 in a 3-dimensional (3D) fit using the program Scientist and is presented as follows:[8]

(i) Figure 8.17 (a) illustrates the good fit obtained using [Cl^-] as x-axis variable and k_{obs} on the y-axis. The different curves on Figure 8.17 (a) represents the step-wise increase in [H_2O] in steps 0.005M.

(ii) Similarly, Figure 8.17 (b) illustrates the good fit obtained using [H_2O] as x-axis variable and k_{obs} on the y-axis. The different curves on Figure 8.17 (a) represents the step-wise increase in [Cl^-] in steps 0.005M.

(iii) Finally, by variation of both [Cl^-] and [H_2O] on the x- and y-axis simultaneously, and using k_{obs} on the z-axis, the complete 3-dimensional representation as given in Figure 8.17 (c) and defined by Eq. 8.11 is clear. And indeed, it describes (Figure 8.6) the data obtained very well. Plateaus in both directions, i.e. upon increase of [Cl^-] and [H_2O] are reached; that is typical of "saturation" kinetics, precisely as predicted by Eq. 8.11.

Based on this, it is assumed that Eq. 8.11 gives an acceptable rate law for the general simplified substitution reaction given in Figure 8.1. The values used to model Eq. 8.11 and produced the 3D surface, as illustrated in Figure 8.17 (c), are as follows:

(i) As dependant variable: k_{obs}; (ii) As independent variables [Cl^-] and [H_2O]; (iii) As parameters to be determined, fixed for the best fit: k_{11} = 0.94 $M^{-1}.s^{-1}$, k_{21} = 0.90 $M^{-1}.s^{-1}$, k_{31} = 0.10 $M^{-1}.s^{-1}$, k_{MeCN} = 0.2 M^{-1}, k_{2MeCN} = 0.1 M^{-1}, K'_{ox} = 500 and k_{rev} = 0.0055 s^{-1}. (iv) The concentration of the β-diketone was [ttfaH] = 0.025 M.

These were all introduced in Eq. 8.11 in Micromath Scientist and were assumed to have approximately 20 % esd estimates as reflected in other systems.[31]

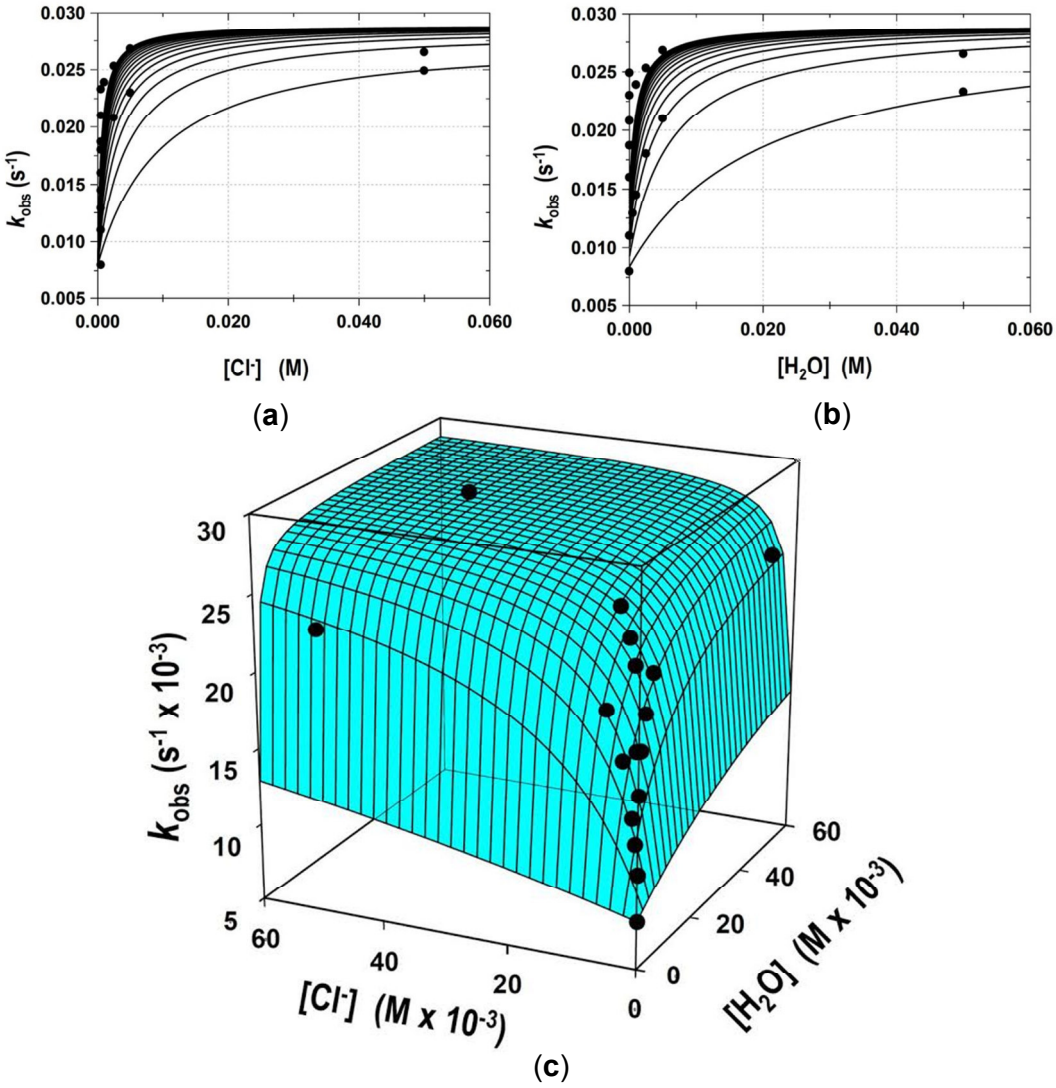

Figure 8.17 (**a**) 2D illustration of the influence of additional [Cl^-] on k_{obs} for the reaction of (Et_4N)[$NbCl_6$] (5.00 x 10^{-4} M) with trifluoroacetylacetone (tfaaH) (2.50 x 10^{-2} M). (**b**) 2D illustration of the influence of additional [H_2O] on k_{obs} for the reaction of (Et_4N)[$NbCl_6$] (5.00 x 10^{-4} M) and trifluoroacetylacetone (tffaH) (2.50 x 10^{-2} M). (**c**) 3D illustration of the influence of additional [H_2O], [Cl^-] and [H_2O/Cl^-] on k_{obs} the reaction of (Et_4N)[$NbCl_6$] (5.00 x 10^{-4} M) and trifluoroacetylacetone (tffaH) (2.50 x 10^{-2} M).

An accurate reaction mechanism is given above, and may be used further to study and evaluate the effect of differing *β*-diketone ligands (see Figure 8.2) on the Nb(V) metal centres. For a specific ligand, and at fixed $[Cl^-]_{free}$ and $[H_2O]_{free}$ values, the first term in Eq. 8.11 is actually constant, defined by k_{fwd}. By varying different *β*-diketones, the effect of them on k_{fwd}, as given directly below, can be studied.

$$k_{obs} = k_{\mathrm{fwd}}[\beta - \mathrm{diket}] + k_{\mathrm{rev}} \qquad \text{Eq. 8.12}$$

with, $$k_{\mathrm{fwd}} = \frac{k_{11}[\mathrm{H_2O}]K_{\mathrm{ox}}[\mathrm{Cl^-}] + k_{21}K_{\mathrm{MeCN}}[\mathrm{Cl^-}] + k_{31}K_{2\mathrm{MeCN}}K_{\mathrm{MeCN}}}{[\mathrm{Cl^-}]^2 + [\mathrm{Cl^-}]K_{\mathrm{ox}}[\mathrm{H_2O}] + [\mathrm{Cl^-}]K_{\mathrm{MeCN}} + K_{2\mathrm{MeCN}}K_{\mathrm{MeCN}}} \qquad \text{Eq. 8.13}$$

For all the variations of *β*-diketones reported further, Eq. 8.12 is used and evaluated for [*β*-diketone] as well as the effects of temperature.

8.4 Results

In order to determine the effect of varying temperature, ligand concentrations and ligand pK_a values on these systems, various experiments were undertaken. The aim of this is to quantify the effect of these varying aspects on reaction rates. These observations should not only increase the insight into the solution state properties of Nb(V) and Ta(V) solution properties but could reveal an ideal nuance to exploit for separation purposes in future.

8.4.1 Effect of Temperature on the Rate of Formation of $(NEt_4)[NbOCl_3(ttfa)]$ and $(NEt_4)[NbCl_4(ttfa)]$ in "Wet" and "Dry" MeCN, Respectively

A kinetic investigation on the reaction between of thenoyltrifluoroacetylacetone (ttfaH) and $(Et_4N)[NbCl_6]$ at temperatures between 15 - 45 °C was performed in both "wet" and "dry" MeCN. The synthesis and preliminary characterization of this niobium(V) complex has been reported in Section 3.3.1.4 and a detailed crystallographic structural characterization of the solid state product obtained, was described in Section 5.4. As with other acacH ligands, ttfaH yields a clear and definite colour change to a reaction solution when coordinated to Nb(V), making it an

ideal candidate for a UV/Vis absorbance spectroscopic solution kinetic evaluation. An example of this reaction is illustrated in Figure 8.18.

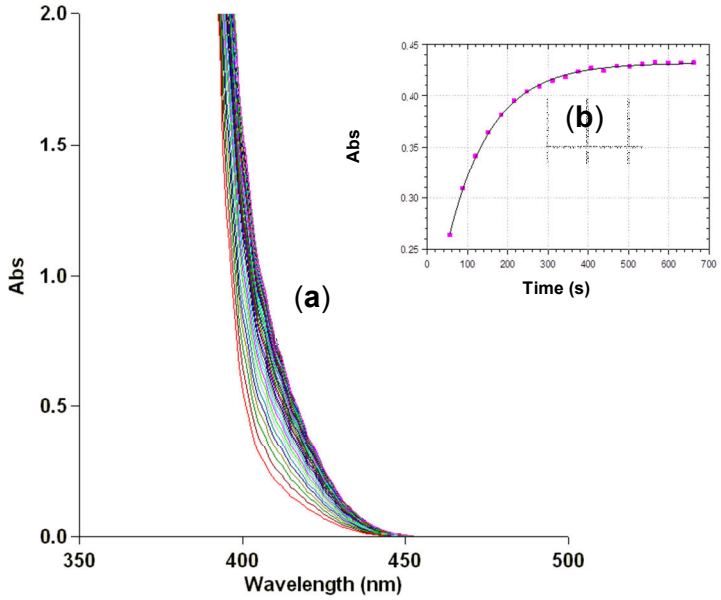

Figure 8.18 Graphical representation of data obtained from UV/Vis spectroscopic kinetics for the formation of $(Et_4N)[NbOCl_3(ttfa)]$: (**a**) Wavelengths scans over time: (~2h); (**b**) Absorbance vs. time trace at 422 nm (k_{obs} = 0.0258(1) s^{-1}) (25 s intervals between scans, insert illustrates initial 12 minutes). $[(NEt_4)[NbCl_6]]$ = 5.00 x 10^{-4} M, $[H_2O]$ = 5 x 10^{-1} M, [ttfaH] = 1.00 x 10^{-2} M, Solvent: MeCN, 25 °C.

The coordination of ttfaH to $(Et_4N)[NbCl_6]$ was followed over the 350-500 nm spectral range to determine the best wavelength to follow product formation. As illustrated in Figure 8.18, the selected wavelength in this case was 422 nm for hydrous (410 nm for anhydrous) MeCN. Absorbance *vs.* time traces were obtained for five ligand concentrations of ttfaH at four different temperatures. Two sets of experiments; (a) in anhydrous and (b) hydrous acetonitrile were performed and the results reported below.

By employing *pseudo*-first order conditions, the concentration of the entering ligand is in excess ([*β* - diket] >> $[(Et_4N)[NbCl_6]]$). Accordingly, by using Eq. 8.12 above, it enables one to determine the k_{fwd} by calculating the slope of k_{obs} *vs.* different ligand concentrations as described below. Similarly, k_{rev} is also calculated from a plot of k_{obs}

vs. [tfaaH], which yields a straight line, with k_{rev} as the intercept. The equilibrium constant, K_1, was determined throughout this study by means of Equation 8.13.

$$K_1 = \frac{k_{\mathrm{fwd}}}{k_{\mathrm{rev}}} \qquad \text{Eq. 8.13}$$

For the kinetic investigation at hand, the coordination of ttfaH to $(Et_4N)[NbCl_6]$ in MeCN was performed at four different temperatures, in a 15 ºC – 45 ºC range. The absorbance data obtained from each of these experiments was subjected to mathematical modelling (Eq. 8.1) and a k_{obs} value obtained. A plot of k_{obs} *vs.* [ttfaH] in anhydrous MeCN is given in Figure 8.19 and the corresponding trace for hydrous MeCN given in Figure 8.20. Figures 8.21 and 8.22 illustrate the Eyring plots for the both sets of reactions to determine activation parameters. Tables 8.2 and 8.3 summarize the kinetic data for this reaction.

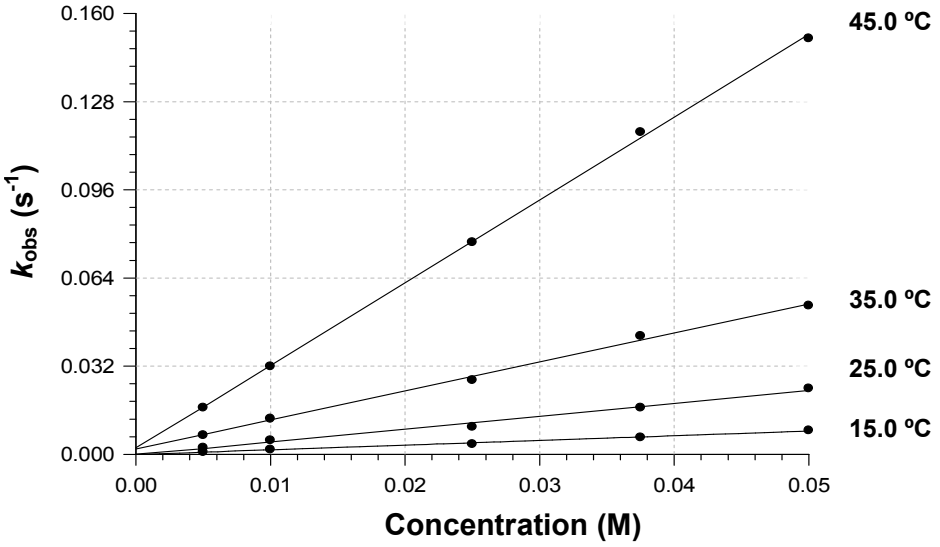

Figure 8.19 k_{obs} *vs.* [ttfaH] plot for the reaction of $(Et_4N)[NbCl_6]$ and thenoyltrifluoroacetone (ttfaH) at four different temperatures. [Nb] = 5.00 x 10^{-4} M, λ = 410 nm, anhydrous MeCN.

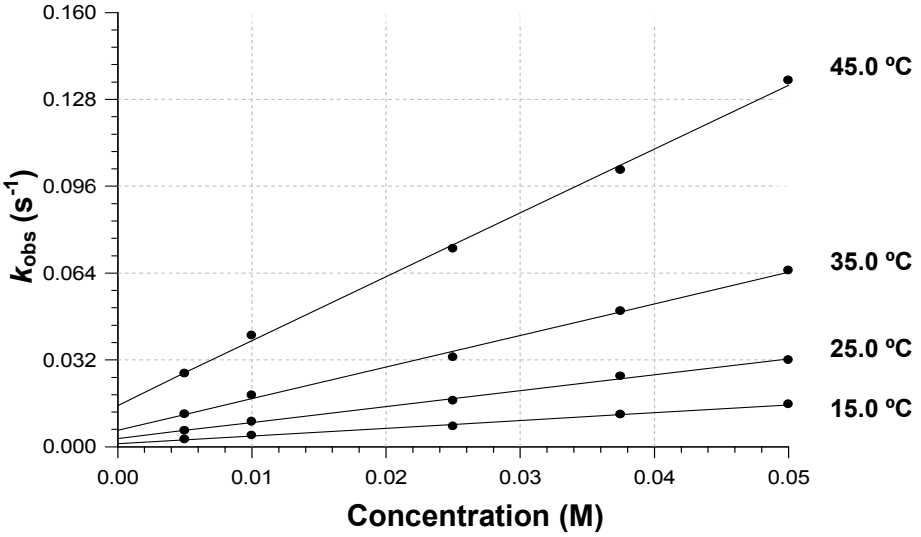

Figure 8.20 k_{obs} *vs.* [ttfaH] plot for the reaction of $(Et_4N)[NbCl_6]$ and thenoyltrifluoroacetone (ttfaH) at four different temperatures. [Nb] = 5.00 x 10^{-4} M, [H_2O] = 5 x 10^{-1} M, λ = 422 nm, hydrous MeCN.

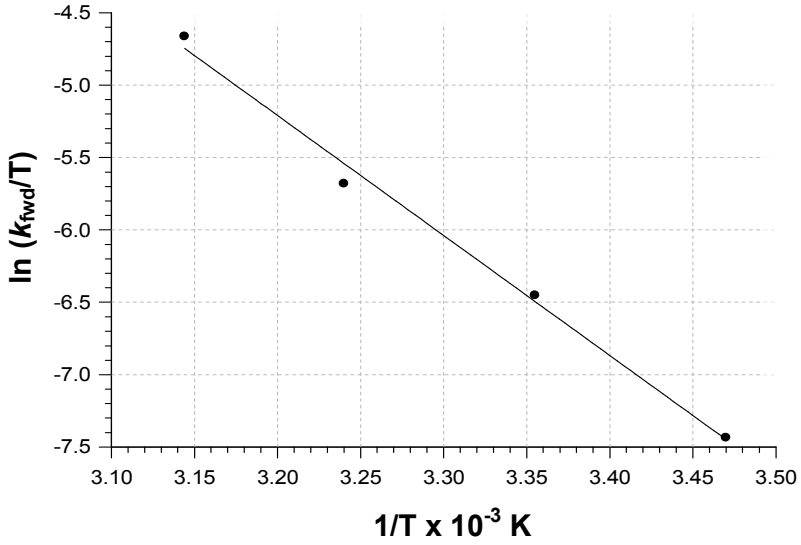

Figure 8.21 Eyring plot of ln(k_{fwd}/T) *vs.* 1/T for the reaction of $(Et_4N)[NbCl_6]$ and thenoyltrifluoroacetone (ttfaH) at four different temperatures. [Nb] = 5.00 x 10^{-4} M, λ = 410 nm, anhydrous MeCN.

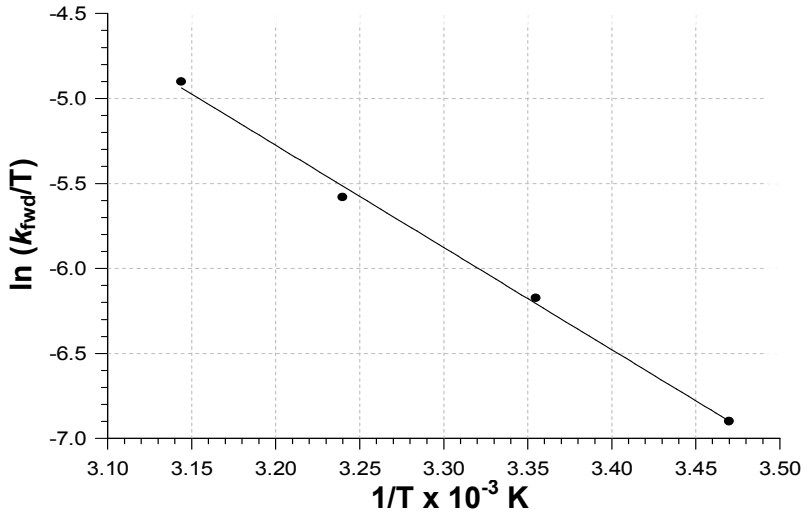

Figure 8.22 Eyring plot of ln(k_{fwd}/T) *vs.* 1/T for the reaction of $(Et_4N)[NbCl_6]$ and thenoyltrifluoroacetone (ttfaH) at four different temperatures. [Nb] = 5.00 x 10^{-4} M, [H_2O] = 5 x 10^{-1} M, λ = 422 nm, hydrous MeCN.

All of the slope and intercept values (k_{fwd} and k_{rev}); as well as the activation parameters are listed in Tables 8.2 and 8.3.

Table 8.2 Summary of the rate constants and activation parameters of the reaction between $(Et_4N)[NbCl_6]$ and thenoyltrifluoroacetone (ttfaH) in anhydrous MeCN at different temperatures.

	15.0 ºC	**25.0 ºC**	**35.0 ºC**	**45.0 ºC**
k_{fwd} ($M^{-1}s^{-1}$)	0.17(1)	0.47(3)	1.05(2)	3.00(4)
k_{rev} (s^{-1})	0.000063(1)	0.000198(8)	0.0019(1)	0.0022(1)
K_1 (M^{-1})	2689(1)	2358(6)	553(1)	1363(1)
$\Delta H^{\ddagger}_{(fwd)}$ (kJ mol^{-1})		77(2)		
$\Delta S^{\ddagger}_{(fwd)}$ (J K^{-1} mol^{-1})		4(5)		

Table 8.3 Summary of the rate constants and activation parameters of the reaction between $(Et_4N)[NbCl_6]$ and thenoyltrifluoroacetone (ttfaH) in hydrous MeCN, at different temperatures.

	15 ºC	25 ºC	35 ºC	45 ºC
k_{fwdd} ($M^{-1}s^{-1}$)	0.29(5)	0.62(2)	1.16(4)	2.36(5)
k_{rev} (s^{-1})	0.0011(4)	0.0066(8)	0.0061(1)	0.0156(2)
K_1 (M^{-1})	263(16)	94(1)	190(1)	150(1)
$\Delta H^{\ddagger}_{(fwd)}$ (kJ mol^{-1})		51(2)		
$\Delta S^{\ddagger}_{(fwd)}$ (J K^{-1} mol^{-1})		-77(5)		
$\Delta H^{\ddagger}_{(rev)}$ (kJ mol^{-1})		76(12)		
$\Delta S^{\ddagger}_{(rev)}$ (J K^{-1} mol^{-1})		-39(38)		

8.4.2 Effect of Ligand pKa on the Reaction Rate of *β*-diketone Coordination to $(NEt_4)[MCl_6]$; M = Nb(V), Ta(V)

As was mentioned in Chapter 1, one of the main objectives of this solution state study, was to determine the effect of the different the electron withdrawing and -donating capabilities of entering ligand systems on Nb(V) and Ta(V) metal centres. The ligands illustrated in Figure 8.2 were selected to include a series of substituents that influence the electron donating and -withdrawing ability (pK_a) of the *β*-diketones, with the main focus being placed on fluorinated *β*-diketones.

In an attempt to accurately determine the influence of ligand pKa on *β*-diketone coordination to both Ta(V) and Nb(V) metal centres a generalized kinetic experiment was conducted. During this investigation, all the *β*-diketone ligands were reacted with $(NEt_4)[MCl_6]$ (5.00×10^{-4} M) at 25.0 ºC. The absorbance data obtained from each of these experiments was fitted to Eq. 8.1 and a k_{obs} value obtained. A plot of k_{obs} *vs.* [*β*-diket] in anhydrous MeCN is given in Figure 8.23 and Figure 8.25 for Nb(V) and Ta(V) metal centres, respectively, whereas the corresponding traces for hydrous MeCN are shown in Figure 8.24 and Figure 8.26, respectively.

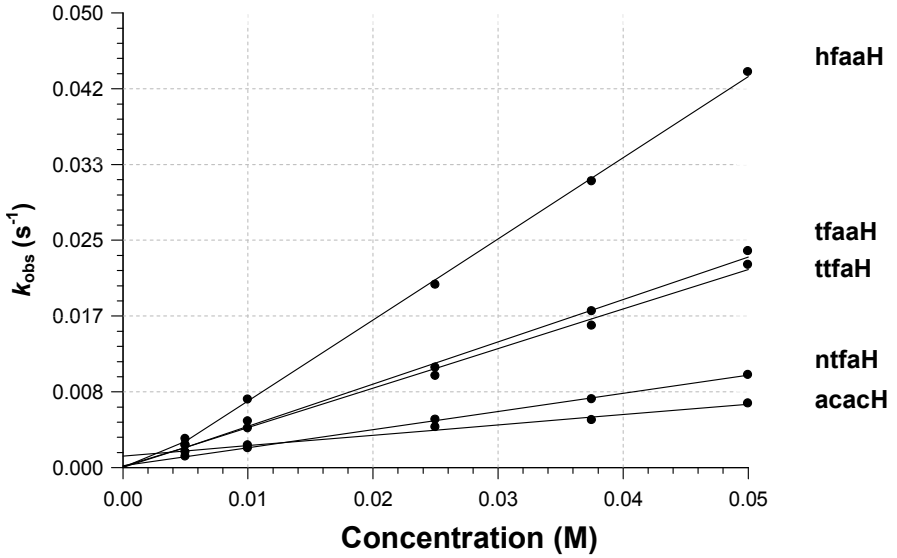

Figure 8.23 k_{obs} *vs.* [*β*-diket] plot for the reaction of $(Et_4N)[NbCl_6]$ and the five different acetylacetone ligands in anhydrous MeCN. [Nb] = 5.00 x 10^{-4} M.

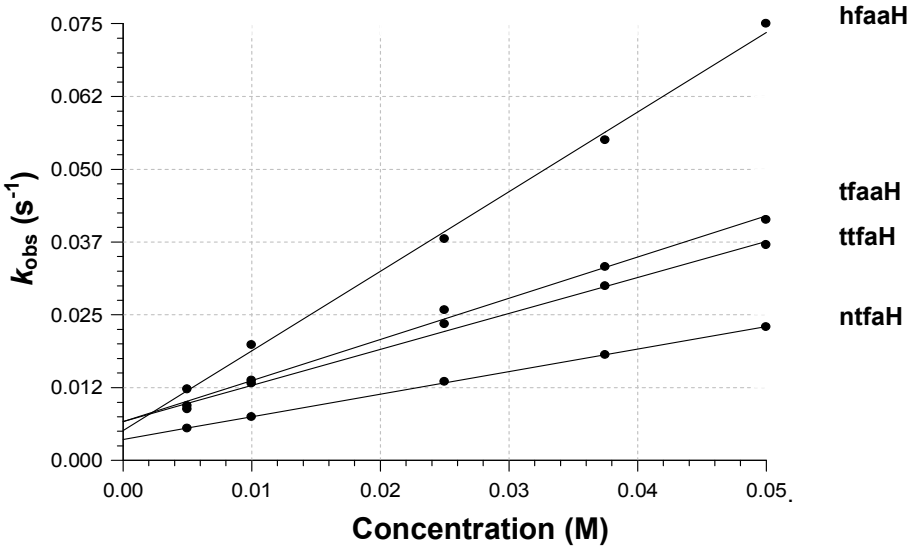

Figure 8.24 k_{obs} *vs.* [*β*-diket] plot for the reaction of $(Et_4N)[NbCl_6]$ and the five different acetylacetone ligands in hydrous MeCN. [Nb] = 5.00 x 10^{-4} M, $[H_2O]$ = 5 x 10^{-1} M.

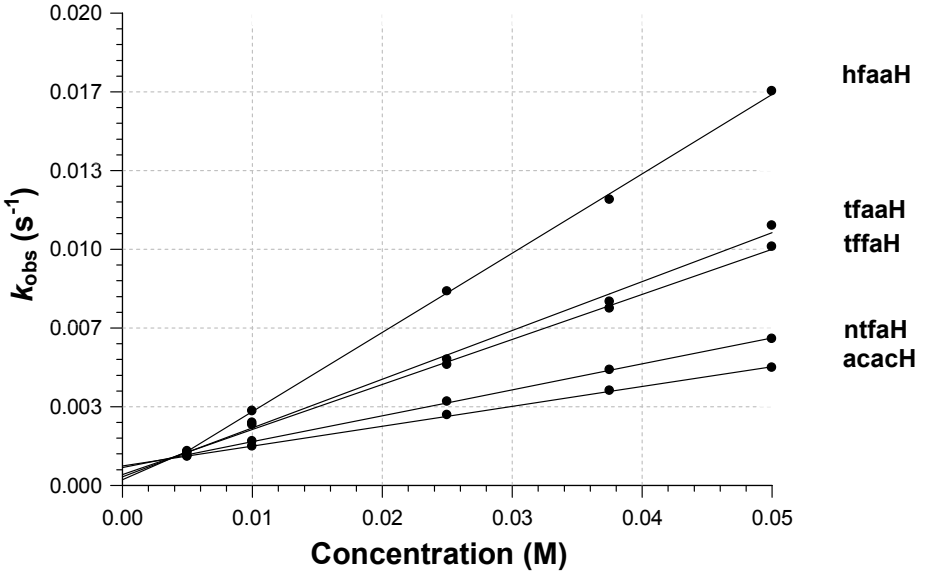

Figure 8.25 k_{obs} *vs.* [*β*-diket] plot for the reaction of $(Et_4N)[TaCl_6]$ and the five different acetylacetonate ligands in anhydrous MeCN. [Ta] = 5.00 x 10^{-4} M.

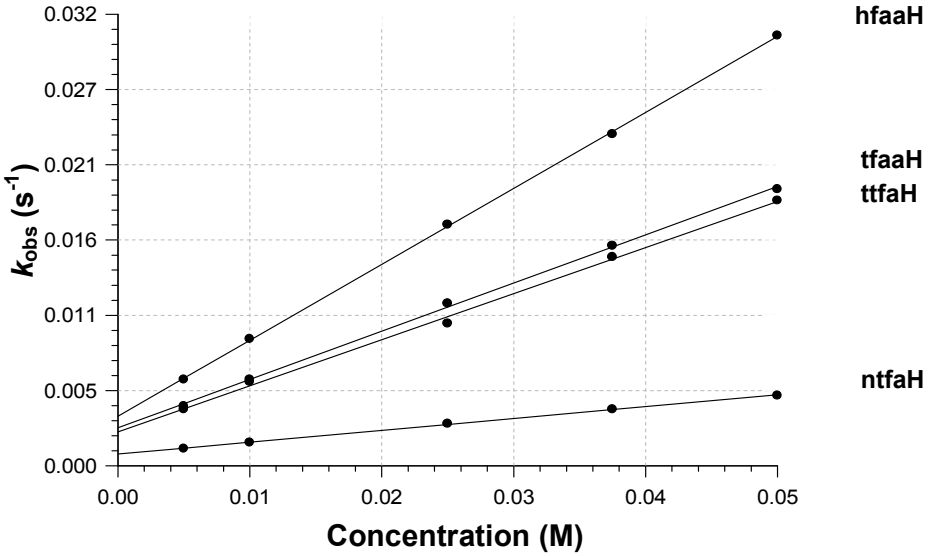

Figure 8.26 k_{obs} *vs.* [*β*-diket] plot for the reaction of $(Et_4N)[TaCl_6]$ and the five different acetylacetone ligands in "wet" MeCN. [Ta] = 5.00 x 10^{-4} M, $[H_2O]$ = 5 x 10^{-1} M.

The slopes and intercepts were once again obtained using Eq. 8.12 and the corresponding rate constants are reported in Tables 8.4 and 8.5.

Table 8.4 Comparison of the rate constants the reaction between $(Et_4N)[NbCl_6]$ and various β-diketone ligands.

	acacH	ntfaH	ttfaH	tfaaH	hfaaH
pKa of Ligand	8.95	>6.60	6.50	6.30	4.60
Anhydrous MeCN					
k_{fwd} ($M^{-1}s^{-1}$)	0.11(1)	0.19(1)	0.47(1)	0.43(1)	0.89(1)
k_{rev} (s^{-1})	0.0012(2)	0.00019(9)	0.00012(8)	0.000041(4)	0.000016(4)
K_1 (M^{-1})	91(10)	1000(72)	3916(163)	10487(475)	51520(311)
Hydrous MeCN					
k_{fwd} ($M^{-1}s^{-1}$)	n/a	0.39(1)	0.62(3)	0.71(3)	1.37(4)
k_{rev} (s^{-1})	n/a	0.0036(4)	0.0066(8)	0.0067(8)	0.0051(12)
K_1 (M^{-1})	n/a	108(3)	94(5)	106(5)	269(18)

Table 8.5 Comparison of the rate constants the reaction between $(Et_4N)[TaCl_6]$ and various β-diketone ligands.

	acacH	ntfaH	ttfaH	tfaaH	hfaaH
pKa of Ligand	8.95	>6.60	6.50	6.30	4.60
Anhydrous MeCN					
k_{fwd} ($M^{-1}s^{-1}$)	0.08(1)	0.11(1)	0.19(1)	0.21(1)	0.34(1)
k_{rev} (s^{-1})	0.0008(3)	0.0008(4)	0.0005(3)	0.0004(3)	0.0002(1)
K_1 (M^{-1})	100(5)	138(6)	380(47)	525(112)	1700(120)
Hydrous MeCN					
k_{fwd} ($M^{-1}s^{-1}$)	n/a	0.21(1)	0.33(1)	0.34(1)	0.53(4)
k_{rev} (s^{-1})	n/a	0.0023(2)	0.0024(3)	0.0027(2)	0.0035(3)
K_1 (M^{-1})	n/a	70(1)	136(5)	127(3)	154(9)

8.5 Discussion

The data presented above in Sections 8.2 - 8.4 are now systematically discussed with respect to the influences it shows on the reactivity and mechanism.

8.5.1 General Rate Law and Mechanism

The different experiments described above in Section 8.2 allowed the mechanism (Figure 8.15) and the associated rate law in Eq. 8.11 to be presented with a fair amount of confidence. It has to be stressed that it can obviously not be proven without doubt. In spite of that, it gives a very reasonable explanation all the

experimental (both in solution and solid state) observations made to date. In particular, it gives an acceptable interpretation of the observations made under hydrous conditions.

8.5.2 Comparison of Reactivity of $[MCl_6]^-$ Under Hydrous/Anhydrous Conditions

From the data presented in Sections 8.2 and 8.4, and in particular Tables 8.2, 8.3 and 8.4, some interesting observations were made can now be discussed relating to reactivity of $[MCl_6]^-$ in both anhydrous and hydrous conditions. These can be summarized as follows.

(a) The overall forward rate constant, k_{fwd}, measured in solutions containing H_2O is in general two times faster than anhydrous solutions. This probably means that the niobium metal is slightly more labilized by the coordinated oxido ligand than otherwise. This is better illustrated in Figure 8.27, where the influence in hydrous conditions is clearly observed.

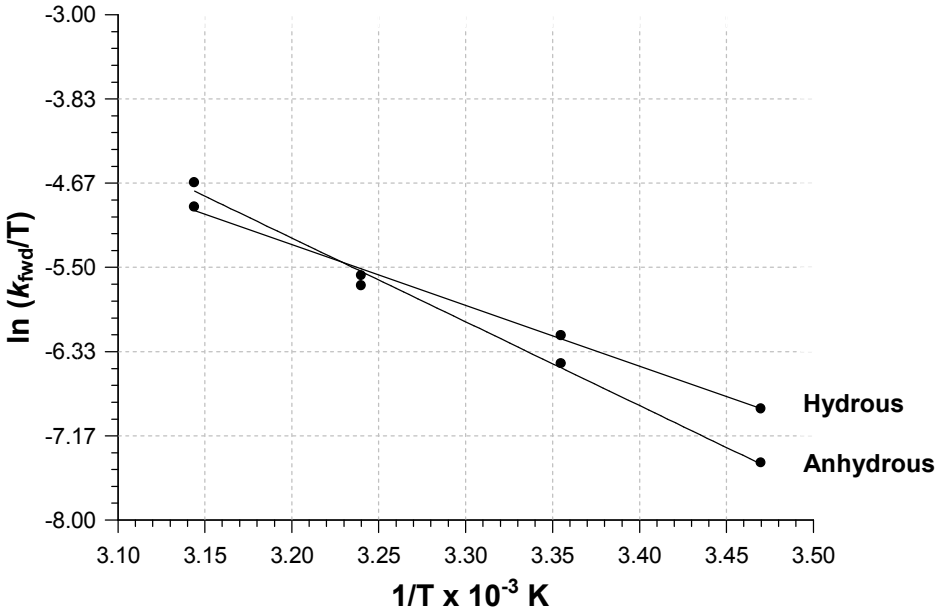

Figure 8.27 Eyring plot of ln(k_{fwd}/T) *vs.* 1/T comparing the activation parameters of the reaction of $(Et_4N)[NbCl_6]$ and thenoyltrifluoroacetone (ttfaH) in both anhydrous and hydrous MeCN, respectively. [Nb] = 5.00 x 10^{-4} M, [H_2O] = 5 x 10^{-1} M.

(b) In general it seems as if the stability constants for the oxido species are larger than the MeCN-chlorido complexes. This is probably why the crystalline species are more easily obtained which contain oxido ligands in the coordination sphere.

(c) The relatively high negative $\Delta S^{\ddagger}$ values obtained under hydrous conditions points towards some form of association in the transition state, but more information is required before such an assumption can be made with more authority.

(d) The $\Delta H^{\ddagger}$ values (see Tables 8.2 and 8.3) are indicative of the reactivity observed. However, it cannot be ruled out that it represents a multi-step process, as inferred by Figure 8.15.

8.5.3 Effect of Entering Ligand pK_a Value

From the data presented in Tables 8.4 and 8.5, several observations are made with respect to the observed rate and equilibrium constants.

(a) There is a marked increase in the rate of the forward reaction (k_{fwd}) that is associated with a decrease of pK_a of the incoming *β*-diketone ligands for both metal centres.

This relationship between the k_{fwd} rate constant and pK_a of the uncoordinated *β*-diketone ligands is schematically illustrated in Figure 8.28 in anhydrous MeCN and in Figure 8.29 in hydrous MeCN.

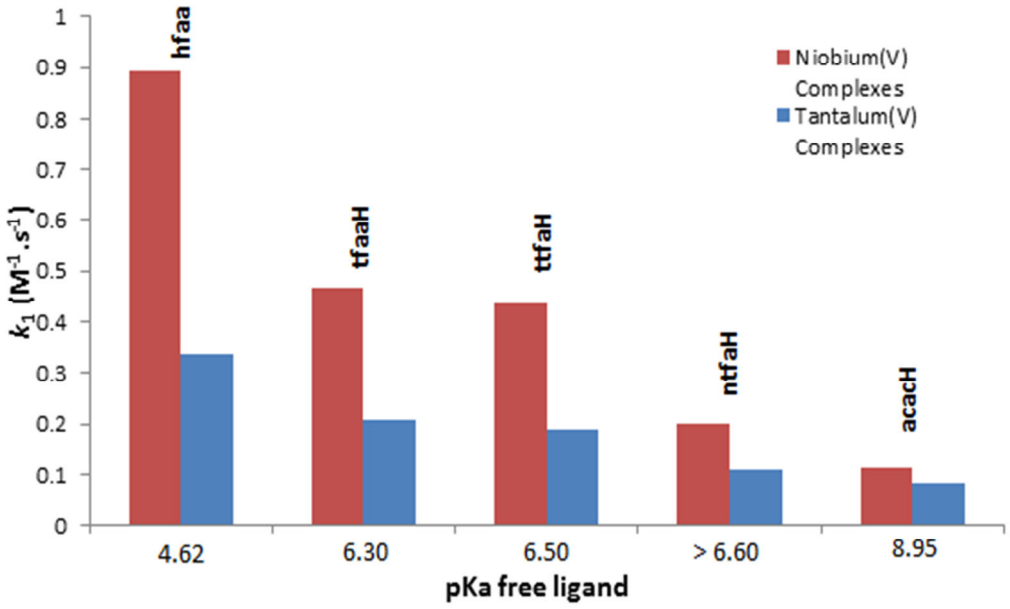

Figure 8.28 Comparison of forward rate constants (k_{fwd}) *vs.* pK_a of the entering *β*-diketone ligands in the formation reaction of $(NEt_4)[NbCl_4(\beta\text{-diket})]$ and $(NEt_4)[TaCl_4(\beta\text{-diket})]$ in anhydrous MeCN.

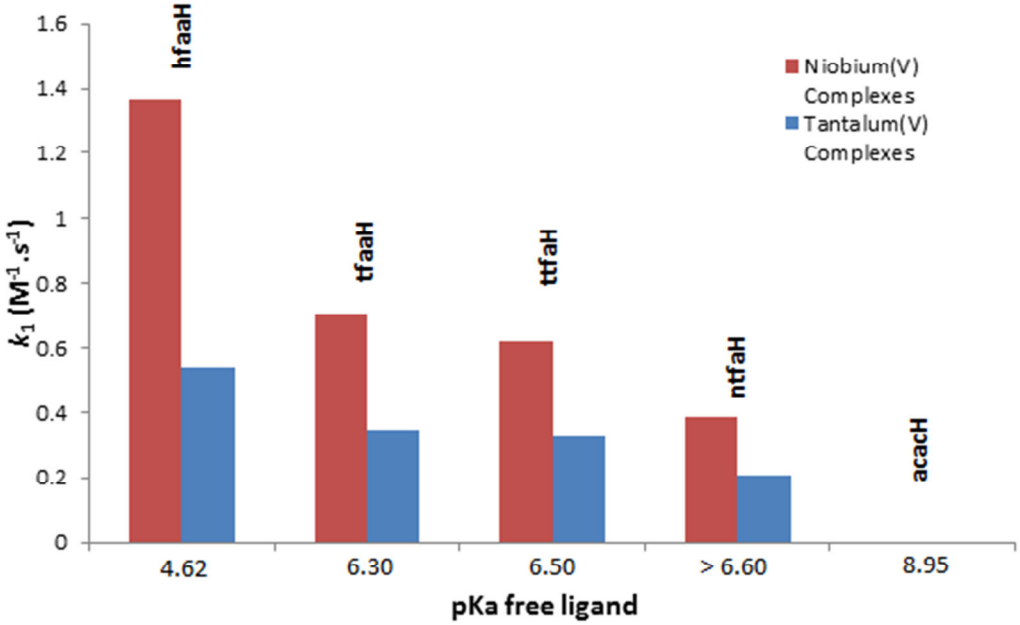

Figure 8.29 Comparison of rate constants (k_{fwd}) *vs.* pK_a of the entering *β*-diketone ligands in the formation reaction of $(NEt_4)[NbOCl_3(\beta\text{-diket})]$ and $(NEt_4)[TaOCl_3(\beta\text{-diket})]$ in hydrous MeCN.

When considering Figures 8.27 and 8.28, it can be seen that the pK_a of 8.95 for the incoming acacH ligand displayed the slowest reaction rates. When considering anhydrous MeCN, values of k_{fwd} = 0.11(1) $M^{-1}.s^{-1}$ and 0.08(1) $M^{-1}.s^{-1}$ for the formation of $(NEt_4)[NbCl_4(acac)]$ and $(NEt_4)[TaCl_4(acac)]$ were observed. This observation is in contrast with entering ligands with lower pK_a values. For example, hfaaH resulted in much faster substitution rates with value of k_{fwd} = 0.89(1) $M^{-1}.s^{-1}$ and 0.34(1) $M^{-1}.s^{-1}$ for the formation of $(NEt_4)[NbOCl_3(hfaa)]$ and $(NEt_4)[TaOCl_3(hfaa)]$ in anhydrous MeCN, respectively.

The decrease in pK_a value of the free ligand can be related to more electron withdrawing substituents on the coordinating *β*-diketonato backbone. This trend then suggests that by altering the substituents (electronic influence) of the entering *β*-diketonato ligands in the niobium(V) and tantalum(V) complexes, by decreasing the electron density at these metal centres, faster substitutions will occur. In contrast, as electron density is increased around the metal centres by electron donating substituents in the coordinating *β*-diketonato ligands, the substitution rates will decrease significantly. If true, it is indicative of an associative type mechanism.

It is also important to note that the varying pK_a values of the ligands could cause differences in the pH of solution, which in turns influences reaction rates. This was not systematically addressed in this investigation but will have to be investigated in future.

(b) Secondly, when comparing Figures 8.23 and 8.25 with Figures 8.24 and 8.26, the influence of H_2O addition on the reaction rates of these systems, is noted to be quite substantial.

As was discussed in Section 8.2.5.3, by introducing H_2O into the reaction mixture leads to the formation of the more reactive $[MOCl_5]^{2-}$ (M = Nb, Ta) synthon in solution. This synthon substantially increased the rate of ligand substitution when compared to the $[MCl_5(MeCN)]$ and $[MCl_4(MeCN)_2]^+$ counterparts found in “dry” MeCN solutions. Tables 8.6 and 8.7 illustrate the ratio at which the reaction rates increase as a result of H_2O addition for the formation of both sets of complexes. In

the case of the incoming acacH ligand, no reaction can be observed in "wet" MeCN, this can be ascribed to protonation of the acacH ligand at the lower pH solution pH (due to excess H_2O addition).

Table 8.6 Comparison of k_{fwd} rate constants for the formation of various Nb(V) complexes in both anhydrous ("dry") and hydrous ("wet") MeCN.

Formation Complex	pK_a of Free Ligand	k_{fwd} ($M^{-1}.s^{-1}$) ("Dry" MeCN)	k_{fwd} ($M^{-1}.s^{-1}$) ("Wet" MeCN)	Ratio of Rate Increase
$(NEt_4)[NbOCl_3(hfaa)]$	4.60	0.82(2)	1.37(4)	1.67
$(NEt_4)[NbOCl_3(tfaa)]$	6.30	0.43(2)	0.71(3)	1.65
$(NEt_4)[NbOCl_3(ttfa)]$	6.50	0.47(3)	0.62(3)	1.31
$(NEt_4)[NbOCl_3(ntfa)]$	>6.60	0.19(1)	0.39(1)	2.05
$(NEt_4)[NbOCl_3(acac)]$	8.95	0.11(1)	No reaction	n/a

Table 8.7 Comparison of k_{fwd} rate constants for the formation of various Ta(V) complexes in both anhydrous ("dry") and hydrous ("wet") MeCN.

Formation Complex	pK_a of Free Ligand	k_{fwd} ($M^{-1}.s^{-1}$) ("Dry" MeCN)	k_{fwd} ($M^{-1}.s^{-1}$) ("Wet" MeCN)	Ratio of Rate Increase
$(NEt_4)[TaOCl_3(hfaa)]$	4.60	0.34(5)	0.54(4)	1.58
$(NEt_4)[TaOCl_3(tfaa)]$	6.30	0.21(8)	0.34(1)	1.62
$(NEt_4)[TaOCl_3(ttfa)]$	6.50	0.19(4)	0.33(1)	1.74
$(NEt_4)[TaOCl_3(ntfa)]$	>6.60	0.11(1)	0.21(1)	1.91
$(NEt_4)[TaOCl_3(acac)]$	8.95	0.08(1)	No reaction	n/a

It is clear from Table 8.6 and Table 8.7 that H_2O addition increases the rate of *β*-diketonate coordination by a factor of between 1.5 and 2.0. This ratio also increases slightly as the pK_a of the free ligand increases from hfaaH to ntfaH. From these observations it can be postulated that the $[MOCl_5]$ synthon is indeed more reactive to all types of *β*-diketone ligands and more receptive to an influx of electron density than its $[MCl_5(MeCN)]$ and $[MCl_4(MeCN)_2]^+$ counterpart.

(c) The k_{rev} for these reactions are relatively small and varied

All of the ligands studied, yielded relatively large K_1 values for the overall reactions. This is indicative of a reaction equilibrium that is substantially shifted towards product formation.

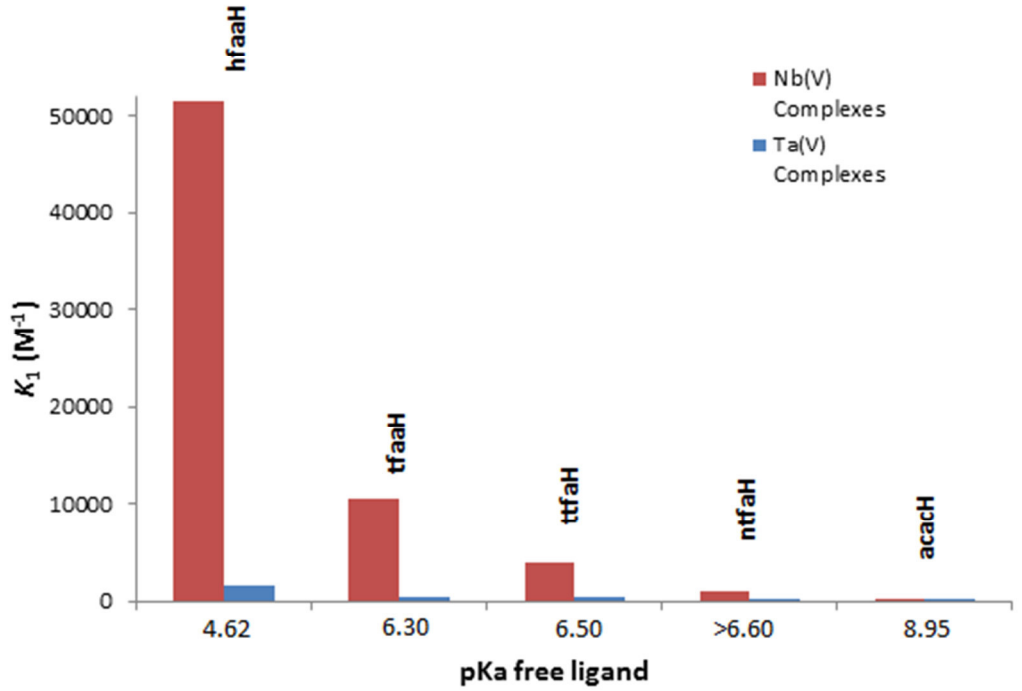

Figure 8.30 Comparison of rate constants (K_1) *vs.* pK_a of the entering *β*-diketone ligands in the formation reaction of $(NEt_4)[NbOCl_3(\beta\text{-diket})]$ and $(NEt_4)[TaOCl_3(\beta\text{-diket})]$ in hydrous MeCN.

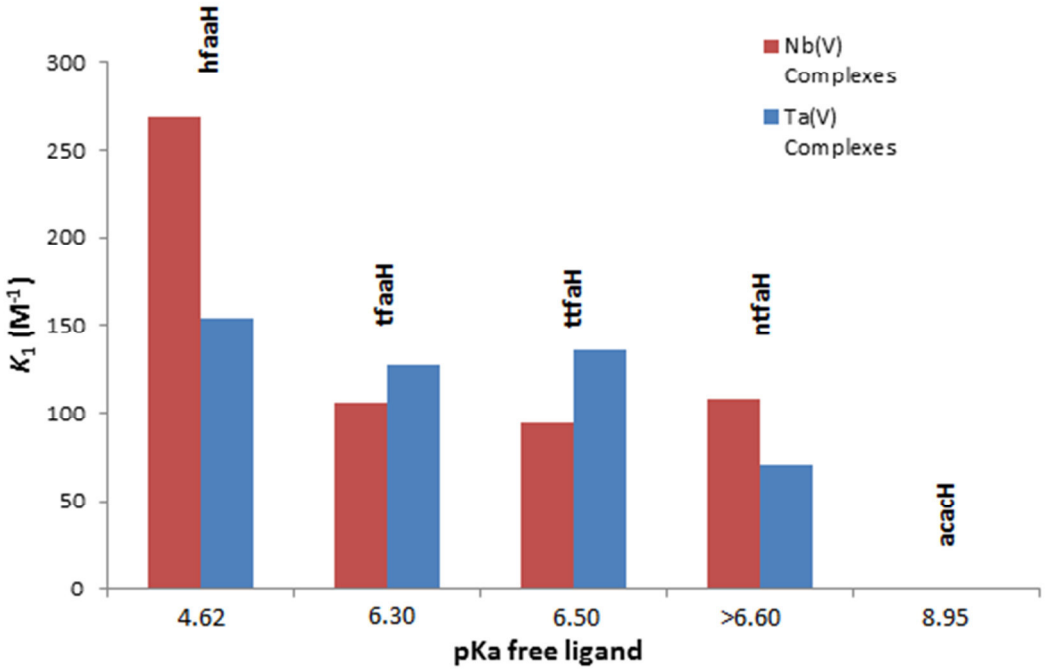

Figure 8.31 Comparison of rate constants (K_1) *vs.* pK_a of the entering *β*-diketone ligands in the formation reaction of $(NEt_4)[NbOCl_3(\beta\text{-diket})]$ and $(NEt_4)[TaOCl_3(\beta\text{-diket})]$ in hydrous MeCN.

It is clear from Tables 8.4 and 8.5, and illustrated in Figures 8.30 and 8.31 that the equilibrium constant (K_1) for the reaction (formation of the final product, Eq. 8.12 and Eq. 8.13) significantly increases from acacH to hfaaH. In the case of the Nb(V) complex formation, this values increases three order-of-magnitude under anhydrous conditions (Table 8.4). However, upon using hydrous MeCN, the K_1 values become significantly smaller and vary only *ca.* 2.5 times, with no reaction observed for acacH addition. This suggests a significant contribution of $[H_2O]_{free}$ to the reverse reaction, indicating a hydrolysis of the *β*-diketonate ligand. However this needs to be investigated systematically in future.

The results for Ta(V) (Table 8.5 and Figures 8.30 and 8.31) are seemingly less significant, with an increase of more than only two orders-of-magnitude observed for anhydrous MeCN, and only a two-fold difference for hydrous MeCN with no reaction with acacH. Once again, additional systematic research is also required for the Ta(V) systems.

(d) Finally, there is a noticeable difference in Nb(V) and Ta(V) coordinative behaviour.

This solution state investigation yields an ideal opportunity to compare coordinative behaviour of these two systems. Tables 8.8 and 8.9 compares the k_{fwd} values of the Ta(V) and Nb(V) systems in both anhydrous and hydrous MeCN.

Table 8.8 Comparison of k_{fwd} rate constants for the formation of Nb(V) and Ta(V) complexes in anhydrous MeCN. (M = Nb(V), Ta(V)).

Formation Complex	pK_a of Free Ligand	k_{fwd} ($M^{-1}.s^{-1}$) (M = Nb(V))	k_{fwd} ($M^{-1}.s^{-1}$) (M = Ta(V))	Ratio of Rate Increase
$(NEt_4)[MOCl_3(hfaa)]$	4.60	0.82(2)	0.34(5)	2.41
$(NEt_4)[MOCl_3(tfaa)]$	6.30	0.43(2)	0.21(8)	2.05
$(NEt_4)[MOCl_3(ttfa)]$	6.50	0.47(3)	0.19(4)	2.40
$(NEt_4)[MOCl_3(ntfa)]$	>6.60	0.19(1)	0.11(1)	1.72
$(NEt_4)[MOCl_3(acac)]$	8.95	0.11(1)	0.08(1)	1.38

Table 8.9 Comparison of k_{fwd} rate constants for the formation of Nb(V) and Ta(V) complexes in hydrous MeCN. (M = Nb(V), Ta(V)).

Formation Complex	pK_a of Free Ligand	k_{fwd} ($M^{-1}.s^{-1}$) (M = Nb(V))	k_{fwd} ($M^{-1}.s^{-1}$) (M = Ta(V))	Ratio of Rate Increase
$(NEt_4)[MOCl_3(hfaa)]$	4.60	1.37(4)	0.54(4)	2.54
$(NEt_4)[MOCl_3(tfaa)]$	6.30	0.71(3)	0.34(1)	2.09
$(NEt_4)[MOCl_3(ttfa)]$	6.50	0.62(3)	0.33(1)	1.88
$(NEt_4)[MOCl_3(ntfa)]$	>6.60	0.39(1)	0.21(1)	1.86
$(NEt_4)[MOCl_3(acac)]$	8.95	No reaction	No reaction	n/a

Tables 8.8 and 8.9 indicate that the ligand coordination occurs at a much faster rate in the Nb(V) systems. To some extent this is contradictory for a proposed associative activation that is mentioned above. However, more systematic research on this is required to give even better explanations. Additionally, it is noted that as the pK_a (electron-withdrawing ability) of the free ligand decreases, the factor in reaction rate difference increases substantially. In theory this could be the ideal anomaly to exploit for industrial separation purposes.

8.6 Conclusion

The data reported above could be used in a systematic way to successfully derive an overall reaction mechanism and rate law, which accounts for all current experimental observations.

The specified aim set out in Chapter 1 was thus successfully completed, albeit that some observations relating to the formation of additional products or precise identification of complex structures still need to be explained in more detail.

In spite of this, the complex system's solution behaviour has been adequately described. It clearly illustrates that although the systems as defined in Figure 8.1 seems quite simple and straight forward, extreme care, and thus a complete and detailed mechanistic study is required for proper evaluation of many a chemical process.

Chapter 9: Comparison of Various Solution and Solid State Characteristics of $(NEt_4)[NbOCl_3(\beta\text{-diket})]$ Complexes

9.1 Introduction

An overarching theme throughout the preceding chapters has focused on the investigation of various physical and electronic ligand effects which have been introduced to the solid and solution state properties of Nb(V)-*β*-diketonates. From the in-depth literature study reported in Chapter 2, it was anticipated that the introduction of different steric and electronic changes to the metal centre could potentially provide a better insight into the intrinsic properties of these systems. These influences were brought about by utilizing different coordinating *β*-diketonato ligands with electron withdrawing/donating (as manifested by the different Bronsted pK_a values) or sterically bulky substituents.

In Chapters 5 and 6 the crystallographic investigation of six Nb(V)-*β*-diketonate complexes was undertaken. Various solid state properties such as intermolecular interactions, solid-state crystal packing and coordination modes were discussed in great detail. This study shed much light with relation to coordination preferences, stability of the compounds and the effects of ligand substituents on the crystal systems.

In this chapter, the systematic integration of the specific data is further combined, compared and correlated for the different niobium(V) and tantalum(V) complexes, from the evaluations in Chapters 3, 5 and 6. The subsections below attempt to systematically present the correlations drawn between the different properties of the

complexes such as electronic and steric changes which were introduced on the metal centres.

The different coordinated *β*-diketonato ligands involved in the comparisons to be discussed in this chapter (already noted in Chapter 3) are again represented in Figure 9.1 to allow for more easy discussion.

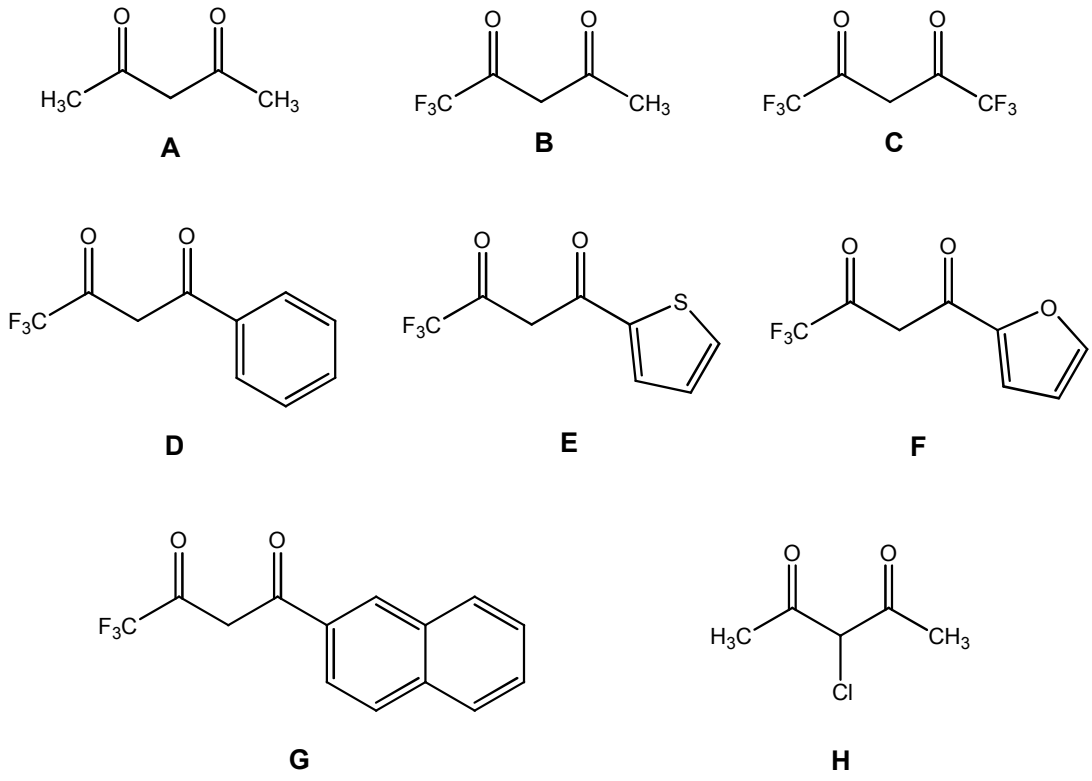

Figure 9.1 Graphical representation of the *β*-diketone ligands (mono-anionic when coordinated) employed in the synthesis of the niobium(V) and tantalum(V) complexes. **A** *2,4-pentanedione* (acacH), **B** *1,1,1*-Trifluoro-*2,4*-pentanedione (tfaaH), **C** *1,1,1,5,5,5*-Hexafluoro-*2,4*-pentanedione (hfaaH), **D** *4,4,4*-Trifluoro-*1*-phenyl-*1,3*-butanedione (btfaH), **E** *4,4,4*-Trifluoro-*1*(*2*-thienyl)-*1,3*-butanedione (ttfaH), **F** *4,4,4*-Trifluoro-*1*(*2*-furyl)-*1,3*-butanedione (tffaH), **G** *4,4,4*-Trifluoro-*1*(*2*-naphtyl)-*1,3*-butanedione (ntfaH), **F** *3*-Chloro-*2,4*-pentanedione (3-ClacacH).

9.2 Effect of the pK_a of the Free *β*-diketone Ligand on Reaction Systems

The acid dissociation constant (K_a), is a quantitative measure of the strength of an acid in solution.[1] It is the equilibrium constant for a chemical reaction known as dissociation in the context of acid-base reactions. In aqueous solution, the equilibrium of acid dissociation can be written symbolically as:

$$HA + H_2O \rightleftharpoons A^- + H_3O^+ \qquad \text{Eq. 9.1}$$

where HA is a weak acid that dissociates into the conjugate base A^- and a hydrogen ion which combines with a water molecule to form a hydronium ion.

When equilibrium is reached, the concentration of the chemical species HA, A^- and H_3O^+ do not change as time progresses. The dissociation constant is usually written as a quotient of the equilibrium concentrations (in mol/dm^3), denoted by [HA], [A^-] and [H_3O^+].[1]

$$K_a = \frac{[A^-][H_3O^+]}{[HA][H_20]} \qquad \text{Eq. 9.2}$$

Barring all but the most concentrated aqueous solutions of an acid, the concentration of H_2O can be taken as constant and be assigned a value of 1. Accordingly, the definition can then be written more simply;

$$HA \rightleftharpoons A^- + H^+$$

$$K_a = \frac{[A^-][H_3O^+]}{[HA]} \qquad \text{Eq. 9.3}$$

But for more practical purposes it is more to discuss the logarithmic constant, pK_a;[2]

$$pK_a = -\log_{10} K_a \qquad \text{Eq. 9.4}$$

[1] W. L. Jolly, (1984). *Modern Inorganic Chemistry*. McGraw-Hill, New York, United States of America.

[2] C. E. Housecroft, A. G. Sharpe, (2008). *Inorganic Chemistry*, **3**, Prentice Hall, New Jersey, United States of America.

For this investigation, consideration of pK_a values of the various *β*-diketones is vital as this property relates to the Lewis acidity (as well as potential strength of coordination and thus also by implication extraction efficiency) for the obtained complexes of harder metal centres e.g. Nb(V).[3] Fluorinated substituents have often been introduced into these types of ligand extractants. The acidity of the extracting agent is increased by the electron-withdrawing effect of the fluorinated group, and the extracting agent can thus be used to selectively remove metal ions from more acidic aqueous solutions provided that strong enough bonds with the acid metal centres are formed.[4] In past investigations, a decrease in pK_a value has been found to be more efficient for the synergistic extraction of harder metal species which are more easily hydrolysed.[5] Similar studies undertaken on lanthanide- and actinide-*β*-diketonates are reported to confirm this postulation.[6]

The pK_a values of the eight substituted *β*-diketones illustrated in Figure 9.1 are noted in Table 9.1. In the following sections, the pK_a of the free ligand will be related to various aspects of the Nb(V)-*β*-diketonate complexes in an attempt to distinguish how the electronic properties of the ligands potentially influence the physical properties of the coordination compounds.

[3] J. C. Reid and M. Calvin, (1950). *J. Am. Chem. Soc.*, **72**, 2048-2065.

[4] S. Umetani, Y. Kawase and M. Matsui, (2000). *J. Chem. Soc. Dalton Trans.*, **33**, 2787-2799.

[5] M. L. Bhaumik, (1965). *J. Inorg. Nucl. Chem.*, **27**, 243-252.

[6] N. E. Holden, (2004). *CRC Handbook of Chemistry and Physics,* **85**, CRC Press, Boca Raton, United States of America.

Table 9.1 A list of the pK_a values for the various *β*-diketones used in this study.

***β*-diketone Ligand**	**Abbreviation**	***pK*$_a$ Values**
2,4-Pentanedione	acacH[7]	8.95
3-Chloro-2,4-pentanedione	3Cl-acacH[8]	6.77
4,4,4-Trifluoro-1(2-naphtyl)-1,3-butanedione	ntfaH[8]	>6.60
4,4,4-Trifluoro-1(2-furyl)-1,3-butanedione	tffaH[8]	6.50
4,4,4-Trifluoro-1(2-thienyl)-1,3-butanedione	ttfaH[9]	6.48
4,4,4-Trifluoro-1-benzoyl-1,3-butanedione	btfaH[7]	6.30
1,1,1-Trifluoro-2,4-pentanedione	tfaaH[7]	6.30
1,1,1,5,5,5-Hexafluoro-2,4-pentanedione	hfaaH[7]	4.60

9.2.1 Relationship Between the Bronsted pK_a Values of the Free *β*-diketone Ligands, the M=O Infrared Stretching Frequencies and the Metal-Oxido Bond Distances of the Coordinated Complexes

9.2.1.1 pK_a *vs.* υ(M=O)

During the course of the synthetic investigation reported in Chapter 3 (Section 3.5) a potential relationship was noted between the pK_a values of the free ligands and the IR metal-oxido infrared stretching frequencies reported for the different coordinated niobium(V) and tantalum(V) complexes. To illustrate this, the pK_a values of the free ligands along with the corresponding stretching frequencies of the niobium(V) and tantalum(V) complexes are given in Tables 9.2 and 9.3. It is clear that a fair relationship is observed for both the Nb(V) and Ta(V) complexes in good agreement with the electron-donating ability of the *β*-diketonato ligand. This reflects in a asymmetric weakening of the M=O bond as more electron density is introduced by the ligand which results in a lowering of the υ(M=O) stretching frequency. This phenomenon is illustrated in Figure 9.2.

[7] P. Ebenebe, (1998). *A Mechanistic and Structural Study of Carbonyl Substitution in Square-Planar Rh(I)-β-diketone Complexes*. MSc Dissertation, University of the Free State, Bloemfontein, South Africa.

[8] C. Pretorius, (2015). *Structural and Reactivity Study of Rhodium(I) Carbonyl Complexes as Model Nano Assemblies.* PhD Thesis, University of the Free State, Bloemfontein, South Africa.

[9] H. Watarai and I. Takahashi, (1998). *Anal. Commun.*, **38**, 289-292.

Table 9.2 Correlation of the pK_a values of the free ligands and the reported IR M=O stretching frequencies (Chapter 3, Table 3.1) of the coordinated niobium(V) complexes.

Nb(V) Complex	pK_a of β-diketonate	υ (Nb=O) (cm^{-1})
$(NEt_4)[NbOCl_3(hfaa)]$	4.60	949
$(NEt_4)[NbOCl_3(btfa)]$	6.30	935
$(NEt_4)[NbOCl_3(tfaa)]$	6.30	931
$(NEt_4)[NbOCl_3(tffa)]$	6.48	934
$(NEt_4)[NbOCl_3(ttfa)]$	6.50	936
$(NEt_4)[NbOCl_3(ntfa)]$	Unknown	942
$(NEt_4)[NbOCl_3(3\text{-}Clacac)]$	6.77	929
$(NEt_4)[NbOCl_3(acac)]$	8.95	922

Table 9.3 Correlation of the pK_a values of the free ligands and the reported IR M=O stretching frequencies (Chapter 3, Table 3.2) of the coordinated tantalum(V) complexes.

Ta(V) Complex	pK_a of β-diketonate	υ (Ta=O) (cm^{-1})
$(NEt_4)[TaOCl_3(hfaa)]$	4.60	933
$(NEt_4)[TaOCl_3(btfa)]$	6.30	919
$(NEt_4)[TaOCl_3(tfaa)]$	6.30	921
$(NEt_4)[TaOCl_3(tffa)]$	6.48	911
$(NEt_4)[TaOCl_3(ttfa)]$	6.50	917
$(NEt_4)[TaOCl_3(ntfa)]$	Unknown	927
$(NEt_4)[TaOCl_3(3\text{-}Clacac)]$	6.77	918
$(NEt_4)[TaOCl_3(acac)]$	8.95	909

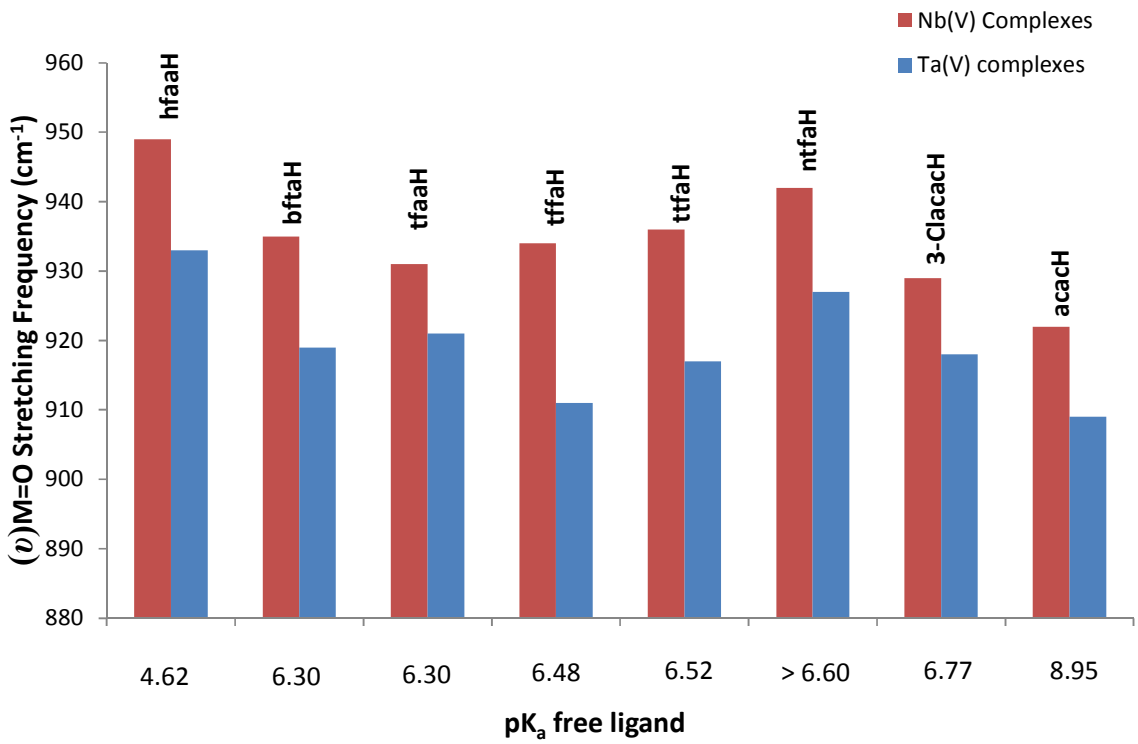

Figure 9.2 Schematic representation of the relationship between the pK_a values of the free *β*-diketone ligands and the reported M=O stretching frequency (cm^{-1}) of the coordinated complexes.

From the aforementioned, the IR spectra recorded for the synthesized products provided valuable insight into the electronic effects of the ligands to the tantalum and niobium metal centres. The well-defined Nb=O and Ta=O bonds have characteristic IR stretching frequencies in the region of ~ 930 cm^{-1} and ~ 920 cm^{-1}.[10]

9.2.1.2 pK_a *vs.* M-O bond lengths

It was further noted that the pK_a values of these ligands influence the Nb-oxido bond distances as illustrated in Table 9.4. A generalized depiction of the numbering scheme of $[NbOCl_3(\beta\text{-diket})]^-$ anion is shown in a perspective drawing in Figure 9.3.

[10] F. D. Hardcastle and I. E. Wachs, (1990). *J. Raman Spectrosc.*, **21**, 683-691.

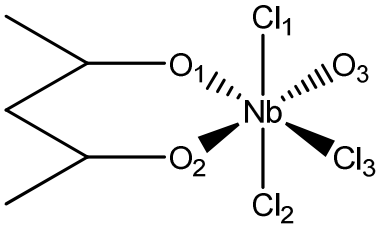

Figure 9.3 Generalized depiction of the numbering scheme of the $[NbOCl_3(\beta\text{-diket})]^-$ anion.

Table 9.4 Correlation of the pK_a values of the free ligands and the reported Nb-oxido bond distances (Chapters 5 and 6) of the coordinated niobium(V) complexes.

Nb(V) Complex	pK_a of *β*-diketonate	Nb-O1 Bond Distance (Å)	Nb-O2 Bond Distance (Å)	Nb-O3 Bond Distance (Å)
$(NEt_4)[NbOCl_3(hfaa)]$	4.60	2.223(1)*	2.223(1)*	1.836(1)*
$(NEt_4)[NbOCl_3(btfa)]$	6.30	2.046(1)	2.266(1)	1.806(1)
$(NEt_4)[NbOCl_3(tfaa)]$	6.30	---	---	---
$(NEt_4)[NbOCl_3(tffa)]$	6.48	2.069(1)	2.295(1)	1.715(1)
$(NEt_4)[NbOCl_3(ttfa)]$	6.50	2.066(1)*	2.306(1)*	1.739(1)*
$(NEt_4)[NbOCl_3(ntfa)]$	>6.60	2.046(1)	2.314(1)	1.711(1)
$(NEt_4)[NbOCl_3(3\text{-}Clacac)]$	6.77	2.023(1)	2.280(1)	1.704(1)
$(NEt_4)[NbOCl_3(acac)]$	8.95	---	---	---

* Probably influenced due to substantial disorder within the crystal structure (see Sections 5.4 and 6.4).

The oxido bonds (O3) of the complexes noted in Table 9.4 are classified as multiple covalent bonds formed by the donation of p_π electrons of oxygen to the d_π orbitals of the metal centres, superimposed upon the sigma bond. The extent of $p_\pi - d_\pi$ donation is dependent upon the tendency of oxygen to donate and the capacity of the metal to accept electrons. The donor capacity of oxygen is not expected to change appreciably by coordination of different ligands to the metal centres. In contrast, the acceptor ability of the metal complexes should be greatly affected. The coordinated ligands, which donate electron density into the metal *d*-orbitals and consequently it is expected that the $p_\pi - d_\pi$ donation from the oxygen to the metal will be reduced depending upon the donor ability of the ligands. As a result the M=O bond order should be lowered (and in principle should become shorter) as well as the corresponding M=O stretching frequency, as discussed in Section 9.2.1.1 above.

Evidence of this postulation was noted in Figure 9.3 when considering the ligand with the most electron-donating (acacH) ability, yielded a complex in which the M=O stretching frequency has the lowest value (υ(Ta=O), 909 cm^{-1} and υ(Nb=O), 922 cm^{-1}). In contrast, the most electron-withdrawing (hfaaH) ligand, afforded much higher M=O stretching frequencies value (υ(Ta=O), 922 cm^{-1} and υ(Nb=O), 949 cm^{-1}).

When comparing the pK_a of the free ligand with the Nb=O bond distances (Table 9.4) of the various crystal structures, a substantial shortening of bond length is noted as the electron-donating ability of the ligand increases. However, the *trans*- Nb-O2 (*β*-diketone) bonds follow exactly the same trend, i.e., a systematic shortening of the bond *trans* to the Nb-O3 bond. Superficially, this suggests that the Nb-O2 bond become stronger as the hardness of the metal increases. Since the Nb-O1 bond distances are seen to be less influenced by the *β*-diketone ligands, it might suggest that the total *trans*- O3=Nb-$O2^-$ moiety accommodates the added electron density introduced by the *β*-diketonate ligands and that the other equatorial bonds are less affected. This also manifests in the Nb-Cl3 bond distances.

This observation is directly in contrast with the results observed from IR analysis. As has been mentioned, various electronic and steric effects may disturb the solid state metal-oxido (M-O3) bond distances but slight crystallographic disorders substantially complicate the placement of atoms within the unit cell and could further clarify this anomaly.

9.2.2 Relationship Between the Bronsted pK_a Values of the Free *β*-diketone Ligands and the ^{19}F-NMR Chemical Shift of the Coordinated Complexes

As was presented in Chapter 3 (Section 3.5) a fair correlation was observed between the pK_a values of the free *β*-diketone ligands and the ^{19}F-NMR chemical shifts reported for the different coordinated niobium(V) and tantalum(V) complexes. The pK_a values of the free ligands along with the corresponding ^{19}F-NMR chemical shifts of the niobium(V) and tantalum(V) complexes are given in Tables 9.5 and 9.6. From

these tables an increase in chemical shift is observed as the pK_a values increase for the different coordinating *β*-diketone ligands, which is further illustrated in Figure 9.4.

Table 9.5 Correlation of the pK_a values of the free ligands and the reported ^{19}F-NMR chemical shifts (Chapter 3) of the coordinated niobium(V) complexes.

Nb(V) Complex	pK_a of *β*-diketonate	δ (^{19}F) (ppm)
$(NEt_4)[NbOCl_3(hfaa)]$	4.60	-76.34, -77.96
$(NEt_4)[NbOCl_3(btfa)]$	6.30	-73.66
$(NEt_4)[NbOCl_3(tfaa)]$	6.30	-73.22
$(NEt_4)[NbOCl_3(tffa)]$	6.48	-73.41
$(NEt_4)[NbOCl_3(ttfa)]$	6.50	-73.37
$(NEt_4)[NbOCl_3(ntfa)]$	>6.60	-73.25
$(NEt_4)[NbOCl_3(3\text{-}Clacac)]$	6.77	No CF_3 group
$(NEt_4)[NbOCl_3(acac)]$	8.95	No CF_3 group

Table 9.6 Correlation of the pK_a values of the free ligands and the reported ^{19}F-NMR chemical shifts (Chapter 3) of the coordinated tantalum(V) complexes.

Ta(V) Complex	pK_a of *β*-diketonate	δ (^{19}F) (ppm)
$(NEt_4)[TaOCl_3(hfaa)]$	4.60	-75.01, 75.52
$(NEt_4)[TaOCl_3(btfa)]$	6.30	-72.59
$(NEt_4)[TaOCl_3(tfaa)]$	6.30	-72.83
$(NEt_4)[TaOCl_3(tffa)]$	6.48	-72.71
$(NEt_4)[TaOCl_3(ttfa)]$	6.50	-72.89
$(NEt_4)[TaOCl_3(ntfa)]$	>6.60	-71.07
$(NEt_4)[TaOCl_3(3\text{-}Clacac)]$	6.77	No CF_3 group
$(NEt_4)[TaOCl_3(acac)]$	8.95	No CF_3 group

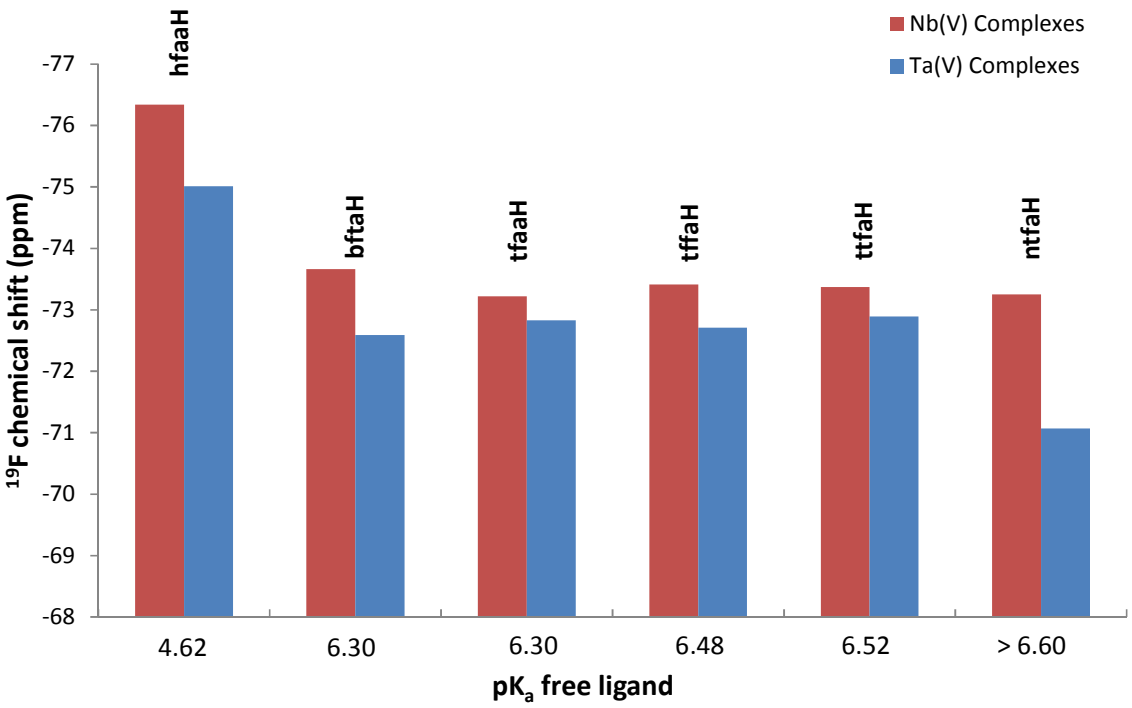

Figure 9.4 Schematic representation of the relationship between the pK_a values of the free *β*-diketone ligands and the observed ^{19}F-NMR chemical shifts (ppm) of the coordinated complexes.

NMR chemical shifts can provide valuable information on the electronic environment experienced by the nuclei under investigation. The practically of such NMR investigations have been noted in past examinations undertaken by Roodt *et al.* [11,12,13,14] During these studies, the protonation behaviour of *trans*-dioxidootetracyanido complexes of tungsten(IV), technetium(V), rhenium(V) and molybdenum(IV) was studied, by subjection to ^{13}C- and ^{17}O-NMR spectroscopy in order to examine the proton exchange within these complexes. The use of NMR spectroscopy was effective in elucidating effect of pH on the complex structures.

Studies relating to the modification of the electron-donating and -withdrawing properties of *β*-diketone ligands, by changing substituents on the acac backbone

[11] A. Roodt, J. G. Leipoldt, L. Helm, A. Abou-Hamdann and A. E. Merbach, (1995). *Inorg. Chem.*, **34**, 560-568.

[12] A. Roodt, J. G. Leipoldt and E. A. Deutsch and J. C. Sullivan, (1992). *Inorg Chem.*, **31**, 1080-1085.

[13] W. Purcell, A. Roodt, S. S. Basson and J. G. Leipoldt, (1991). *Trans. Met. Chem.*, **16**, 60-61.

[14] A. Roodt, J. G. Leipoldt, S. S. Basson and I. M. Potgieter, (1988). *Trans. Met. Chem.*, **13**, 336-339.

have given greater insight to the influence of these varying groups on the electronic properties (NMR shifts) of the compounds.[8]

In a study conducted by Pretorius *et al.* a very thorough ^{103}Rh-NMR investigation of fluorinated Rh(I)-*β*-diketonate complexes was effective in revealing the various electronic effects caused by ligand modification at the Rh metal centre.[8] It was found that as electron density is increased around the rhodium(I) centre (addition of electron-donating group), the shielding experienced by the rhodium nucleus will increase. As the shielding is increased, the chemical shift will move upfield. Accordingly, investigating the ^{103}Rh chemical shifts of the different coordinated rhodium(I) complexes provided information on the electron density present at the rhodium(I) centre.

In contrast, for this current Ph.D. investigation focus was placed on the electronic environment around the ^{19}F nuclei on the periphery of the acac backbone rather than the metal centre as such. It has been mentioned in Chapters 2, 5, 6, 8 and Section 9.1 that the extent of fluorination (electron-withdrawing effect) could be crucial in obtaining more effective separation methods for Ta(V) from Nb(V), either by solvent extraction or sublimation. The premise being that in the solid state, the degree of fluorination increases volatility of compounds, whereas in solution this effect causes a decrease in Lewis acidity of the compound. The various advantages of these properties have been discussed in significant detail throughout the text. With this in mind, it was concluded that more insight of the effect of ligand basicity on the electronic environment around the ^{19}F nuclei of the Nb(V) complexes could be advantageous to better understand the resulting characteristics of varying the electron density also on e.g. relative intermolecular interactions or complex acidity.

Tables 9.5 and 9.6 illustrates a fair but obvious trend when comparing ligand pK_a and the ^{19}F NMR chemical shift for the various Nb(V) and Ta(V) compounds. As the ligand pK_a decreases (more electron-withdrawing ligand), an upfield shift of the ^{19}F nuclei of the various corresponding complexes is noted. When comparing $(NEt_4)[NbOCl_3(hfaa)]$ (hfaaH; pK_a = 4.6) complex with a ^{19}F shift of δ = -76.34 ppm (-77.96 ppm) and $(NEt_4)[NbOCl_3(btfa)]$ (btfaH; pK_a = 6.3) complex with a ^{19}F shift of δ

= -73.66 ppm, this phenomenon becomes quite evident. This is a clear indication that the ^{19}F nuclei are more shielded and more electron density is found around the ^{19}F nuclei in the $[NbOCl_3(hfaa)]^-$ complex. This might contribute to the fact that this compound has the least intermolecular interactions (Chapter 5 and 6) as the complex periphery, might be more electronically saturated when compared to the other Nb(V) counterparts. Even though this trend is noted for both metal centres, the resonance peaks for the Ta(V) compounds were found to resonate in a more upfield environment.

9.3 Quantification of the Influence of Intermolecular Interactions (Hydrogen Bonding) on Sublimation Properties of $(NEt_4)[MOCl_3(\beta\text{-diket})]$ (M = Nb, Ta)

Intermolecular interactions occur between all types of molecules or ions in all states of matter resulting in spontaneous assembly when carefully controlled.[15]. These communications range from the strong, long-distance electrical attractions and repulsions between ions to relatively weak dispersion forces.[16] It is further critical in e.g. the assembly of bonds in DNA.[17] There are four types of these interactions and all are different indicators of the fact that "opposite charges attract" (ionic bonds > hydrogen bonding > van der Waals dipole-dipole interactions > van der Waals dispersion forces).[18] It all flows from this general principle: as chemical bonds become more polarized, the induced charges on the various atoms become greater. This in turn affords to stronger intermolecular attractions, which conversely lead to higher melting and boiling points, and also potentially increase in sublimation temperatures. For this investigation, focus was placed on varying electronic aspects

[15] J. M. Lehn, (1987). *Supramolecular Chemistry - Scope and Perspectives, Molecules - Supermolecules – Molecular Devices,* Nobel Prize lecture.

[16] A. J. Wallace, C. D. Jayasinghe, M. I. Polson and O. J. Curnow, (2015). *J. Am. Chem. Soc.*, **137**, 15528-15532.

[17] B. E. Tropp, (2008). *Molecular Biology*, Jones and Bartlett Learning, Burlington, United States of America.

[18] C. Starr, R. Taggart, C. Evans and L. Starr, (2008). *Cell Biology and Genetics*, Cengage Learning, Boston, United States of America.

(changing *β*-diketone ligands) of the various compounds and qualitatively evaluating the effect thereof on sublimation properties.

The advantages of using sublimation purification as an effective separation method for Nb(V) and Ta(V) are clear and have been described in Section 2.4.2. Accordingly, the aspects of the various metal(V) compounds that could in principle influence sublimation properties and retrieval yields need to be evaluated. In Chapters 5 and 6, emphasis was placed on determining the various intermolecular hydrogen-bonding interactions within the crystal lattice of the Nb(V) compounds and a summary of these are listed again Table 9.7. It is important to note that these interactions can only be determined from systematic and accurate XRD studies. These interactions are known to stabilize the crystal lattice and accordingly, potentially may directly influence the sublimation properties of a compound. In an attempt to qualitatively quantify the strength of these intermolecular hydrogen interactions all hydrogen bonds with angles > 165 º are defined as strong interactions (highlighted in red), between 145 – 165 º intermediate interactions (highlighted in green) and < 145 º as weak interactions (highlighted in blue).

Table 9.7 Summary of intermolecular hydrogen bonding interactions from the XRD studies in Chapters 5 and 6 for different oxygen, chlorine, carbon and fluorine donor/accepting atoms.

$(NEt_4)[NbOCl_3$ (3-Clacac)]	$(NEt_4)[NbOCl_3$ (hfaa)]	$(NEt_4)[NbOCl_3$ (ntfa)]	$(NEt_4)[NbOCl_3$ (btfa)]	$(NEt_4)[NbOCl_3$ (tffa)]	$(NEt_4)[NbOCl_3$ (ttfa)]
(a) Oxygen					
C21-H21C···O3	-	C24-H24A···O1	C25-H25B···O3	C25-H25B···O3	-
145.50 (2) °		**172.00 (2) °**	**142.07 (3) °**	**150.46 (2) °**	
C21-H21B···O3	-	C25-H25A···O1	C21-H21B···O3	C28-H28B···O3	-
168.82 (2) °		**149.90 (2) °**	**150.23 (2) °**	**161.63 (1) °**	
C26-H26B···O3	-	C25-H25A···O3	C26-H26C···O3	C27-H27B···O3	-
139.66 (2) °		**144.76 (2) °**	**162.92 (1) °**	**140.97 (3) °**	
-	-	C26-H26C···O3	-	-	-
		140.51 (3) °			
(b) Chlorine (Inter-anionic)					
C1-H1B···Cl3	C21-H21B···Cl3	C6-H6···Cl1	C8-H8···Cl1	C7-H7···Cl2	C6A-H6A···Cl2A
153.29 (2) °	**134.95 (3) °**	**119.00 (3) °**	**132.71 (3) °**	**161.77 (1) °**	**176.35 (2) °**
C5-H5C···Cl4	C21-H21B···Cl3	C6-H6···Cl3	C10-H10···Cl3	C6-H6···Cl3	C3A-H3A···Cl2A
135.86 (3) °	**134.95 (3) °**	**151.34 (2) °**	**160.48 (1) °**	**162.15 (1) °**	**131.41 (3) °**
C1-H1C···Cl4	C21-H21B···Cl3	-	C9-H9···Cl1	-	-
148.20 (3)°	**134.95 (3) °**		**149.71 (2) °**		
-	C21-H21B···Cl3	-	C27-H27A···Cl3	-	-
	134.95 (3) °		**135.62 (3) °**		
(c) Chlorine (Counter-ionic)					
C20-H20A···Cl1	-	C21-H21B···Cl3	-	C21-H21B···Cl3	-
178.88 (1) °		**159.75 (2) °**		**143.18 (3) °**	
C24-H24B···Cl2	-	C27-H27B···Cl2	-	-	-
151.95 (2) °		**135.23 (2) °**			
C27-H27A···Cl2	-	C21-H21A···Cl3	-	-	-
148.20 (2) °		**170.55 (1) °**			
-	-	C22-H22A···Cl2	-	-	-
		172.60 (1) °			
(d) Carbon					
C5-H5C···H27C	-	-	C6-H6···C24A	C27-H27A···C6	-
145.40 (2) °			**136.91 (3) °**	**161.77 (1) °**	
-	-	-	C25-H25A···C9	C27-H27A···C7	-
			150.61 (2) °	**162.15 (1) °**	
(e) Fluorine					
-	-	C25-H25B···F1	C26-H26A···F2	C26-H28C···F1	-
		122.06 (3) °	**122.06 (3) °**	**121.51 (3) °**	
-	-	C28-H28B···F1	C26-H26B···F2	-	-
		122.06 (3) °	**122.06 (3) °**		
-	-	C26-H26B···F1	C28-H28A···F3	-	-
		135.68 (3) °	**135.68 (3) °**		

Table 9.8 Summary of the number of different types of intermolecular hydrogen bonding interactions observed for the compounds in Chapters 5 and 6.

Sample	Weak Interactions (Blue)	Intermediate Interactions (Green)	Strong Interactions (Red)	Total Number of Interactions
$(NEt_4)[NbOCl_3(ttfa)]$	1	0	1	2
$(NEt_4)[NbOCl_3(hfaa)]$	4	0	0	4
$(NEt_4)[NbOCl_3(tffa)]$	3	6	0	9
$(NEt_4)[NbOCl_3(3\text{-}Clacac)]$	2	6	2	10
$(NEt_4)[NbOCl_3(btfa)]$	7	5	0	12
$(NEt_4)[NbOCl_3(ntfa)]$	7	3	3	13

Tables 9.7 and 9.8 effectively illustrate the fact that as the size of the substituent opposite the CF_3 substituent increases, the number of stabilizing hydrogen interactions also increases. Thus for the $(NEt_4)[NbOCl_3(ntfa)]$ compound, thirteen non-classical hydrogen interactions are noted, whereas in the case of $(NEt_4)[NbOCl_3(hfaa)]$ only four are observed. Although no study to the authors knowledge has ever confirmed that the stoichiometric amount of hydrogen bonding interactions relates directly to complex stability (not all hydrogen interactions have identical energy potentials), it must be noted that from the current study, the substantial increase of these interactions with increase with substituent size indeed has to significantly influence different physical properties, and thus also lattice stability.

A further point worth noting is that these interactions found for the different $(NEt_4)[NbOCl_3(\beta\text{-diket})]$ complexes also correlate quite well with the postulation in Chapter 2, that as the degree of fluorination on the acetylacetonato backbone increases, a significant reduction of hydrogen bonding will/can occur. This in principle should potentially imply that $(NEt_4)[NbOCl_3(hfaa)]$ (6 fluorines, 4 hydrogen bonding interactions) should sublimate much easier than the more stable $(NEt_4)[NbOCl_3(ntfa)]$ (3 fluorines, 13 hydrogen interactions).

Based on the above information, in the following section, a standardized experiment was designed and is described which was used to determine the percentage recovery of Nb from a pure powdered sample of the different $(NEt_4)[NbOCl_3(\beta\text{-diket})]$ compounds in a simple sublimation experiment. This was done with the aim of obtaining/postulating a prediction model based on the number of hydrogen-bonding interactions within the different compounds, reporting the percentage Nb that could be retrieved from a crushed sample. It is important to note that the Ta(V) compounds could not be related to hydrogen bonding interactions as no crystal structures of these compounds were obtained in this study.

9.3.1 Sublimation of Nb(V)-*β*-diketonato Compounds

The discussions in the preceding sections enabled different observations from the simple sublimation experimental runs. From these studies, the following assumptions are made;

- A relatively small amount of Nb(V) should be retrieved from each of the experiments. This can be ascribed to that fact that even though these compounds show a marked improvement in stability *vs.* similar compounds, decomposition still remains a problem at elevated temperatures (melting and charring).

- The percentage recovery of Nb from the sublimation of $(NEt_4)[NbOCl_3(ntfa)]$ is expected to be the lowest, owing to the fact that this compound is the "most stable" when considering the greater amount of intermolecular hydrogen interactions.

- The percentage recovery of from the sublimation of $(NEt_4)[NbOCl_3(hfaa)]$ is expected to be the be the highest due to the fact that the increased degree of fluorination should decrease hydrogen bonding interactions.

- It has to be noted that the current experiments (or study) just serves as a "proof of concept"; and that much more work is required to refine the model.

9.3.1.1 Determining Optimum Temperatures and Pressures of Maximum Percentage Recovery of Niobium from Samples.

The sublimation of Nb(V)-bidentate complexes, and in particular the development of a model towards predicting it, is considered a very novel field of research and not much literature relating to ideal experimental conditions for optimum sublimation has been defined. Accordingly, a vast amount of preliminary studies will be required to attempt to define these conditions more systematically. When considering the investigation at hand, three properties that could influence % Nb recovery were noted in particular. These include, but not restricted to, sample mass, temperature as well as pressure.

- The amount of sample required relates directly to the size of the surface area avaliable on which the product will/can sublime. Sample sizes ranging from 0.050 g to 2.000 g of the Nb(V)-*β*-diketonates were tested, but the mass of the sublimated product did not increase substantially in the setup as employed, above a 0.450 g Nb(V) sample. Thus, a standardized mass of 0.500 g of Nb(V) product was selected.

- For this process to be economically viable, the temperatures required for sublimation must be substantially lower than the industrial norm. For this investigation, samples were exposed to temperatures ranging from 50 – 400 ºC. The first observations made were that at temperatures below 100 ºC no sublimation product was obtained, whereas at temperatures above 200 ºC significant decomposition of the starting material was observed. Accordingly, a 150 ºC standardized temperature was selected as it affords the same sublimation yields as any increased temperature would, without significantly damaging the sample.

- The same argument for industrial applicability of the selected pressure applies as what was described for normal temperature selection. The basic reasoning for obtaining an ideal pressure was to define the highest value at which sublimation yields do not increase significantly. For this investigation, pressures ranging from atmospheric pressure to 5 mBar were utilized. From this analysis it was found that at pressures below 1 mBar, no substantial increase in sublimation yields were noted and accordingly this pressure was selected as the norm of this sublimation study.

9.3.1.2 Normalized Sublimation Experiment

A basic schematic of the experimental setup was noted in Section 2.4.1 (Figure 2.27). For this experiment a pure sample of the $(NEt_4)[NbOCl_3(\beta\text{-diket})]$ (0.500 g) was crushed and placed in a sublimation tube. This was placed in a sublimation oven and heated to 150 ºC, at 1 mBar for 2 hours to ensure maximum recovery of niobium from the samples. The sublimate recovered was collected from the cold finger and sent for ICP analysis on a Shimadzu ICPS-7510 ICP-OES sequential plasma spectrometer to determine the amount of niobium collected. This was done in triplicate with the average results obtained from this investigation given in Table 9.9.

Table 9.9 Results obtained from the standardized sublimation investigation.

Sample	Mass of Sample (g)	Mass of Nb in Sample (g)	% Nb in Sample	Mass of Sublimate (mg)	Mass Nb in Sublimate (mg)	% Nb Retrieved
$(NEt_4)[NbOCl_3(hfaa)]$	0.500	0.079	15.80	12.0	n/a	n/a
$(NEt_4)[NbOCl_3(btfa)]$	0.500	0.081	16.23	45.0	5.12	6.33
$(NEt_4)[NbOCl_3(tffa)]$	0.500	0.083	16.52	33.0	2.86	3.45
$(NEt_4)[NbOCl_3(ttfa)]$	0.500	0.080	16.02	30.0	3.80	4.75
$(NEt_4)[NbOCl_3(ntfa)]$	0.500	0.074	14.80	75.0	8.89	12.01
$(NEt_4)[NbOCl_3(3\text{-}Clacac)]$	0.500	0.095	19.04	33.0	3.91	4.12

9.3.1.3 Discussion

The results documented in Table 9.9, show some interesting tendencies with respect to the sublimation properties of the Nb(V) complexes utilized. These observations were found to be mostly counter intuitive with the potential expected results as postulated in Section 9.3.1.

The first anomaly that was noted from the above was the fact that as the size of the non-CF_3 substituent increases, the amount of niobium retrieved in the sublimate increased. Interestingly, in previous sections it has also been noted that as the size of this substituent increases so does the amount of intermolecular hydrogen bonding. Accordingly, in an attempt to correlate the number of hydrogen bonding interactions with the percentage recovery of Nb from the sublimation experiment, Table 9.10 and Figure 9.5 are presented.

Table 9.10 Correlation of the number of hydrogen bonding interactions with % recovery of Nb for this Investigation.

Sample	Number of Hydrogen Interactions (From Table 9.8)	% Nb retrieved
$(NEt_4)[NbOCl_3(ttfa)]$	2	4.75
$(NEt_4)[NbOCl_3(hfaa)]$	4	0.00
$(NEt_4)[NbOCl_3(tffa)]$	9	3.45
$(NEt_4)[NbOCl_3(3\text{-}Clacac)]$	10	4.12
$(NEt_4)[NbOCl_3(btfa)]$	12	6.33
$(NEt_4)[NbOCl_3(ntfa)]$	13	12.01

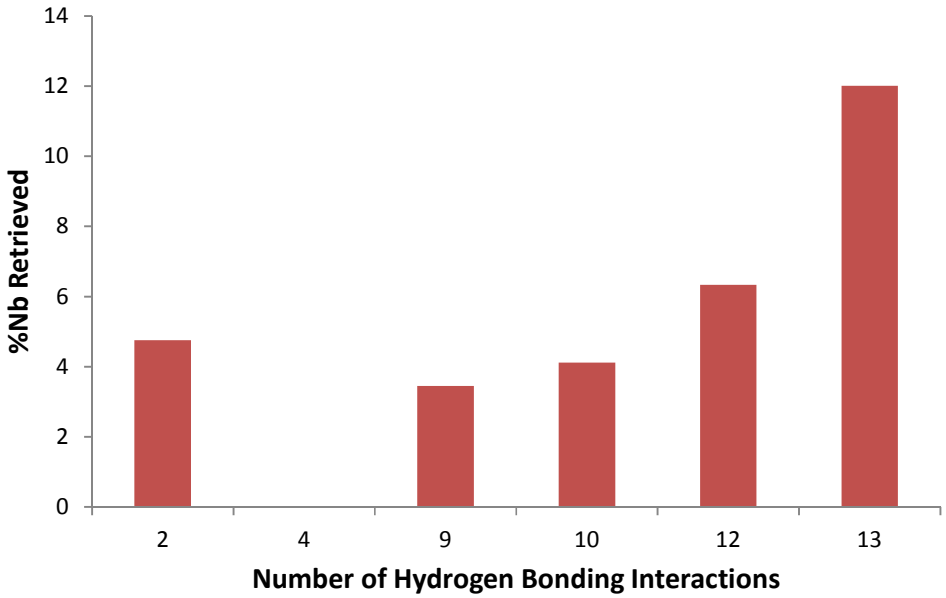

Figure 9.5 Schematic representation of the relationship between the number of hydrogen bonding interactions and the % Nb retrieved from the sublimation experiments.

Figure 9.5 indicates obvious that as the number of intermolecular hydrogen bonding interactions increases, so does the % Nb retrieved from the sublimation experiment. This contradicts the theory noted in Section 2.3.1.3 that reducing the hydrogen bonding interactions (by an increased degree of fluorination) destabilizes the complex to such an extent that an increased sublimation yield is obtained. It might therefore be concluded that hydrogen bonding can affect the degree of sublimation in a different way (e.g. by forming conglomerates which might have better sublimation properties).

An outlier in this trend was found to be the $(NEt_4)[NbOCl_3(ttfa)]$ compound which only displays two H-interactions. This number can be ascribed to the severe disorder within the crystal lattice making it difficult to accurately define the various additional hydrogen bonding interactions. If the qualitative relationship shown in Figure 9.5 holds, based on the other Nb(V) complexes investigated, this compound should display roughly ten interactions, resulting in a good relation to the expected % recovery of niobium.

In the case of $(NEt_4)[NbOCl_3(ntfa)]$, the percentage Nb retrieved is slightly greater than what would be anticipated when noted the aforementioned trend. If an increased stability of the particular compound indeed causes more niobium to be retrieved from a sample, then some additional stabilization interactions will be required for this compound. When considering the discussion in Section 5.7 it was found that the $(NEt_4)[NbOCl_3(ntfa)]$ crystal lattice displays additional π-π-stacking interactions (see Figure 5.29). Even though these connections are not as resilient as the hydrogen bonding interactions they do contribute considerably to complex stability.[19]

If all the information regarding the sublimation properties of these compounds is considered, it follows that $(NEt_4)[NbOCl_3(\beta\text{-diket})]$ complexes might in fact sublimate in molecular "clusters". The size and stability of these "clusters" could relate to the amount of intermolecular interactions, forming pseudo oligomeric compounds in the gaseous state. This might explain why the more "stable" compounds (when considering intermolecular interactions) are sublimated with greater success.

9.4 Conclusion

It was noted in Chapter 2 that there is a substantial lack of knowledge regarding the physical properties and in particular that of sublimation, of these types of metal-*β*-diketonate chemical systems. This opinion has mainly been attributed to the difficulty in obtaining the final coordinated metal(V) complex, due to hydrolysis of the metal centres causing an instability of the formed compounds. In Chapter 3 of this study, a number of these relatively stable Nb(V)- and Ta(V)-*β*-diketonate complexes, with a range of different *β*-diketone ligands, were successfully synthesized and fully characterized by means of ^{1}H-, ^{13}C-, ^{19}F-NMR and infrared spectroscopy. All of these aforementioned ligands have varying electronic properties as denoted by their pK_a values, which influence the corresponding complex in different ways. For the major part of this investigation, emphasis was placed on the influence of this pK_a value of the free ligand (electron-donating or -withdrawing ability) on the physical properties corresponding Nb(V) or Ta(V) complexes.

[19] C. A. Hunter and J. K. M. Sanders, (1990). *J. Am. Chem. Soc.*, **112**, 5525-5534.

Several trends were noted as a result of the differing electronic properties of the various *β*-diketonate ligands. All of these observations contribute to a better insight into the properties that govern the chemical and physical properties of these systems. These include;

- An increased influx of electrons as a result of electron donating substituents on the *β*-diketonate backbone (higher pK_a value of free ligand) which correspondingly influences the electron density around (and on) the metal centre. This causes the metal centre to be less dependent on electrons from the oxido group for its electronic needs and reduces $p_\pi - d_\pi$ donation from the oxygen to the metal (decreased *trans* effect). This was corroborated by a decrease in M=O stretching frequency with an increase of free ligand pK_a (electron-donating ability)

- When considering the ^{19}F-NMR spectra of these compounds, an upfield shift of the resonance peaks for ^{19}F nuclei of the various corresponding complexes was observed as the free ligand pK_a decreases (more electron-withdrawing ligand). This is a clear indication that the ^{19}F nuclei are more electronically shielded due to increased electron density around the ^{19}F nuclei.

- Finally, it was found that sublimation yields of these compounds are significantly influenced by the number of intermolecular hydrogen bonding interactions within the crystal lattice. It is thus a preliminary conclusion that $(NEt_4)[NbOCl_3(\beta\text{-diket})]$ complexes might sublimate in molecular “clusters”. The size and stability of these “clusters” could relate to the amount of intermolecular interactions, forming pseudo oligomeric compounds in the gaseous state.

These observations yielded an improved perspective as to the effect of electron-donating or -withdrawing ligands on the electron flow within the molecular structure of the various compounds. It was noted that as electron-withdrawing capabilities (lower pK_a) of the *β*-diketonate is increased more electron density will be

encountered within the periphery of this ligand. This in turn decreases the amount of intermolecular hydrogen bonding interactions, which probably impacts on the sublimation properties of the compounds. In contrast, more electron-donating substituents (higher pK_a) have a substantial influence on the oxido, *trans* effect of the compounds, as well as seemingly causing an increase in intermolecular hydrogen bonding interactions. When all of these pieces are combined it seems that by increasing electron-donation capabilities of the *β*-diketonate substituent, improved recovery of niobium can be expected from sublimation separation studies.

Even though significant and systematic supplementary research is required to fully substantiate this postulation, correlation of various aspects by means of different characterization techniques has substantially improved the understanding of the chemical and physical properties of these systems. Clearly this field of research needs to be further explored.

Chapter 10: Evaluation of Study and Future Aims

10.1 Overview

As was noted in Chapter 1, the synthesis, characterization and quantification of solid- and solution state behaviour of the niobium(V) and tantalum(V) compounds, highlights the comprehensive aims of this research study focusing on the separation of niobium and tantalum. During the course of this investigation various novel findings relating to the coordinative behaviour of these complexes have been noted and discussed in detail in each respective chapter relating to each individual field of the investigation. The aim of this final chapter is to elaborate on the aforementioned successes attained and discuss the significance of these results on the current knowledge base regarding tantalum(V) and niobium(V) chelation behaviour. This investigation concludes by deliberating on future research opportunities for separation.

10.2 Synthesis of New Synthons and Nb(V)- and Ta(V) complexes

One of the central objectives in this study involved the synthesis of various niobium(V) and tantalum(V) complexes with different coordinating bidentate ligands. This was done to evaluate the influence of different substituents on the *O,O'*-ligand backbones on these metal centres. Two sets of ligand types, functionalized acetylacetones and tropolones, were identified as excellent candidates for this chelation study. The theoretical considerations of these compounds were discussed in detail in Chapter 2.

Most of the recorded literature highlighted in Chapter 2, indicated that tantalum(V) and niobium(V) *O,O'*-bidentate complexes could only be synthesized under inert and

anhydrous conditions.[1,2] This was attributed to the $[MCl_5]_2$ (M = Ta(V), Nb(V)) starting material hydrolizing to various unreactive oxido-metal species.[3] In an attempt to overcome this problem, a more robust synthon for both metal centres was required for application in atmospheric conditions.

Chapters 3 and 4 described the use of an ammonium-type counter-ion that has led to the development of two novel synthons $(NEt_4)[NbCl_6]$ and $(NEt_4)[TaCl_6]$. The simplicity and efficiency (90+ % yields) of the syntheses in atmospheric conditions is exactly what is required when producing an ideal synthon with the air-stability of this $(NEt_4)[MCl_6]$ compound being quite noteworthy. These compounds, even when stored under atmospheric conditions, have been found to be functional for coordination reactions to *β*-diketones weeks after synthesis.

A series of seven *β*-diketone ligands was identified and by utilization of the novel synthons, applied in synthesis. These ligands were all successful in yielding coordination compound products, as confirmed by UV/Vis-, IR- and ^{1}H-, ^{13}C- and ^{19}F NMR spectroscopy. The different substituents on the acac-backbone of the ligands were selected for their electron withdrawing/donating as well as steric influences. An overview as to the effect of these properties on the solid- and solution state behaviour of the obtained complexes will be summarized in the following sections. Furthermore, the significance of the application of these ligands as chelators also lies in the fact that very few examples of niobium(V) and tantalum(V) complexes containing acetylacetonato-type ligands were previously known in literature.[4]

A notable feature worth citing here, lies in the value of the technique applied to obtain these metal(V)-*β*-diketonate complexes. The simple method utilized in all cases associated with *β*-diketone coordination, involved simple bench-top synthesis

[1] H. O. Davies, T. J. Leedlam and A. C. Jones, (1999). *Polyhedron*, **18**, 3165-3180.

[2] G. J. Bullen, R. Mason and P. Pauling, (1965). *Inorg. Chem.*, **4**, 456-465.

[3] R. Koen, (2012). *High Oxidation State Tantalum Coordination Chemistry: A Solution and Solid State Investigation*, M.Sc. Dissertation, University of the Free State, South Africa.

[4] Cambridge Structural Database (CSD) Version 5.35, November 2013 update. F.H. Allen, (2002). *Acta Cryst.*, **B58**, 380-388.

without any special precautions regarding anaerobic conditions (pre-dried solvents and reagents or an inert atmosphere reaction setup). This is ideal for an industrially applicable and a more economically viable process.

The second group of the aforementioned ligand systems used during the course of this investigation, tropolones, was chosen to expand on the *O,O'*-chelation possibilities for niobium(V) and tantalum(V). In Section 3.3, unmodified tropolone (tropH) was coordinated to Ta(V) and Nb(V) metal centres, while studying the influence of pH on the coordination geometry of these systems. It was mentioned in earlier sections that in most cases, the $[TaCl_5]_2$ and $[NbCl_5]_2$ synthons do not yield stable complexes when coordinated to bidentate ligands in atmospheric conditions. Interestingly, in this case, it was found that the metal-tropolonato complexes form quite readily with very high yields, in hydrous conditions and were found to remain stable for weeks after synthesis.

It was illustrated that the synthesis of Nb(V)- and Ta(V)-*β*-diketonate and -tropolonato complexes do not require rigorous synthetic procedures and laborious crystallization methods. Formation reactions are often self-catalyzed and crystallization can occur in ambient environments. Several of these compounds yielded crystalline products. For those of sufficient quality and stability, the structural characterization of the Nb(V)- and Ta(V) complexes was performed by means of single crystal X-Ray Diffraction studies (XRD). Unfortunately, in the case of the Ta(V)-*β*-diketonates the crystalline products were unstable and could not yield measurable X-ray diffraction data.

10.3 Single Crystal X-ray Diffraction Studies

During the course of the in-depth single crystal X-Ray diffraction characterization investigations discussed in Chapters 4, 5, 6 and 7; the crystal structures of two synthons (Nb(V) and Ta(V)), six Nb(V)-*β*-diketonate- and three metal(V)-tropolonate complexes (Ta(V) and Nb(V)) were successfully obtained and characterized.

From Chapter 4 it was noted that in the case of the Nb(V) metal centre, three realistic options for the ideal synthon for bidentate ligand coordination were identified, namely; $(Et_4N)[NbCl_6]$, $(Pr_4N)[NbCl_6]$ and $(Bu_4N)[NbCl_6]$. After taking into account properties such as synthon stability (intermolecular hydrogen bonding), chlorido lability and past successes, it was deemed that the $(Et_4N)[NbCl_6]$ and $(Et_4N)[TaCl_6]$ analogues were deemed to be the ideal synthons to further study the coordinative behaviour for both metal centres.

In Chapters 5 and 6 the description of the six Nb(V)-acetylacetonato complexes yielded more insight into the intimate geometric coordination characteristics around the niobium(V) metal centre, as well as the crystal lattice packing stabilization as a whole. Correlation of these structures was shown to highlight general trends relating to structural properties (i.e. bond lengths, ligand bite angles, etc.), especially noting the influence of the electron donating or -withdrawing ability of the substituents on the acetylacetonato backbone. These trends were discussed in detail in Chapter 9.

The crystallographic investigation concluded with an in-depth study relating solution pH with Nb(V)- and Ta(V)-tropolonato coordination and packing modes. Some very interesting observations and conclusions could be drawn from the comparison of the $[Ta(Trop)_4]Cl$ and $[Nb(Trop)_4]Cl$ solid state crystal structures. During a study by Muetteries *et al*. it was noted that the Nb(V) analogue is more susceptible to increasing temperature and pH than its Ta(V) counterpart in solution.[5] Chapter 7 of this study was aimed at giving possible explanations observed in the solid state, which contribute to this anomaly.

Firstly, it was noted that the $[Nb(Trop)_4]Cl$ compound experiences a higher degree of strain within the chelate ring. When considering the higher degree of strain (less energetically favourable) within the Nb(V) chelate ring, this complex could more readily offer up one of its tropolone ligands for the sake of obtaining the more stable $[NbO(Trop)_3]$. Secondly, the $[Ta(Trop)_4]^+$ cation exhibits a more distorted square antiprismatic geometry when compared with $[Nb(Trop)_4]^+$. In fact the coordination

[5] E. L. Muetteries and C. M. Wright, (1965). *J. Am. Chem. Soc.*, **87**, 4706-4717.

geometry is so distorted that could be deemed that $[Ta(Trop)_4]Cl$ in more inclined towards the more energetically favourable dodecahedral geometry. This might also contribute to the Ta(V) complex stability.

From the preceding chapters the importance of a solid-state crystallographic investigation becomes quite evident. The various solid-state characteristics within each crystal structure shed much light on coordination preferences and ligand influences on the complex structure of both Nb(V)- and Ta(V)-type complexes. This enhanced insight contributes to enhancing the knowledge base for Nb(V)- and Ta(V) bidentate complexes.

10.4 Solution Mechanistic Study

To further evaluate the electronic environment experienced by the niobium(V) and tantalum(V) centres in these complexes, a study of the substitution reactions of $[NbCl_6]^-$ and $[TaCl_6]^-$ with a range of *β*-diketones as entering ligand was undertaken and discussed in Chapter 8. A standardized kinetic substitution study in the formation of $(NEt_4)[NbOCl_3(ttfa)]$ - Tetraethylammonium *mer*-trichlorido oxido(thenoyltrifluoro acetylacetonato-κ^2O,O')niobate(V) was effective in yielding a postulated reaction mechanism and complicated rate law for the acac-type ligand coordination to the Nb(V) metal centre in both anhydrous and hydrous MeCN. For a specific ligand, and at fixed $[Cl^-]_{free}$ and $[H_2O]_{free}$ values, the first term in of the complicated rate law could actually be simplified to a constant value, defined by k_{fwd}. Accordingly, by varying different *β*-diketones, the effect of them on k_{fwd} could be studied. From the obtained results and observations using this equation, various previously unknown chemical characteristics for these systems could be identified.

For instance, it was found that the addition of H_2O to the reaction mixture affords the more reactive $[NbOCl_5)]^{2-}$ synthon *in situ vs.* $[NbCl_4(MeCN)_2]^+$ and $[NbCl_5(MeCN)]^+$ in anhydrous MeCN solutions which increases the rate of bidentate ligand coordination by factor 1.5-2.0.

Additionally, a relationship could also be established between the pK_a of the uncoordinated *β*-diketonato entering ligands and the rate of ligand substitution. These substitution rates were noted to increase significantly as the pK_a of the free ligand was decreased. This was ascribed to a decrease in electron density at the metal centre, which causes it to be more prone to nucleophilic attack. It was seen that the four order-of-magnitude increase in Bronsted basicity of the free bidentate ligands results in an eight and six times decrease in substitution reactivity at the Nb(V) and Ta(V) centres respectively.

10.5 Correlation Study

This investigation concluded in Chapter 9, which focused on comparing different properties associated with the niobium(V) and tantalum(V) complexes and relating those properties to the changes that were introduced in each complex by using different coordinating *β*-diketonato ligands. Several trends were noted as a result of the differing electronic properties of the various *β*-diketonate ligands. All of these observations give a better insight into the properties that govern the chemical and physical properties of these systems. A general schematic representation to illustrate the relationship of all the parameters used to evaluate the niobium(V) and tantalum(V) complexes was also presented.

These observations yielded an improved perspective as to the effect of electron-donating or -withdrawing ligands on the electron flow within the molecular structure of the various compounds. It was noted that as electron-withdrawing capabilities (lower pK_a) of the *β*-diketonate is increased more electron density will be encountered within the periphery of this ligand. This in turn decreases the amount of intermolecular hydrogen bonding interactions, which seems to impact the sublimation properties of the compounds. In contrast, more electron-donating substituents (higher pK_a) have a substantial influence on the oxido, *trans* effect of the compounds, as well as seemingly causing an increase in intermolecular hydrogen bonding interactions. When all of these pieces are combined, it seems that by

increasing electron-donation capabilities of the *β*-diketonate substituent, improved recovery of niobium can be expected from sublimation separation studies.

Due to the to the direct relation between intermolecular interactions and % recovery of Nb, it could then be concluded that these $(NEt_4)[NbOCl_3(\beta\text{-diket})]$ complexes sublimate in molecular "clusters". The size and stability of these "clusters" could relate to the amount of intermolecular interactions, forming pseudo polymeric compounds in the gaseous state.

10.6 Future Aims

The research outputs presented throughout this investigation has yielded a significant amount of novel insights and fundamental knowledge into niobium(V) and tantalum(V) coordination behaviour for solid, solution and gaseous phase behaviours. When considering these results and observations from this study, certain aspects could be identified that might be improved upon or new approaches that require additional investigation. These future aims will be crucial in completely understanding the chemical and physical behaviour of chloride substitution reactions and the implication thereof as it relates to niobium(V) and tantalum(V) separation. A few key issues for immediate further investigation can be summarised, as below:

i) As was noted in Chapter 3, in most cases, the bench-top synthesis of various Nb(V)- and Ta(V)-bidentate complexes proved to yield numerous crystalline products. However, some of the compounds afforded crystals that were of too low quality to analyze via XRD analysis, especially noting the Ta(V)-*β*-diketonates. Effort into the production of better quality crystals would greatly increase the possibility of structural characterization possibility, in turn expanding on the knowledge base of niobium(V) and tantalum(V) coordination behaviour properties.

ii) Expansion of the scope of research by the investigation of these Nb(V)- and Ta(V) complexes to include theoretical calculations to gain a better understanding of the orbital overlap that takes place between the metal

centres and the various ligands. This will also aid in understanding the electronic effects brought about by using different substituents in the coordinating *β*-diketonato ligands.

iii) The application of the rudimentary findings of the kinetic investigation presented in Chapter 8 could directly be applied on various sets of separation studies, involving either liquid-liquid- or solution extraction experimentation. From the observations concerning the manipulation of chloride substitution (by electron withdrawing groups on the acac backbone), nuances in coordination rates were controllably enhanced. Capitalization on this observation could in principle lead to improved separation in solution. Other ligand systems need also to be investigated.

iv) It was noted in Chapter 9 that an increase in intermolecular hydrogen bonding interactions relates to improved Nb recovery by means of solid-state sublimation studies. Although this is a very important observation, the % Nb recovery noted during this investigation was quite low (*c.a.* 10 % recovered) for the *β*-diketonato ligands. However, other ligand systems that are known to be easily functionalized, such as the aromatic tropolones or quinolines, could yield greater percentage recovery of Nb owing to an increased number of intermolecular interactions. It has been noted in past investigations that due to the larger size and physical and electronic properties of these ligand systems they are more prone afford hydrogen bonding interaction within the crystal lattices of their corresponding complexes. Accordingly, further research regarding the solid-state properties of the ligands is required.

The scope surrounding this research is great and diverse, and establishing a knowledge base of how fundamental chemistry impacts the coordinative properties of both tantalum and niobium metal centres will become vital in developing techniques that improve separation of these elements.

Summary

Niobium and tantalum, chemical twins of the vanadium triad of the periodic table, are notoriously difficult to separate from one another and from their naturally occurring ores due to their near identical chemical properties. The significance of the separation of these two elements lies in the value and application of these elements in various fields of uses, especially noting the nuclear industry. Niobium with its high melting point, strength, resistance properties to chemical attack and the low neutron absorption cross-section (NAC) is ideally suited when alloyed with zirconium for cladding material in control rods of nuclear reactors to prevent leakage of nuclear reactive materials. Tantalum, on the other hand, has a much more limited application in the nuclear industry. It is mainly used in combination with carbon to form tantalum carbide which is used as a lining agent within the nuclear reactor (due to the corrosion resistance of tantalum). Due to that fact tantalum and niobium are always found together in mineral ores, tantalum is actually seen as a “pollutant” by nuclear chemists. This is why an efficient separation method is required because even the smallest impurity of one metal in the other would seriously degrade the ability of the metal to function in its particular role in a nuclear reactor.

The principle aim of this study was to gain insight into the coordination and kinetic behaviour of Nb(V)- and Ta(V)-tropolonato and -acetylacetonato complexes. A detailed description of the synthesis of ten niobium(V)- and eight tantalum(V) complexes with the two ligand families (*O,O'*-donating) are reported and characterized by means of IR, UV/Vis and NMR (^{1}H, ^{13}C, ^{19}F) spectroscopies. Furthermore, the solid state structural characterization, by means of single crystal X-Ray diffraction spectroscopy, yielded eleven of these synthesized compounds which were described in detail in three separate sections.

The original focus of this crystallographic investigation was placed on the characterization of the more robust Nb(V)- and Ta(V) synthons, $(NEt_4)[NbCl_6]$ and $(NEt_4)[TaCl_6]$ and the factors that govern their stability for coordinative purposes. Secondly, six solid-state crystal structures of Nb(V)-*β*-diketonates -

$(NEt_4)[NbOCl_3(ttfa)]$, $(NEt_4)[NbOCl_3(tffa)]$, $(NEt_4)[NbOCl_3(ntfa)]$, $(NEt_4)[NbOCl_3(btfa)]$, $(NEt_4)[NbOCl_3(hffa)]$ and $(NEt_4)[NbOCl_3(3Cl\text{-}acac)]$ (where ttfa = thenoyl trifluoroacetylacetonato, tffa = trifluorofurylacetylacetonato, ntfa = naphtyltrifluoro acetylacetonato, btfa = benzoyltrifluoroacetonato, hfaa = hexafluoroacetylacetonato and 3Cl-acac = 3-chloroacetylacetonato) were discussed and compared with regard to the intimate geometric environment around the niobium(V) metal centre. And finally, the in-depth characterization relating to the solid state *tris*- and *tetrakis*-coordination modes of three M(V)-tropolonato (Trop) complexes, $[NbO(Trop)_3]$, $[Ta(Trop)_4Cl]$ and $[Nb(Trop)_4Cl]$ was effective in relating solid-state coordination preferences with complex stability in solution.

To further evaluate the electronic environment experienced by the niobium(V) and tantalum(V) centres in these complexes, a kinetic study of the substitution reactions of $[NbCl_6]^-$ and $[TaCl_6]^-$ with a range of *β*-diketones as entering ligand was undertaken. The data reported from this study could be used in a systematic way to successfully derive an overall reaction mechanism and rate law, which accounts for all current experimental observations. It was also found that for a specific ligand, at fixed $[Cl^-]_{free}$ and $[H_2O]_{free}$ values, the first term in of the complicated rate law could actually be simplified to a constant value, defined by k_{fwd}. From the obtained results and observations noted during this study, by using this equation, various previously unknown chemical characteristics for these systems such as enhancement of reaction rates by hydrolization could be quantified.

Additionally, a relationship could also be established between the pK_a of the uncoordinated *β*-diketonato entering ligands and the rate of ligand substitution. These substitution rates were seen to increase significantly as the pK_a of the free ligand was decreased. This was ascribed to a decrease in electron density at the metal centre, which causes it to be more prone to nucleophilic attack. It was seen that the four order-of-magnitude increase in Bronsted basicity of the free bidentate ligands results in an eight and six times decrease in substitution reactivity at the Nb(V) and Ta(V) centres respectively.

This investigation concluded by comparing different properties associated with the niobium(V)- and tantalum(V) complexes and relating those properties to the changes that were introduced in each complex by using different coordinating *β*-diketonato ligands. Several trends were noted as a result of the differing electronic properties of the various *β*-diketonate ligands.

It was noted that as more electron-donating substituents (higher pK_a) are encountered on the acac backbone of the complex causes a substantial influence on the oxido, *trans* effect of the compounds, as well as seemingly causing an increase in intermolecular hydrogen bonding interactions. In contrast, as electron-withdrawing capabilities of the substituents on the *β*-diketonate ligand are increased more electron density will be encountered within the periphery of this ligand. This in turn decreases the amount of intermolecular hydrogen bonding interactions, which seems to impact the sublimation properties of the compounds. If all of these fragments of information are combined it was found that by increasing electron-donation capabilities of the *β*-diketonate substituent, improved recovery of niobium can be expected from sublimation separation studies.

All of these observations give a better insight into the properties that govern the chemical and physical properties of these systems. These deductions that have been discussed, are only a proof of concept regarding the significance of a study to elucidate the intimate geometric nature and characteristics of Nb(V)- and Ta(V) coordination with organic ligands for separation purposes.

Opsomming

Niobium en tantaal, chemiese tweeling van die vanadium drietal van die periodieke tabel, is berug daarvoor dat skeiding tussen die twee en vanuit hulle natuurlike ertse besonder moeilik is danksy hulle amper identiese chemiese eienskappe. Die belangrikheid van die skeiding van hierdie twee elemente lê in die waarde en toepassing van hierdie elemente in verskillende velde van gebruik, veral in die kern bedryf. Niobium, met sy hoë smeltpunt, sterkte, weerstandseienskappe teen chemiese aanval en die lae neutron absorpsie deursnee (NAD) is ideaal vir gebruik as bekleding materiaal in beheerstawe van kernreaktore om lekkasie van kernreaktiewe materiaal te voorkom wanneer dit met sirkonium gelegeer is. Daarenteen het tantaal 'n baie meer beperkte toepassing in die kernnywerheid. Dit word grotendeels in kombinasie met koolstof gebruik om tantaalkarbied te vorm wat as voeringsagent binne die kernreaktor gebruik word weens die roesweerstand van tantaal. Aangesien tantaal en niobium altyd saam in mineraalerts gevind word, word tantaal as "besoedeling" beskou deur kernchemici. 'n Effektiewe skeidingsmetode word dus vereis aangesien selfs die kleinste onsuiwerheid van een metaal in die ander die vermoë van die metaal om sy funksie in die kernreaktor te verrig ernstig sal belemmer.

Die hoofdoel van hierdie studie was om insig in te win rakende die koördinering en kinetiese gedrag van Nb(V)- en Ta(V)-tropolonato en -asetielasetonato komplekse. 'n Breedvoerige beskrywing van die sintese van tien niobium(V) en agt tantaal(V) komplekse met die twee ligandfamilies (*O,O'*-skenkend) word gerapporteer; die komplekse is gekarakteriseer deur middel van IR, UV/Vis en KMR (^{1}H, ^{13}C, ^{19}F) spektroskopie. Daarbenewens het die vaste toestand struktuurkarakterisering deur middel van enkelkristal X-straal diffraksie elf van hierdie vervaardigde verbindings opgelewer en dit word breedvoerig in drie afdelings bespreek.

Die oorspronklike fokus van hierdie kristallografiese ondersoek was die karakterisering van die meer robuuste Nb(V)- en Ta(V) sintone, $(NEt_4)[NbCl_6]$ en

(NEt_4)[$TaCl_6$], en die faktore wat hulle stabiliteit vir koördineringsdoeleindes beheer. Tweedens is ses vaste toestand kristalstrukture Nb(V)-*β*-diketonate - (NEt_4)[$NbOCl_3$(ttfa)], (NEt_4)[$NbOCl_3$(tffa)], (NEt_4)[$NbOCl_3$(ntfa)], (NEt_4)[$NbOCl_3$(btfa)], (NEt_4)[$NbOCl_3$(hffa)] en (NEt_4)[$NbOCl_3$(3Cl-acac)] (waar ttfa = tenoïel trifluoroasetielasetonato, tffa = trifluorofurielasetielasetonato, ntfa = naftieltrifluoro asetielasetonato, btfa = bensoïeltrifluoroasetonato, hfaa = heksafluoroasetiel-asetonato en 3Cl-acac = 3-chloroasetielasetonato) - bespreek en vergelyk met betrekking tot die intieme geometriese omgewing rondom die niobium(V) metaalkern. Laastens was die diepgaande karakterisering met betrekking tot die vaste toestand *tris*- en *tetrakis*- koördineringsmodusse van drie M(V)-tropolonato (Trop) komplekse, [$NbO(Trop)_3$], [$Ta(Trop)_4Cl$] en [$Nb(Trop)_4Cl$], effektief daarin om die verband tussen vastetoestand koördinasievoorkeure en kompleks stabiliteit in oplossing daar te stel.

Ten einde die elektroniese omgewing wat deur die niobium(V) en tantaal(V) kerne in hierdie komplekse ervaar word verder te evalueer is 'n kinetiese studie van die substitusie reaksies van $[NbCl_6]^-$ en $[TaCl_6]^-$ met 'n reeks *β*-diketone in inkomende ligande onderneem. Die data wat uit hierdie studie verkry is kon sistematies gebruik word om 'n algehele reaksie meganisme en tempowet af te lei wat alle huidige eksperimentele waarnemings verklaar. Dit is ook gevind dat die eerste term in die ingewikkelde tempowet vereenvoudig kon word na 'n konstante waarde, gedefinieer deur k_{fwd}, vir 'n spesifieke ligand teen vasgestelde $[Cl^-]_{vry}$ en $[H_2O]_{vry}$ waardes. Vanuit die verkrygde resultate en waarnemings aangeteken gedurende studie kan, deur hierdie vergelyking te gebruik, verskeie voorheen onbekende chemiese eienskappe vir hierdie stelsels, soos die bevordering van reaksiesnelhede deur hidrolisering, gekwantifiseer word.

Bykomend hiertoe kon 'n verband tussen die pK_a van die ongekoördineerde *β*-diketonato inkomende ligande en die tempo van ligandsubstitusie ook vasgestel word. Hierdie substitusietempo's neem merkbaar toe wanneer die pK_a van die vry ligand verlaag word. Dit kan toegeskryf word aan die afname in elektrondigtheid by die metaalkern, wat veroorsaak dat die metaal meer vatbaar is vir nukleofiliese

aanval. Die vier orde-groottes toename in Brønsted basisiteit van die vry bidentate ligande lei tot ŉ agt en ses maal afname in substitusie reaktiwiteit by die Nb(V) en Ta(V) kerne onderskeidelik.

Hierdie ondersoek is afgesluit deur die verskillende eienskappe wat aan niobium(V) en tantaal(V) komplekse gekoppel word te vergelyk, en daardie eienskappe in verband te bring met veranderinge wat in elke kompleks teweeg gebring is deur verskillende koördinerende *β*-diketonato ligande te gebruik. Verskeie tendense is waargeneem as gevolg van die verskillende elektroniese eienskappe van die onderskeie *β*-diketonato ligande.

Dit was opgemerk dat meer elektronskenkende substituente (hoër pK_a) op die acac ruggraat van die kompleks lei tot ŉ beduidende invloed op die oksido, *trans* effek van die verbindings, asook ŉ skynbare toename in intermolekulêre waterstofbindingsinter-aksies. In teenstelling hiermee word meer elektrondigtheid binne die rand van die *β*-diketonato ligand aangetref wanneer die elektrononttrekkende vermoë van die substituente op die ligand toeneem. Dit verminder weer die hoeveelheid intermolekulêre waterstof bindingsinteraksies, wat blyk ŉ impak op die sublimasie-eienskappe van die verbindings te hê. Indien al hierdie brokkies inligting saamgevoeg word kan dit dus afgelei word dat verbeterde herwinning van niobium uit sublimasiestudies verwag kan word deur die elektronskenkende vermoë van die *β*-diketonato substituente te verhoog.

Al hierdie waarnemings lei tot beter insigte rakende die eienskappe wat die chemiese en fisiese eienskappe van hierdie stelsels beheer. Die afleidings wat hier bespreek is, is slegs ŉ bewys van die begrip rakende die belangrikheid van ŉ studie om die intieme geometriese natuur en eienskappe van Nb(V)- en Ta(V) koördinering met organiese ligande vir skeidingsdoeleindes toe te lig.

Sleutelwoorde: niobium(V); tantaal(V); sintese; kristallografiese karaktirisering; *β*-diketoon; tropoloon; kinetiese meganistiese studie; sublimasie; pK_a.

Supplementary Crystallographic Geometric Data

A1 Supplementary Geometric Data for Tetraethylammonium hexachloridoniobate(V); ($(Et_4N)[NbCl_6]$, (Nb_1))

Table A1.1 Atomic coordinates (x 10^4) and equivalent isotropic displacement parameters ($Å^2$ x 10^3) for **Nb_1**.

	x	y	z	U(eq)
Nb(1)	0	5000	5000	35(1)
Cl(1)	-783(1)	6128(1)	6377(1)	67(1)
Cl(2)	3407(1)	5662(1)	5937(1)	50(1)
Cl(3)	-764(1)	6897(1)	3831(1)	59(1)
N(1)	5000	0	5000	39(1)
C(1)	3563(8)	-693(5)	3920(4)	41(1)
C(2)	4110(40)	-2080(20)	3745(16)	50(3)
C(3)	7216(9)	-85(5)	5036(5)	47(1)
C(4)	7450(20)	457(12)	4029(11)	59(3)
C(1)'	5620(8)	-1394(5)	5051(4)	41(1)
C(2)'	4420(30)	-2240(20)	4004(14)	50(3)
C(3)'	4870(9)	705(5)	3930(4)	48(1)
C(4)'	6833(17)	700(11)	3763(11)	55(3)

Table A1.2 Anisotropic displacement parameters ($Å^2 \times 10^3$) for **Nb_1**.

	U^{11}	U^{22}	U^{33}	U^{23}	U^{13}	U^{12}
Nb(1)	41(1)	33(1)	28(1)	0(1)	10(1)	-1(1)
Cl(1)	68(1)	85(1)	48(1)	-19(1)	23(1)	9(1)
Cl(2)	43(1)	53(1)	45(1)	4(1)	9(1)	-8(1)
Cl(3)	57(1)	49(1)	60(1)	22(1)	12(1)	-1(1)
N(1)	44(2)	32(1)	30(2)	4(1)	6(1)	2(1)
C(1)	41(3)	46(3)	28(2)	1(2)	8(2)	-1(2)
C(2)	60(7)	31(5)	49(7)	-2(5)	13(5)	-6(4)
C(3)	39(3)	42(3)	52(3)	-7(2)	10(3)	2(2)
C(4)	64(7)	54(6)	70(8)	1(5)	37(6)	-1(5)
C(1)'	47(3)	35(2)	37(3)	7(2)	13(2)	12(2)
C(2)'	59(8)	35(5)	59(8)	-1(5)	28(6)	-3(5)
C(3)'	69(4)	36(2)	32(3)	7(2)	12(2)	0(3)
C(4)'	75(8)	43(5)	46(4)	11(3)	23(5)	-6(4)

Table A1.3 Bond lengths [Å] for **Nb_1**.

Bond	Bond length [Å]
Nb(1)-Cl(1)’	2.342(1)
Nb(1)-Cl(1)	2.342(1)
Nb(1)-Cl(2)	2.348(2)
Nb(1)-Cl(2)’	2.348(2)
Nb(1)-Cl(3)’	2.355(1)
Nb(1)-Cl(3)	2.355(1)
N(1)-C(1)’	1.478(5)
N(1)-C(1)	1.478(5)
N(1)-C(2)’	1.511(5)
N(1)-C(2)	1.511(5)
N(1)-C(3)’	1.502(5)
N(1)-C(3)	1.502(5)
N(1)-C(4)	1.583(6)
N(1)-C(4)’	1.583(6)
C(2)-C(1)	1.500(2)
C(1')-C(2')	1.520(2)
C(4)-C(3)	1.462(2)
C(3)’-C(4)’	1.515(1)

Table A1.4 Bond angles [º] for **Nb_1**.

Bond	Bond angle [º]
Cl(1)'-Nb(1)-Cl(1)	180.0
Cl(1)'-Nb(1)-Cl(2)	89.73(4)
Cl(1)-Nb(1)-Cl(2)	90.27(4)
Cl(1)'-Nb(1)-Cl(2)'	90.27(4)
Cl(1)-Nb(1)-Cl(2)'	89.73(4)
Cl(2)-Nb(1)-Cl(2)'	180.0
Cl(1)'-Nb(1)-Cl(3)'	90.16(4)
Cl(1)-Nb(1)-Cl(3)'	89.84(4)
Cl(2)-Nb(1)-Cl(3)'	89.37(3)
Cl(2)'-Nb(1)-Cl(3)'	90.63(3)
Cl(1)'-Nb(1)-Cl(3)	89.84(4)
Cl(1)-Nb(1)-Cl(3)	90.16(4)
Cl(2)-Nb(1)-Cl(3)	90.63(3)
Cl(2)'-Nb(1)-Cl(3)	89.37(3)
Cl(3)'-Nb(1)-Cl(3)	180.0
C(1)'-N(1)-C(1)	180.0(4)
C(1')'-N(1)-C(3')'	113.7(3)
C(1')-N(1)-C(3')'	66.3(3)
C(1')'-N(1)-C(3')	66.3(3)
C(1')-N(1)-C(3')	113.7(3)
C(3')'-N(1)-C(3')	180.0
C(1)'-N(1)-C(1)	180.0
C(1)'-N(1)-C(3)	71.9(3)
C(1)-N(1)-C(3)	108.1(3)
C(1)'-N(1)-C(3)'	108.1(3)
C(1)-N(1)-C(3)'	71.9(3)
C(3)-N(1)-C(3)'	180.0
N(1)-C(1)-C(2)	116.6(8)

A2 Supplementary Geometric Data for Tetraethylammonium hexachloridotantalate(V); ($(Et_4N)[TaCl_6]$, (Ta_1))

Table A2.1 Atomic coordinates (x 10^4) and equivalent isotropic displacement parameters ($Å^2$ x 10^3) for **Ta_1**.

	x	y	z	U(eq)
Ta	0	0	5000	16(1)
Cl(1)	349(1)	-1940(1)	6155(1)	29(1)
Cl(2)	2473(1)	-692(1)	4022(1)	23(1)
Cl(3)	2182(1)	1107(1)	6376(1)	32(1)
N(1)	5000	5000	5000	23(1)
C(1)	2775(10)	4888(5)	5060(6)	22(1)
C(1A)	4121(9)	5705(6)	3918(5)	21(1)
C(2)	1542(16)	5479(12)	4021(9)	22(2)
C(2A)	2007(17)	5689(13)	3756(11)	27(2)
C(3)	5352(9)	4289(6)	3908(5)	21(1)
C(3A)	4471(9)	3592(7)	5069(4)	23(1)
C(4)	4647(15)	2739(11)	4000(7)	23(1)
C(4A)	4653(15)	2879(10)	3729(7)	21(1)

Table A2.2 Anisotropic displacement parameters ($Å^2$ x 10^3) for **Ta_1**.

	U^{11}	U^{22}	U^{33}	U^{23}	U^{13}	U^{12}
Ta	19(1)	16(1)	14(1)	0(1)	3(1)	0(1)
Cl(2)	24(1)	26(1)	21(1)	2(1)	7(1)	4(1)
Cl(1)	38(1)	23(1)	28(1)	10(1)	13(1)	7(1)
Cl(3)	30(1)	42(1)	24(1)	-11(1)	1(1)	-9(1)
N(1)	32(2)	18(2)	18(2)	1(1)	7(2)	4(2)
C(1A)	36(4)	13(3)	14(3)	1(2)	4(2)	2(3)
C(2A)	40(7)	26(5)	15(5)	4(3)	10(4)	5(5)
C(4)	25(2)	20(2)	24(3)	6(2)	7(2)	4(2)
C(1)	23(3)	26(3)	19(3)	1(2)	10(3)	-1(3)
C(3)	26(2)	20(2)	18(2)	0(2)	8(2)	4(2)
C(3A)	25(2)	20(2)	24(3)	6(2)	7(2)	4(2)
C(2)	28(5)	17(5)	22(6)	-1(4)	7(4)	6(4)
C(4A)	26(2)	20(2)	18(2)	0(2)	8(2)	4(2)

Table A2.3 Bond lengths [Å] for **Ta_1**.

Bond	Bond length [Å]
Ta-Cl(1)	2.353(1)
Ta-Cl(1)'	2.353(1)
Ta-Cl(2)	2.345(1)
Ta-Cl(2)'	2.345(1)
Ta-Cl(3)	2.343(1)
Ta-Cl(3)'	2.343(1)
N(1)-C(1)	1.608(7)
N(1)-C(1)'	1.608(7)
N(1)-C(1A)	1.498(5)
N(1)-C(1A)'	1.498(5)
N(1)-C(3)	1.509(5)
N(1)-C(3)'	1.509(5)
N(1)-C(3A)	1.465(7)
N(1)-C(3A)'	1.465(7)
C(1)-C(2)	1.508(1)
C(1A)-C(2A)	1.497(1)
C(3)-C(4A)	1.502(1)
C(4)-C(3A)	1.529(1)

Table A2.4 Bond angles [º] for **Ta_1**.

Bond	Bond angle [º]
Cl(1)'-Ta-Cl(1)	180.00(4)
Cl(2)'-Ta-Cl(1)	89.47(3)
Cl(2)-Ta-Cl(1)	90.53(3)
Cl(2)-Ta-Cl(1)'	89.47(3)
Cl(2)'-Ta-Cl(1)'	90.53(3)
Cl(2)-Ta-Cl(2)'	180.00(3)
Cl(3)-Ta-Cl(1)	89.79(4)
Cl(3)-Ta-Cl(1)'	90.21(4)
Cl(3)'-Ta-Cl(1)	90.21(4)
Cl(3)-Ta-Cl(2)	89.81(5)
Cl(3)'-Ta-Cl(2)	90.19(5)
Cl(3)-Ta-Cl(2)'	90.19(5)
Cl(3)'-Ta-Cl(2)'	89.81(5)
Cl(3)'-Ta-Cl(1)'	89.79(4)
Cl(3)-Ta-Cl(3)'	180.0
C(3A)-N(1)-C(3A)'	180.0(5)
C(1A)'-N(1)-C(1A)	180.0(5)
C(3)'-N(1)-C(3)	180.0
C(1)-N(1)-C(1)'	180.0
C(2A)-C(1A)-N(1)	113.1(5)
C(2)-C(1)-N(1)	113.8(5)
C(4A)-C(3)-N(1)	117.8(5)

A3 Supplementary Geometric Data for Tetraethylammonium *mer*-trichloridooxido(thenoyltrifluoroacetylacetonato-κ^2O,O') niobate(V); ((NEt_4) $[NbOCl_3(ttfa)]$), (Nb_2))

Table A3.1 Atomic coordinates (x 10^4) and equivalent isotropic displacement parameters ($Å^2$ x 10^3) for **Nb_2**.

	x	y	z	U(eq)
Nb(1)	7877(2)	2413(1)	5430(1)	24(1)
Cl(1)	6756(4)	1288(4)	4408(2)	57(1)
Cl(2)	6335(6)	3817(7)	5372(5)	42(1)
Cl(3)	9138(5)	805(5)	5631(5)	48(1)
F(1)	10171(6)	3818(12)	7736(5)	100(3)
F(2)	8888(12)	5017(8)	7584(6)	131(4)
F(3)	8994(9)	3881(9)	8507(4)	105(3)
S(1)	5473(6)	-146(8)	6855(6)	59(1)
O(1)	7020(20)	1510(20)	6361(12)	43(2)
O(2)	8564(16)	3263(17)	6452(11)	39(2)
O(3)	8430(8)	3268(12)	4782(7)	34(1)
C(1)	9121(9)	3905(10)	7744(6)	49(2)
C(2)	8390(17)	3013(19)	7274(11)	38(3)
C(3)	7688(10)	2512(13)	7556(9)	29(2)
C(4)	7000(40)	1650(40)	7087(19)	30(2)
C(5)	6211(15)	945(16)	7483(10)	33(2)
C(6)	5873(11)	1210(9)	8133(9)	29(2)
C(7)	5142(16)	320(20)	8202(10)	51(3)
C(8)	4845(17)	-460(20)	7715(12)	51(3)
Nb(1')	7833(2)	2391(2)	5429(1)	37(1)
Cl(2')	6728(3)	1309(3)	4396(1)	32(1)
Cl(3')	6373(6)	3688(7)	5477(6)	56(2)

Cl(4')	9083(5)	858(6)	5764(6)	62(2)
F(1')	10237(5)	3470(8)	7822(5)	83(2)
F(2')	9225(7)	4931(6)	7539(4)	77(2)
F(3')	9138(8)	3797(8)	8560(4)	82(2)
S(1')	5507(6)	-214(7)	6916(6)	64(2)
O(1')	6969(18)	1360(20)	6279(10)	37(2)
O(2')	8574(14)	3070(16)	6532(10)	35(2)
O(3')	8651(8)	3246(12)	4926(6)	32(1)
C(1')	9246(8)	3872(8)	7838(6)	48(2)
C(2')	8447(14)	3136(16)	7186(11)	29(2)
C(3')	7733(13)	2288(13)	7509(9)	36(3)
C(4')	6980(40)	1540(40)	7002(18)	30(2)
C(5')	6230(15)	909(17)	7367(9)	30(2)
C(6')	5999(10)	945(8)	8183(8)	27(2)
C(7')	5123(12)	228(17)	8339(9)	38(2)
C(8')	4800(20)	-460(20)	7569(12)	58(4)
N(1)	7712(3)	7799(4)	9571(3)	41(1)
C(9)	7832(6)	6788(7)	9056(3)	61(1)
C(10)	7864(4)	8991(4)	9169(4)	50(1)
C(11)	6592(4)	7825(5)	9759(3)	61(1)
C(12)	8612(3)	7674(3)	10314(2)	55(1)
C(13)	7059(7)	6825(9)	8246(6)	121(3)
C(14)	8905(6)	9121(7)	8899(6)	91(2)
C(15)	6296(5)	6780(5)	10220(4)	95(2)
C(16)	8631(3)	8616(3)	10931(2)	90(1)
N(1')	7850(40)	7940(40)	9640(30)	45(5)
C(9')	7790(40)	6730(50)	8860(30)	50(7)
C(10')	7740(40)	8760(40)	9150(30)	43(5)
C(11')	6610(50)	8040(40)	9940(30)	60(7)
C(12')	8820(30)	7670(40)	10040(30)	83(8)

C(13')	7230(50)	6720(50)	8190(30)	67(9)
C(14')	8970(30)	9270(50)	8920(30)	46(7)
C(15')	6330(60)	6990(50)	10570(30)	100(14)
C(16')	10190(40)	8510(60)	10230(50)	230(30)

Table A3.2 Anisotropic displacement parameters ($Å^2 \times 10^3$) for **Nb_2**.

	U^{11}	U^{22}	U^{33}	U^{23}	U^{13}	U^{12}
Nb(1)	23(1)	23(1)	26(1)	-1(1)	6(1)	-9(1)
Cl(2)	66(2)	40(2)	60(2)	-8(2)	0(2)	-1(2)
Cl(3)	44(1)	35(1)	49(1)	-4(1)	17(1)	7(1)
Cl(4)	43(1)	47(1)	54(2)	7(1)	6(1)	12(1)
F(1)	58(4)	168(8)	82(4)	-62(4)	28(3)	-65(3)
F(2)	174(9)	55(3)	133(5)	-28(3)	-51(5)	-21(4)
F(3)	120(6)	166(7)	40(3)	-60(3)	42(4)	-100(5)
S(1)	58(2)	77(3)	46(2)	-19(1)	21(1)	-43(2)
O(1)	55(3)	44(4)	30(4)	-12(3)	8(3)	-29(2)
O(2)	54(3)	38(5)	25(3)	4(3)	7(2)	-22(3)
O(3)	25(3)	40(2)	31(3)	6(2)	-7(2)	-3(2)
C(1)	47(4)	82(5)	19(3)	-3(3)	8(3)	-20(3)
C(2)	46(5)	47(6)	19(3)	-2(4)	4(3)	-13(3)
C(3)	31(3)	28(5)	26(3)	-12(2)	3(2)	-13(2)
C(4)	35(1)	33(5)	24(5)	-4(3)	6(4)	-8(3)
C(5)	33(3)	32(3)	35(6)	-3(4)	5(3)	-17(2)
C(6)	37(3)	16(4)	33(3)	13(3)	7(2)	4(3)
C(7)	64(4)	63(6)	31(5)	16(4)	23(3)	-6(3)
C(8)	44(4)	59(5)	51(6)	11(4)	17(4)	-22(3)
Nb(1')	41(1)	46(1)	23(1)	2(1)	8(1)	7(1)
Cl(2')	35(1)	39(2)	19(1)	-5(1)	-3(1)	-4(1)
Cl(3')	55(1)	48(2)	68(3)	-3(2)	21(1)	19(1)
Cl(4')	53(1)	68(2)	62(3)	18(2)	2(1)	27(1)
F(1')	46(2)	103(4)	84(3)	6(3)	-27(2)	-10(2)
F(2')	106(4)	53(3)	57(3)	8(2)	-23(2)	-44(2)
F(3')	84(3)	121(5)	33(2)	4(3)	-9(2)	-63(3)
S(1')	76(3)	57(2)	61(3)	-20(2)	18(2)	-32(2)

O(1')	47(3)	44(5)	20(3)	-9(3)	10(2)	-22(3)
O(2')	39(2)	41(5)	24(3)	5(3)	6(2)	-22(3)
O(3')	21(3)	45(2)	27(3)	6(2)	-2(2)	-5(2)
C(1')	49(4)	49(3)	37(4)	-2(3)	-14(3)	-31(3)
C(2')	28(3)	30(3)	29(4)	5(3)	8(3)	-16(2)
C(3')	56(4)	30(5)	26(3)	-7(3)	17(2)	-12(3)
C(4')	35(1)	33(5)	24(5)	-4(3)	6(4)	-8(3)
C(5')	39(3)	40(3)	12(2)	-3(2)	9(2)	-3(2)
C(6')	35(3)	17(4)	28(2)	11(3)	2(2)	2(3)
C(7')	39(3)	51(3)	26(4)	19(3)	16(3)	-15(2)
C(8')	59(5)	59(5)	56(7)	-2(5)	9(4)	-30(4)
N(1)	35(1)	32(2)	58(2)	2(2)	10(1)	2(1)
C(9)	63(2)	50(2)	71(3)	-19(2)	13(2)	1(2)
C(10)	45(2)	37(2)	69(2)	10(2)	14(2)	0(2)
C(11)	47(2)	46(2)	96(4)	6(2)	33(2)	8(2)
C(12)	56(2)	49(1)	57(2)	5(1)	4(1)	8(1)
C(13)	120(6)	115(5)	110(5)	-49(4)	-23(4)	6(4)
C(14)	82(4)	75(3)	131(6)	22(3)	56(4)	-6(3)
C(15)	87(3)	71(3)	147(6)	29(3)	70(4)	1(2)
C(16)	118(3)	77(2)	66(2)	-16(2)	-10(2)	3(2)
N(1')	51(9)	24(7)	68(9)	-35(6)	31(7)	-7(8)
C(9')	46(13)	37(10)	77(14)	-43(12)	36(10)	-4(9)
C(10')	28(8)	33(10)	77(12)	-18(8)	32(8)	-24(8)
C(11')	73(11)	42(13)	87(15)	-18(10)	72(11)	-8(10)
C(12')	73(10)	92(16)	80(16)	-19(13)	5(12)	-1(11)
C(13')	89(19)	66(17)	56(12)	-37(13)	41(11)	20(14)
C(14')	18(10)	65(16)	65(18)	-19(12)	28(10)	0(9)
C(15')	140(30)	80(20)	100(30)	15(19)	70(20)	-10(20)
C(16')	100(20)	270(60)	280(60)	0(50)	-50(40)	-70(30)

Table A3.3 Bond lengths [Å] for **Nb_2**.

Bond	Bond length [Å]
Nb(1)-O(3)	1.721(13)
Nb(1)-O(2)	2.05(2)
Nb(1)-O(1)	2.33(2)
Nb(1)-Cl(2)	2.405(5)
Nb(1)-Cl(4)	2.415(7)
Nb(1)-Cl(3)	2.508(8)
F(1)-C(1)	1.325(9)
F(2)-C(1)	1.328(10)
F(3)-C(1)	1.345(8)
S(1)-C(5)	1.791(16)
S(1)-C(8)	1.83(2)
O(1)-C(4)	1.26(3)
O(2)-C(2)	1.49(3)
C(1)-C(2)	1.50(2)
C(2)-C(3)	1.23(2)
C(3)-C(4)	1.46(3)
C(4)-C(5)	1.53(4)
C(5)-C(6)	1.30(2)
C(6)-C(7)	1.39(2)
C(7)-C(8)	1.23(3)
Nb(1')-O(3')	1.758(12)
Nb(1')-O(2')	2.092(19)
Nb(1')-O(1')	2.30(2)
Nb(1')-Cl(4')	2.357(7)
Nb(1')-Cl(3')	2.376(9)
Nb(1')-Cl(2')	2.381(3)
F(1')-C(1')	1.333(10)
F(2')-C(1')	1.317(8)
F(3')-C(1')	1.271(9)
S(1')-C(8')	1.57(2)
S(1')-C(5')	1.680(17)
O(1')-C(4')	1.25(3)

O(2')-C(2')	1.16(3)
C(1')-C(2')	1.596(19)
C(2')-C(3')	1.50(2)
C(3')-C(4')	1.44(3)
C(4')-C(5')	1.43(4)
C(5')-C(6')	1.479(19)
C(6')-C(7')	1.439(17)
C(7')-C(8')	1.52(3)
N(1)-C(9)	1.482(8)
N(1)-C(11)	1.502(7)
N(1)-C(12)	1.541(6)
N(1)-C(10)	1.560(7)
C(9)-C(13)	1.536(12)
C(10)-C(14)	1.474(9)
C(11)-C(15)	1.520(8)
C(12)-C(16)	1.508(5)
N(1')-C(10')	1.26(7)
N(1')-C(12')	1.32(6)
N(1')-C(11')	1.73(7)
N(1')-C(9')	1.91(6)
C(9')-C(13')	1.23(9)
C(10')-C(14')	1.76(6)
C(11')-C(15')	1.69(8)
C(12')-C(16')	1.95(6)

Table A3.4 Bond angles [º] for **Nb_2**.

Bond	Bond angle [º]
O(3)-Nb(1)-O(2)	97.0(6)
O(3)-Nb(1)-O(1)	171.7(8)
O(2)-Nb(1)-O(1)	78.6(6)
O(3)-Nb(1)-Cl(2)	95.2(4)
O(2)-Nb(1)-Cl(2)	166.6(5)
O(1)-Nb(1)-Cl(2)	88.6(5)
O(3)-Nb(1)-Cl(4)	101.2(5)
O(2)-Nb(1)-Cl(4)	94.7(6)
O(1)-Nb(1)-Cl(4)	86.2(7)
Cl(2)-Nb(1)-Cl(4)	88.4(2)
O(3)-Nb(1)-Cl(3)	90.6(5)
O(2)-Nb(1)-Cl(3)	85.7(6)
O(1)-Nb(1)-Cl(3)	82.2(7)
Cl(2)-Nb(1)-Cl(3)	88.54(19)
Cl(4)-Nb(1)-Cl(3)	168.0(3)
C(5)-S(1)-C(8)	84.7(9)
C(4)-O(1)-Nb(1)	136(2)
C(2)-O(2)-Nb(1)	126.9(12)
F(1)-C(1)-F(2)	104.6(8)
F(1)-C(1)-F(3)	108.0(9)
F(2)-C(1)-F(3)	99.1(9)
F(1)-C(1)-C(2)	116.8(12)
F(2)-C(1)-C(2)	117.1(13)
F(3)-C(1)-C(2)	109.5(10)
C(3)-C(2)-O(2)	134.9(18)
C(3)-C(2)-C(1)	121.3(16)
O(2)-C(2)-C(1)	101.0(13)
C(2)-C(3)-C(4)	120(2)

O(1)-C(4)-C(3)	121(3)
O(1)-C(4)-C(5)	121(2)
C(3)-C(4)-C(5)	119(2)
C(6)-C(5)-C(4)	126.7(17)
C(6)-C(5)-S(1)	117.5(11)
C(4)-C(5)-S(1)	114.1(14)
C(5)-C(6)-C(7)	103.2(13)
C(8)-C(7)-C(6)	126.6(17)
C(7)-C(8)-S(1)	106.2(14)
O(3')-Nb(1')-O(2')	91.8(5)
O(3')-Nb(1')-O(1')	170.2(6)
O(2')-Nb(1')-O(1')	78.7(6)
O(3')-Nb(1')-Cl(4')	96.4(4)
O(2')-Nb(1')-Cl(4')	84.0(6)
O(1')-Nb(1')-Cl(4')	80.5(7)
O(3')-Nb(1')-Cl(3')	101.1(5)
O(2')-Nb(1')-Cl(3')	87.2(6)
O(1')-Nb(1')-Cl(3')	80.8(7)
Cl(4')-Nb(1')-Cl(3')	160.5(4)
O(3')-Nb(1')-Cl(2')	104.0(4)
O(2')-Nb(1')-Cl(2')	164.2(4)
O(1')-Nb(1')-Cl(2')	85.6(4)
Cl(4')-Nb(1')-Cl(2')	93.4(2)
Cl(3')-Nb(1')-Cl(2')	90.4(2)
C(8')-S(1')-C(5')	97.9(10)
C(4')-O(1')-Nb(1')	128.4(19)
C(2')-O(2')-Nb(1')	140.8(13)
F(3')-C(1')-F(2')	116.2(8)
F(3')-C(1')-F(1')	105.5(8)
F(2')-C(1')-F(1')	105.2(7)

F(3')-C(1')-C(2')	118.4(9)
F(2')-C(1')-C(2')	104.7(10)
F(1')-C(1')-C(2')	105.7(10)
O(2')-C(2')-C(3')	120.9(16)
O(2')-C(2')-C(1')	121.7(13)
C(3')-C(2')-C(1')	115.3(13)
C(4')-C(3')-C(2')	122.2(18)
O(1')-C(4')-C(5')	118(2)
O(1')-C(4')-C(3')	126(3)
C(5')-C(4')-C(3')	117(2)
C(4')-C(5')-C(6')	131.6(16)
C(4')-C(5')-S(1')	122.4(14)
C(6')-C(5')-S(1')	105.7(10)
C(7')-C(6')-C(5')	116.8(12)
C(6')-C(7')-C(8')	102.8(13)
C(7')-C(8')-S(1')	115.5(14)
C(9)-N(1)-C(11)	110.4(5)
C(9)-N(1)-C(12)	106.1(4)
C(11)-N(1)-C(12)	113.3(4)
C(9)-N(1)-C(10)	113.0(5)
C(11)-N(1)-C(10)	105.9(4)
C(12)-N(1)-C(10)	108.2(4)
N(1)-C(9)-C(13)	113.4(6)
C(14)-C(10)-N(1)	114.6(5)
N(1)-C(11)-C(15)	115.2(4)
C(16)-C(12)-N(1)	115.1(3)
C(10')-N(1')-C(12')	120(5)
C(10')-N(1')-C(11')	99(4)
C(12')-N(1')-C(11')	131(5)
C(10')-N(1')-C(9')	95(4)

C(12')-N(1')-C(9')	96(3)
C(11')-N(1')-C(9')	109(3)
C(13')-C(9')-N(1')	127(5)
N(1')-C(10')-C(14')	114(4)
C(15')-C(11')-N(1')	117(4)
N(1')-C(12')-C(16')	132(5)

A4 Supplementary Geometric Data for Tetraethylammonium *mer*-trichlorido(furyltrifluoroacetylacetonato-κ^2O,O')oxidoniobate(V) ($(NEt_4)[NbOCl_3(tffa)]$), (Nb_3))

Table A4.1 Atomic coordinates (x 10^4) and equivalent isotropic displacement parameters ($Å^2$ x 10^3) for **Nb_3**.

	x	y	z	U(eq)
Nb(01)	2781(1)	2491(1)	409(1)	17(1)
Cl(2)	1249(1)	3873(1)	379(1)	30(1)
Cl(1)	4070(1)	875(1)	697(1)	28(1)
Cl(3)	1649(1)	1377(1)	-633(1)	24(1)
O(3)	3514(2)	3364(2)	-159(2)	22(1)
O(1)	3492(2)	3256(3)	1483(2)	24(1)
C(25)	6236(4)	2584(4)	-350(3)	30(1)
C(3)	2630(3)	2421(3)	2503(2)	22(1)
O(2)	1889(2)	1459(3)	1266(2)	24(1)
N(1)	7229(3)	2694(3)	341(2)	26(1)
C(8)	18(5)	-565(6)	2507(5)	68(2)
C(1)	4118(4)	3974(4)	2787(2)	28(1)
C(6)	990(3)	979(4)	3127(2)	26(1)
C(5)	1189(3)	837(3)	2374(2)	20(1)
O(4)	624(3)	-97(3)	1972(2)	50(1)
C(4)	1915(3)	1582(3)	2004(2)	19(1)
C(27)	7171(4)	3853(4)	802(3)	31(1)
C(2)	3343(3)	3150(4)	2214(2)	21(1)
C(23)	8328(4)	2741(4)	57(4)	44(1)
C(21)	7190(4)	1601(4)	866(3)	35(1)
C(7)	210(5)	52(7)	3190(4)	68(2)
C(22)	8069(6)	1574(6)	1631(4)	70(2)

C(28)	6147(5)	3999(5)	1155(4)	47(1)
C(26)	6155(6)	3584(5)	-966(4)	52(2)
C(24)	8528(5)	1696(5)	-482(5)	66(2)
F(1)	5238(18)	3660(20)	2777(9)	36(3)
F(2)	4001(19)	5130(20)	2577(16)	43(4)
F(3)	3960(30)	3950(30)	3550(20)	32(4)
F(1')	5050(40)	3920(70)	2750(20)	63(9)
F(2')	3770(70)	5090(50)	2580(30)	81(14)
F(3')	4080(50)	3720(60)	3520(30)	27(6)

Table A4.2 Anisotropic displacement parameters ($Å^2$ x 10^3) for **Nb_3**.

	U^{11}	U^{22}	U^{33}	U^{23}	U^{13}	U^{12}
Nb(01)	19(1)	20(1)	13(1)	1(1)	5(1)	1(1)
Cl(2)	25(1)	24(1)	45(1)	-5(1)	15(1)	5(1)
Cl(3)	26(1)	23(1)	22(1)	-3(1)	-1(1)	-1(1)
O(3)	17(1)	16(1)	34(2)	2(1)	5(1)	0(1)
O(1)	30(2)	28(1)	15(1)	-3(1)	6(1)	-13(1)
C(25)	33(2)	25(2)	31(2)	2(2)	5(2)	2(2)
C(3)	26(2)	25(2)	14(2)	-2(1)	4(1)	-5(2)
O(2)	29(2)	28(1)	16(1)	-1(1)	7(1)	-11(1)
N(1)	19(2)	19(2)	41(2)	2(1)	11(2)	-1(1)
C(8)	37(3)	56(4)	98(6)	51(4)	-17(3)	-25(3)
C(1)	35(2)	33(2)	18(2)	-1(2)	7(2)	-14(2)
C(6)	28(2)	37(2)	13(2)	5(2)	10(2)	7(2)
C(5)	19(2)	24(2)	16(2)	2(1)	3(1)	-4(1)
O(4)	54(2)	39(2)	50(2)	2(2)	-4(2)	-15(2)
C(4)	18(2)	22(2)	18(2)	1(1)	4(1)	-3(1)
C(27)	26(2)	23(2)	44(3)	-5(2)	7(2)	0(2)
C(2)	25(2)	24(2)	15(2)	-2(1)	4(1)	-5(2)
C(23)	26(2)	30(2)	85(4)	1(3)	31(3)	-1(2)
C(21)	30(2)	27(2)	46(3)	10(2)	0(2)	0(2)
C(7)	28(3)	114(6)	69(4)	73(4)	29(3)	25(3)
C(22)	73(5)	46(3)	72(4)	17(3)	-31(4)	-3(3)
C(28)	44(3)	43(3)	63(4)	-18(3)	29(3)	-5(2)
C(26)	70(4)	38(3)	45(3)	14(2)	3(3)	6(3)
C(24)	55(4)	40(3)	121(6)	-14(3)	59(4)	2(3)
F(1)	17(5)	64(6)	28(5)	-12(5)	4(3)	-8(4)

F(2)	66(8)	22(5)	33(5)	0(3)	-12(3)	-25(3)
F(3)	44(10)	36(9)	17(3)	-16(5)	13(5)	-19(6)
F(1')	17(11)	110(20)	66(13)	-60(13)	14(8)	-22(12)
F(2')	150(30)	42(11)	39(10)	-9(8)	-8(19)	-39(18)
F(3')	34(8)	37(17)	11(8)	-8(9)	6(6)	-9(10)

Table A4.3 Bond lengths [Å] for **Nb_3**.

Bond	Bond length [Å]
Nb(01)-O(3)	1.740(3)
Nb(01)-O(1)	2.045(3)
Nb(01)-O(2)	2.297(3)
Nb(01)-Cl(3)	2.369(1)
Nb(01)-Cl(1)	2.378(1)
Nb(01)-Cl(2)	2.420(1)
O(1)-C(2)	1.298(4)
C(25)-C(26)	1.518(7)
C(25)-N(1)	1.518(6)
C(3)-C(2)	1.354(5)
C(3)-C(4)	1.436(5)
O(2)-C(4)	1.256(5)
N(1)-C(21)	1.515(6)
N(1)-C(27)	1.519(5)
N(1)-C(23)	1.519(5)
C(8)-C(7)	1.328(1)
C(8)-O(4)	1.387(8)
C(1)-F(1')	1.16(5)
C(1)-F(3')	1.28(6)
C(1)-F(2)	1.33(2)
C(1)-F(2')	1.33(5)
C(1)-F(3)	1.36(3)
C(1)-F(1)	1.42(2)
C(1)-C(2)	1.524(5)

C(6)-C(5)	1.360(5)
C(6)-C(7)	1.424(8)
C(5)-O(4)	1.356(5)
C(5)-C(4)	1.449(5)
C(27)-C(28)	1.504(6)

Table A4.4 Bond angles [º] for **Nb_3**.

Bond	Bond angle [º]
O(3)-Nb(01)-O(1)	95.05(12)
O(3)-Nb(01)-O(2)	174.21(12)
O(1)-Nb(01)-O(2)	79.21(10)
O(3)-Nb(01)-Cl(3)	99.64(10)
O(1)-Nb(01)-Cl(3)	165.08(8)
O(2)-Nb(01)-Cl(3)	86.05(8)
O(3)-Nb(01)-Cl(1)	98.19(9)
O(1)-Nb(01)-Cl(1)	89.11(9)
O(2)-Nb(01)-Cl(1)	82.61(8)
Cl(3)-Nb(01)-Cl(1)	91.32(4)
O(3)-Nb(01)-Cl(2)	96.71(9)
O(1)-Nb(01)-Cl(2)	86.75(9)
O(2)-Nb(01)-Cl(2)	82.27(9)
Cl(3)-Nb(01)-Cl(2)	88.98(4)
Cl(1)-Nb(01)-Cl(2)	164.82(4)
C(2)-O(1)-Nb(01)	134.5(2)
C(26)-C(25)-N(1)	113.9(4)
C(2)-C(3)-C(4)	122.4(4)
C(4)-O(2)-Nb(01)	131.3(2)
C(21)-N(1)-C(25)	106.0(3)
C(21)-N(1)-C(27)	111.6(4)
C(25)-N(1)-C(27)	110.8(3)
C(21)-N(1)-C(23)	110.5(4)
C(25)-N(1)-C(23)	112.3(4)
C(27)-N(1)-C(23)	105.7(3)
C(7)-C(8)-O(4)	110.8(5)
F(1')-C(1)-F(3')	106(3)
F(1')-C(1)-F(2')	107(3)

F(3')-C(1)-F(2')	113(3)
F(2)-C(1)-F(3)	105(2)
F(2)-C(1)-F(1)	106.5(13)
F(3)-C(1)-F(1)	109.3(19)
F(1')-C(1)-C(2)	115(2)
F(3')-C(1)-C(2)	111(3)
F(2)-C(1)-C(2)	112.9(11)
F(2')-C(1)-C(2)	105(3)
F(3)-C(1)-C(2)	114.3(16)
F(1)-C(1)-C(2)	109.0(9)
C(5)-C(6)-C(7)	103.6(5)
O(4)-C(5)-C(6)	113.2(4)
O(4)-C(5)-C(4)	121.1(4)
C(6)-C(5)-C(4)	125.7(4)
C(5)-O(4)-C(8)	104.1(5)
O(2)-C(4)-C(3)	123.5(3)
O(2)-C(4)-C(5)	118.4(3)
C(3)-C(4)-C(5)	118.1(3)
C(28)-C(27)-N(1)	115.3(4)
O(1)-C(2)-C(3)	128.8(4)
O(1)-C(2)-C(1)	111.7(3)
C(3)-C(2)-C(1)	119.5(3)
N(1)-C(23)-C(24)	115.0(4)
C(22)-C(21)-N(1)	114.9(4)
C(8)-C(7)-C(6)	108.3(4)

A5 Supplementary Geometric Data for Tetraethylammonium *mer*-(benzoyltrifluoroacetylacetonato-κ^2*O,O'*)trichloridooxidoniobate(V) ($(NEt_4)[NbOCl_3(btfa)]$), (Nb_4))

Table A5.1 Atomic coordinates (x 10^4) and equivalent isotropic displacement parameters ($Å^2$ x 10^3) for **Nb_4**.

	x	y	z	U(eq)
Nb(1)	2821(1)	2494(1)	461(1)	51(1)
O(3)	3550(3)	3330(3)	-147(3)	65(1)
O(2)	1968(4)	1565(4)	1310(2)	57(1)
O(1)	3543(3)	3273(4)	1492(2)	58(1)
Cl(2)	4082(2)	917(2)	752(1)	83(1)
Cl(1)	1343(1)	3878(1)	411(1)	64(1)
Cl(3)	1739(2)	1382(1)	-504(1)	67(1)
N(1)	2733(4)	-2723(4)	-409(3)	59(1)
C(2)	3430(4)	3164(5)	2194(3)	49(1)
C(3)	2746(5)	2444(5)	2486(3)	50(1)
C(4)	2013(4)	1652(4)	2024(3)	42(1)
C(5)	1277(4)	891(4)	2367(3)	44(1)
C(6)	775(6)	-49(6)	1945(3)	68(2)
C(7)	92(7)	-780(7)	2237(4)	85(2)
C(8)	-160(6)	-556(7)	2942(4)	74(2)
C(9)	303(5)	381(6)	3365(3)	58(1)
C(10)	1042(5)	1091(5)	3093(3)	49(1)
C(21)	3671(9)	-2606(7)	268(6)	97(2)
C(22)	3746(8)	-3591(7)	861(5)	97(2)
C(23)	1610(7)	-2795(7)	-191(7)	109(3)
C(24)	1361(8)	-1780(8)	299(8)	109(3)

C(25)	2830(7)	-3866(7)	-832(6)	88(2)
C(26)	3867(6)	-3973(7)	-1151(5)	88(2)
C(27)	2805(8)	-1651(9)	-907(6)	113(2)
C(28)	1983(8)	-1607(9)	-1649(6)	113(2)
C(1)	4195(6)	3964(6)	2740(4)	71(2)
F(1)	4460(40)	3500(40)	3410(17)	110(30)
F(2)	5040(30)	4260(50)	2480(30)	114(3)
F(3')	3600(30)	4890(30)	2780(30)	133(4)
F(1')	4037(7)	3964(8)	3446(4)	100(3)
F(3)	4145(9)	5045(5)	2497(4)	133(4)
F(2')	5227(4)	3639(8)	2781(5)	114(3)

Table A5.2 Anisotropic displacement parameters ($Å^2$ x 10^3) for **Nb_4**.

	U^{11}	U^{22}	U^{33}	U^{23}	U^{13}	U^{12}
Nb(1)	61(1)	54(1)	39(1)	9(1)	14(1)	10(1)
O(3)	43(2)	40(2)	115(4)	16(2)	21(2)	1(2)
O(2)	75(3)	62(2)	34(2)	0(2)	10(2)	-25(2)
O(1)	68(3)	64(2)	40(2)	1(2)	6(2)	-24(2)
Cl(2)	71(1)	67(1)	104(1)	25(1)	0(1)	18(1)
Cl(1)	68(1)	58(1)	71(1)	-3(1)	27(1)	13(1)
Cl(3)	86(1)	57(1)	53(1)	-5(1)	0(1)	-2(1)
N(1)	56(3)	40(2)	85(4)	-2(2)	22(3)	-3(2)
C(2)	49(3)	51(3)	43(3)	0(2)	0(2)	-11(2)
C(3)	56(3)	57(3)	37(3)	-1(2)	4(2)	-12(3)
C(4)	49(3)	39(2)	37(2)	0(2)	6(2)	-5(2)
C(5)	53(3)	41(2)	38(2)	4(2)	7(2)	-6(2)
C(6)	93(5)	71(4)	43(3)	-13(3)	19(3)	-38(4)
C(7)	107(6)	86(5)	61(4)	-6(4)	10(4)	-55(5)
C(8)	74(4)	90(5)	56(4)	18(3)	12(3)	-31(4)
C(9)	63(4)	72(4)	43(3)	10(3)	17(3)	-3(3)
C(10)	60(3)	45(3)	41(3)	-1(2)	10(2)	-4(2)
C(21)	120(5)	70(3)	91(4)	2(3)	-2(4)	-11(3)
C(22)	120(5)	70(3)	91(4)	2(3)	-2(4)	-11(3)
C(23)	89(5)	68(4)	194(8)	-32(4)	82(5)	-9(3)
C(24)	89(5)	68(4)	194(8)	-32(4)	82(5)	-9(3)
C(25)	73(3)	78(3)	117(5)	-25(3)	33(3)	-5(3)
C(26)	73(3)	78(3)	117(5)	-25(3)	33(3)	-5(3)
C(27)	102(5)	89(4)	136(6)	40(4)	-7(4)	-9(4)
C(28)	102(5)	89(4)	136(6)	40(4)	-7(4)	-9(4)
C(1)	76(5)	78(5)	54(4)	-6(3)	4(3)	-33(4)
F(1)	130(50)	110(40)	50(30)	10(20)	-70(30)	-20(30)

F(2)	71(3)	176(8)	87(5)	-24(5)	-6(3)	-42(4)
F(3')	221(9)	72(3)	84(4)	8(3)	-27(5)	-81(4)
F(1')	123(6)	122(6)	57(4)	-31(3)	24(4)	-72(5)
F(3)	221(9)	72(3)	84(4)	8(3)	-27(5)	-81(4)
F(2')	71(3)	176(8)	87(5)	-24(5)	-6(3)	-42(4)

Table A5.3 Bond lengths [Å] for **Nb_4**.

Bond	Bond length [Å]
Nb(1)-O(3)	1.808(4)
Nb(1)-O(1)	2.065(4)
Nb(1)-O(2)	2.264(4)
Nb(1)-Cl(3)	2.3272(17)
Nb(1)-Cl(2)	2.3696(19)
Nb(1)-Cl(1)	2.4096(17)
O(2)-C(4)	1.255(6)
O(1)-C(2)	1.282(6)
N(1)-C(21)	1.505(10)
N(1)-C(25)	1.514(9)
N(1)-C(27)	1.515(10)
N(1)-C(23)	1.526(9)
C(2)-C(3)	1.355(8)
C(2)-C(1)	1.517(8)
C(3)-C(4)	1.419(7)
C(3)-H(3)	0.86(7)
C(4)-C(5)	1.476(7)
C(5)-C(6)	1.380(7)
C(5)-C(10)	1.389(7)
C(6)-C(7)	1.361(9)
C(6)-H(6)	0.9500
C(7)-C(8)	1.368(10)
C(7)-H(7)	0.9500
C(8)-C(9)	1.361(9)
C(8)-H(8)	0.9500
C(9)-C(10)	1.380(8)
C(9)-H(9)	0.9500
C(10)-H(10)	0.9500

C(21)-C(22)	1.522(12)
C(21)-H(21A)	0.9900
C(21)-H(21B)	0.9900
C(22)-H(22A)	0.9800
C(22)-H(22B)	0.9800
C(22)-H(22C)	0.9800
C(23)-C(24A)	1.510(12)
C(23)-H(23A)	0.9900
C(23)-H(23B)	0.9900
C(24A)-H(24A)	0.9800
C(24A)-H(24B)	0.9800
C(24A)-H(24C)	0.9800
C(25)-C(26)	1.514(10)
C(25)-H(25A)	0.9900
C(25)-H(25B)	0.9900
C(26)-H(26A)	0.9800
C(26)-H(26B)	0.9800
C(26)-H(26C)	0.9800
C(27)-C(28)	1.497(13)
C(27)-H(27A)	0.9900
C(27)-H(27B)	0.9900
C(28)-H(28A)	0.9800
C(28)-H(28B)	0.9800
C(28)-H(28C)	0.9800
C(1)-F(2)	1.275(14)
C(1)-F(1)	1.277(14)
C(1)-F(3')	1.297(15)
C(1)-F(3)	1.297(8)
C(1)-F(1')	1.301(8)
C(1)-F(2')	1.326(8)

Table A5.4 Bond angles [º] for **Nb_4**.

Bond	Bond angle [º]
O(3)-Nb(1)-O(1)	96.76(19)
O(3)-Nb(1)-O(2)	174.79(18)
O(1)-Nb(1)-O(2)	78.16(14)
O(3)-Nb(1)-Cl(3)	97.75(17)
O(1)-Nb(1)-Cl(3)	165.42(12)
O(2)-Nb(1)-Cl(3)	87.31(11)
O(3)-Nb(1)-Cl(2)	97.77(13)
O(1)-Nb(1)-Cl(2)	88.71(14)
O(2)-Nb(1)-Cl(2)	83.32(13)
Cl(3)-Nb(1)-Cl(2)	90.77(7)
O(3)-Nb(1)-Cl(1)	96.09(13)
O(1)-Nb(1)-Cl(1)	87.15(14)
O(2)-Nb(1)-Cl(1)	82.64(13)
Cl(3)-Nb(1)-Cl(1)	89.86(7)
Cl(2)-Nb(1)-Cl(1)	165.91(7)
C(4)-O(2)-Nb(1)	134.0(3)
C(2)-O(1)-Nb(1)	134.5(3)
C(21)-N(1)-C(25)	110.0(6)
C(21)-N(1)-C(27)	105.4(6)
C(25)-N(1)-C(27)	112.5(7)
C(21)-N(1)-C(23)	114.3(8)
C(25)-N(1)-C(23)	104.2(5)
C(27)-N(1)-C(23)	110.6(7)
O(1)-C(2)-C(3)	128.6(5)
O(1)-C(2)-C(1)	112.5(5)
C(3)-C(2)-C(1)	118.9(5)

C(2)-C(3)-C(4)	123.0(5)
C(2)-C(3)-H(3)	118(5)
C(4)-C(3)-H(3)	119(5)
O(2)-C(4)-C(3)	121.7(5)
O(2)-C(4)-C(5)	117.3(4)
C(3)-C(4)-C(5)	121.0(4)
C(6)-C(5)-C(10)	118.0(5)
C(6)-C(5)-C(4)	118.8(5)
C(10)-C(5)-C(4)	123.1(5)
C(7)-C(6)-C(5)	121.1(6)
C(7)-C(6)-H(6)	119.5
C(5)-C(6)-H(6)	119.5
C(6)-C(7)-C(8)	120.4(6)
C(6)-C(7)-H(7)	119.8
C(8)-C(7)-H(7)	119.8
C(9)-C(8)-C(7)	119.8(6)
C(9)-C(8)-H(8)	120.1
C(7)-C(8)-H(8)	120.1
C(8)-C(9)-C(10)	120.3(6)
C(8)-C(9)-H(9)	119.9
C(10)-C(9)-H(9)	119.9
C(9)-C(10)-C(5)	120.3(5)
C(9)-C(10)-H(10)	119.9
C(5)-C(10)-H(10)	119.9
N(1)-C(21)-C(22)	114.6(7)
N(1)-C(21)-H(21A)	108.6
C(22)-C(21)-H(21A)	108.6
N(1)-C(21)-H(21B)	108.6
C(22)-C(21)-H(21B)	108.6
H(21A)-C(21)-H(21B)	107.6

C(21)-C(22)-H(22A)	109.5
C(21)-C(22)-H(22B)	109.5
H(22A)-C(22)-H(22B)	109.5
C(21)-C(22)-H(22C)	109.5
H(22A)-C(22)-H(22C)	109.5
H(22B)-C(22)-H(22C)	109.5
C(24A)-C(23)-N(1)	114.0(7)
C(24A)-C(23)-H(23A)	108.7
N(1)-C(23)-H(23A)	108.7
C(24A)-C(23)-H(23B)	108.7
N(1)-C(23)-H(23B)	108.7
H(23A)-C(23)-H(23B)	107.6
C(23)-C(24A)-H(24A)	109.5
C(23)-C(24A)-H(24B)	109.5
H(24A)-C(24A)-H(24B)	109.5
C(23)-C(24A)-H(24C)	109.5
H(24A)-C(24A)-H(24C)	109.5
H(24B)-C(24A)-H(24C)	109.5
N(1)-C(25)-C(26)	114.2(6)
N(1)-C(25)-H(25A)	108.7
C(26)-C(25)-H(25A)	108.7
N(1)-C(25)-H(25B)	108.7
C(26)-C(25)-H(25B)	108.7
H(25A)-C(25)-H(25B)	107.6
C(25)-C(26)-H(26A)	109.5
C(25)-C(26)-H(26B)	109.5
H(26A)-C(26)-H(26B)	109.5
C(25)-C(26)-H(26C)	109.5
H(26A)-C(26)-H(26C)	109.5
H(26B)-C(26)-H(26C)	109.5

C(28)-C(27)-N(1)	115.3(8)
C(28)-C(27)-H(27A)	108.4
N(1)-C(27)-H(27A)	108.4
C(28)-C(27)-H(27B)	108.4
N(1)-C(27)-H(27B)	108.4
H(27A)-C(27)-H(27B)	107.5
C(27)-C(28)-H(28A)	109.5
C(27)-C(28)-H(28B)	109.5
H(28A)-C(28)-H(28B)	109.5
C(27)-C(28)-H(28C)	109.5
H(28A)-C(28)-H(28C)	109.5
H(28B)-C(28)-H(28C)	109.5
F(2)-C(1)-F(1)	111.2(15)
F(2)-C(1)-F(3')	109.1(15)
F(1)-C(1)-F(3')	109.3(15)
F(3)-C(1)-F(1')	108.0(7)
F(3)-C(1)-F(2')	105.3(6)
F(1')-C(1)-F(2')	106.1(6)
F(2)-C(1)-C(2)	113(2)
F(1)-C(1)-C(2)	111(2)
F(3')-C(1)-C(2)	103(2)
F(3)-C(1)-C(2)	111.9(5)
F(1')-C(1)-C(2)	114.5(6)
F(2')-C(1)-C(2)	110.5(6)

A6 Supplementary Geometric Data for Tetraethylammonium *mer*-oxidotrichlorido(naphtyltrifluoroacetylacetonato-κ^2O,O') niobate(V) ($(NEt_4)[NbOCl_3(ntfa)]$), (Nb_5))

Table A6.1 Atomic coordinates (x 10^4) and equivalent isotropic displacement parameters ($Å^2$ x 10^3) for **Nb_5**.

	x	y	z	U(eq)
Nb(1)	5983(1)	2836(1)	8024(1)	23(1)
F(1)	10554(6)	5443(4)	8303(4)	45(1)
F(2)	11644(6)	4696(4)	7190(4)	46(1)
F(3)	9329(6)	5528(4)	6826(4)	49(1)
Cl(1)	4274(2)	2797(2)	6414(1)	29(1)
Cl(2)	8090(2)	2525(2)	9439(1)	34(1)
Cl(3)	4290(2)	1240(1)	8351(1)	28(1)
O(1)	7782(6)	3881(4)	7667(4)	27(1)
O(2)	7427(6)	1483(4)	7298(3)	24(1)
O(3)	5115(6)	3999(4)	8511(4)	28(1)
N(1)	6109(8)	-2581(5)	8595(4)	25(1)
C(21)	6592(10)	-1338(6)	9084(6)	37(2)
C(1)	10189(9)	4841(6)	7441(6)	29(2)
C(2)	9220(9)	3679(5)	7441(5)	22(2)
C(22)	8363(11)	-882(6)	9051(6)	46(2)
C(3)	9809(9)	2640(5)	7195(5)	25(2)
C(23)	6088(10)	-2600(6)	7542(5)	28(2)
C(4)	8827(9)	1547(6)	7067(5)	23(2)
C(24)	5401(10)	-3731(6)	6924(5)	35(2)
C(25)	7342(10)	-3441(6)	9039(5)	26(2)
C(5)	9374(9)	473(5)	6622(5)	21(2)
C(6)	10955(9)	432(5)	6428(5)	20(1)

C(26)	7508(10)	-3565(7)	10096(6)	40(2)
C(27)	4386(9)	-2920(6)	8733(5)	29(2)
C(7)	11447(9)	-592(5)	5997(5)	19(1)
C(8)	13048(9)	-637(6)	5801(5)	26(2)
C(28)	2997(9)	-2226(6)	8208(6)	34(2)
C(12)	10332(9)	-1608(5)	5750(5)	20(2)
C(14)	8270(9)	-541(6)	6365(5)	25(2)
C(9)	13499(9)	-1619(6)	5368(5)	31(2)
C(13)	8721(9)	-1528(6)	5950(5)	24(2)
C(11)	10850(10)	-2609(6)	5306(5)	26(2)
C(10)	12388(10)	-2619(6)	5108(5)	29(2)

Table A6.2 Anisotropic displacement parameters ($Å^2 \times 10^3$) for **Nb_5**.

	U^{11}	U^{22}	U^{33}	U^{23}	U^{13}	U^{12}
Nb(1)	21(1)	18(1)	31(1)	0(1)	8(1)	1(1)
F(1)	49(3)	28(2)	56(3)	-11(2)	14(3)	-16(2)
F(2)	26(3)	28(2)	91(4)	-7(2)	32(3)	-5(2)
F(3)	37(3)	35(2)	76(4)	32(3)	8(3)	-2(2)
Cl(1)	26(1)	30(1)	31(1)	1(1)	6(1)	2(1)
Cl(2)	27(1)	39(1)	33(1)	3(1)	3(1)	1(1)
Cl(3)	28(1)	21(1)	35(1)	3(1)	9(1)	0(1)
O(1)	24(3)	21(2)	36(3)	1(2)	9(2)	-2(2)
O(2)	24(3)	16(2)	33(3)	-3(2)	11(2)	-1(2)
O(3)	29(3)	19(2)	36(3)	-4(2)	12(2)	-2(2)
N(1)	25(4)	21(3)	31(3)	6(3)	7(3)	7(3)
C(21)	36(5)	21(4)	50(5)	-2(4)	4(4)	-5(3)
C(1)	19(4)	23(4)	43(5)	-4(3)	9(3)	-3(3)
C(2)	21(4)	17(3)	25(4)	-1(3)	4(3)	-4(3)
C(22)	56(6)	23(4)	48(5)	0(4)	-11(5)	-2(4)
C(3)	23(4)	20(3)	30(4)	-2(3)	6(3)	-1(3)
C(23)	28(4)	25(4)	31(4)	6(3)	10(3)	-1(3)
C(4)	26(4)	26(4)	18(3)	3(3)	8(3)	-1(3)
C(24)	39(5)	31(4)	31(4)	2(3)	1(4)	5(4)
C(25)	30(4)	22(3)	26(4)	2(3)	6(3)	3(3)
C(5)	23(4)	16(3)	22(4)	1(3)	3(3)	1(3)
C(6)	20(4)	15(3)	25(4)	5(3)	7(3)	1(3)
C(26)	33(5)	43(5)	42(5)	6(4)	1(4)	14(4)
C(27)	26(4)	27(4)	35(4)	5(3)	14(4)	1(3)
C(7)	21(4)	19(3)	19(3)	1(3)	11(3)	4(3)
C(8)	28(4)	26(4)	25(4)	4(3)	10(3)	3(3)
C(28)	22(4)	31(4)	52(5)	11(4)	9(4)	3(3)

C(12)	22(4)	15(3)	26(4)	1(3)	11(3)	5(3)
C(14)	18(4)	24(3)	31(4)	3(3)	2(3)	3(3)
C(9)	16(4)	43(4)	33(4)	0(4)	4(3)	8(3)
C(13)	22(4)	19(3)	28(4)	1(3)	4(3)	-6(3)
C(11)	33(5)	20(3)	25(4)	-1(3)	9(3)	1(3)
C(10)	35(5)	33(4)	20(4)	-2(3)	8(3)	14(4)

Table A6.3 Bond lengths [Å] for **Nb_5**.

Bond	Bond length [Å]
O(1)-Nb(1)	2.047(5)
O(2)-Nb(1)	2.314(4)
O(3)-Nb(1)	1.711(5)
Cl(1)-Nb(1)	2.412(2)
Cl(2)-Nb(1)	2.414(2)
Cl(3)-Nb(1)	2.395(2)
C(21)-N(1)	1.530(9)
C(21)-C(22)	1.541(12)
C(1)-F(1)	1.330(8)
C(1)-F(3)	1.334(8)
C(1)-F(2)	1.340(8)
C(1)-C(2)	1.523(9)
C(2)-O(1)	1.321(8)
C(2)-C(3)	1.354(9)
C(3)-C(4)	1.438(9)
C(23)-N(1)	1.506(9)
C(23)-C(24)	1.520(10)
C(4)-O(2)	1.271(8)
C(4)-C(5)	1.475(9)
C(25)-C(26)	1.510(10)
C(25)-N(1)	1.517(8)
C(5)-C(6)	1.394(9)
C(5)-C(14)	1.414(9)
C(6)-C(7)	1.399(8)
C(27)-C(28)	1.513(10)
C(27)-N(1)	1.516(9)
C(7)-C(8)	1.411(9)
C(7)-C(12)	1.421(9)

C(8)-C(9)	1.347(9)
C(12)-C(11)	1.396(9)
C(12)-C(13)	1.424(9)
C(14)-C(13)	1.341(9)
C(9)-C(10)	1.406(10)

Table A6.4 Bond angles [º] for **Nb_5**.

Bond	Bond angle [º]
O(3)-Nb(1)-O(1)	93.2(2)
O(3)-Nb(1)-O(2)	171.0(2)
O(1)-Nb(1)-O(2)	77.80(18)
O(3)-Nb(1)-Cl(3)	100.39(17)
O(1)-Nb(1)-Cl(3)	166.06(14)
O(2)-Nb(1)-Cl(3)	88.59(13)
O(3)-Nb(1)-Cl(1)	96.76(18)
O(1)-Nb(1)-Cl(1)	90.46(15)
O(2)-Nb(1)-Cl(1)	82.72(13)
Cl(3)-Nb(1)-Cl(1)	90.78(7)
O(3)-Nb(1)-Cl(2)	97.68(18)
O(1)-Nb(1)-Cl(2)	86.06(15)
O(2)-Nb(1)-Cl(2)	82.61(13)
Cl(3)-Nb(1)-Cl(2)	89.25(7)
Cl(1)-Nb(1)-Cl(2)	165.32(7)
N(1)-C(21)-C(22)	113.5(7)
F(1)-C(1)-F(3)	107.1(6)
F(1)-C(1)-F(2)	106.5(6)
F(3)-C(1)-F(2)	106.6(6)
F(1)-C(1)-C(2)	112.0(6)
F(3)-C(1)-C(2)	111.8(6)
F(2)-C(1)-C(2)	112.4(6)
O(1)-C(2)-C(3)	128.8(6)
O(1)-C(2)-C(1)	109.5(6)
C(3)-C(2)-C(1)	121.6(7)
C(2)-C(3)-C(4)	122.6(7)
N(1)-C(23)-C(24)	116.3(6)
O(2)-C(4)-C(3)	121.2(6)

O(2)-C(4)-C(5)	117.6(6)
C(3)-C(4)-C(5)	121.1(6)
C(26)-C(25)-N(1)	116.4(6)
C(6)-C(5)-C(14)	118.5(6)
C(6)-C(5)-C(4)	121.6(6)
C(14)-C(5)-C(4)	119.9(6)
C(5)-C(6)-C(7)	120.8(6)
C(28)-C(27)-N(1)	114.9(6)
C(6)-C(7)-C(8)	120.9(6)
C(6)-C(7)-C(12)	120.1(6)
C(8)-C(7)-C(12)	118.9(6)
C(9)-C(8)-C(7)	120.6(7)
C(11)-C(12)-C(7)	118.7(6)
C(11)-C(12)-C(13)	123.8(6)
C(7)-C(12)-C(13)	117.5(6)
C(13)-C(14)-C(5)	121.4(7)
C(8)-C(9)-C(10)	120.6(7)
C(14)-C(13)-C(12)	121.7(6)
C(10)-C(11)-C(12)	121.0(7)
C(11)-C(10)-C(9)	120.2(7)
C(23)-N(1)-C(27)	110.5(6)
C(23)-N(1)-C(25)	108.6(5)
C(27)-N(1)-C(25)	109.7(5)
C(23)-N(1)-C(21)	109.7(5)
C(27)-N(1)-C(21)	107.1(6)
C(25)-N(1)-C(21)	111.1(6)
C(2)-O(1)-Nb(1)	133.6(4)
C(4)-O(2)-Nb(1)	132.8(4)

A7 Supplementary Geometric Data for Tetraethylammonium *mer*-(3-chloroacetylacetonato-κ^2*O,O'*)trichloridooxidoniobate(V) ($(NEt_4)[NbOCl_3(3Cl\text{-}acac)]$), (Nb_6))

Table A7.1 Atomic coordinates (x 10^4) and equivalent isotropic displacement parameters ($Å^2$ x 10^3) for **Nb_6**.

	x	y	z	U(eq)
Nb(1)	2266(1)	1651(1)	9391(1)	38(1)
Cl(2)	1516(1)	2741(2)	8193(1)	46(1)
Cl(3)	1721(1)	-1364(2)	9107(1)	45(1)
Cl(1)	3354(1)	506(2)	10409(1)	50(1)
Cl(4)	5171(1)	4581(3)	8649(1)	67(1)
O(3)	1513(2)	2398(6)	9909(2)	44(1)
O(2)	3353(2)	917(6)	8734(2)	43(1)
O(1)	2994(2)	3975(6)	9475(2)	45(1)
C(5)	4654(4)	706(10)	8223(3)	60(2)
C(3)	4226(3)	3568(8)	8880(3)	42(1)
C(2)	3714(3)	4601(8)	9267(3)	42(1)
C(4)	4035(3)	1729(9)	8628(3)	45(2)
C(1)	3928(4)	6522(8)	9481(3)	52(2)
N(1)	1577(3)	-1955(6)	6546(2)	34(1)
C(25)	615(4)	-4827(9)	6278(4)	57(2)
C(24)	1245(4)	-3507(8)	6016(3)	43(1)
C(20)	809(3)	-826(8)	6713(3)	44(1)
C(23)	2884(4)	-3797(9)	7244(3)	52(2)
C(21)	234(4)	38(8)	6046(4)	53(2)
C(22)	2066(3)	-2692(8)	7282(3)	41(1)
C(27)	2591(4)	837(9)	6583(3)	52(2)
C(26)	2192(3)	-814(8)	6160(3)	40(1)

Table A7.2 Anisotropic displacement parameters ($Å^2$ x 10^3) for **Nb_6**.

	U^{11}	U^{22}	U^{33}	U^{23}	U^{13}	U^{12}
Nb(1)	23(1)	72(1)	19(1)	-4(1)	5(1)	-6(1)
Cl(2)	33(1)	84(1)	21(1)	1(1)	5(1)	-3(1)
Cl(3)	31(1)	76(1)	29(1)	-6(1)	7(1)	-10(1)
Cl(1)	33(1)	89(1)	26(1)	-3(1)	-1(1)	-2(1)
Cl(4)	41(1)	100(1)	65(1)	39(1)	23(1)	-5(1)
O(3)	32(2)	77(3)	25(2)	-6(2)	8(2)	-2(2)
O(2)	25(2)	79(3)	27(2)	1(2)	12(1)	-2(2)
O(1)	27(2)	78(3)	30(2)	-4(2)	5(2)	-11(2)
C(5)	34(3)	110(5)	38(3)	20(3)	17(2)	17(3)
C(3)	23(2)	78(4)	26(3)	22(3)	7(2)	-1(2)
C(2)	27(2)	69(4)	26(3)	13(2)	-4(2)	-10(2)
C(4)	21(2)	91(5)	22(3)	20(3)	1(2)	4(3)
C(1)	41(3)	75(4)	38(3)	12(3)	1(3)	-9(3)
N(1)	25(2)	60(3)	18(2)	5(2)	5(2)	7(2)
C(25)	40(3)	72(4)	56(4)	-5(3)	4(3)	1(3)
C(24)	37(3)	68(4)	23(3)	-3(2)	4(2)	11(3)
C(20)	31(3)	69(4)	34(3)	-5(3)	15(2)	7(3)
C(23)	41(3)	76(4)	35(3)	10(3)	-2(2)	16(3)
C(21)	34(3)	68(4)	58(4)	10(3)	11(3)	13(3)
C(22)	37(3)	65(4)	20(2)	8(2)	2(2)	6(3)
C(27)	42(3)	70(4)	45(3)	12(3)	10(3)	5(3)
C(26)	33(3)	66(4)	22(2)	10(2)	6(2)	10(2)

Table A7.3 Bond lengths [Å] for **Nb_6**.

Bond	Bond length [Å]
Nb(1)-O(3)	1.704(3)
Nb(1)-O(1)	2.022(4)
Nb(1)-O(2)	2.280(3)
Nb(1)-Cl(3)	2.382(2)
Nb(1)-Cl(1)	2.413(1)
Nb(1)-Cl(2)	2.419(1)
Cl(4)-C(3)	1.740(5)
O(2)-C(4)	1.243(6)
O(1)-C(2)	1.309(6)
C(5)-C(4)	1.501(8)
C(3)-C(2)	1.371(8)
C(3)-C(4)	1.435(9)
C(2)-C(1)	1.480(8)
N(1)-C(20)	1.509(6)
N(1)-C(22)	1.516(6)
N(1)-C(24)	1.520(7)
N(1)-C(26)	1.521(7)
C(25)-C(24)	1.501(8)
C(20)-C(21)	1.509(8)
C(23)-C(22)	1.501(7)
C(27)-C(26)	1.502(8)

Table A7.4 Bond angles [º] for **Nb_6**.

Bond	Bond angle [º]
O(3)-Nb(1)-O(1)	95.99(17)
O(3)-Nb(1)-O(2)	174.13(16)
O(1)-Nb(1)-O(2)	78.21(15)
O(3)-Nb(1)-Cl(3)	99.99(14)
O(1)-Nb(1)-Cl(3)	164.01(11)
O(2)-Nb(1)-Cl(3)	85.81(11)
O(3)-Nb(1)-Cl(1)	97.06(12)
O(1)-Nb(1)-Cl(1)	86.54(11)
O(2)-Nb(1)-Cl(1)	81.88(10)
Cl(3)-Nb(1)-Cl(1)	90.74(6)
O(3)-Nb(1)-Cl(2)	98.01(13)
O(1)-Nb(1)-Cl(2)	87.51(11)
O(2)-Nb(1)-Cl(2)	82.68(10)
Cl(3)-Nb(1)-Cl(2)	90.99(6)
Cl(1)-Nb(1)-Cl(2)	164.29(5)
C(4)-O(2)-Nb(1)	132.7(4)
C(2)-O(1)-Nb(1)	138.7(4)
C(2)-C(3)-C(4)	125.4(5)
C(2)-C(3)-Cl(4)	117.7(5)
C(4)-C(3)-Cl(4)	116.9(4)
O(1)-C(2)-C(3)	122.9(5)
O(1)-C(2)-C(1)	114.4(5)
C(3)-C(2)-C(1)	122.7(5)
O(2)-C(4)-C(3)	121.7(5)
O(2)-C(4)-C(5)	117.3(6)
C(3)-C(4)-C(5)	121.0(5)
C(20)-N(1)-C(22)	107.1(4)

C(20)-N(1)-C(24)	110.8(4)
C(22)-N(1)-C(24)	110.8(4)
C(20)-N(1)-C(26)	111.1(4)
C(22)-N(1)-C(26)	111.1(4)
C(24)-N(1)-C(26)	106.1(4)
C(25)-C(24)-N(1)	115.9(4)
N(1)-C(20)-C(21)	115.3(4)
C(23)-C(22)-N(1)	115.7(4)
C(27)-C(26)-N(1)	115.5(4)

A8 Supplementary Geometric Data for Tetraethylammonium *mer*-trichlorido(hexafluoroacetylacetonato-κ^2*O,O'*)oxidoniobate(V) ($(NEt_4)[NbOCl_3(hffa)]$), (Nb_7))

Table A8.1 Atomic coordinates (x 10^4) and equivalent isotropic displacement parameters ($Å^2$ x 10^3) for **Nb_7**.

x	y	z	U(eq)	x
Nb(1)	7500	7500	691(1)	67(1)
Cl(1)	8974(1)	6027(1)	880(1)	70(1)
N(1)	7500	2500	0	55(2)
O(1)	6622(3)	6622(3)	1681(3)	60(2)
C(22)	6260(7)	3489(7)	1054(4)	93(3)
C(21)	6391(6)	2467(6)	492(3)	65(2)
C(1)	5935(6)	5935(6)	2858(6)	68(2)
C(3)	7500	7500	2772(7)	66(3)
C(2)	6750(5)	6750(5)	2392(4)	54(2)
F(1)	5780(30)	6060(40)	3530(20)	96(11)
F(1')	6149(18)	6149(18)	3630(20)	89(8)
F(2)	6390(20)	4790(30)	2767(16)	112(8)
F(2')	5880(20)	4890(30)	2630(13)	128(10)
O(3)	8464(16)	8464(16)	116(9)	55(5)

Table A8.2 Anisotropic displacement parameters ($Å^2$ x 10^3) for **Nb_7**.

	U^{11}	U^{22}	U^{33}	U^{23}	U^{13}	U^{12}
Nb(1)	82(1)	82(1)	37(1)	0	0	33(1)
Cl(1)	61(1)	61(1)	89(2)	14(1)	-14(1)	9(1)
N(1)	53(3)	53(3)	59(6)	0	0	-7(4)
O(1)	67(2)	67(2)	46(3)	1(2)	1(2)	-22(3)
C(22)	106(6)	84(5)	90(5)	-29(4)	25(4)	-7(4)
C(21)	63(4)	64(4)	68(4)	-6(3)	14(3)	-8(3)
C(1)	75(4)	75(4)	53(6)	3(4)	3(4)	-13(5)
C(3)	78(5)	78(5)	43(6)	0	0	-24(7)
C(2)	61(3)	61(3)	40(4)	9(3)	9(3)	-5(4)
F(1)	100(20)	140(20)	48(15)	-44(14)	45(17)	-80(18)
F(1')	111(11)	111(11)	45(9)	-8(6)	-8(6)	-84(12)
F(2)	150(20)	77(8)	105(9)	25(7)	25(11)	-9(12)
F(2')	190(20)	81(12)	112(13)	-31(11)	97(13)	-62(15)
O(3)	55(6)	55(6)	54(11)	21(8)	21(8)	0(6)
Cl(3)	61(2)	61(2)	44(3)	10(3)	10(3)	3(2)

Table A8.3 Bond lengths [Å] for **Nb_8**.

Bond	Bond length [Å]
Nb(1)-O(3)	1.84(2)
Nb(1)-O(3)'	1.84(2)
Nb(1)-Cl(3)	2.198(8)
Nb(1)-Cl(3)'	2.198(8)
Nb(1)-O(1)	2.223(5)
Nb(1)-O(1)'	2.223(5)
Nb(1)-Cl(1)'	2.374(2)
Nb(1)-Cl(1)	2.374(2)
N(1)-C(21)	1.518(5)
N(1)-C(21)'	1.518(5)
O(1)-C(2)	1.257(8)
C(22)-C(21)	1.520(8)
C(1)-F(1)	1.19(4)
C(1)-F(1)'	1.19(4)
C(1)-F(2')	1.24(3)
C(1)-F(2')'	1.24(3)
C(1)-F(1')	1.39(4)
C(1)-F(2)	1.40(3)
C(1)-F(2)'	1.40(3)
C(1)-C(2)	1.532(11)
C(3)-C(2)	1.368(10)
C(3)-C(2)'	1.368(10)
F(1)-F(2)'	1.77(6)
F(2)-F(1)'	1.77(6)
F(2')-F(2')'	1.57(6)

Table A8.4 Bond angles [º] for **Nb_7**.

Bond	Bond angle [º]
O(3)-Nb(1)-O(3)'	113.9(13)
O(3)-Nb(1)-Cl(3)	11.9(8)
O(3)'-Nb(1)-Cl(3)	102.0(5)
O(3)-Nb(1)-Cl(3)'	102.0(5)
O(3)'-Nb(1)-Cl(3)'	11.9(8)
Cl(3)-Nb(1)-Cl(3)'	90.1(5)
O(3)-Nb(1)-O(1)	162.1(7)
O(3)'-Nb(1)-O(1)	84.0(7)
Cl(3)-Nb(1)-O(1)	174.0(3)
Cl(3)'-Nb(1)-O(1)	95.9(3)
O(3)-Nb(1)-O(1)'	84.0(7)
O(3)'-Nb(1)-O(1)'	162.1(7)
Cl(3)-Nb(1)-O(1)'	95.9(3)
Cl(3)'-Nb(1)-O(1)'	174.0(3)
O(1)-Nb(1)-O(1)'	78.1(3)
O(3)-Nb(1)-Cl(1)'	94.34(8)
O(3)'-Nb(1)-Cl(1)'	94.34(8)
Cl(3)-Nb(1)-Cl(1)'	95.62(5)
Cl(3)'-Nb(1)-Cl(1)'	95.62(5)
O(1)-Nb(1)-Cl(1)'	83.82(6)
O(1)'-Nb(1)-Cl(1)'	83.82(6)
O(3)-Nb(1)-Cl(1)	94.34(8)
O(3)'-Nb(1)-Cl(1)	94.34(8)
Cl(3)-Nb(1)-Cl(1)	95.62(5)
Cl(3)'-Nb(1)-Cl(1)	95.62(5)
O(1)-Nb(1)-Cl(1)	83.82(6)
O(1)'-Nb(1)-Cl(1)	83.82(6)
Cl(1)'-Nb(1)-Cl(1)	164.06(14)

C(21)-N(1)-C(21)'	106.2(5)
C(21)-N(1)-C(21)'	111.1(5)
C(21)'-N(1)-C(21)'	111.1(5)
C(21)-N(1)-C(21)'	111.1(5)
C(21)'-N(1)-C(21)'	111.1(5)
C(21)'-N(1)-C(21)'	106.2(5)
C(2)-O(1)-Nb(1)	131.7(5)
N(1)-C(21)-C(22)	115.2(5)
F(1)-C(1)-F(1)'	22(5)
F(1)-C(1)-F(2')	115(3)
F(1)'-C(1)-F(2')	100(2)
F(1)-C(1)-F(2')'	100(2)
F(1)'-C(1)-F(2')'	115(3)
F(2')-C(1)-F(2')'	78(3)
F(1)-C(1)-F(1')	19(2)
F(1)'-C(1)-F(1')	19(2)
F(2')-C(1)-F(1')	118.9(16)
F(2')'-C(1)-F(1')	118.9(16)
F(1)-C(1)-F(2)	106(3)
F(1)'-C(1)-F(2)	86(3)
F(2')-C(1)-F(2)	27(2)
F(2')'-C(1)-F(2)	105.4(15)
F(1')-C(1)-F(2)	101.9(13)
F(1)-C(1)-F(2)'	86(3)
F(1)'-C(1)-F(2)'	106(3)
F(2')-C(1)-F(2)'	105.4(15)
F(2')'-C(1)-F(2)'	27(2)
F(1')-C(1)-F(2)'	101.9(14)
F(2)-C(1)-F(2)'	132(2)
F(1)-C(1)-C(2)	122.5(17)

F(1)'-C(1)-C(2)	122.5(17)
F(2')-C(1)-C(2)	115.4(13)
F(2')'-C(1)-C(2)	115.4(13)
F(1')-C(1)-C(2)	107.8(16)
F(2)-C(1)-C(2)	105.7(12)
F(2)'-C(1)-C(2)	105.7(12)
C(2)-C(3)-C(2)'	122.1(11)
O(1)-C(2)-C(3)	128.2(8)
O(1)-C(2)-C(1)	112.7(7)
C(3)-C(2)-C(1)	119.0(8)
F(1)'-F(1)-C(1)	79(3)
F(1)'-F(1)-F(2)'	126.3(16)
C(1)-F(1)-F(2)'	52(2)
F(1)'-F(1')-C(1)	55(9)
C(1)-F(2)-F(1)'	42.2(16)
C(1)-F(2')-F(2')'	50.8(13)

A9 Supplementary Geometric Data for Oxido-*tris*(tropolonato -κ^2*O,O'*)niobium(V) ([$NbO(Trop)_3$]), (Nb_8))

Table A9.1 Atomic coordinates (x 10^4) and equivalent isotropic displacement parameters ($Å^2$ x 10^3) for **Nb_8**.

	x	y	z	U(eq)
Nb(1)	7874(1)	2785(1)	1861(1)	38(1)
O(7)	4863(9)	2666(3)	1432(4)	42(2)
O(6)	7408(9)	2501(3)	584(3)	41(2)
O(3)	7799(9)	1508(3)	1765(3)	41(2)
O(2)	7932(10)	2265(3)	3038(3)	42(2)
O(5)	7289(9)	3921(3)	1219(3)	48(2)
O(4)	7556(9)	3665(3)	2737(4)	50(2)
O(1)	10241(8)	2864(3)	1869(4)	42(2)
C(26)	6845(14)	5308(5)	1247(6)	51(3)
C(27)	7172(13)	4574(5)	1641(6)	44(2)
C(35)	2117(16)	1821(6)	-1061(6)	56(3)
C(37)	5564(15)	2033(5)	-616(5)	45(2)
C(23)	7289(18)	5818(6)	3094(7)	76(4)
C(36)	3946(16)	1807(5)	-1160(5)	52(3)
C(33)	2410(14)	2347(5)	386(6)	45(2)
C(32)	4267(14)	2442(5)	674(5)	38(2)
C(25)	6806(15)	6058(5)	1591(7)	61(3)
C(31)	5749(13)	2314(4)	190(5)	35(2)
C(22)	7418(15)	5003(6)	3156(6)	62(3)
C(34)	1461(14)	2075(6)	-366(6)	51(3)
C(11)	8029(14)	1509(5)	3176(5)	42(2)
C(12)	7866(14)	1061(5)	2411(5)	44(2)
C(24)	7050(17)	6277(6)	2406(8)	71(4)

C(21)	7379(14)	4428(5)	2527(5)	45(2)
C(17)	8176(14)	1232(5)	3970(5)	49(3)
C(16)	8228(15)	456(5)	4245(6)	53(3)
C(14)	7945(15)	-329(6)	2953(6)	58(3)
C(15)	8151(15)	-247(5)	3802(6)	59(3)
C(13)	7824(15)	252(5)	2329(6)	56(3)

Table A9.2 Anisotropic displacement parameters ($Å^2$ x 10^3) for **Nb_8**.

	U^{11}	U^{22}	U^{33}	U^{23}	U^{13}	U^{12}
Nb(1)	52(1)	33(1)	30(1)	-3(1)	8(1)	0(1)
O(7)	43(4)	44(3)	43(4)	-5(3)	15(3)	-1(3)
O(6)	51(5)	43(3)	28(3)	-11(3)	7(3)	-9(3)
O(3)	65(5)	26(3)	31(3)	-2(2)	9(3)	5(3)
O(2)	64(5)	37(3)	30(3)	0(2)	17(3)	-4(3)
O(5)	64(5)	42(3)	40(4)	-3(3)	11(3)	-2(3)
O(4)	73(5)	35(3)	42(4)	3(3)	14(3)	-2(3)
O(1)	28(4)	51(4)	46(4)	-4(3)	1(3)	-7(3)
C(26)	61(7)	48(6)	44(6)	12(4)	13(5)	13(5)
C(27)	42(6)	43(5)	49(6)	-8(4)	15(4)	5(5)
C(35)	63(8)	59(6)	44(6)	-9(5)	0(5)	-10(6)
C(37)	65(7)	41(5)	28(5)	-3(4)	7(4)	5(5)
C(23)	116(12)	45(6)	67(8)	-31(6)	14(7)	15(6)
C(36)	81(9)	46(5)	29(5)	0(4)	12(5)	11(6)
C(33)	44(6)	54(6)	35(5)	1(4)	3(4)	6(5)
C(32)	58(7)	28(4)	29(5)	-6(3)	12(4)	-3(4)
C(25)	70(9)	28(5)	86(8)	4(5)	13(6)	2(5)
C(31)	47(6)	32(4)	27(4)	6(3)	5(4)	10(4)
C(22)	81(9)	54(6)	48(6)	-13(5)	8(6)	2(6)
C(34)	36(6)	66(6)	50(6)	4(5)	7(5)	12(5)
C(11)	56(7)	33(5)	38(5)	0(4)	11(4)	4(4)
C(12)	60(7)	28(4)	42(5)	9(4)	5(5)	-6(4)
C(24)	89(10)	35(6)	91(9)	-20(6)	22(7)	-11(6)
C(21)	54(7)	41(5)	40(5)	-14(4)	5(5)	4(5)
C(17)	71(8)	36(5)	41(5)	1(4)	14(5)	7(5)
C(16)	67(8)	52(6)	42(5)	2(5)	15(5)	7(5)
C(14)	64(8)	44(5)	60(7)	0(5)	-6(6)	-4(5)
C(15)	68(8)	46(6)	60(7)	12(5)	5(6)	3(5)

Table A9.3 Bond lengths [Å] for **Nb_8**.

Bond	Bond length [Å]
Nb(1)-O(1)	1.754(7)
Nb(1)-O(4)	2.113(6)
Nb(1)-O(6)	2.125(6)
Nb(1)-O(2)	2.126(6)
Nb(1)-O(3)	2.152(6)
Nb(1)-O(5)	2.186(6)
Nb(1)-O(7)	2.216(7)
O(7)-C(32)	1.302(9)
O(6)-C(31)	1.315(10)
O(3)-C(12)	1.299(9)
O(2)-C(11)	1.288(9)
O(5)-C(27)	1.311(10)
O(4)-C(21)	1.328(10)
C(26)-C(25)	1.384(12)
C(26)-C(27)	1.394(11)
C(27)-C(21)	1.463(12)
C(35)-C(34)	1.394(14)
C(35)-C(36)	1.394(14)
C(37)-C(31)	1.395(11)
C(37)-C(36)	1.407(13)
C(23)-C(24)	1.358(15)
C(23)-C(22)	1.374(14)
C(33)-C(32)	1.376(13)
C(33)-C(34)	1.385(12)
C(32)-C(31)	1.489(13)
C(25)-C(24)	1.374(14)
C(22)-C(21)	1.416(12)
C(11)-C(17)	1.377(11)

C(11)-C(12)	1.456(12)
C(12)-C(13)	1.365(11)
C(17)-C(16)	1.379(11)
C(16)-C(15)	1.384(12)
C(14)-C(15)	1.389(14)
C(14)-C(13)	1.410(13)

Table A9.4 Bond angles [º] for **Nb_8**.

Bond	Bond angle [º]
O(1)-Nb(1)-O(4)	100.5(3)
O(1)-Nb(1)-O(6)	90.0(3)
O(4)-Nb(1)-O(6)	144.9(2)
O(1)-Nb(1)-O(2)	100.1(3)
O(4)-Nb(1)-O(2)	69.3(2)
O(6)-Nb(1)-O(2)	141.9(2)
O(1)-Nb(1)-O(3)	95.0(2)
O(4)-Nb(1)-O(3)	138.0(2)
O(6)-Nb(1)-O(3)	72.9(2)
O(2)-Nb(1)-O(3)	69.7(2)
O(1)-Nb(1)-O(5)	92.6(3)
O(4)-Nb(1)-O(5)	71.6(2)
O(6)-Nb(1)-O(5)	74.6(2)
O(2)-Nb(1)-O(5)	140.4(2)
O(3)-Nb(1)-O(5)	146.6(2)
O(1)-Nb(1)-O(7)	162.1(3)
O(4)-Nb(1)-O(7)	92.7(2)
O(6)-Nb(1)-O(7)	72.4(2)
O(2)-Nb(1)-O(7)	95.8(2)
O(3)-Nb(1)-O(7)	82.9(2)
O(5)-Nb(1)-O(7)	80.1(2)
C(32)-O(7)-Nb(1)	118.1(6)
C(31)-O(6)-Nb(1)	120.5(6)
C(12)-O(3)-Nb(1)	121.3(5)
C(11)-O(2)-Nb(1)	123.9(5)
C(27)-O(5)-Nb(1)	120.0(5)
C(21)-O(4)-Nb(1)	120.9(5)

C(25)-C(26)-C(27)	128.9(9)
O(5)-C(27)-C(26)	121.0(8)
O(5)-C(27)-C(21)	112.7(8)
C(26)-C(27)-C(21)	126.3(8)
C(34)-C(35)-C(36)	126.8(9)
C(31)-C(37)-C(36)	128.3(10)
C(24)-C(23)-C(22)	128.7(10)
C(35)-C(36)-C(37)	130.4(9)
C(32)-C(33)-C(34)	130.8(10)
O(7)-C(32)-C(33)	120.1(9)
O(7)-C(32)-C(31)	114.1(8)
C(33)-C(32)-C(31)	125.8(8)
C(24)-C(25)-C(26)	129.6(10)
O(6)-C(31)-C(37)	117.9(9)
O(6)-C(31)-C(32)	114.3(7)
C(37)-C(31)-C(32)	127.7(9)
C(23)-C(22)-C(21)	129.3(10)
C(33)-C(34)-C(35)	130.0(10)
O(2)-C(11)-C(17)	119.5(8)
O(2)-C(11)-C(12)	111.4(7)
C(17)-C(11)-C(12)	129.0(8)
O(3)-C(12)-C(13)	119.8(8)
O(3)-C(12)-C(11)	113.5(7)
C(13)-C(12)-C(11)	126.7(8)
C(23)-C(24)-C(25)	129.8(9)
O(4)-C(21)-C(22)	118.6(8)
O(4)-C(21)-C(27)	114.2(7)
C(22)-C(21)-C(27)	127.1(8)
C(11)-C(17)-C(16)	128.8(9)
C(17)-C(16)-C(15)	129.6(9)

A10 Supplementary Geometric Data for *Tetrakis*(tropolonato -κ^2*O,O'*)niobium(V) chloride ([Nb(Trop)$_4$]Cl), (Nb_9))

Table A10.1 Atomic coordinates (x 10^4) and equivalent isotropic displacement parameters (Å^2 x 10^3) for **Nb_9**.

	x	y	z	U(eq)
Nb(1)	7116(2)	2579(1)	-728(1)	29(1)
O(1)	8182(11)	1027(9)	-502(8)	27(3)
O(2)	7951(12)	2452(10)	-2099(9)	39(3)
O(3)	8896(11)	2795(9)	-366(8)	29(3)
O(4)	7705(11)	4186(9)	-1603(8)	32(3)
O(5)	5716(11)	3476(9)	-1621(8)	30(3)
O(6)	5655(11)	1534(9)	-573(9)	31(3)
O(7)	6087(11)	3592(9)	57(9)	32(3)
O(8)	6886(11)	1650(9)	781(8)	29(3)
Cl(1)	2697(10)	50(8)	4584(8)	113(3)
C(11)	8803(16)	717(13)	-1208(12)	27(4)
C(12)	9560(17)	-348(15)	-1042(14)	34(4)
C(13)	10308(17)	-863(19)	-1700(14)	45(5)
C(14)	10495(19)	-489(18)	-2785(16)	53(6)
C(15)	9926(19)	580(20)	-3392(14)	49(6)
C(16)	9152(18)	1502(17)	-3139(13)	38(5)
C(17)	8681(18)	1540(15)	-2204(15)	37(5)
C(21)	9474(16)	3717(14)	-783(12)	28(4)
C(22)	10707(15)	3784(14)	-509(12)	28(4)
C(23)	11490(17)	4702(15)	-877(14)	35(4)
C(24)	11314(17)	5747(15)	-1567(13)	36(5)
C(25)	10225(18)	6141(16)	-2022(12)	34(4)
C(26)	9084(18)	5651(14)	-2005(12)	32(4)

C(27)	8787(15)	4540(14)	-1483(12)	26(4)
C(31)	4716(15)	2958(14)	-1677(14)	35(5)
C(32)	3859(17)	3636(16)	-2419(14)	35(4)
C(33)	2759(17)	3276(16)	-2578(14)	36(4)
C(34)	2226(17)	2232(17)	-2213(15)	41(5)
C(35)	2700(16)	1233(15)	-1488(13)	32(4)
C(36)	3784(16)	1095(14)	-1000(12)	29(4)
C(37)	4655(16)	1879(15)	-1092(12)	30(4)
C(41)	5812(15)	3246(14)	1037(13)	27(4)
C(42)	5119(17)	3921(15)	1504(12)	33(4)
C(43)	4680(20)	3739(18)	2536(14)	48(6)
C(44)	5000(20)	2773(16)	3273(14)	40(5)
C(45)	5661(19)	1809(16)	3275(12)	38(5)
C(46)	6227(17)	1464(17)	2445(13)	43(6)
C(47)	6288(15)	2125(14)	1446(11)	28(4)

Table A10.2 Anisotropic displacement parameters ($Å^2$ x 10^3) for **Nb_9**.

	U^{11}	U^{22}	U^{33}	U^{23}	U^{13}	U^{12}
Nb(1)	31(1)	24(1)	30(1)	5(1)	-15(1)	-16(1)
O(1)	29(6)	27(6)	27(7)	-5(5)	-6(5)	-15(5)
O(2)	39(7)	33(7)	33(7)	14(6)	-15(6)	-24(6)
O(3)	33(6)	28(6)	26(6)	3(5)	-12(5)	-22(5)
O(4)	37(6)	31(7)	25(6)	11(5)	-19(5)	-28(5)
O(5)	33(6)	21(6)	38(7)	3(5)	-23(5)	-20(5)
O(6)	33(6)	23(6)	39(7)	-6(5)	-10(5)	-20(5)
O(7)	39(6)	20(6)	32(7)	3(5)	-11(5)	-17(5)
O(8)	37(6)	18(6)	27(7)	8(5)	-9(5)	-16(5)
Cl(1)	124(7)	104(7)	112(7)	-32(6)	-30(6)	-11(6)
C(11)	31(8)	25(9)	22(9)	11(8)	-12(7)	-27(7)
C(12)	33(9)	30(10)	44(11)	-9(9)	-12(8)	-19(8)
C(13)	32(9)	76(16)	31(11)	-15(11)	-7(8)	-26(10)
C(14)	40(11)	51(14)	52(14)	5(11)	-3(10)	-27(10)
C(15)	35(10)	74(16)	23(11)	2(11)	-3(8)	-9(11)
C(16)	35(9)	48(12)	28(10)	1(9)	-13(8)	-22(9)
C(17)	39(10)	26(10)	44(13)	-3(9)	-18(9)	-7(8)
C(21)	28(8)	22(9)	30(10)	2(8)	-10(7)	-13(7)
C(22)	27(8)	31(9)	28(9)	-5(8)	-2(7)	-21(7)
C(23)	31(9)	34(10)	47(12)	-13(9)	-12(8)	-18(8)
C(24)	37(9)	40(11)	37(11)	-10(9)	-4(8)	-31(8)
C(25)	47(10)	42(11)	14(9)	-1(8)	-16(8)	-15(9)
C(26)	46(10)	24(9)	25(10)	3(8)	-12(8)	-20(8)
C(27)	25(8)	30(9)	24(9)	1(7)	-17(7)	-15(7)
C(31)	23(8)	25(9)	65(13)	-15(9)	-18(8)	-15(7)
C(32)	29(9)	40(11)	38(11)	-8(9)	-18(8)	-4(8)
C(33)	28(9)	37(10)	45(12)	-5(9)	-23(8)	-6(8)

C(34)	27(9)	45(12)	57(13)	-19(10)	-14(9)	-12(8)
C(35)	26(8)	39(11)	34(10)	-9(9)	-10(8)	-15(8)
C(36)	32(9)	31(9)	25(9)	-4(8)	-6(7)	-19(8)
C(37)	32(9)	35(10)	24(9)	0(8)	-12(7)	-23(8)
C(41)	23(8)	27(9)	33(10)	-6(8)	-13(7)	-12(7)
C(42)	33(9)	41(11)	25(10)	-4(9)	-8(7)	-22(8)
C(43)	67(14)	49(13)	31(11)	1(10)	-24(10)	-30(11)
C(44)	53(12)	35(11)	39(12)	-17(10)	-9(9)	-10(9)
C(45)	54(11)	32(11)	15(9)	15(8)	-15(8)	-13(9)
C(46)	36(10)	62(14)	18(10)	18(9)	-16(8)	-35(10)
C(47)	27(8)	36(10)	12(8)	18(8)	-16(7)	-25(8)

Table A10.3 Bond lengths [Å] for **Nb_9**.

Bond	Bond length [Å]
O(1)-Nb(1)	2.090(12)
O(2)-Nb(1)	2.083(14)
O(3)-Nb(1)	2.088(9)
O(4)-Nb(1)	2.104(10)
O(5)-Nb(1)	2.085(10)
O(6)-Nb(1)	2.082(9)
O(7)-Nb(1)	2.089(13)
O(8)-Nb(1)	2.093(11)
C(11)-O(1)	1.27(2)
C(11)-C(12)	1.44(2)
C(11)-C(17)	1.49(2)
C(12)-C(13)	1.41(3)
C(13)-C(14)	1.47(3)
C(14)-C(15)	1.47(3)
C(15)-C(16)	1.45(3)
C(16)-C(17)	1.38(3)
C(17)-O(2)	1.34(2)
C(21)-O(3)	1.292(17)
C(21)-C(27)	1.41(2)
C(21)-C(22)	1.43(2)
C(22)-C(23)	1.40(2)
C(23)-C(24)	1.38(3)
C(24)-C(25)	1.36(2)
C(25)-C(26)	1.40(2)
C(26)-C(27)	1.40(2)
C(27)-O(4)	1.326(15)
C(31)-O(5)	1.334(14)

C(31)-C(37)	1.35(2)
C(31)-C(32)	1.49(2)
C(32)-C(33)	1.37(2)
C(33)-C(34)	1.40(3)
C(34)-C(35)	1.44(3)
C(35)-C(36)	1.40(2)
C(36)-C(37)	1.396(19)
C(37)-O(6)	1.337(18)
C(41)-O(7)	1.33(2)
C(41)-C(42)	1.34(2)
C(41)-C(47)	1.41(2)
C(42)-C(43)	1.44(3)
C(43)-C(44)	1.38(3)
C(44)-C(45)	1.33(3)
C(45)-C(46)	1.44(3)
C(46)-C(47)	1.40(2)
C(47)-O(8)	1.34(2)

Table A10.4 Bond angles [º] for **Nb_9**.

Bond	Bond angle [º]
O(6)-Nb(1)-O(2)	90.3(4)
O(6)-Nb(1)-O(5)	71.2(4)
O(2)-Nb(1)-O(5)	76.5(5)
O(6)-Nb(1)-O(3)	148.9(5)
O(2)-Nb(1)-O(3)	96.2(4)
O(5)-Nb(1)-O(3)	139.9(4)
O(6)-Nb(1)-O(7)	101.3(4)
O(2)-Nb(1)-O(7)	147.2(5)
O(5)-Nb(1)-O(7)	78.4(5)
O(3)-Nb(1)-O(7)	89.5(4)
O(6)-Nb(1)-O(1)	77.1(4)
O(2)-Nb(1)-O(1)	71.6(5)
O(5)-Nb(1)-O(1)	134.3(4)
O(3)-Nb(1)-O(1)	76.2(4)
O(7)-Nb(1)-O(1)	140.7(5)
O(6)-Nb(1)-O(8)	78.1(4)
O(2)-Nb(1)-O(8)	141.5(5)
O(5)-Nb(1)-O(8)	131.0(5)
O(3)-Nb(1)-O(8)	78.0(4)
O(7)-Nb(1)-O(8)	71.3(5)
O(1)-Nb(1)-O(8)	70.0(5)
O(6)-Nb(1)-O(4)	139.5(4)
O(2)-Nb(1)-O(4)	75.4(5)
O(5)-Nb(1)-O(4)	68.7(4)
O(3)-Nb(1)-O(4)	71.3(4)
O(7)-Nb(1)-O(4)	76.0(5)
O(1)-Nb(1)-O(4)	130.1(5)
O(8)-Nb(1)-O(4)	134.8(4)

C(11)-O(1)-Nb(1)	122.6(10)
C(17)-O(2)-Nb(1)	122.9(11)
C(21)-O(3)-Nb(1)	121.8(10)
C(27)-O(4)-Nb(1)	120.2(10)
C(31)-O(5)-Nb(1)	119.4(10)
C(37)-O(6)-Nb(1)	121.8(9)
C(41)-O(7)-Nb(1)	123.1(11)
C(47)-O(8)-Nb(1)	120.3(9)
O(1)-C(11)-C(12)	122.0(15)
O(1)-C(11)-C(17)	114.2(16)
C(12)-C(11)-C(17)	123.7(17)
C(13)-C(12)-C(11)	131.7(17)
C(12)-C(13)-C(14)	130(2)
C(15)-C(14)-C(13)	123(2)
C(16)-C(15)-C(14)	132.0(19)
C(17)-C(16)-C(15)	127.0(18)
O(2)-C(17)-C(16)	119.4(17)
O(2)-C(17)-C(11)	108.6(17)
C(16)-C(17)-C(11)	131.9(19)
O(3)-C(21)-C(27)	113.7(12)
O(3)-C(21)-C(22)	118.1(14)
C(27)-C(21)-C(22)	128.1(14)
C(23)-C(22)-C(21)	127.0(16)
C(24)-C(23)-C(22)	131.3(15)
C(25)-C(24)-C(23)	125.4(14)
C(24)-C(25)-C(26)	132.9(17)
C(25)-C(26)-C(27)	126.7(16)
O(4)-C(27)-C(26)	119.1(14)
O(4)-C(27)-C(21)	112.8(13)
C(26)-C(27)-C(21)	128.1(13)

O(5)-C(31)-C(37)	115.9(15)
O(5)-C(31)-C(32)	115.3(14)
C(37)-C(31)-C(32)	128.8(13)
C(33)-C(32)-C(31)	124.8(16)
C(32)-C(33)-C(34)	132.3(17)
C(33)-C(34)-C(35)	126.8(14)
C(36)-C(35)-C(34)	127.7(15)
C(37)-C(36)-C(35)	128.8(16)
O(6)-C(37)-C(31)	111.7(12)
O(6)-C(37)-C(36)	117.7(15)
C(31)-C(37)-C(36)	130.5(15)
O(7)-C(41)-C(42)	120.7(16)
O(7)-C(41)-C(47)	110.7(15)
C(42)-C(41)-C(47)	128.5(17)
C(41)-C(42)-C(43)	131.1(18)
C(44)-C(43)-C(42)	124(2)
C(45)-C(44)-C(43)	133.5(19)
C(44)-C(45)-C(46)	128.2(17)
C(47)-C(46)-C(45)	126(2)
O(8)-C(47)-C(46)	117.0(17)
O(8)-C(47)-C(41)	114.6(13)
C(46)-C(47)-C(41)	128.4(19)
O(1)-C(11)-C(12)	122.0(15)
O(1)-C(11)-C(17)	114.2(16)
C(12)-C(11)-C(17)	123.7(17)
C(13)-C(12)-C(11)	131.7(17)
C(12)-C(13)-C(14)	130(2)
C(15)-C(14)-C(13)	123(2)
C(16)-C(15)-C(14)	132.0(19)
C(17)-C(16)-C(15)	127.0(18)

A11 Supplementary Geometric Data for *Tetrakis*(tropolonato -κ^2*O,O'*)tantalum(V)chloride ([Ta(Trop)$_4$]Cl), (Ta_2))

Table 11.1 Atomic coordinates (x 10^4) and equivalent isotropic displacement parameters (Å^2 x 10^3) for **Ta_2**.

	x	y	z	U(eq)
Ta(2)	10000	4067(1)	7500	24(1)
Ta(1)	7889(1)	1048(1)	6442(1)	24(1)
O(1)	8051(6)	96(6)	6788(6)	28(3)
O(2)	7504(6)	384(6)	5683(6)	28(3)
O(3)	7495(5)	1904(6)	6804(6)	25(3)
O(4)	8540(6)	1783(6)	6491(6)	27(3)
O(5)	9269(10)	5468(11)	5179(11)	94(7)
O(6)	9215(6)	4346(6)	7920(6)	29(3)
O(7)	8212(6)	1092(6)	7480(6)	26(3)
O(8)	7597(6)	1583(6)	5556(6)	31(3)
O(9)	9730(6)	4892(6)	6900(6)	36(3)
O(10)	9684(5)	3763(6)	6516(6)	25(3)
O(11)	8615(6)	722(6)	5940(6)	29(3)
O(12)	9476(6)	3226(6)	7639(6)	29(3)
O(13)	8665(8)	2687(9)	8008(9)	63(5)
O(14)	7077(6)	799(7)	6759(6)	33(3)
C(11)	8330(8)	4137(8)	8403(9)	23(4)
C(12)	8358(8)	-683(9)	7674(9)	28(4)
C(13)	6763(8)	2468(9)	7337(9)	27(4)
C(14)	7193(9)	123(10)	4550(9)	35(5)
C(15)	8468(8)	620(9)	8563(9)	27(4)
C(16)	6242(10)	2506(11)	7647(11)	43(5)
C(21)	6212(10)	1021(10)	7312(11)	38(5)

C(22)	9433(9)	2231(9)	6260(9)	29(4)
C(23)	7814(9)	3060(9)	8625(9)	33(4)
C(24)	7002(9)	225(9)	3888(9)	32(4)
C(25)	9423(11)	5386(12)	5827(12)	55(6)
C(26)	8112(8)	2600(9)	8325(9)	28(4)
C(27)	10093(10)	1137(10)	5447(10)	35(5)
C(31)	8295(8)	555(9)	7857(8)	25(4)
C(32)	8585(8)	122(9)	9060(8)	26(4)
C(33)	8827(8)	3921(8)	8114(8)	21(4)
C(34)	6899(13)	812(13)	3463(13)	59(7)
C(35)	9992(9)	2256(9)	6001(9)	33(4)
C(36)	8253(8)	-23(9)	7463(8)	26(4)
C(37)	10311(10)	1764(10)	5647(10)	41(5)
C(41)	7889(9)	3752(10)	8652(10)	33(4)
C(42)	7229(10)	1666(10)	4397(10)	40(5)
C(43)	7373(8)	583(9)	5063(9)	28(4)
C(44)	9077(9)	1080(9)	5893(9)	28(4)
C(45)	7392(8)	1303(9)	5002(9)	26(4)
C(46)	8609(9)	-553(10)	8927(10)	37(5)
C(47)	9356(11)	3953(10)	5375(12)	45(6)
C(51)	8524(9)	-901(9)	8313(9)	27(4)
C(52)	8985(8)	3273(8)	7915(8)	22(3)
C(53)	9545(9)	828(10)	5560(10)	35(4)
C(54)	9034(8)	1712(9)	6223(9)	27(4)
C(55)	5807(11)	1365(12)	7612(11)	50(6)
C(56)	5813(10)	2071(10)	7762(10)	41(5)
C(57)	9535(9)	4192(10)	6020(10)	33(4)
C(61)	6726(8)	1241(9)	7051(9)	28(4)
C(62)	7063(10)	1486(11)	3724(11)	45(5)
C(63)	9202(11)	4277(13)	4779(12)	54(6)

C(64)	9561(8)	4838(9)	6263(9)	29(4)
C(65)	7015(9)	1865(9)	7047(9)	30(4)
C(66)	9186(12)	4929(13)	4674(12)	58(7)
Cl(1)	7127(3)	-1490(3)	3998(3)	61(2)

Table A11.3 Bond lengths [Å] for **Ta_2**.

Bond	Bond length [Å]
Ta(2)-O(9)	2.080(11)
Ta(2)-O(9)'	2.080(11)
Ta(2)-O(10)	2.100(13)
Ta(2)-O(10)'	2.100(13)
Ta(2)-O(11)	2.103(13)
Ta(2)-O(11)'	2.103(13)
Ta(2)-O(12)	2.112(12)
Ta(2)-O(12)'	2.112(12)
Ta(1)-O(1)	2.049(13)
Ta(1)-O(2)	2.072(12)
Ta(1)-O(3)	2.088(12)
Ta(1)-O(4)	2.090(12)
Ta(1)-O(5)	2.097(12)
Ta(1)-O(6)	2.100(13)
Ta(1)-O(7)	2.111(12)
Ta(1)-O(8)	2.126(12)
O(5)-C(45)	1.375(19)
O(6)-C(54)	1.29(2)
O(7)-C(77)	1.23(2)
O(8)-C(62)	1.28(2)
O(9)-C(35)	1.29(3)
O(9)-C(78)	1.48(3)
O(10)-C(41)	1.31(2)
O(11)-C(39)	1.32(2)
O(12)-C(56)	1.27(2)
O(15)-C(69)	1.32(2)

O(16)-C(55)	1.28(2)
O(17)-C(60)	1.28(2)
O(18)-C(60)	1.41(2)
O(18)-C(36)	1.46(2)
C(20)-C(41)	1.38(2)
C(20)-C(47)	1.39(3)
C(23)-C(59)	1.35(2)
C(23)-C(45)	1.42(2)
C(24)-C(29)	1.37(3)
C(26)-C(34)	1.34(2)
C(26)-C(54)	1.40(3)
C(27)-C(39)	1.41(2)
C(27)-C(40)	1.41(2)
C(31)-C(65)	1.33(3)
C(31)-C(71)	1.39(3)
C(32)-C(62)	1.38(3)
C(32)-C(44)	1.40(3)
C(33)-C(36)	1.32(3)
C(33)-C(47)	1.42(3)
C(34)-C(43)	1.46(3)
C(35)-C(75)	1.42(3)
C(38)-C(46)	1.41(3)
C(38)-C(61)	1.42(3)
C(39)-C(45)	1.41(2)
C(40)-C(57)	1.40(3)
C(41)-C(60)	1.43(2)
C(44)-C(46)	1.45(3)
C(51)-C(56)	1.41(3)
C(54)-C(56)	1.47(3)
C(55)-C(61)	1.39(3)

Table A11.4 Bond angles [º] for **Ta_2**.

Bond	Bond angle [º]
O(9)-Ta(2)-O(9)'	145.4(7)
O(9)-Ta(2)-O(10)	103.1(5)
O(9)'-Ta(2)-O(10)	86.2(5)
O(9)-Ta(2)-O(10)'	86.2(5)
O(9)'-Ta(2)-O(10)'	103.1(5)
O(10)-Ta(2)-O(10)'	148.7(7)
O(10)'-Ta(2)-O(9)'	70.6(5)
O(12)'-Ta(2)-O(11)	143.8(5)
O(10)-Ta(2)-O(13)	78.5(5)
O(10)'-Ta(2)-O(9)	76.7(5)
O(10)-Ta(2)-O(9)'	143.8(5)
O(9)'-Ta(2)-O(11)'	70.6(5)
O(6)-Ta(1)-O(8)	76.7(5)
O(6)-Ta(1)-O(7)	78.5(5)
O(2)-Ta(1)-O(5)	74.0(7)
O(2)-Ta(1)-O(1)	74.9(5)
O(2)'-Ta(1)-O(3)	77.2(5)
O(5)-Ta(1)-O(4)	70.5(5)
O(7)-Ta(1)-O(2)	140.5(5)
O(5)-Ta(1)-O(3)	126.0(5)
O(7)-Ta(1)-O(8)	135.0(5)
O(5)-Ta(1)-O(6)	77.2(5)
O(5)-Ta(1)-O(7)	74.9(5)
O(4)-Ta(1)-O(1)	140.5(5)
C(35)-O(9)-C(78)	124(2)
C(41)-O(10)-Ta(1)	123.1(11)
C(39)-O(11)-Ta(2)	121.6(10)
C(56)-O(12)-Ta(2)	122.1(11)

C(75)-O(1)-Ta(1)	121.3(12)
C(69)-O(2)-Ta(1)	121.5(12)
C(55)-O(3)-Ta(1)	122.0(12)
C(60)-O(4)-Ta(1)	120.6(11)
C(60)-O(18)-C(36)	128.6(16)
C(41)-C(20)-C(47)	127.1(17)
C(59)-C(23)-C(45)	127.4(17)
C(29)-C(24)-C(77)	126.2(18)
C(34)-C(26)-C(54)	129.1(19)
C(39)-C(27)-C(40)	128.7(17)
C(65)-C(31)-C(71)	129(2)
C(62)-C(32)-C(44)	127.5(18)
C(36)-C(33)-C(47)	130.9(19)
C(26)-C(34)-C(43)	134(2)
C(46)-C(38)-C(61)	130(2)
O(11)-C(39)-C(45)	112.8(15)
O(11)-C(39)-C(27)	118.8(16)
C(45)-C(39)-C(27)	128.1(16)
C(57)-C(40)-C(27)	125.8(17)
O(10)-C(41)-C(20)	120.0(15)
O(10)-C(41)-C(60)	109.7(15)
C(20)-C(41)-C(60)	130.0(16)
C(32)-C(44)-C(46)	130.8(18)
O(5)-C(45)-C(39)	112.2(15)
O(5)-C(45)-C(23)	118.5(15)
C(39)-C(45)-C(23)	129.2(16)
C(38)-C(46)-C(44)	126(2)
C(20)-C(47)-C(33)	129.2(19)
C(73)-C(51)-C(56)	133(2)
O(6)-C(54)-C(26)	119.2(17)

O(6)-C(54)-C(56)	112.7(15)
C(26)-C(54)-C(56)	127.9(16)
O(6)-C(55)-C(61)	118.8(17)
O(6)-C(55)-C(62)	112.3(17)
C(61)-C(55)-C(62)	128.9(18)
O(8)-C(56)-C(51)	121.5(17)
O(8)-C(56)-C(54)	112.8(15)
C(51)-C(56)-C(54)	125.6(16)
C(59)-C(57)-C(40)	130.9(18)
C(23)-C(59)-C(57)	129.5(18)
O(12)-C(60)-C(41)	115.7(15)
O(8)-C(62)-C(32)	118.4(16)
O(8)-C(62)-C(55)	112.7(16)
C(32)-C(62)-C(55)	128.9(18)

Supplementary Kinetic Data

B1 Derivation of Rate Law in Section 8.3.2

In Figure 8.15 six possible species in solution are available for ligand coordination were identified. The various equilibriums between four of these species are illustrated in Figure 8.16. When considering the K_{ox} equilibrium depiction in Figure 8.16 between $[NbOCl_5]$ and $[NbCl_6^-]$, it indicates an overarching representation of the total of $[NbCl_6^-]$ – $[NbCl_5(H_2O)]$ – $[NbCl_5(OH)]$ – $[NbOCl_5]$ equilibriums.

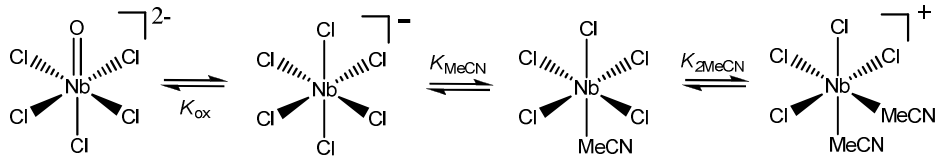

Figure 8.16 Illustration of kinetic equilibriums between the various synthons in solution.

From the definition of the three equilibrium constants defined in the mechanism in Figures 8.15 and 8.16, K_{ox}, K_{MeCN} and K_{2MeCN}, the following equations could be derived:

$$K'_{ox} = \frac{[M(ox)Cl_5][Cl]}{[MCl_6][H_2O]} \quad \text{Eq. 1}$$

$$K_{MeCN} = \frac{[M(MeCN)Cl_5][Cl]}{[MCl_6]} \quad \text{Eq. 2}$$

$$K_{2MeCN} = \frac{[M(MeCN)_2Cl_4][Cl]}{[M(MeCN)Cl_5]} \quad \text{Eq. 3}$$

To accurately obtain the total metal species available for coordination, the $[M(ox)Cl_5]$, $[M(MeCN)Cl_5]$ and $[M(MeCN)_2Cl_5]$ concentrations need to derived in terms of $[M]_{tot}$. The total metal(V) concentration in solution ($[M]_{tot}$) at any time, is defined by:

$$[M]_{tot} = [MCl_6] + [M(ox)Cl_5] + [M(MeCN)Cl_5] + [M(MeCN)_2Cl_4] \quad \text{Eq. 4}$$

By substituting Eq. 8.2, Eq. 8.3 and Eq. 8.4 into Eq. 8.5 three expressions for $[M(ox)Cl_5]$, $[M(MeCN)Cl_5]$ and $[M(MeCN)_2Cl_5]$ are obtained:

From Eq. 2

$$[MCl_6] = \frac{[M(MeCN)Cl_5][Cl]}{[K_{MeCN}]} \quad \text{Eq. 5}$$

and

From Eq. 1

$$[MCl_6] = \frac{[M(ox)Cl_5][Cl]}{K_{ox}[H_2O]} \quad \text{Eq. 6}$$

$$[M(ox)Cl_5] = \frac{[MCl_6]K_{ox}[H_2O]}{[\mathrm{Cl}]} \quad \text{Eq. 7}$$

By substituting Eq. 2 into Eq. 7

$$[M(ox)Cl_5] = \frac{[M(MeCN)Cl_5]K_{ox}[H_2O]}{K_{MeCN}} \quad \text{Eq. 8}$$

From Eq.3

$$[M(MeCN)_2Cl_4] = \frac{[M(MeCN)Cl_5]K_{2MeCN}}{[\mathrm{Cl}]} \quad \text{Eq. 9}$$

By substituting Eq. 5, Eq. 8 and Eq. 9 into Eq. 4

$$[M]_{tot} = \frac{[M(ox)Cl_5][Cl]}{K_{ox}[H_2O]} + \frac{[M(MeCN)Cl_5]K_{ox}[H_2O]}{K_{MeCN}} + [M(MeCN)Cl_5] + \frac{[M(MeCN)Cl_5]K_{2MeCN}}{[\mathrm{Cl}]} \quad \text{Eq. 10}$$

$$[M(MeCN)Cl_5] = \frac{[\mathrm{M}]_{tot}}{\frac{[Cl]}{K_{MeCN}} + \frac{K_{ox}[H_2O]}{K_{MeCN}} + 1 + \frac{K_{2MeCN}}{[Cl]}} \; x \; \frac{K_{MeCN}[Cl]}{K_{MeCN}[Cl]} \quad \text{Eq. 11}$$

$$[M(MeCN)Cl_5] = \frac{[\mathrm{M}]_{tot}K_{MeCN}[Cl]}{[Cl^-]^2 + [Cl^-]K_{ox}[H_2O] + [Cl^-]K_{MeCN} + K_{2MeCN}K_{MeCN}} \quad \text{Eq. 12}$$

Similarly the expression for $[M]_{tot}$ in terms of $[M(MeCN)_2Cl_4]$

$$[M]_{tot} = \frac{[M(MeCN)_2Cl_4][Cl^-]^2}{K_{2MeCN}K_{MeCN}} + \frac{[M(MeCN)_2Cl_4][Cl^-]K_{ox}[H_2O]}{K_{2MeCN}K_{MeCN}} + \frac{[M(MeCN)_2Cl_4][Cl^-]}{K_{2MeCN}} + [M(MeCN)_2Cl_4]$$

Eq. 13

$$[M(MeCN)_2Cl_4] = \frac{[\mathrm{M}]_{tot}}{\frac{[Cl^-]^2}{K_{MeCN}K_{2MeCN}} + \frac{[Cl^-]K_{ox}[H_2O]}{K_{MeCN}K_{2MeCN}} + \frac{[Cl^-]}{K_{2MeCN}} + 1} \; x \; K_{MeCN}K_{2MeCN} \qquad \text{Eq. 14}$$

$$[M(MeCN)_2Cl_4] = \frac{[\mathrm{M}]_{tot}K_{MeCN}K_{2MeCN}}{[Cl^-]^2 + [Cl^-]K_{ox}[H_2O] + [Cl^-]K_{MeCN} + K_{2MeCN}K_{MeCN}} \qquad \text{Eq. 15}$$

Similarly the expression for $[M]_{tot}$ in terms of $[M(ox)Cl_5]$

$$[M]_{tot} = \frac{[M(ox)Cl_5][Cl^-]}{K_{ox}[H_2O]} + [M(ox)Cl_5] + \frac{[M(ox)Cl_5]K_{MeCN}}{K_{ox}[H_2O]} + \frac{[M(ox)Cl_5]K_{2MeCN}K_{MeCN}}{K_{ox}[H_2O][Cl^-]} \qquad \text{Eq. 16}$$

$$[M(ox)Cl_5] = \frac{[\mathrm{M}]_{tot}}{\frac{[Cl]}{K_{ox}[H_2O]} + 1 + \frac{1}{K_{ox}[H_2O]} + \frac{K_{2MeCN}}{K_{ox}[H_2O][Cl^-]}} \; x \; \frac{[H_2O]K_{ox}[Cl^-]}{[H_2O]K_{ox}[Cl^-]} \qquad \text{Eq. 17}$$

$$[M(ox)Cl_5] = \frac{[\mathrm{M}]_{tot}[H_2O]K_{ox}[Cl^-]}{[Cl^-]^2 + [Cl^-]K_{ox}[H_2O] + [Cl^-]K_{MeCN} + K_{2MeCN}K_{MeCN}} \qquad \text{Eq. 18}$$

These three equations define the total amount of reacting M(V) species in solution, i.e. $[M(ox)Cl_5]^{2-}$, $[M(MeCN)Cl_5]$ and $[M(MeCN)_2Cl_4]^+$ for which a complex rate law involving these reactants for the forward reaction, may be written. Thus, an expression for the total rate of the reaction is defined by:

$$Rate^{tot} = Rate^{[M(ox)Cl_5]} + Rate^{[M(MeCN)Cl_5]} + Rate^{[M(MeCN)_2Cl_4]} \qquad \text{Eq. 19}$$

$$Rate^{tot} = k_{11}[M(ox)Cl_5][acac] + k_{21}[M(MeCN)Cl_5][acac] + k_{31}[M(MeCN)_2Cl_4][acac] \qquad \text{Eq. 20}$$

By substituting Eq. 12, Eq. 15 and Eq. 18 into Eq. 20, the total rate law is obtained under conditions where [*β*-diket] >> [M_{tot}], yielding the *pseudo* first-order rate constant:

$$K_{obs}{}^{tot} = \frac{k_{11}[H_2O]K_{ox}[Cl^-] + k_{21}K_{MeCN}[Cl^-] + k_{31}K_{2MeCN}K_{MeCN}}{[Cl^-]^2 + [Cl^-]K_{ox}[H_2O] + [Cl^-]K_{MeCN} + K_{2MeCN}K_{MeCN}} \; [acac] + k_{rev} \qquad \text{Eq. 21}$$

B2 k_{obs} Values Used for Various Graphs in Chapter 8

Table B2.2 k_{obs} values used in kinetic fits in Figure 8.17.

Concentration (M)	Chloride	Water	Chloride + Water
	k_{obs} (s^{-1})	k_{obs} (s^{-1})	k_{obs} (s^{-1})
0	0.011	0.011	0.011
0.0005	0.0129	0.016	0.0187
0.001	0.0145	0.0187	0.0239
0.0025	0.018	0.0208	0.0253
0.005	0.021	0.023	0.0268
0.05	0.0233	0.0249	0.0265

Table B2.2 k_{obs} values used in kinetic fits in Figure 8.19.

Concentration (M)	15 ºC	25 ºC	35 ºC	45 ºC
	k_{obs} (s^{-1})	k_{obs} (s^{-1})	k_{obs} (s^{-1})	k_{obs} (s^{-1})
0.005	0.0009	0.0025	0.007	0.017
0.01	0.0018	0.0051	0.013	0.032
0.025	0.0038	0.01	0.027	0.077
0.0375	0.0062	0.017	0.043	0.117
0.05	0.0087	0.024	0.054	0.151

Table B2.3 k_{obs} values used in kinetic fits in Figure 8.20.

Concentration (M)	15 ºC	25 ºC	35 ºC	45 ºC
	k_{obs} (s^{-1})	k_{obs} (s^{-1})	k_{obs} (s^{-1})	k_{obs} (s^{-1})
0.005	0.0027	0.0059	0.012	0.027
0.01	0.0042	0.0093	0.019	0.041
0.025	0.0075	0.017	0.033	0.073
0.0375	0.0119	0.026	0.05	0.102
0.05	0.0157	0.032	0.065	0.135

Table B2.4 k_{obs} values used in kinetic fits in Figure 8.23.

Concentration (M)	AcacH	Naphtyl	Thenoyl	Trifluoro	Hexafluoro
	k_{obs} (s^{-1})	k_{obs} (s^{-1})	k_{obs} (s^{-1})	k_{obs} (s^{-1})	k_{obs} (s^{-1})
0.005	0.00171	0.00121	0.00253	0.00244	0.00315
0.01	0.00245	0.00212	0.00509	0.00432	0.0075
0.025	0.00445	0.00528	0.0101	0.011	0.0201
0.0375	0.00521	0.00752	0.0172	0.0156	0.0315
0.05	0.00705	0.0102	0.0238	0.0223	0.0435

Table B2.5 k_{obs} values used in kinetic fits in Figure 8.24.

Concentration (M)	AcacH	Naphtyl	Thenoyl	Trifluoro	Hexafluoro
	k_{obs} (s^{-1})	k_{obs} (s^{-1})	k_{obs} (s^{-1})	k_{obs} (s^{-1})	k_{obs} (s^{-1})
0.005	0	0.00548	0.00877	0.00935	0.0122
0.01	0	0.00743	0.0132	0.0137	0.0198
0.025	0	0.0135	0.0234	0.0258	0.038
0.0375	0	0.0181	0.0299	0.0332	0.055
0.05	0	0.0229	0.037	0.0413	0.075

Table B2.6 k_{obs} values used in kinetic fits in Figure 8.25.

Concentration (M)	AcacH	Naphtyl	Thenoyl	Trifluoro	Hexafluoro
	k_{obs} (s^{-1})	k_{obs} (s^{-1})	k_{obs} (s^{-1})	k_{obs} (s^{-1})	k_{obs} (s^{-1})
0.005	0.00122	0.00125	0.00133	0.00141	0.00145
0.01	0.00165	0.00187	0.00256	0.00265	0.00315
0.025	0.00298	0.00355	0.00511	0.00533	0.00822
0.0375	0.00401	0.00489	0.0075	0.00778	0.0121
0.05	0.00498	0.0062	0.0101	0.011	0.0167

Table B2.7 k_{obs} values used in Figure 8.26.

Concentration (M)	AcacH	Naphtyl	Thenoyl	Trifluoro	Hexafluoro
	k_{obs} (s^{-1})	k_{obs} (s^{-1})	k_{obs} (s^{-1})	k_{obs} (s^{-1})	k_{obs} (s^{-1})
0.005	0	0.00399	0.00401	0.00422	0.00611
0.01	0	0.00501	0.00595	0.00612	0.00899
0.025	0	0.0085	0.0101	0.0115	0.0171
0.0375	0	0.0106	0.0148	0.0156	0.0235
0.05	0	0.0135	0.0188	0.0196	0.0305